

CHAPTER 4

RESULTS AND DISCUSSIONS

4.0 INTRODUCTION

The outcomes of different segments are discussed in the forthcoming sections on the ground of basic theories involved and test results reported in the world of green AgNPs synthesis in the absence of back-track records.

4.1 PHASE-I:

ENGINEERING ELEMENTARY SET-UP AND CONFIRMING COMPETENCY OF NOVEL BIO-SYNTHEZIZED NANOPARTICLES

This phase has dealt with the commercially efficacious chemical and till date unexplored Milkweed [*Calotropis Procera* (CP)] leave extract based green synthesis routes for the formation of silver nanoparticles (AgNPs). During the three (Forward, Reverse and Reduction) chemical synthesis routes of AgNO_3 , concentrations of the chemical agents were selected as per the standard laid down methods. But for green synthesis the best performances level reported in the previous studies for other than CP mediums was used in both (Forward and Reverse) routes. The fundamental performance peculiarities of novel green-way nanoparticles from established chemical pathway have been explored in order to distinguish its sustainability.

4.1.1 RESULT'S ANALYSIS

4.1.1.1 Elementary Confirmation of AgNPs formation and Stability by VCCO:

The colour change witnessed reduction of silver ions (Ag^+) to silver nanoparticles (Ag^0). The resultant colour arises due to the collective oscillations of free conduction electrons in the nanoparticles [111,233]. According to vanaja et al. [233], the colour change of the aqueous solution also occurs due to the excitation of the surface plasmon resonance (SPR) and SPR band, issuing preliminary guaranteeing for the formation of the AgNPs. The intensity of the colour changes, that is from light to dark, results as per the alteration in the size of the nanoparticles from nano to the microstructure [5]. Thus, preliminarily confirmation about the formation of the AgNPs and their stability with respect to time was validated by the change in the colour of the colloidal solutions which were prepared by the chemical synthesis (CS) and green synthesis (GS) methods after 0 hour, 24 hours and 48 hours.

**CS-1
Forward
method
(Top-down
approach)**



**CS-2
Reverse
method
(Bottom-up
approach)**



**CS-3
Reduction
method
(by tri-
sodium
citrate)**



Time

(a) 0 hour

(b) 24 hours

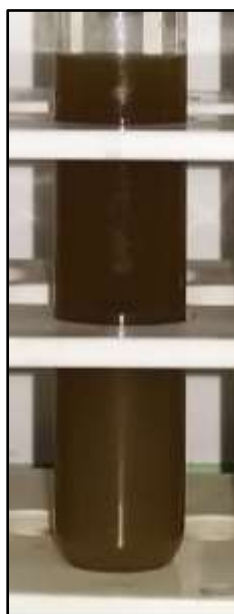
(c) 48 hours

Figure 4.1: Colour change observation of the AgNPs colloidal - Chemical synthesis

**GS-1
Forward
method
(Top-down
approach)**



**GS-2
Reverse
method
(Bottom-up
approach)**



Time

(a) 0 hour

(b) 24 hours

(c) 48 hours

Figure 4.2: Colour change observation of the AgNPs colloidal - Green synthesis

4.1.1.1.1 Chemical Synthesis (CS)

The colour change in the colloidal solution was observed invariably for all three chemical synthesis procedures; forward, reverse, and reduction. This has substantiated occurrence of AgNPs [Figures 4.1 (a–c)].

It can be seen that colour changed from milky white and colourless (after 0 hour), to light-dark brown (after 24 hours) to dark brown (after 48 hours) for the Forward and Reduction synthesis procedures respectively [Figures 4.1 (a–c)]. Thus, almost an identical visual colour change trend was observed with respect to time leap for both the approaches. However, this colour change from light to dark with increased time implies that the size of the nanoparticles has not remained stable and due to clustering turned to unacceptable microstructures [5,111].

Conversely, the reverse (bottom-up) method demonstrated a different but favourable colour change pattern; from colourless (after 0 hour) to light yellowish (after 24 hours) to yellowish (after 48 hours) respectively. This colourless to light yellowish colour change has subjectively supported occurrence of the preferable small size nanoparticles, and light yellow to yellowish colour change has authenticated their size stability or a very negligible but non-objectionable size change over the highest prescribed test time limits [5,111]. Besides this, most of the earlier studies also revealed that the bottom-up approach to the synthesis of the metal nanoparticle gives good nanoparticle formation as well as distribution of the nanoparticles [5,77]. This is attributed to a presence of large amount of reducing and capping agents used during synthesis to reduce the silver ion and stabilise the AgNPs [5,77]. Thus, present study results have gone in line with previous findings and Reverse approach came out with preferable quality and stable nanoparticles.

4.1.1.1.2 Green Synthesis (GS)

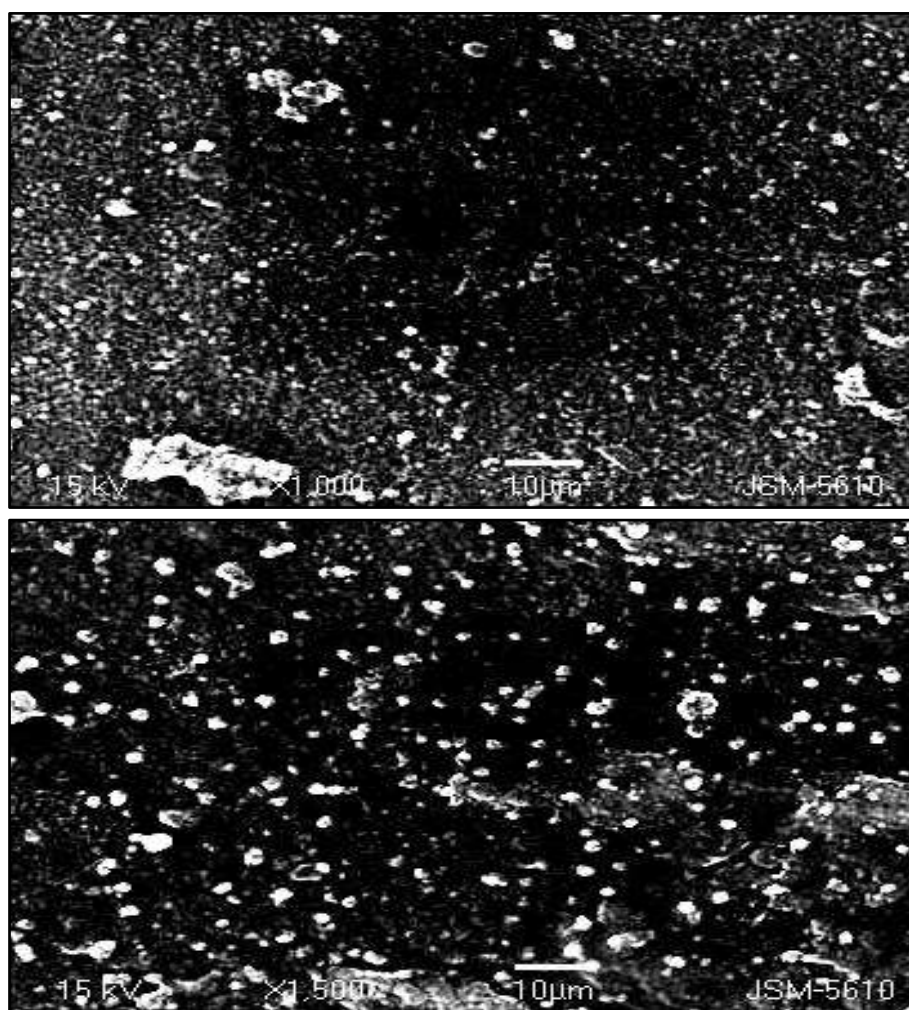
Both the green synthesis routes colour change visuals observed at specified time durations; i.e. after 0 hour, 24 hours, and 48 hours for the AgNPs colloidal solution are illustrated in Figures 4.2 (a–c).

An outlying difference in colour change pattern has been observed for both the methods. In case of forward method (GS-1) the colour has changed from colourless (at 0 hour) to milky white (after 24 hours) to brownish (after 48 hours), whereas in reverse method (GS-2) the colour change pattern was light brownish (at 0 hour) to fuzzy milky brownish

(after 24 hours) to dark brownish (after 48 hours). Hence, the CP leave extract is having inherent light brownish tint and its add-on values for both the approaches [Table 3.1] were not same, thereby difference in their colour change patterns and shade depths are likely. It can be well noted that Reverse approach working with ten times higher CP extract along with ten times lower AgNO_3 add-on have predominantly resumed light brownish tint initially (0 hour) instead of colourless seen in case of forward synthesis. This behaviour also makes visual judgment-based confirmation for the formation of AgNPs and their stability in either of the route misleading. That's why SEM analysis was considered a reliable ground of decision in these regards for both the green synthesis outputs.

4.1.1.2 Surface morphological analysis (by SEM) of the Green synthesised AgNPs

The SEM micrographs of the AgNPs colloidal prepared via the forward (GS-1) and the reverse (GS-2) green synthesis are illustrated in Figures 4.3 (a–b).



(a) Forward Method (GS-1)

(b) Reverse method (GS-2)

Figure 4.3: SEM micrograph of the AgNPs prepared through the Green synthesis

Both the micrographs witness formation of the huge count of AgNPs. This becomes possible due to phytochemicals, viz; alkaloids, steroids, flavonoids, terpenoids, cardenolides, phenols, etc. (Figure 4.4) present in the chemical composition of CP leave similar to other bio mediums used till date. These phytochemicals have invariably contributed in reducing the silver macro-particles to nano size as well as capping them during synthesis process [1,141]. The phenomenon gets approved by the SEM results which have endorsed formation of AgNPs via both the synthesis route.

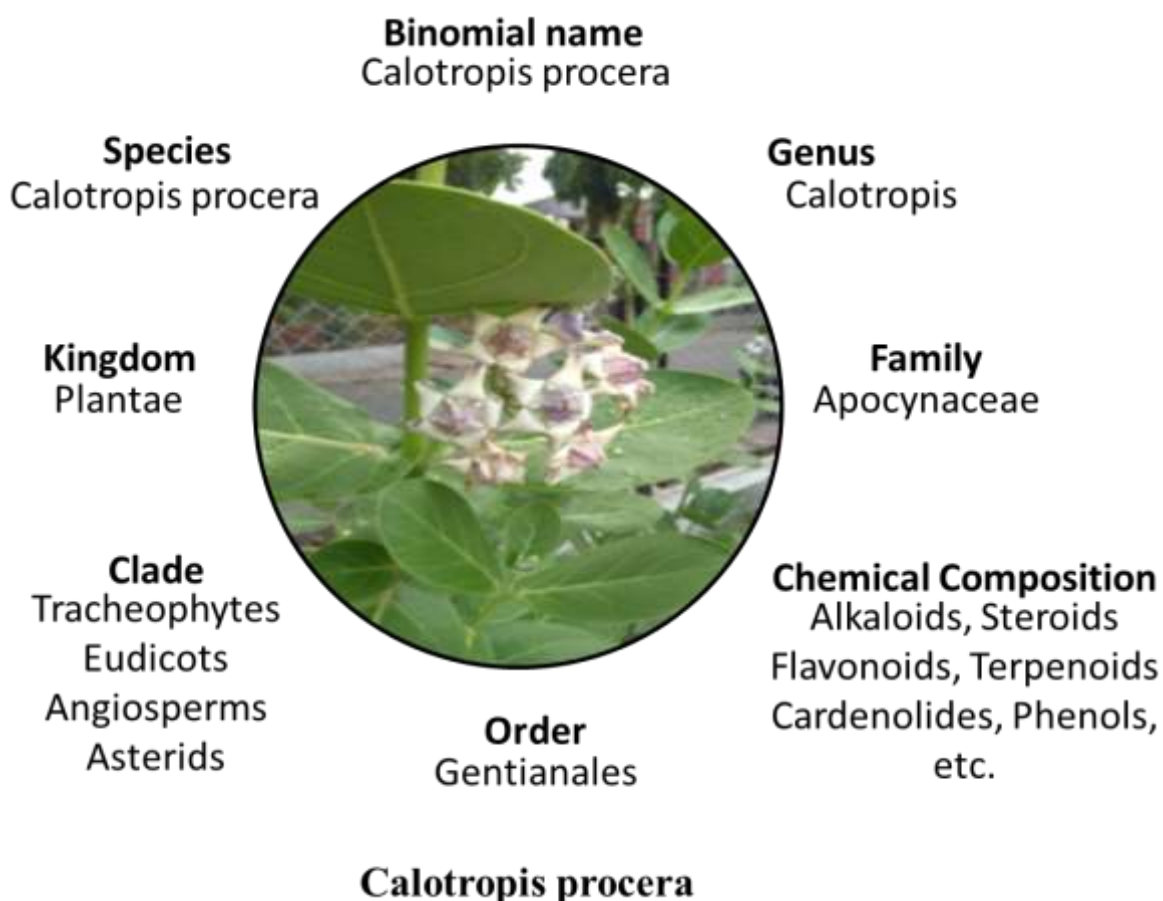


Figure 4.4: Plant specification (Calotropis procera)

The argument found further support from the SEM micrographs [Figures 4.3 (a-b)], executing high degree of AgNPs agglomerations for colloidal solution GS-1 against uniform dispersion of AgNPs with rarely occurring aggregation for sample GS-2. Being AgNPs in reverse path were synthesized with ten times more CP add-on and ten times less AgNO₃ [Table 3.1], higher quantity of CP extract was available to deal with ten times less AgNPs. This has not only enhanced silver macro particles reduction process to form AgNPs, but also prevented micro/macro particle formation by well encapsulating them. On the contrary the small quantity of the CP leave extract used against larger quantum of AgNO₃ during the forward AgNPs synthesis process definitely resulted in the huge numbers of AgNPs formation, but failed in covering/capping them.

4.1.2 PHASE-I: CONCLUSIONS

I) Chemical Synthesis (CS):

During the chemical synthesis of the AgNO₃, the concentrations of the chemical agent were selected as per the previous studies [5,77]. Going in agreement with back stuff record, the reverse method (bottom-up approach) has executed good deal of nanoparticle formation, confirmed by the colour change pattern from colourless to yellowish.

II) Green Synthesis (GS):

Using the CP leave extract, the forward and reverse green synthesis of the AgNO₃ salt was conducted successfully. Similar to the reverse chemical synthesis technique, the reverse method (Bottom-up approach) produced excellent nanoparticle production during green synthesis. The colour change observation and SEM analysis both confirmed this.

Hence, the reverse method produced superior nanoparticle generation and distribution in both cases, i.e. CS and GS; it was considered method of future research.

4.2 PHASE-II:

PREPARATION OF PROTOTYPE NONWOVEN @AgNPs/CP NANO-COMPOSITE AND VALIDATING ITS ANTIBACTERIAL ACTIVITY

This phase was designed to develop the prototype eco-friendly nano-composites for medical health care applications. Antibacterial efficacy is the major concern for the materials used in such applications. Thereby this functionality was introduced to the most commonly used medical textile material; PV (Polyester-Viscose) nonwoven fabric by treating with functional AgNPs, synthesized using innovative ecological medium; CP leave extract. The simple and effective cold dipping technique was used for AgNPs/CP under in-situ deposition on the selected textile material. Antibacterial activity potential of the newly engineered PV-AgNPs/CP nano-composite material and also feasible changes took place in physical, mechanical and comfort-associated parameters with respect to parent fabric on treatment for bio-medical material were measured.

4.2.1 RESULT'S ANALYSIS

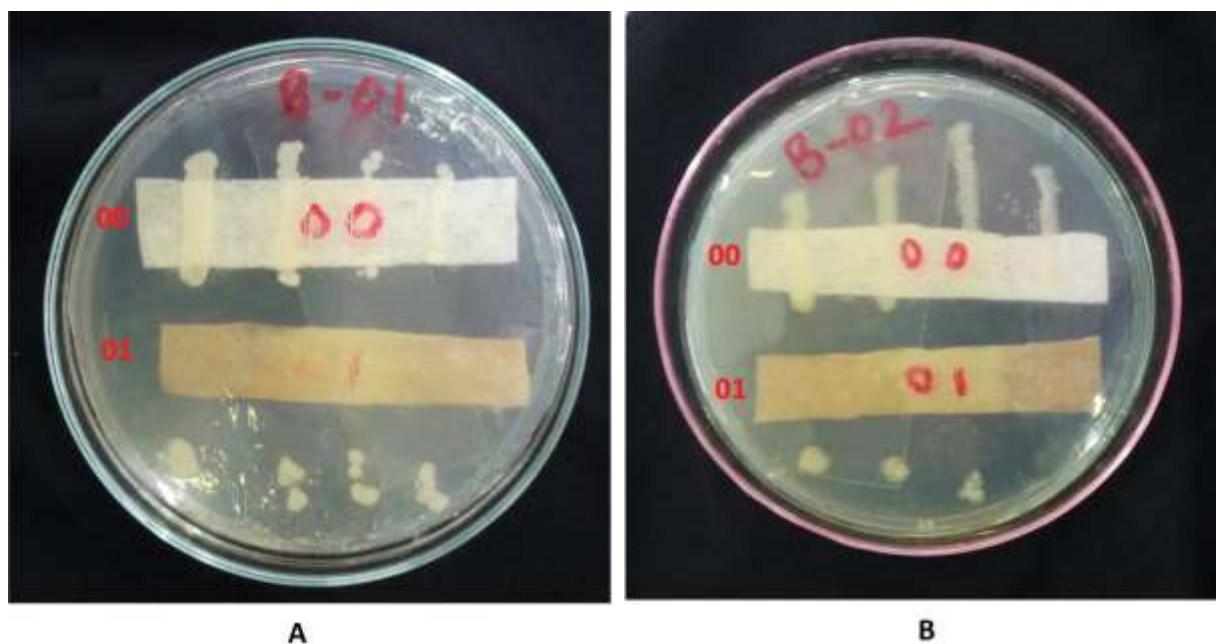
4.2.1.1 Antibacterial assessment of the Nano-composite @PV-AgNPs/CP

The antibacterial activity of PV-AgNPs/CP nano-composite (samples 01) was evaluated against untreated PV non-woven textile material (sample 00). The test was done in accordance with the AATCC-147 (Parallel streak method) standard; against the test bacterial cultures *Staphylococcus Aureus* (SA) and *Escherichia Coli* (EC). Photographs for the test results are shown in Figures 4.5 (a and b) and the average Zone of Inhibition (ZOI) of both samples (00 and 01) for both organisms (SA and EC) are given in Table 4.1.

Table 4.1: Average zone of inhibition (mm)

Organism	Sample 00	Sample 01	SD	CV%
<i>Staphylococcus aureus</i> (SA)	None	23.75	2.49	10.47
<i>Escherichia Coli</i> (EC)	None	24.50	3.57	14.57

SD= Standard deviation, CV%= Coefficient of variation %

(a) *Staphylococcus Aureus*(b) *Escherichia Coli***Figure 4.5: Antibacterial assessment of the Sample (00) and Sample (01)**

It can be seen from the test results that, the average ZOI value measured for AgNPs/CP loaded fabric (sample 01) is 23.75 mm and 24.5 mm against SA and EC test bacterial cultures, respectively. Parent fabric (sample 00), on the other hand, did not exhibit any bacterial inhibition against any of the test bacterial cultures, as expected. The significant antibacterial activity against both bacterial cultures (SA and EC) demonstrated by sample 01 was attributed mainly due to the presence of dynamic antibacterial composition of AgNPs formed with CP leave extract. Milkweed (*Calotropis*) leave have inherently inbuilt high level of antibacterial properties, well proven from its wide span use made in rural areas for treating burns, fungal attack and wound healing mainly [171,209]. Additionally, its capping potential has retained active silver component to the comparable nanoparticle size only without transforming into macro/micro particles in the sample 01 structure, offered increased specific surface for interaction [295]. All the parameters have unanimously contributed in enhancing remarkably antibacterial activities of the AgNPs/CP loaded PV-Nonwoven.

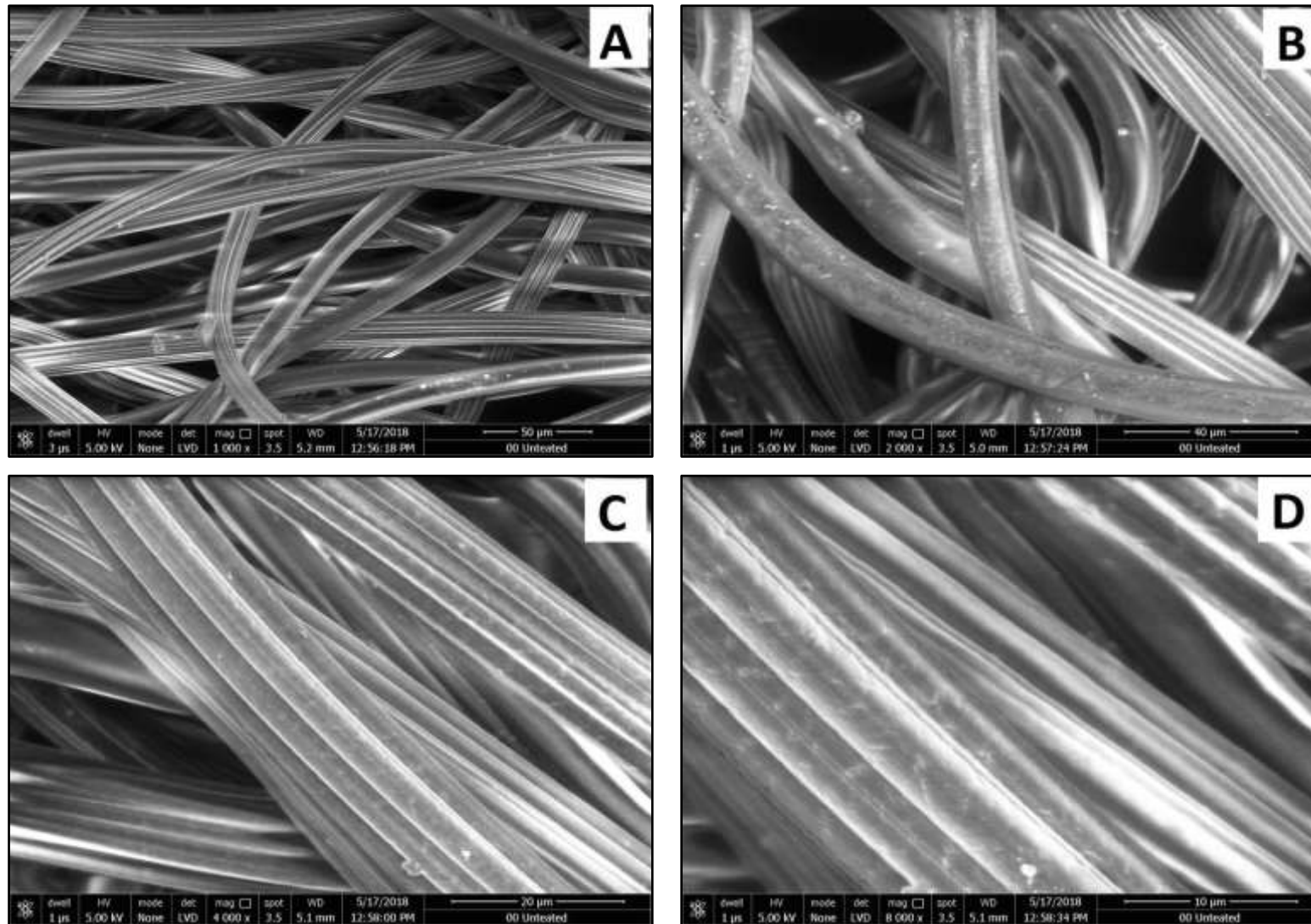


Figure 4.6: ESEM images of Sample 00 at different magnifications (a–d)

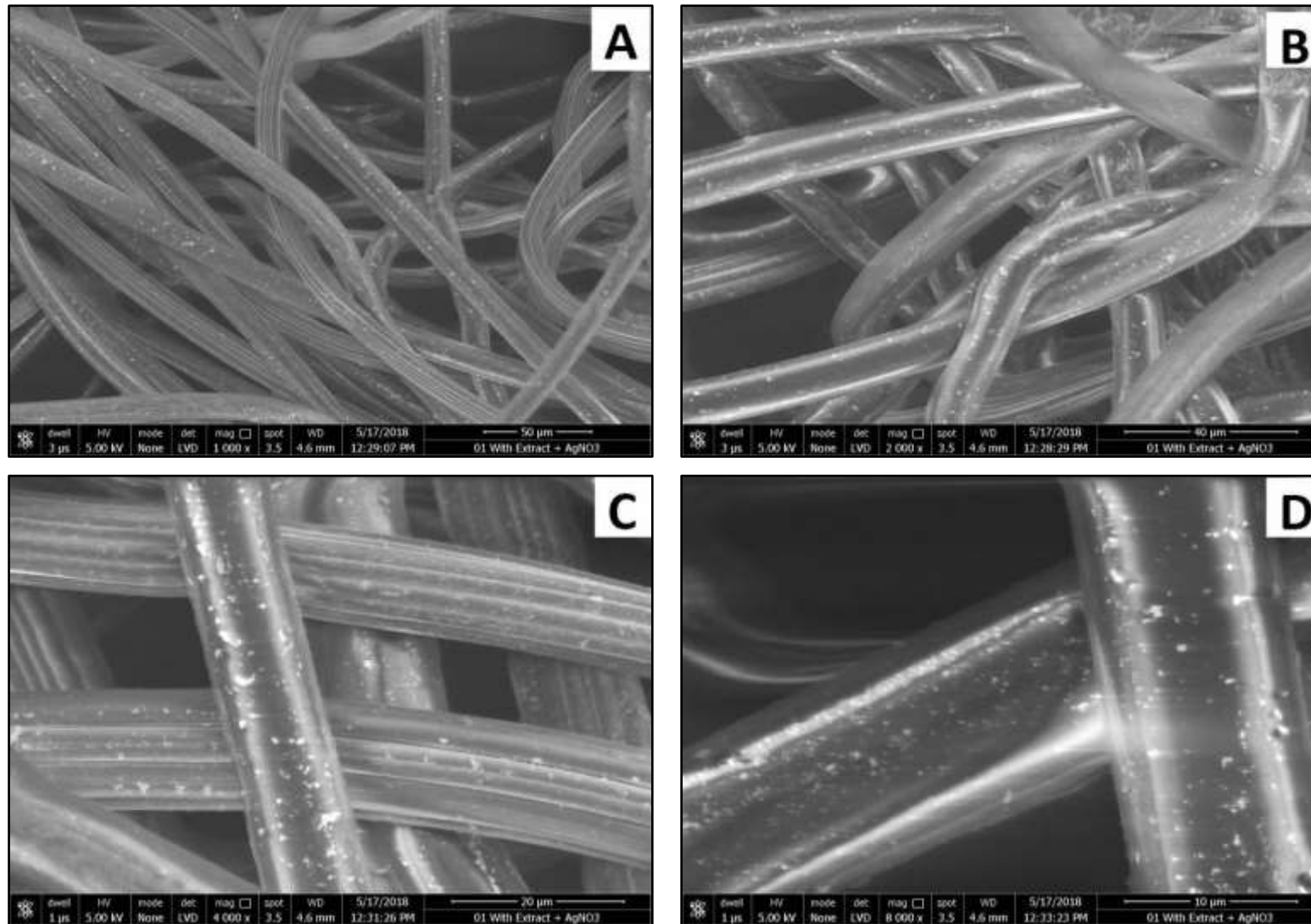


Figure 4.7: ESEM images of Sample 01 at different magnifications (a–d)

4.2.1.2 Structural assessment of the Nano-Composite @PV-AgNPs/CP

4.2.1.2.1 Morphological assessment by Environmental Scanning Electron Microscopy (ESEM)

The ESEM images were taken for both the samples (00 and 01) at different magnification levels; 1000X, 2000X, 4000X, and 8000X with 5 kV are shown in Figures 4.6 and 4.7 (a–d) respectively.

Hence sample 00 represents the untreated PV-Nonwoven fabric (base material) only and sample 01 AgNPs/CP treated sample, execution of apparently similar structure is likely. Thus, sample 00 ESEM images have exclusively revealed the surface morphology, structure, and orientation of the fibres that make up the base material.

Whereas, ESEM images for Sample 01 have shown uniform spreading of AgNPs on the constituent fibers surface for the selected deposition system. Presence of certain tiny aggregates composed of much smaller fundamental nanoparticles has also been detected. Rightfully, the utilised approach found efficient enough in a virtuous deposition of AgNPs on the PV non-woven, with the constituent fibres evenly covered with the particles.

4.2.1.2.2 Elemental assessment by Energy Dispersive X-Ray Spectroscopy (EDAX)

The qualitative and semi-quantitative evaluation of the newly designed AgNPs/CP treated fabric sample (01) was done with reference to untreated sample (00) to avail information about chemical compositions using EDAX. Figures 4.8 and 4.9 show the energy-dispersive spectrums (EDS) obtained for the chosen test areas of the samples (00 and 01). Compared to untreated sample (00), strong signals have been reported from silver atoms in nanoparticles at around 3.0 – 3.2 keV (Figure 4.9), which has a typical peak of metallic silver nano-crystals [3]. This endorses presence of AgNPs in the structure of treated sample (01) and completely absent in the structure of parent sample (00).

Furthermore, elemental mapping was used to characterise green synthesized AgNPs. Figures 4.10 and 4.1 demonstrate the elemental mapping test results for samples 00 and 01 respectively. The results corroborated the preferable even dispersion of the AgNPs across the electron microscopy region of the synthesized product. The system generated chemical composition of mapped specimen in terms of weight (%) and atomic (%) of the elements are

given in Table 4.2. Presence of silver in terms of AgL, silver complex of the order of 3.56% by weight for the specified quantity of AgNO₃ add-on can be seen in the green synthesized AgNPs treated sample 01. Aside from that, unanimously the highest composition (60.97%, 57.80%) of Carbon (C) and the second-highest composition (38.51%, 38.12%) of Oxygen (O) by weight are visible for sample 00 and sample 01 respectively. Figures 4.10 and 4.11(a & b) illustrate the elemental maps of Carbon (C) and Oxygen (O) for both samples. Aluminium (Al), Silicon (Si), and Titanium (Ti) are common additional elements detected in both samples, with a very small but almost comparable proportion in untreated sample 00 and AgNPs/CP treated sample 01.

Table 4.2: Composition of the Elements

Element	Sample 00		Sample 01	
	Weight %	Atomic %	Weight %	Atomic %
C K	60.97	67.72	57.8	66.47
O K	38.51	32.12	38.12	32.91
AlK	0.02	0.01	0.03	0.02
SiK	0.04	0.02	0.06	0.03
TiK	0.46	0.13	0.43	0.12
AgL	-	-	3.56	0.46

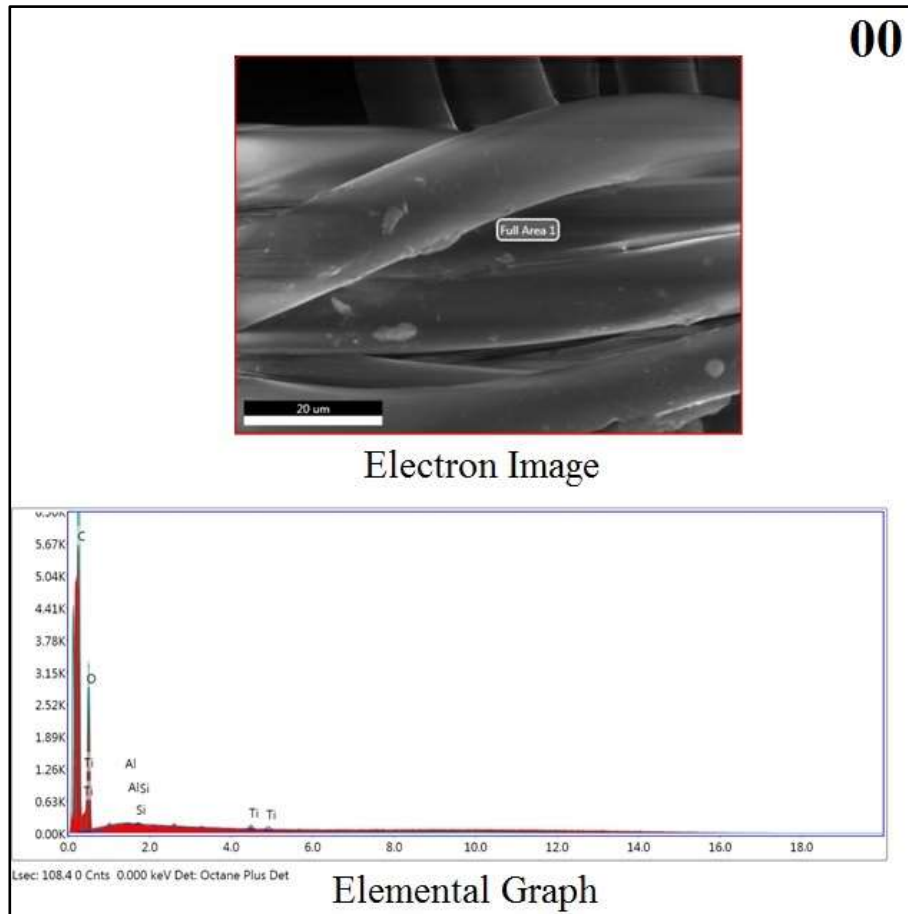


Figure 4.8: Energy dispersive spectrums of Sample 00

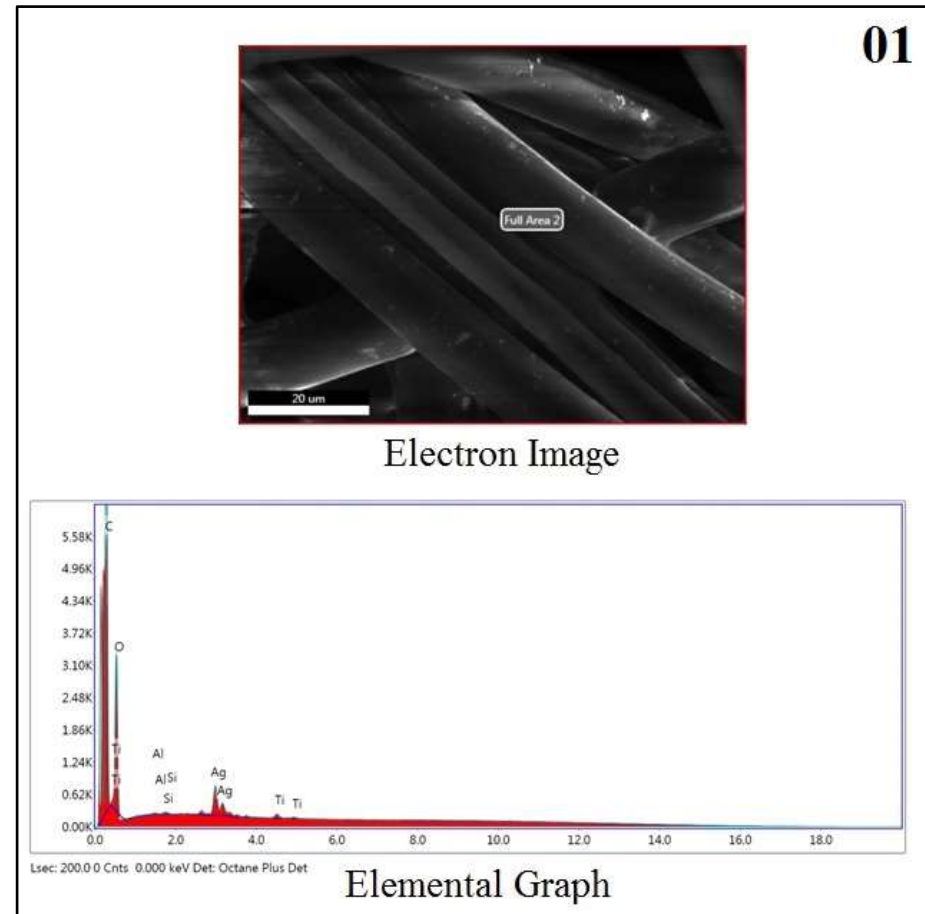


Figure 4.9: Energy dispersive spectrums of Sample 01

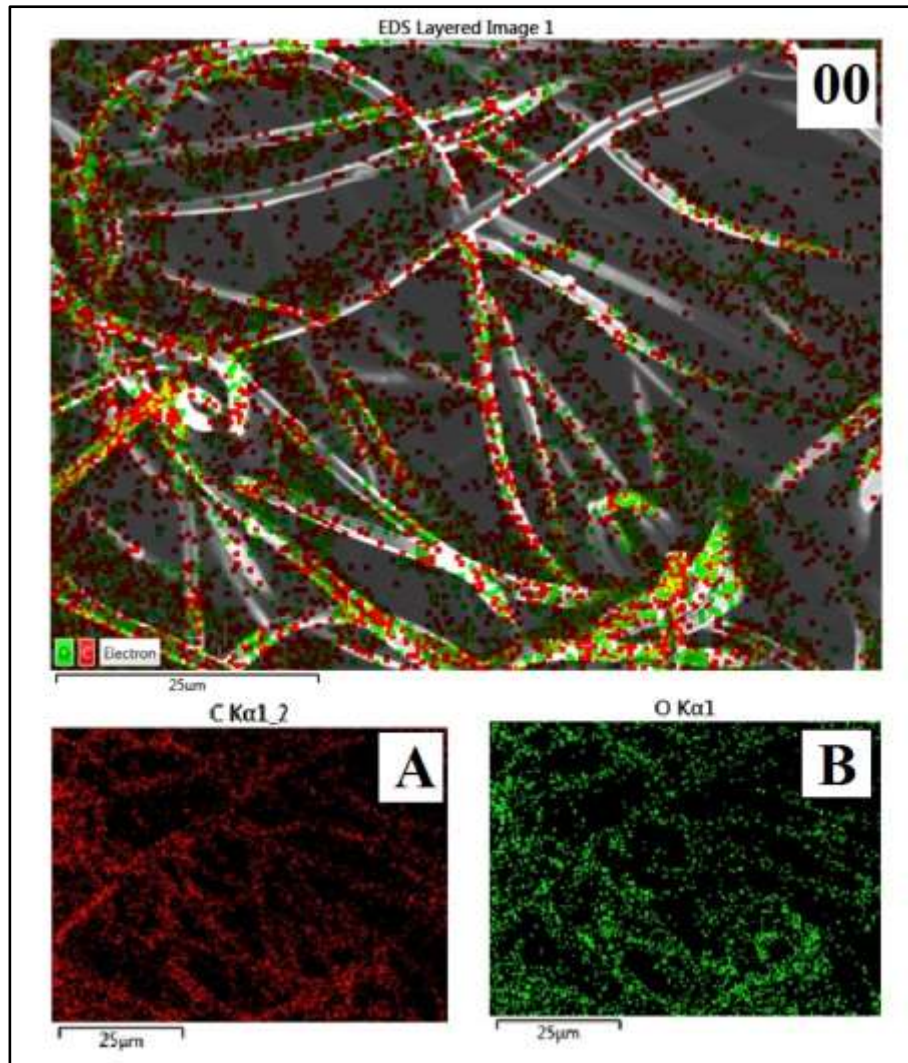


Figure 4.10: Elemental mapping of Sample 00
a) Map of Carbon, and b) Map of Oxygen

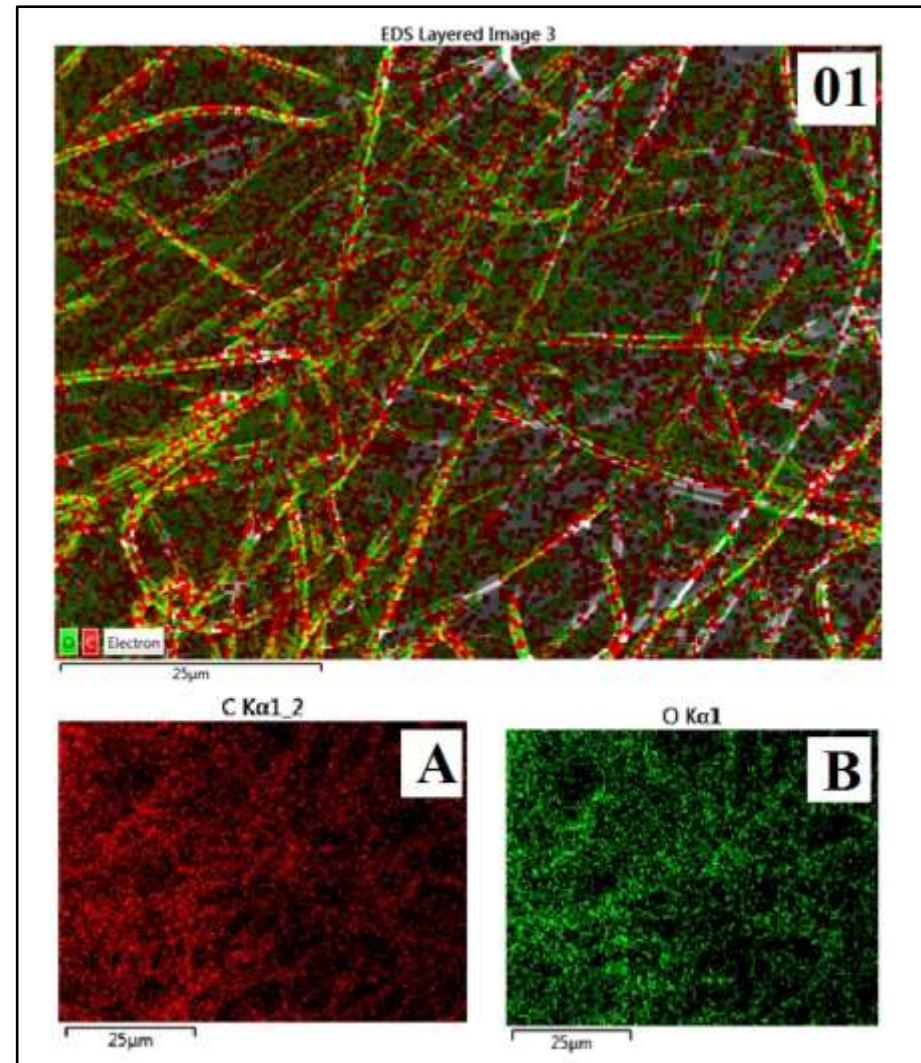


Figure 4.11: Elemental mapping of Sample 01
a) Map of Carbon and b) Map of Oxygen

4.2.1.2.3 Nanoparticles Size distribution

The average nanoparticle size of the AgNPs was preliminary assessed by processing ESEM image by using the 'ImageJ 1.53a' software (Figure 3.12). The micrograph (Figure 4.12) so obtained was analysed to get nanoparticles size and distribution in the selected focal area of the fabric under the study. The test result data was further analysed using Microsoft Excel software to generate particle size normal distribution curve and histogram [Figures 4.13 (a) and (b)] respectively.

It can be observed that the particles' diameter range is following nearly a positive skew distribution starting from 27 nm and ends to 500 nm. The major shuffle of the particles size found in the range of 100nm to 200nm, followed by a second highest populated group in the range of 51nm to 100nm and thence after the number count goes on decreasing from 200nm onwards. Occurrence of a very small frequency (<10) is seen for the particles bigger than 400 nm. These findings support the reducing and capping agent behaviour of the CP leave extract used in the production of AgNPs.

However, the efficacy of the reducing medium is regarded as the best if the majority particle size found less-than 100nm [28]. But in the present test results, the major chunk (>50%) was reported near about 160nm average particle size. No doubt intensity of occurrence for the bigger particle size (>200nm) in the group has shown a sharp declination. This behaviour was further investigated precisely by a particle size analyser before drawing fruitful conclusions. As, the quoted situation can be arisen due to limitations of ESEM judging closely spaced nanoparticle group as a big particle or a light refraction exhibiting striking line at the point of measurement [Figure 4.12].



Figure 4.12: Micrograph used for determination of nanoparticles size distribution [290]

4.2.1.2.4 FTIR analysis of the Nano-composite @PV-AgNPs/CP

Fourier transform infrared spectroscopy was used to assess for the changes happen in chemical structure of the PV non-woven textile material on AgNPs/CP treatment. All measurements were taken in the 400 to 4,000 cm^{-1} range. The FTIR spectral characterization peaks of untreated sample (00) and treated sample (01) are depicted in Figure 4.14 (a & b) and Table 4.3 respectively.

Both the spectrums appear same due to identical base material content. Maximal composition of the polyester and viscose are evidenced from the characterisation peaks in the FTIR bands of both the samples. They show a broad peak around 3432 cm^{-1} associated with the N-H stretching vibration of primary amines, around 2966 cm^{-1} to 2907 cm^{-1} related to symmetric stretching vibrations of hydrogen bond (C-H stretching), the polyester profile has a strong peak around 1714 cm^{-1} related with carboxyl groups (C=O stretching), and a weak peak at 1577 cm^{-1} associated with cyclic alkene (C=C) stretching vibration, around 1455 cm^{-1} and 1372 cm^{-1} related with the bending vibration of alkanic hydrogen bond (C-H), at 1409 cm^{-1} and 1340 cm^{-1} associated with alcoholic (O-H) bending vibration, various other bands observed at around 1242 cm^{-1} , 1174 cm^{-1} , 1097 cm^{-1} , and 1016 cm^{-1} are accompanied with (C-O) stretching vibration of alkyl ether, ester, aliphatic ether, and vinyl ether, respectively [243].

Additionally, the spectrum for PV-AgNPs/CP nano-composite (Sample 01) has demonstrated a peak at 1382 cm^{-1} related to phenolic (O-H) bending vibration and at 1263 cm^{-1} associated with aromatic amine (C-N) stretching vibration. These spectrum peaks associated with phenolic and aromatic amine groups indicate that the AgNPs have been incorporated into the Sample 01 [225].

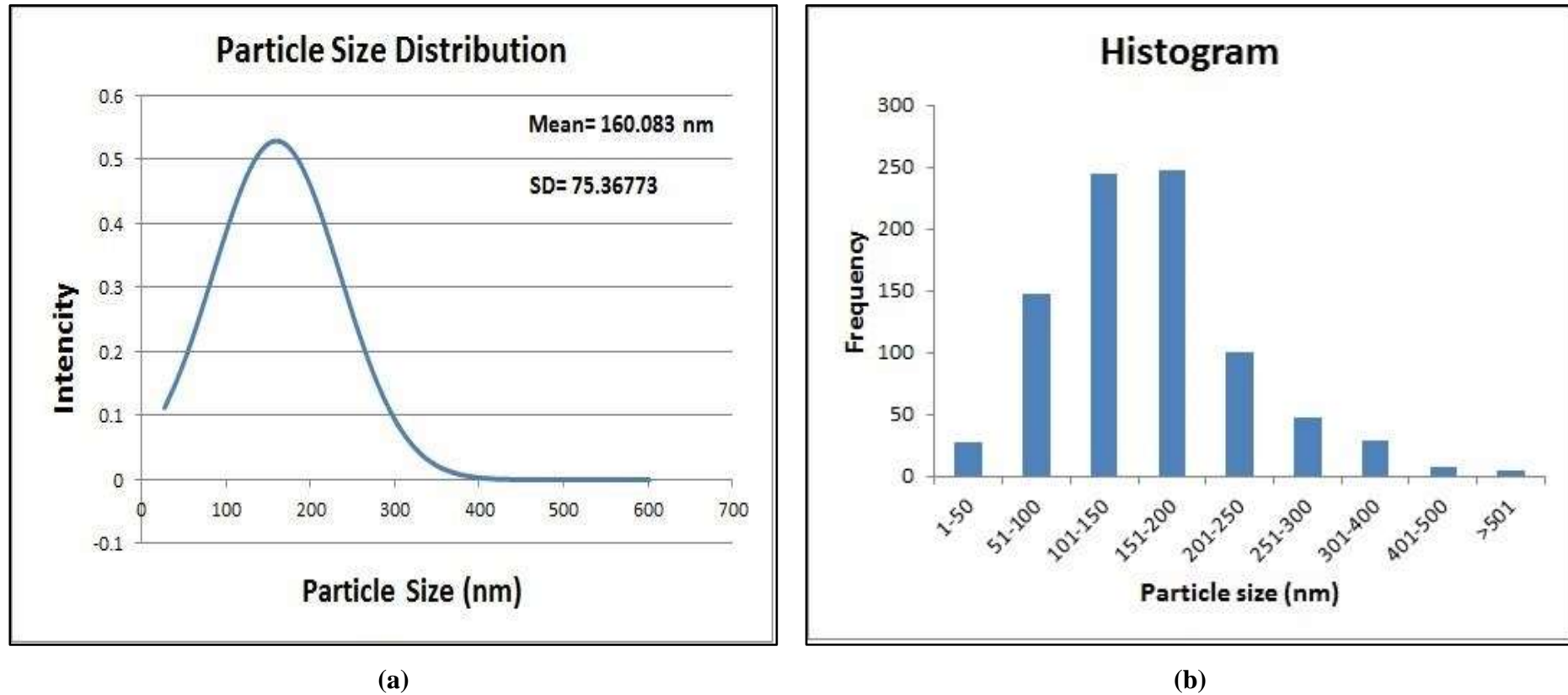
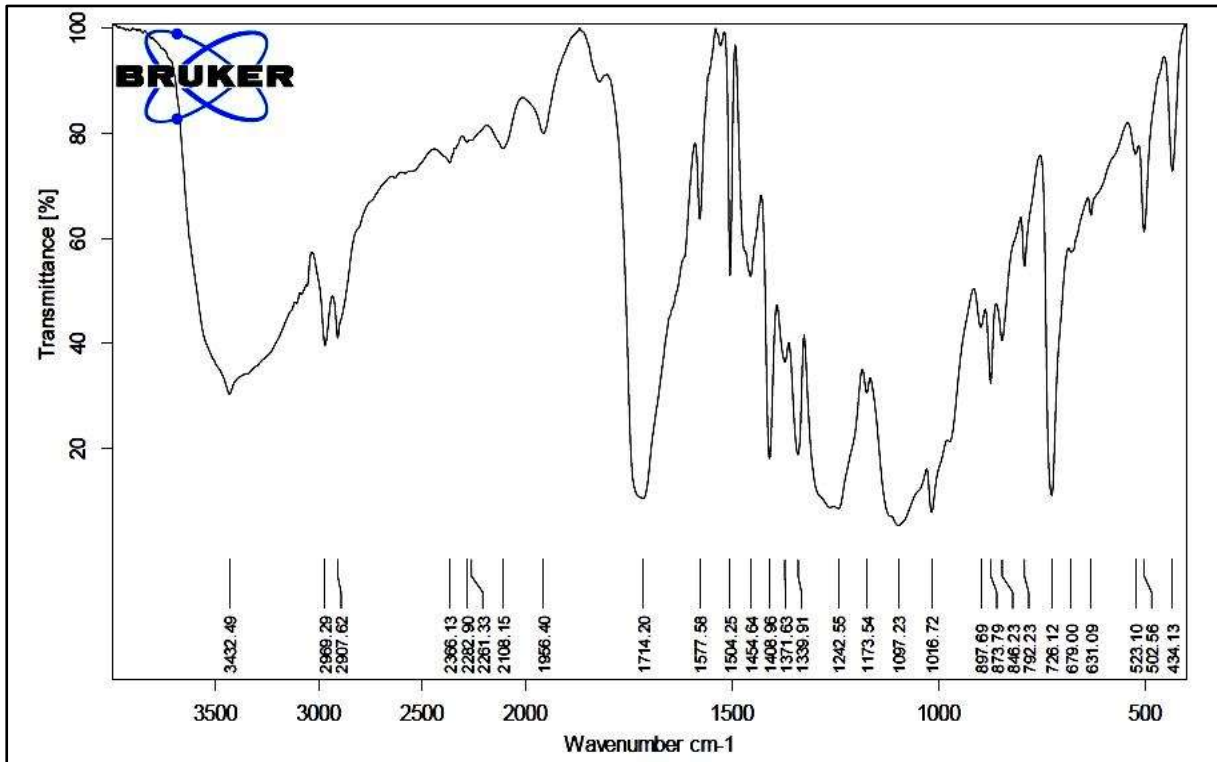
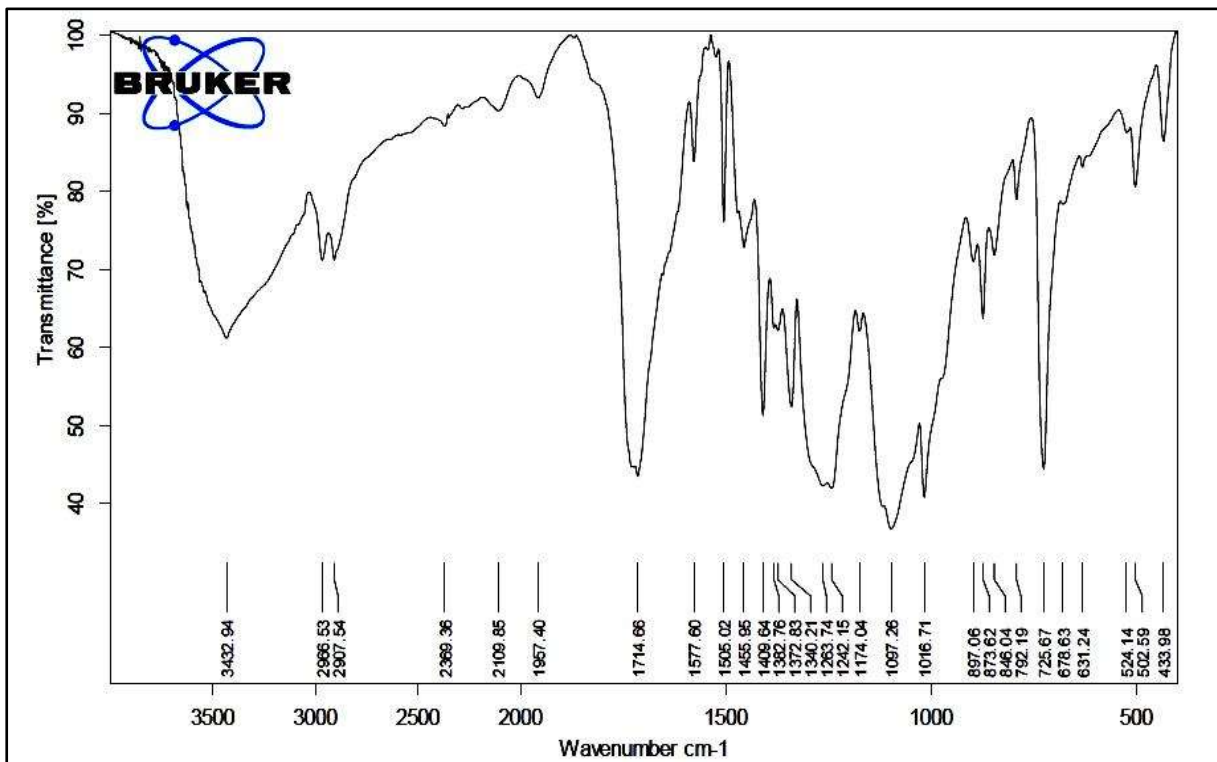


Figure 4.13: a) Nano particle size distribution curve and, b) Histogram [290]



(a)



(b)

Figure 4.14: FTIR spectra of the a) Sample 00, and b) Sample 01

Table 4.3: FTIR characterization peaks of Sample 00 and Sample 01

Wavenumber (cm ⁻¹)		Appearance	Group	Compound Class	Comments
Sample 00	Sample 01				
3432.49	3432.94	Medium, Broad	N-H stretching	Primary amine	
2969.29	2966.53	Medium	C-H stretching	Alkane	
2907.62	2907.54	Medium	C-H stretching	Alkane	
2366.13	2369.36	Weak	O=C=O stretching	Carbon dioxide	
2108.15	2109.85	Weak	C≡C stretching	Alkane	Mono-substituted
1956.40	1957.4	Weak	C-H bending	Aromatic compound	Overtone
1714.20	1714.66	Strong	C=O stretching	Carboxylic acid	Dimer
1577.58	1577.6	Medium	C=C stretching	Cyclic alkene	
1504.25	1505.02	Weak	N-O stretching	Nitro compound	
1454.64	1455.95	Medium	C-H bending	Alkane	
1408.96	1409.64	Medium	O-H bending	Alcohol	
1371.63	1372.83	Medium	C-H bending	Alkane	Gem dimethyl
1339.91	1340.21	Medium	O-H bending	Alcohol	
1242.55	1242.15	Strong	C-O stretching	Alkyl aryl ether	
1173.54	1174.04	Medium	C-O stretching	Ester	
1097.23	1097.26	Strong	C-O stretching	Aliphatic ether	
1016.72	1016.71	Strong	C-O stretching	Vinyl ether	
846.23	846.04	Medium	C=C bending	Alkene	Tri-substituted
726.12	725.67	Strong	C-H bending		1,2,3-Tri-substituted
---	1382.76	Medium	O-H bending	Phenol	
---	1263.74	Strong	C-N stretching	Aromatic amine	

* --- = No peak found

4.2.1.3 Physical and comfort-related properties

The extent of changes ensues on AgNPs/CP loading to the base PV-nonwoven textile material (Sample 01) in its characteristics important for bio-medical application; physical properties, low-stress properties, and comfort-related properties, were evaluated.

4.2.1.3.1 Physical properties

The GSM and Thickness of the PV-AgNPs/CP nano-composite (Sample 01) were investigated and compared with untreated PV non-woven textile material (Sample 00) for any change observed (Table 4.4).

The results indicate no significant change in fabric thickness on treatment but contradicting usual trend GSM has shown perceptible rise even at nano-level add-on [296]. However, the coefficient of variation values reported for both the characteristics are advocating for the inherent structural variations in the manufacturing of spun bonded nonwoven material from the regular or say controlled manmade fibers. The argument gets substantiated by the earlier findings with spun bonded PV-nonwoven [297].

Table 4.4: Physical characteristics

Physical property	Untreated Sample (00)		PV-AgNPs/CP Treated Sample (01)		% Change
	Mean \bar{X}	CV%	Mean \bar{X}	CV%	
GSM	40.90	1.48	42.04	1.32	+2.78
Thickness (mm)	0.415	5.24	0.418	6.75	+0.72

4.2.1.3.2 Low-stress properties

The fabric's low-stress qualities; bending modulus and crease recovery both have a substantial impact on fine and disposable bio-medical fabric handling behaviour. These parameters were examined and compared for the prepared PV-AgNPs/CP nano-composite (Sample 01) with untreated PV non-woven textile material (Sample 00) (Table 4.5).

The similar behaviour to that of physical properties has been found for low-stress properties also for the selected PV-nonwoven with in-built variations on prototype green treatment. However, shuffle in the values is not considered objectionable if it can able to serve well basic duties as bio-medical material. Just like the bending modulus of fabric is a measurement of how freely it can be bent. The movement of the body portions where medical apparel is worn causes more or less bending distortion of the textile material. It is necessary for the material to swiftly curve to the new body contour, which is only achievable if it has a low bending modulus. So, the machine-direction 28% reduction(-) along with almost same cross-direction 47% increase(+) in bending modulus should expectedly not affect draping of the material as per body contour in three dimensions.

Table 4.5: Low-stress characteristics

Low-stress properties	Untreated sample (00)		Treated sample (01)		% Change	
	Machine-direction	Cross-direction	Machine-direction	Cross-direction	Machine-direction	Cross-direction
Bending Modulus						
Mean (g/cm ²)	9.43	0.87	6.70	1.28	-28.95%	47.12%
CV%	10.00%	9.57%	4.54%	12.92%		
Crease Recovery angle						
Mean	116.4	111	112.3	107.7	-3.52%	-2.97%
CV%	3.01%	2.72%	3.03%	2.94%		

Conversely crease recoveries values are not regarded as significant for disposable nonwoven textiles not designed as wash and wear fabrics. Only concern for its measured values is they should be sufficient enough to be recovered from creasing from the beginning till the last uses. Declination in the machine-direction crease recovery value supports reduced fabric stiffness in that direction but cross-direction reduced value contradicts the bending modulus behaviour. Thus, results substantiate the argument about integral structural variation of spun bonded PV-nonwoven material designed for bio-medical purpose only by the reputed firm led to unclear trend for both the characteristics on AgNPs/CP deposition. As mentioned before, changes recorded for both the low-stress characteristics at nano-level add-on behaved similar to other green synthesised nano-composites bio-medical materials, and not shown intolerable values on AgNPs/CP deposition [297].

4.2.1.3.3 Comfort-associated properties

When a textile material is utilised in medical outfits like; apron, gloves, cap, mask, etc. wearer's comfort will be regarded as a vital feature. Air permeability and moisture management capacities of the fabric play an important role in defining their comfort. The newly engineered bio-medical PV-AgNPs/CP nano-composite material was thereby evaluated for its air permeability and overall moisture management capabilities (OMMC) and compared for any change took place with respect to the untreated PV-nonwoven textile material.

D) Air permeability

Test results of the air permeability test done on Samples 00 and 01 are given in Table 4.6.

Table 4.6: Air permeability ($\text{m}^3/\text{m}^2/\text{h}$)

	Sample 00	Sample 01	%Change
Mean (\bar{x})	4752.5	4657.5	-1.99%
CV %	1.15	1.19	

It can be seen that the air permeability of the PV-nonwoven gets reduced by 1.99% on AgNPs/CP deposition along with slight increase in CV%. In general, the air permeability of a non-woven fabric is primarily determined by its GSM, thickness, and fabric porosity, among other factors [255]. Hence, these values have not shown any distinctive trend with AgNPs/CP deposition but they were mainly influenced by inherent base material changes only. The air permeability reduction from 4752.5 m³/m²/hr to 4657.5 m³/m²/hr is also negligible change and within the required limits for bio-medical material only. Thus, they are attributed to the base material variations more rather than presence of very limited quantum of nanoparticles.

II) Overall moisture management capability (OMMC)

The Overall moisture management capability (OMMC) is an index that indicates the fabric's overall ability to control the transport of liquid moisture; this includes three performance aspects: spreading speed or drying speed, moisture absorption rate, and accumulative one-way liquid transport ability. A higher overall moisture management capacity suggests that the fabric has superior overall moisture transport ability [289].

The results of the moisture management test on Samples 00 and 01 are shown in Table 4.7. The OMMC test findings show that without the application of nanoparticles on the surface of the PV non-woven textile material (sample 00); the OMMC value obtained was "poor" (0.3041) (Figure 4.18). Similarly, the one-way transport index percentage (%) of sample 00 was negative (-1117.0243) (Figure 4.19), which qualifies the base material as a 'very poor' grade. This indicates that the fabric has inadequate moisture management qualities and falls into the category of 'fast absorbing and quick drying fabric'.

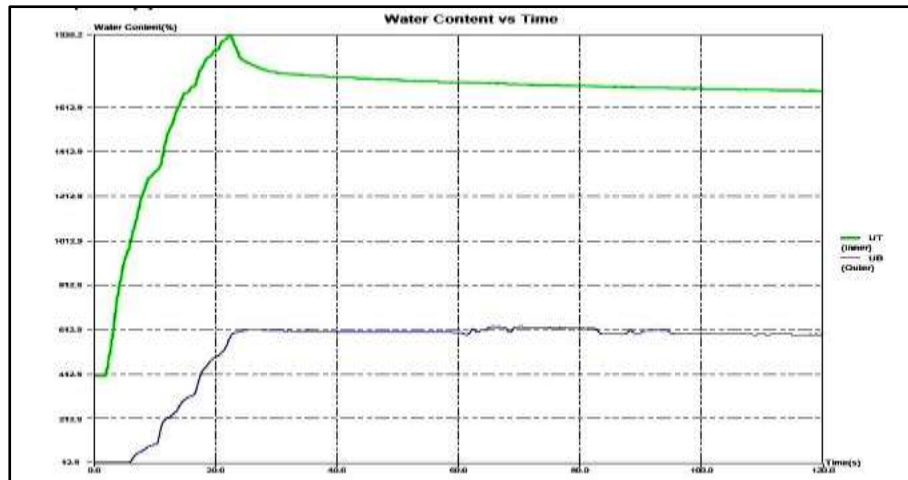
The OMMC value for the same base material but with functional nanoparticles (PV-AgNPs/CP nano-composite) has increased to 0.4132, indicating that sample 01 overall moisture management performance is 'Good'. Similarly, its one-way transport index (%) turned positive (166.1951), demonstrating 'Good' water transportability for sample 01. In an aggregate, the newly engineered nano-composite (Sample 01) has executed strong moisture management characteristics and became 'moisture management fabric' in the presence of AgNPs/CP.

In general, the moisture management capabilities of non-woven fabric are determined by the fabric's constituent and structure [258]. Thus, the improved moisture management

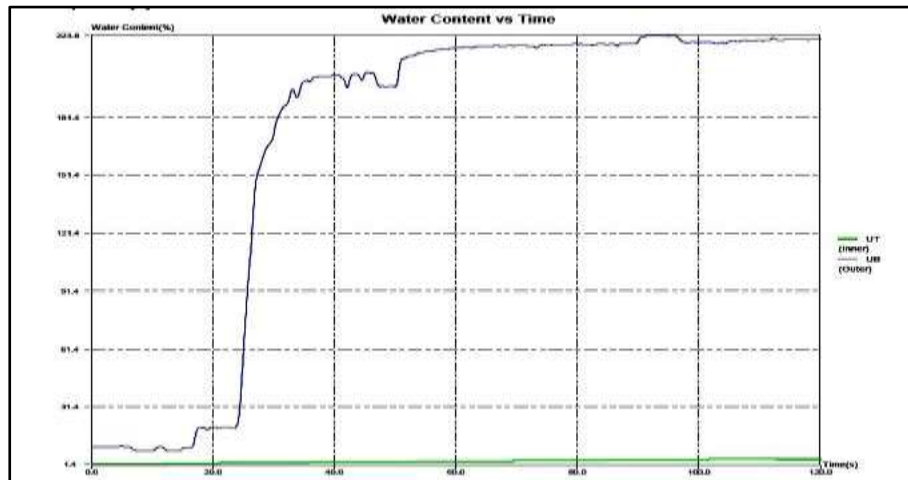
capabilities of the treated sample are attributed to the added constituents for the identical fabric structure. Figures 4.15 to 4.23 illustrate the graphical analysis and result maps of the moisture management test for samples 00 and 01, respectively.

Table 4.7: Moisture management test results

	Sample 00	Sample 01
Wetting Time Top(sec)	1.217 (Very fast)	120 (No wetting)
Wetting Time Bottom(sec)	5.335 (Medium)	16.38 (Medium)
Top Absorption Rate (%/sec)	71.6256 (Fast)	0 (Very slow)
Bottom Absorption Rate (%/sec)	29.486 (Slow)	5.4189 (Very slow)
Top Max Wetted Radius (mm)	30 (Very fast)	0 (No wetting)
Bottom Max Wetted Radius (mm)	25 (Very fast)	15 (Medium)
Top Spreading Speed (mm/sec)	13.0363 (Very fast)	0 (Very slow)
Bottom Spreading Speed (mm/sec)	7.4152 (Very fast)	3.0762 (Fast)
Accumulative one-way transport index (%)	-1117.0243 (Very poor)	166.1951 (Good)
OMMC	0.3041 (Poor)	0.4132 (Good)
Grade	This is fast absorbing and quick drying fabric	This is moisture management fabric

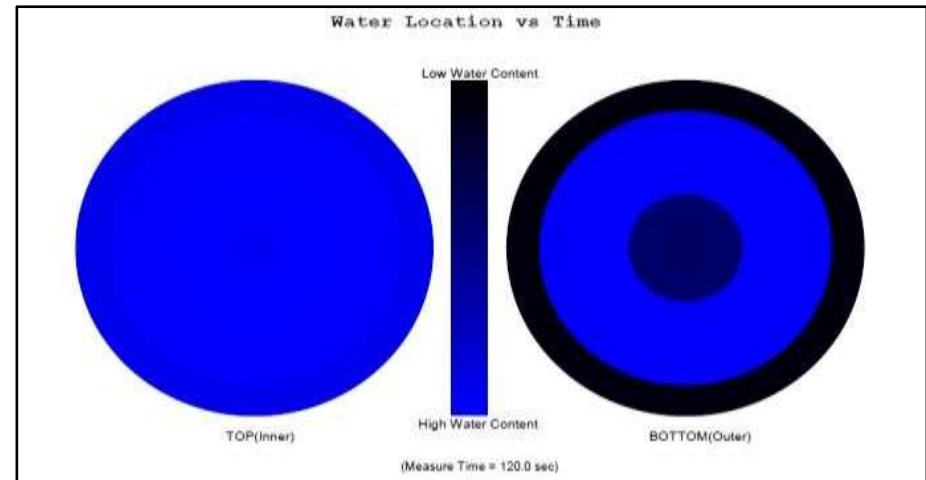


(a)

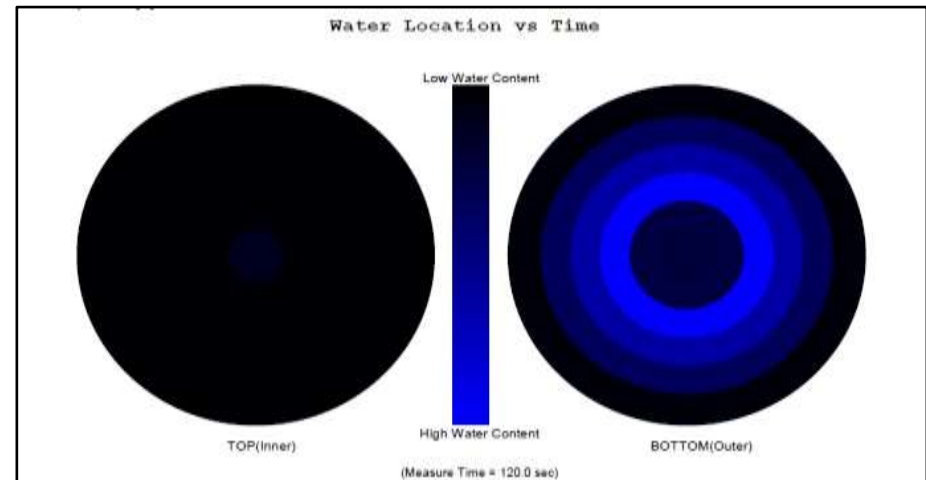


(b)

Figure 4.15: Water content vs Time
a) Sample 00, and b) Sample 01 respectively

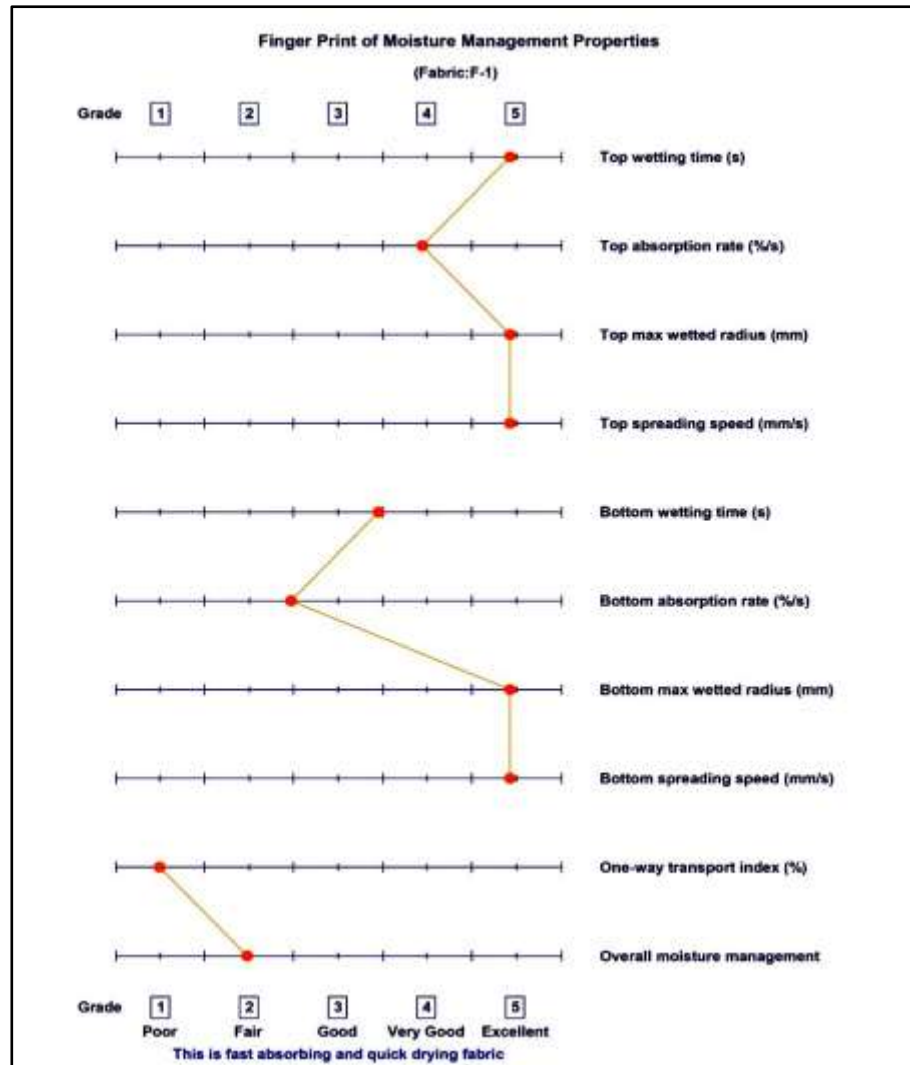


(a)

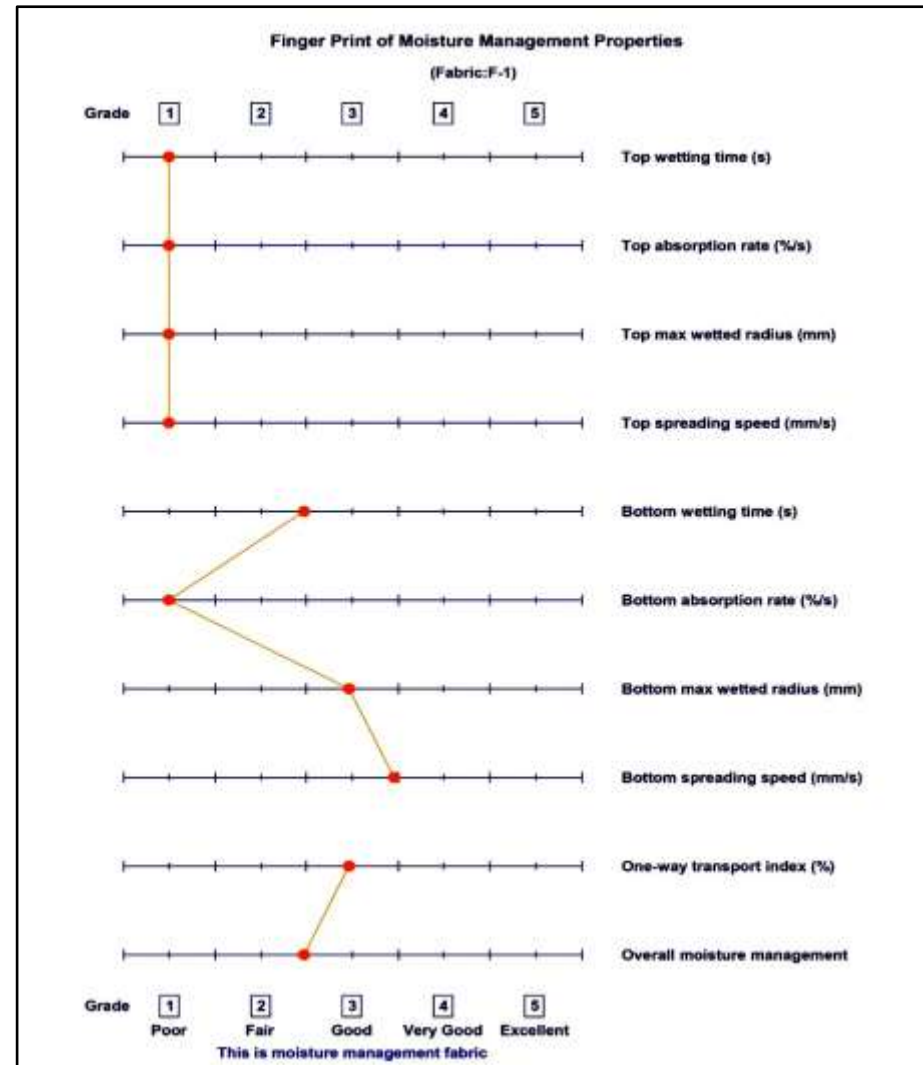


(b)

Figure 4.16: Water location vs Time
a) Sample 00, and b) Sample 01 respectively



(a)



(b)

Figure 4.17: Finger print of moisture management properties for a) Sample 00, and b) Sample 01 respectively

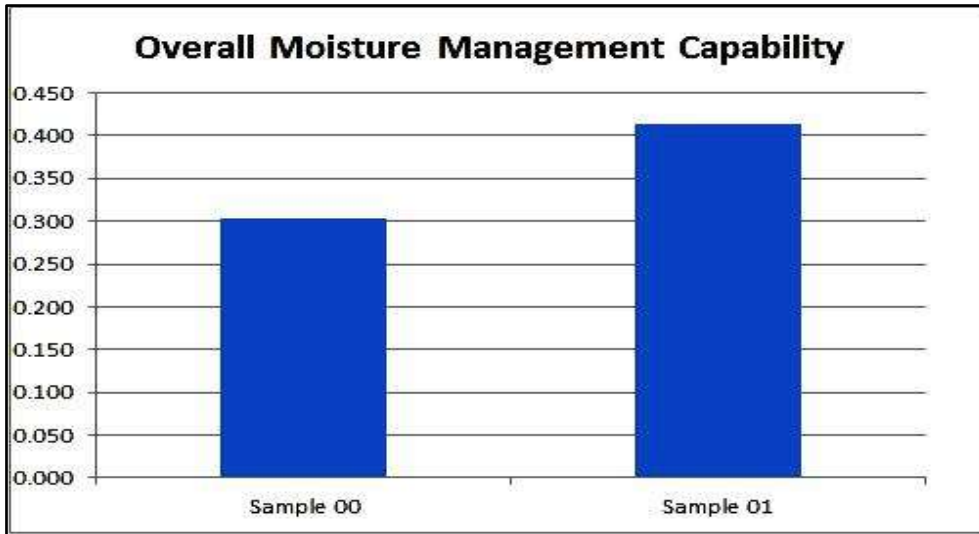


Figure 4.18: Overall moisture management capability of Sample 00 and 01

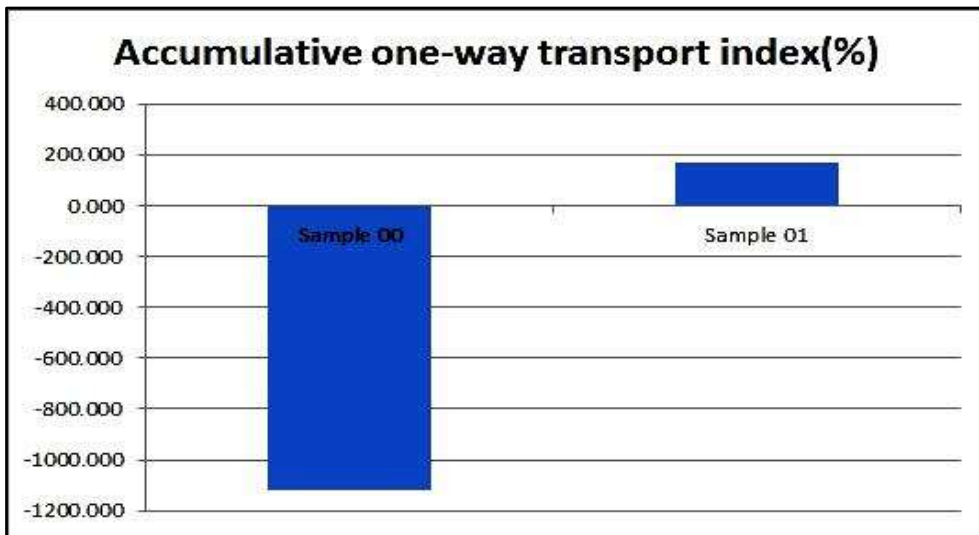


Figure 4.19: Accumulative one-way transport index (%) of Sample 00 and 01

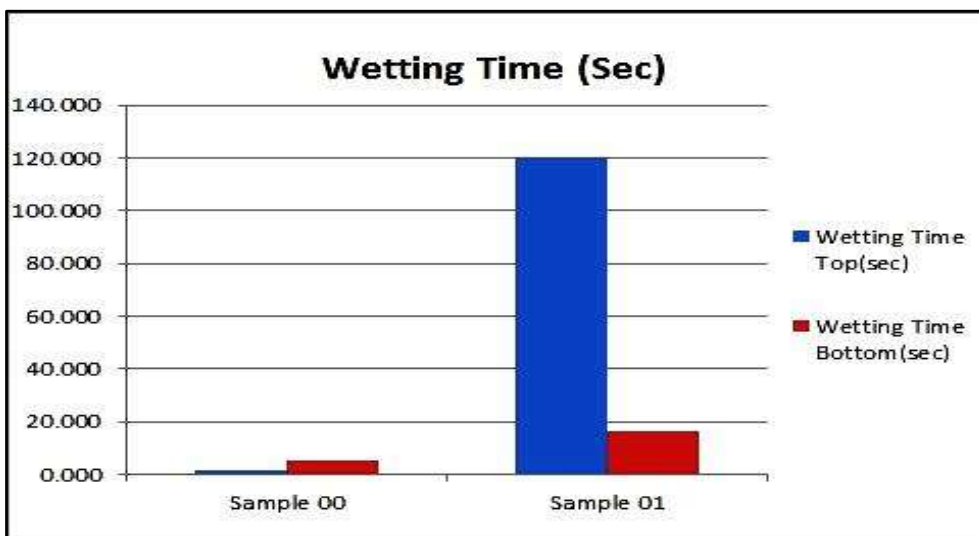


Figure 4.20: Wetting time (sec.) for Top and Bottom surface of Sample 00 and 01

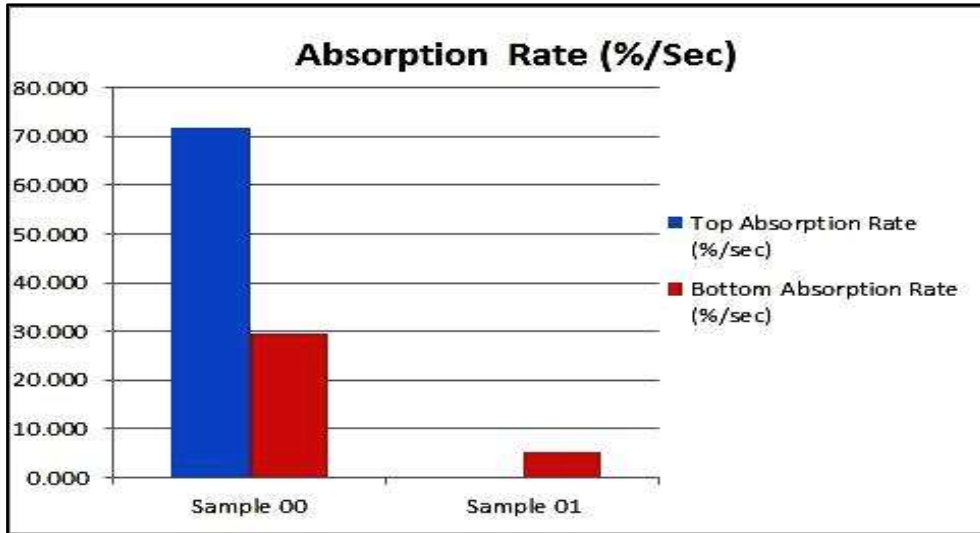


Figure 4.21: Absorption Rate (%/sec) for Top and Bottom surface of Sample 00 and 01

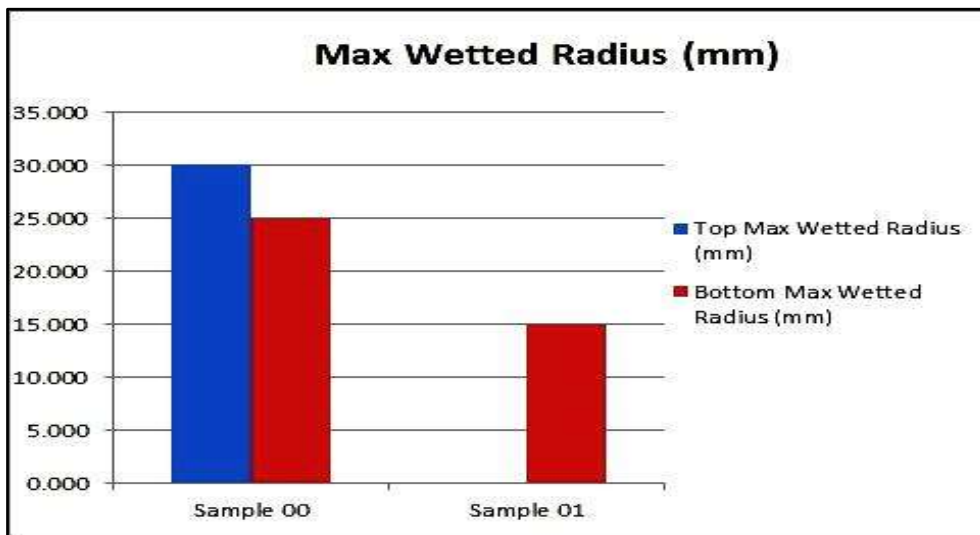


Figure 4.22: Max Wetted Radius (mm) for Top and Bottom surface of Sample 00 and 01

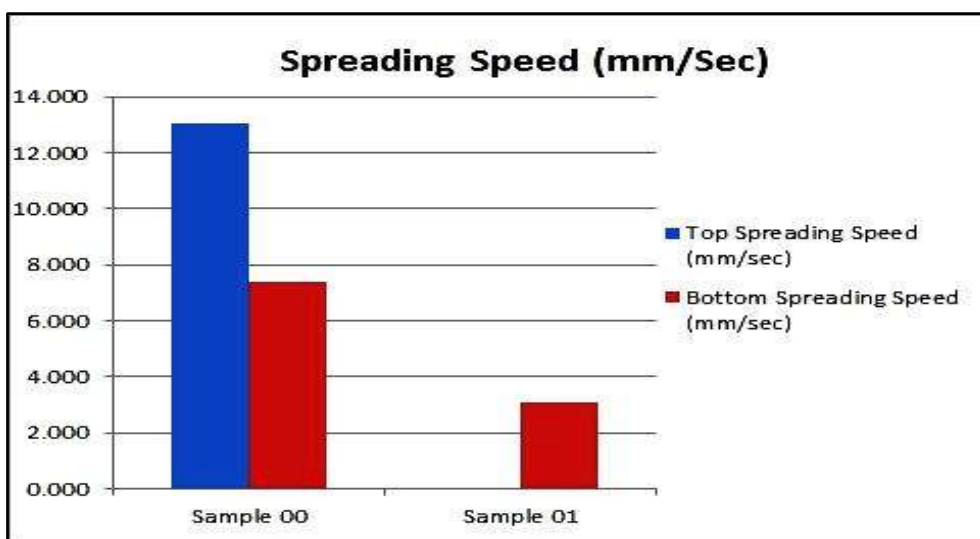


Figure 4.23: Spreading Speed (mm/sec) for Top and Bottom surface of Sample 00 and 01

4.2.1.4 UV Transmission properties

The UPF (Ultraviolet Protection Factor) grading system assesses the UV protection provided by the textile materials. UVA transmittance ranges from 320 to 400 nm and UVB transmittance ranges from 290 to 320 nm are the most dangerous invisible ultraviolet (UV) radiations that can cause erythema or sunburn. Excess UV radiation absorption can result in scarring, which can lead to illnesses such as skin cancer [298].

The UV protection profiles of the PV-AgNPs/CP nano-composite (sample 01) was assessed and compared with untreated PV-nonwoven textile material (sample 00).

Table 4.8 displays the UV transmittance characteristics of Samples 00 and 01. The UPF rating data shows that the untreated PV non-woven textile material (sample 00) has a '5' UPF rating, which is quite low. Similarly, at 384 critical wavelengths, the UVA transmittance % is '34.12', while the UVB transmittance % is '11.54'. Due to application of the AgNPs the UPF rating improved to '8' (sample 01). The UVA and UVB transmittance % have been reduced to 20.75 and 9.18 at 386 critical wavelengths. This made the material more protective against UVA and UVB type of radiations.

This behaviour can be attributed to the deposited of AgNPs/CP, which has dispersed or absorbed the radiations and reduced the UV transmittance.

Table 4.8: UV transmittance profile of the samples

	Sample 00	Sample 01
UPF Rating	5	8
Average UPF	6.48	8.97
T (UVA) %	34.12	20.75
T (UVB) %	11.54	9.18
Critical Wavelength	384	386

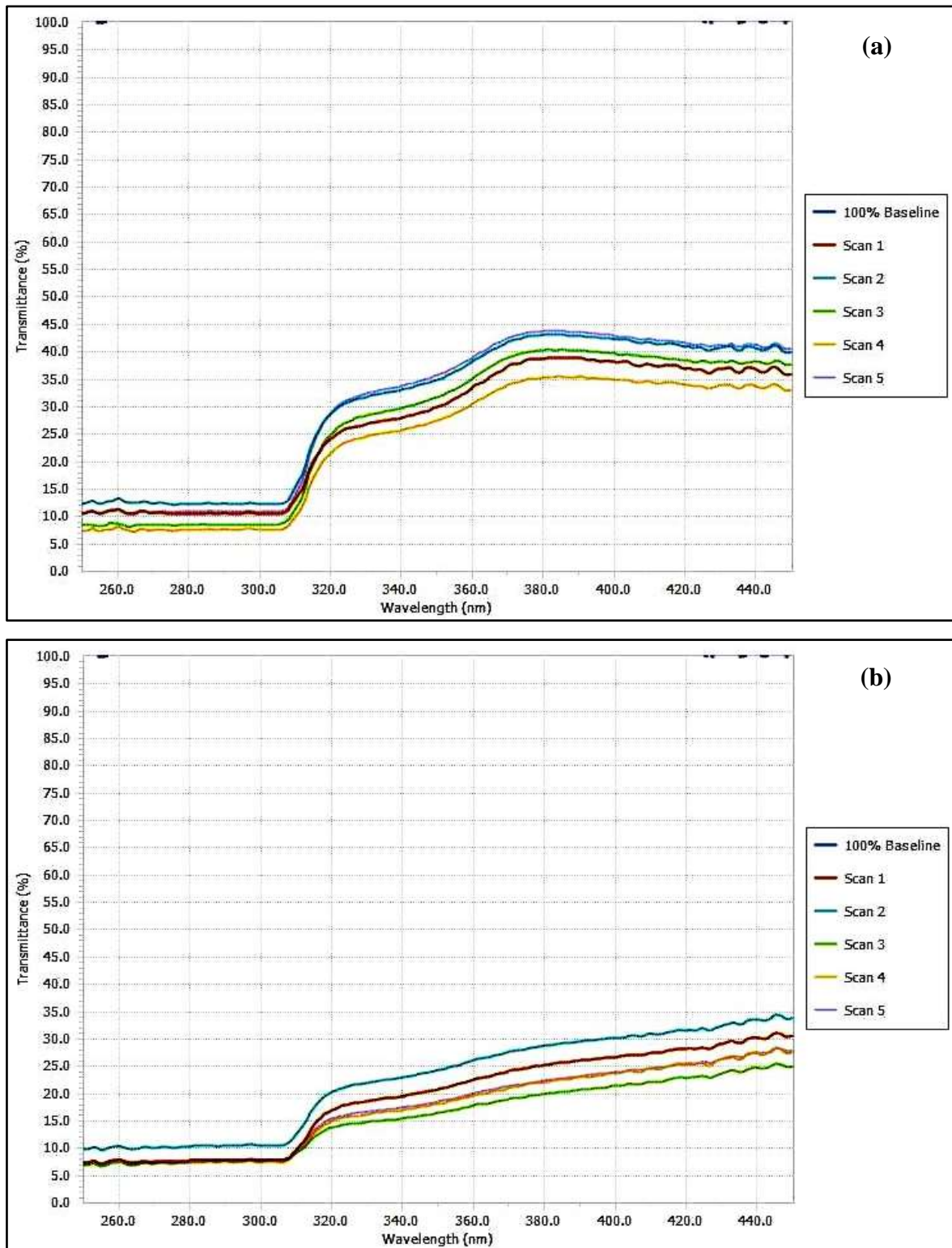


Figure 4.24: UV Transmittance profile of a) Sample 00, b) Sample 01

The graphical representations of the UV transmittance profiles of Samples 00 and 01 also revealed that UVA and UVB transmittance % for all regions of Sample 00 are between 30 to 45 % and 5 to 15 % respectively. While for sample 01, a favourable reduction was observed within 15 to 30 % and 5 to 15 % respectively. This demonstrates an overall improvement in the UV transmission capabilities of the PV-AgNPs/CP nano-composite. Figures 4.24 (a and b) exhibit graphical representations of the UV transmittance profiles of Samples 00 and 01, respectively.

4.2.2 PHASE-II: CONCLUSIONS

I) Antibacterial assessment: The antibacterial test method AATCC-147 (Parallel streak method) findings revealed that the prepared PV-AgNPs/CP nano-composite (Sample 01) demonstrated significant antibacterial activity against both bacterial cultures *Staphylococcus aureus* (23.75 mm) and *Escherichia coli* (24.5 mm).

II) Structural assessments:

Morphological assessment (ESEM): The ESEM analysis demonstrates that, the utilised deposition process results in good deposition of AgNPs on PV-nonwoven material.

Elemental assessment (EDAX): EDAX analysis revealed the presence of AgNPs in the treated sample 01, which has a strong peak of metallic silver nanoparticles.

Nanoparticles Size distribution ('ImageJ' analysis): The average particles of 160nm without an aggregation was confirmed by processing ESEM image using 'ImageJ 1.53a' software.

FTIR analysis: FTIR analysis was used to determine the chemical characteristics of the produced nano-composite (sample 01). The FTIR spectrum characterisation peaks show a common (in samples 00 and 01) as well as additional chemical compositions [i.e. phenolic (O–H) bending vibration and aromatic amine (C–N) stretching vibration] for PV-AgNP/CP nano-composite.

III) Physical assessments:

Physical properties: The results of physical properties demonstrate no substantial change in fabric thickness after treatment, but GSM has showed a discernible increase even at nano-level add-on, which contradicts the normal trend.

Low-stress properties: Low-stress qualities exhibited comparable behaviour to physical properties for the chosen PV-nonwoven with in-built changes on prototype green treatment. No doubt, there are arbitrary fluctuations in the machine and cross-direction bending modulus of the samples under investigation. However, these alterations did not represent a marginal increase or decrease in bending modulus, preventing the material from being suitable for bio-medical usage.

Comfort-associated properties: The air permeability results have not shown any distinctive trend (reduced by 1.99% only) with AgNPs/CP deposition but they were mainly influenced by inherent base material changes only. However, the developed PV-AgNPs/CP nano-composite shows 'excellent' moisture management capabilities and it is classified as a 'moisture management fabric'.

IV) UV Transmission properties: The UV transmittance profile showed no significant changes in the UPF rating when compared to the untreated PV non-woven textile material (Sample 00). However, a favourable decrease in UVA and UVB type radiation transmittance % has been reported, which can lead to improved UVA and UVB type radiation protection by developed PV-AgNPs/CP nano-composite (Sample 01).

Consequently, the antibacterial assessment (AATCC-147) and various structural assessments confirmed the antibacterial activities and nanoparticle distribution for the prepared PV-AgNPs/CP nano-composite with the selected concentration of the AgNPs/CP colloidal solution, the concentration of the AgNO₃ and CP leave extract was optimised with further investigation.

4.3 PHASE-III:

OPTIMIZATION OF AgNPs/CP COLLOIDAL CONSTITUENTS' ADD-ON FOR ANTIBACTERIAL ACTIVITIES IN NONWOVEN @PV-AgNPs/CP NANO-COMPOSITES

This phase aimed to optimise the silver nitrate (AgNO_3) salt and CP leave extract contents in the synthesis of desirable AgNPs and evaluating their antibacterial activity in a prototype bio-medical nonwoven nano-composite.

Pilot trials, divided into two groups: i) Major scale and ii) Minor scale were carried out by altering concentrations of both the ingredients. The concentration of the AgNO_3 salt measure was based on the molarity (Mole, M) of the silver nitrate and varied in the range of 0 mM to 1000 mM, whilst the concentration range of the CP leave extract was kept 5%, 10%, 15%, and 20%, respectively keeping previous green synthesis records as reference. An Optimization always prefers better quality earning at minimum cost for any production house. Thereby minimum level add-on for each component was worked out, also emphasized by the previous researches done on green synthesis ground for AgNO_3 but with different natural mediums. Stability of the colloidal, particle size and antibacterial properties were key performance evaluation tools employed in these sets of pilot trials.

4.3.1 MAJOR SCALE PILOT TRIALS

In this series of trials, the molarities of the AgNO_3 were tested on a large scale, i.e. 1000 mM, 500 mM, 200 mM, and 100 mM with varied concentrations of the CP leave extract, i.e. 5%, 10%, 15%, and 20%. The AgNPs colloidal solution was made in four separate sets i.e. A, B, C, and D based on concentration and each category was having five CP leave extract compositions (Table 3.7). They were subjected for visual colour change based colloidal stability test. The toxicity behaviour of the CP leave extracts; the CP pure latex and its leave extracts prepared at different concentrations were also evaluated using MTT assay. This measure was crucial in determining the appropriate concentration of CP leave extract for its optimisation and selecting the best AgNPs colloidal solution. All prepared PV-AgNPs/CP nano-composite were analysed for their antibacterial activity.

4.3.1.1 Result's Analysis

4.3.1.1.1 Visual colour change observation (VCCO)

All CP leave extract variances as well as colloidal solutions were tested for visual judgment-based colour change observation.

CP leaves Extract:

Hence, the constituent CP leave extract colour has equal impact on colloidal colour; it becomes necessary to note the extent of colour change with its concentration. This can facilitate in drawing true conclusion about AgNPs formation for such subjective assessment [118,280]. The photographs for the beakers containing prepared CP leave extracts; E05, E10, E15, and E20 are shown in figures 4.25.

The extract has achieved natural brownish tint of the leave at the lowest 5% concentration and as per obvious expectation resumed darker tint with increased concentration. Thus, it has behaved similar to other green mediums used earlier [118,282,299].

AgNPs colloidal solutions:

The colour of the various sets of colloidal solutions prepared and kept for time periods: 0 hour, 24 hours, and 48 hours for studying colloidal stability, are shown in Figure 4.26 respectively.

It can be observed that all the colloidal prepared without AgNO₃; E05S00, E10S00, E15S00 and E20S00, have shown obviously the tint identical to that of CP extract [Figure 4.25]. But, on the addition of all major scale except 100mM AgNO₃ add-on, viz; E05S01, E05S02, E05S05, E05S10, E10S02, E10S05, E10S10, E15S02, E15S05, E15S10, E20S02, E20S05, and E20S10 were turned from their original extract colour (light brownish) to undesirable blackish (fuzzy milky blackish) after either after 24 hours or 48 hours' time-leap. This behaviour as mentioned in phases (I-II); was an indicative of colloidal instability on the account of nanoparticles formation from nano to micro scale [5,111]. So, newer green synthesis done with AgNO₃ concentration above 100 mM was found unacceptable for both cost and quality point of view.

The colloidal solutions prepared with the lowest concentration (100mM) AgNO_3 in a major scale group, i.e. E10S01, E15S01, and E20S01, have only retained their original brownish colour to some extent up to 24 hours, advocating colloidal stability. However, they all invariably turned instable and executed an intolerable fuzzy milky blackish colour on agglomeration of nanoparticles to microparticles between 24 hours to 48 hours of the study.

These visual-judgment based colloidal colour change study pattern has uttered partial stability up to 24 hours at 100mM AgNO_3 add-on level, but above that level colloidal failed in attaining stability even for the minimum viable one-day time interval. Thus, it will be fair enough to carry out trials by scaling down AgNO_3 concentration, which can also be beneficial regarding cost point of view, as AgNO_3 is the highest cost bearing component in this synthesis process.

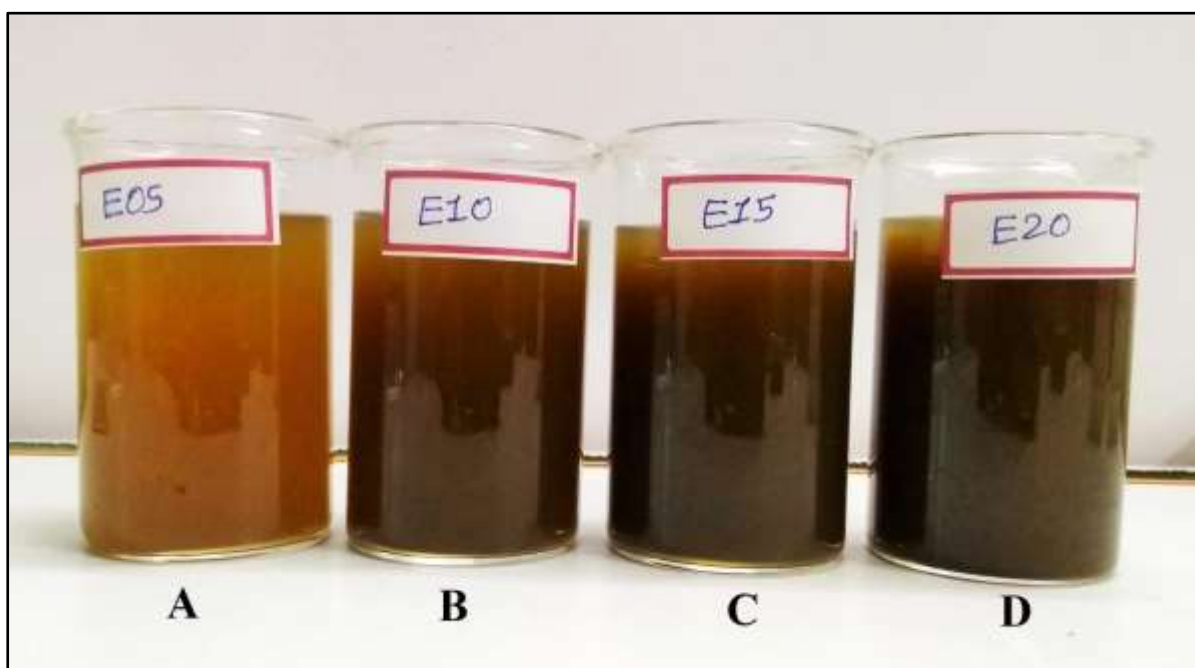


Figure 4.25: CP leaf extracts a) E05, b) E10, c) E15, and d) E20

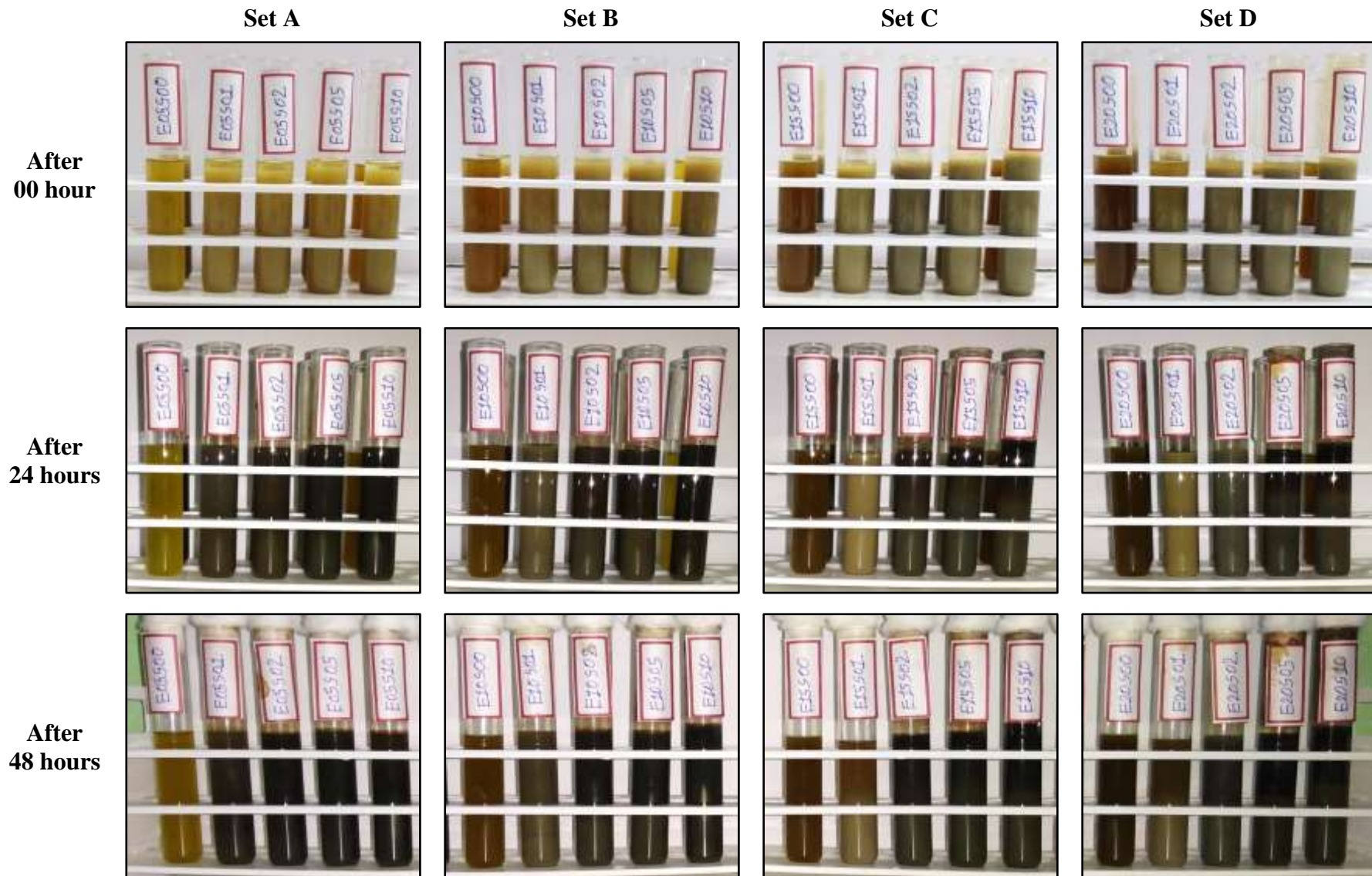


Figure 4.26: Colour change observation of the AgNPs colloidal solutions (Major Trial)

4.3.1.1.2 MTT assay cytotoxicity test of CP leave extract and pure CP latex

The cytotoxicity of CP leave extract and pure CP latex against the Hep-G2 epithelial cell line was investigated using the MTT assay test. The findings of the CP leave extract were compared to the pure CP latex and the positive control of 2,4-dinitrophenol produced in DMSO (Figure 4.27).

It can be seen that the viability of the cell line executed by all the CP leave extracts in comparison to CP pure latex (24%) is quite good and lower than the selected positive reference medium (100%). Regarding the study done to define influence of the CP leave extracts' concentration on the viability of the cell line, a descending trend is observed with the increase in CP leave extract concentration, i.e. E05 (98%), E10 (92%), E15 (85%), and E20 (73%), respectively. Thus, the lowest CP leave extract's concentration has demonstrated highest cell viability (non-toxic behaviour) which deteriorates gradually with the increase in the extract concentration in the present study. Cohen et al. [300] reported a similar behaviour about cytotoxicity measurement carried out for the various concentrations of the CP extract by mitochondrial reduction, utilising the 5-dimethylthiazol-2-yl]-2, 5-diphenyl tetrazolium bromide (MTT) assay against human skin epidermal units.

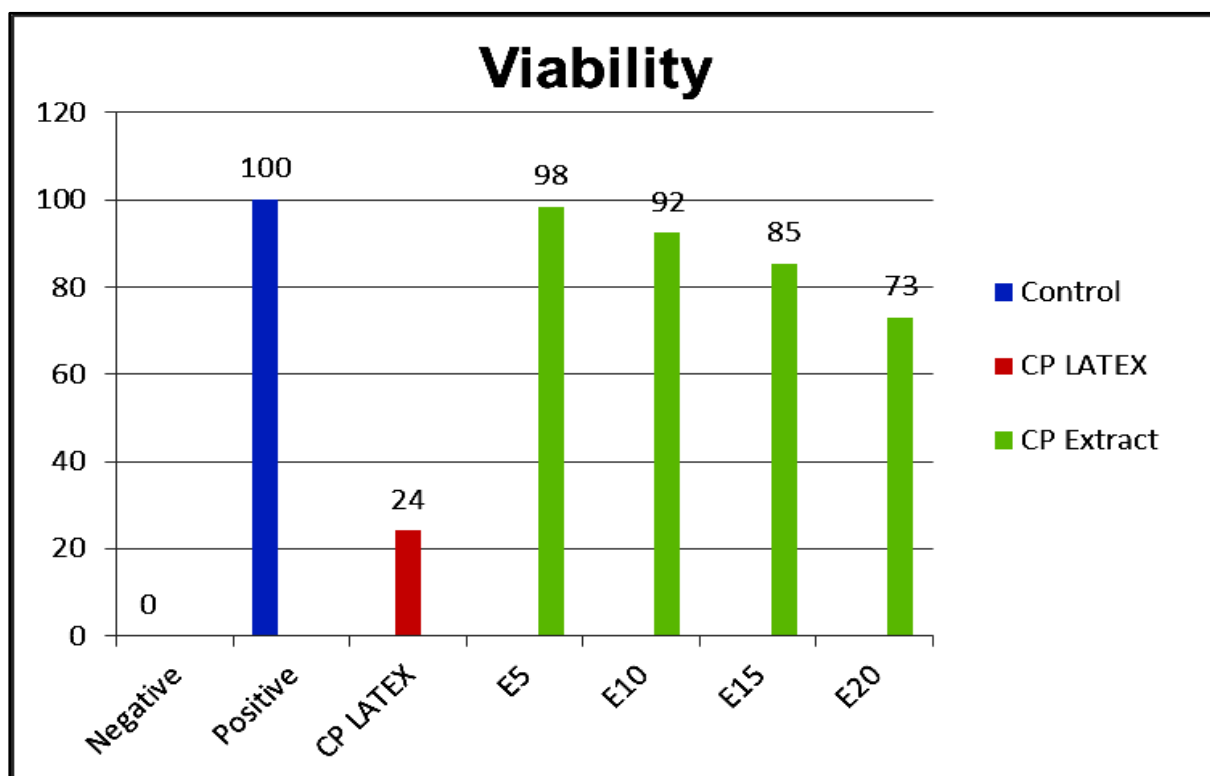


Figure 4.27: Cytotoxicity effects of pure CP latex and CP leave extract with various % concentration

Table 4.9: ZOI (in mm) of various samples against SA and EC bacterial cultures

Sample Code	Colloidal solution (Code)	Staphylococcus aureus (SA)			Escherichia coli (EC)		
		24 Hours	48 Hours	72 Hours	24 Hours	48 Hours	72 Hours
A1	E05S00 [©]	0	0	0	12	0	0
A2	E05S01	15	14	13	21	21	21
A3	E05S02	13	12	11	19	19	19
A4	E05S05	15	13	12	17	17	17
A5	E05S10	13	11	10	15	15	15
B1	E10S00 [©]	17	15	15	21	21	21
B2	E10S01	19	17	16	20	20	20
B3	E10S02	15	12	12	17	17	17
B4	E10S05	10	9	9	14	14	14
B5	E10S10	13	12	12	13	13	13
C1	E15S00 [©]	11	9	9	15	15	15
C2	E15S01	19	16	16	17	17	17
C3	E15S02	16	13	13	15	15	15
C4	E15S05	13	11	11	13	13	13
C5	E15S10	11	10	10	13	13	13
D1	E20S00 [©]	13	10	10	17	17	17
D2	E20S01	17	16	16	20	20	20
D3	E20S02	12	11	11	15	15	15
D4	E20S05	13	11	11	14	14	14
D5	E20S10	12	11	11	13	13	13

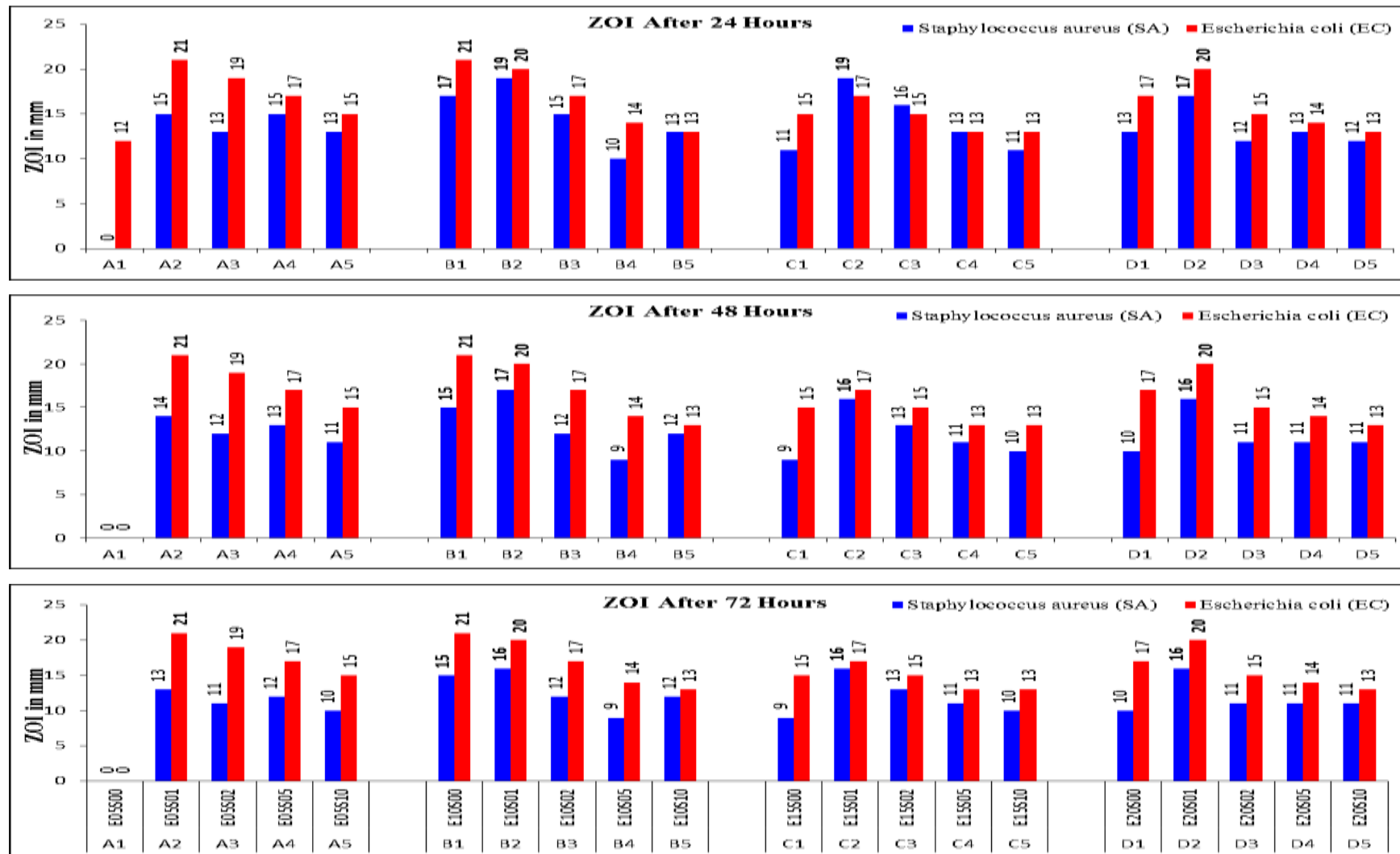


Figure 4.28: Zone of Inhibition (ZOI) in (mm) for each group (major scale)

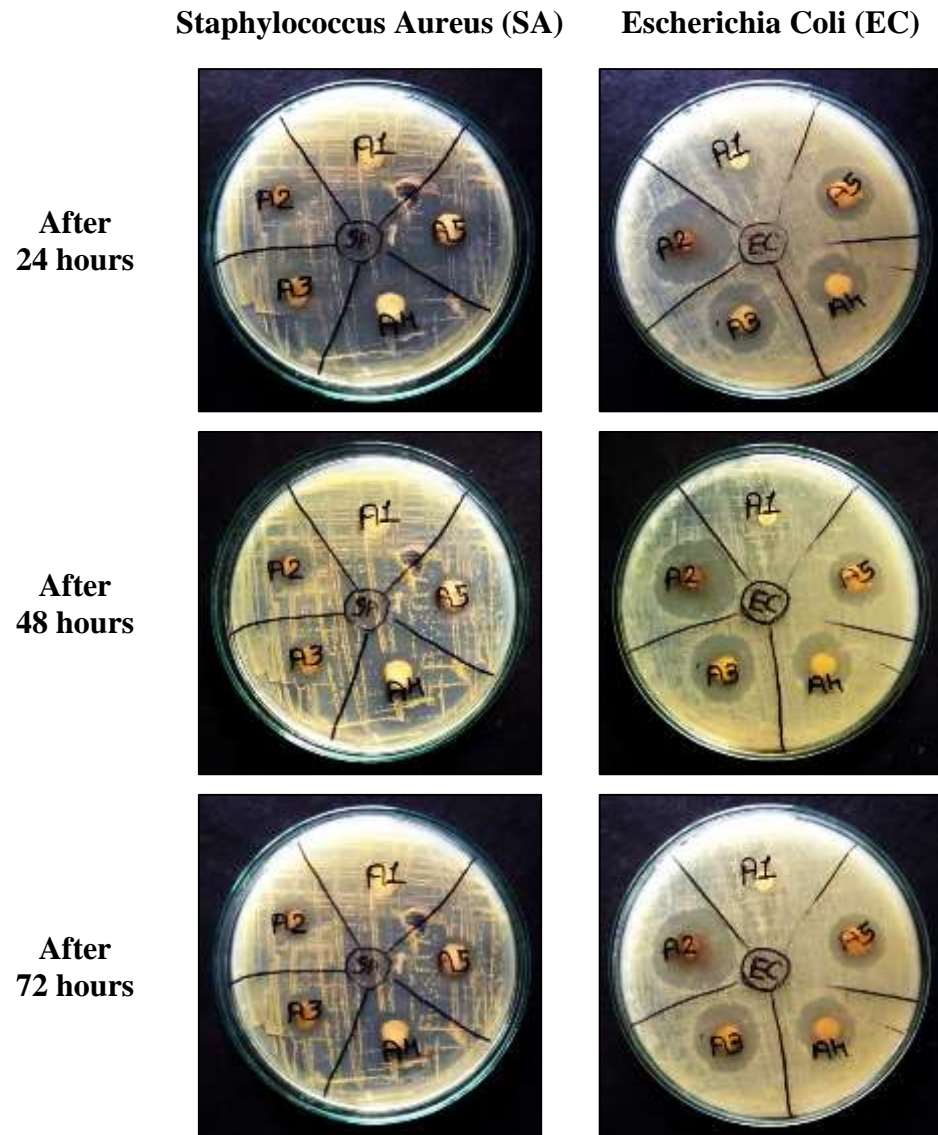


Figure 4.29: Antibacterial assessment (Set A)

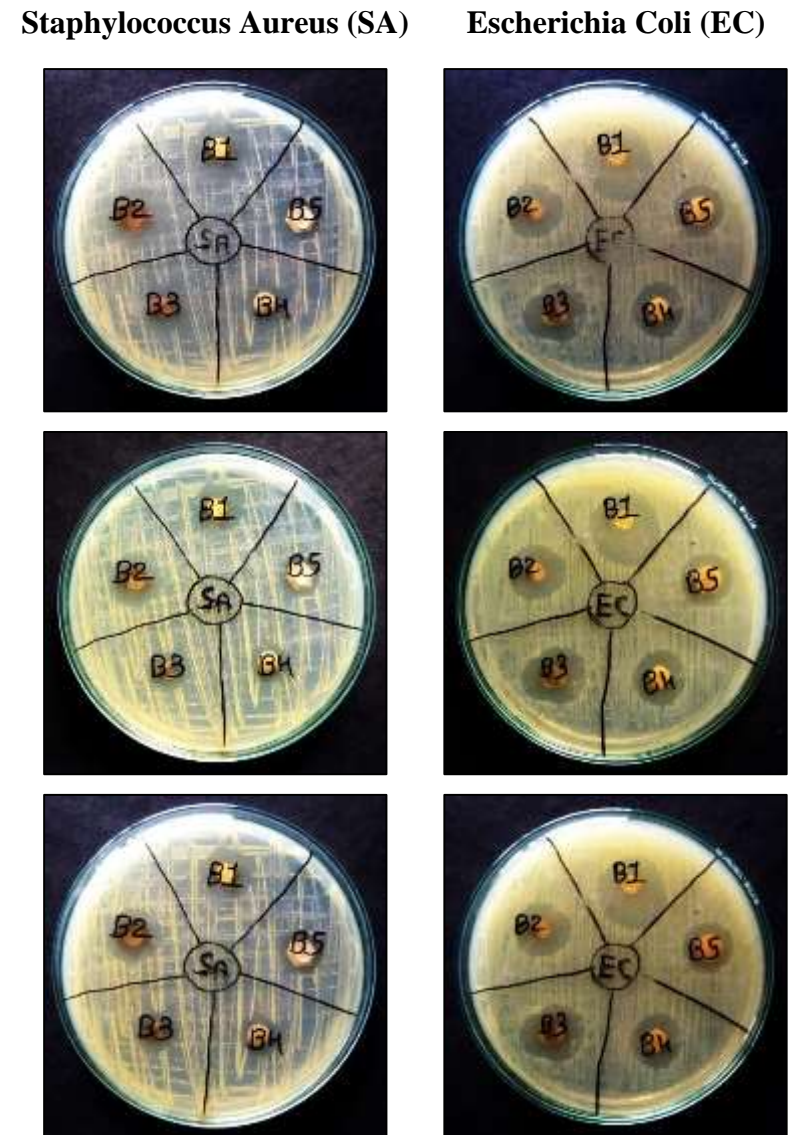


Figure 4.30: Antibacterial assessment (Set B)

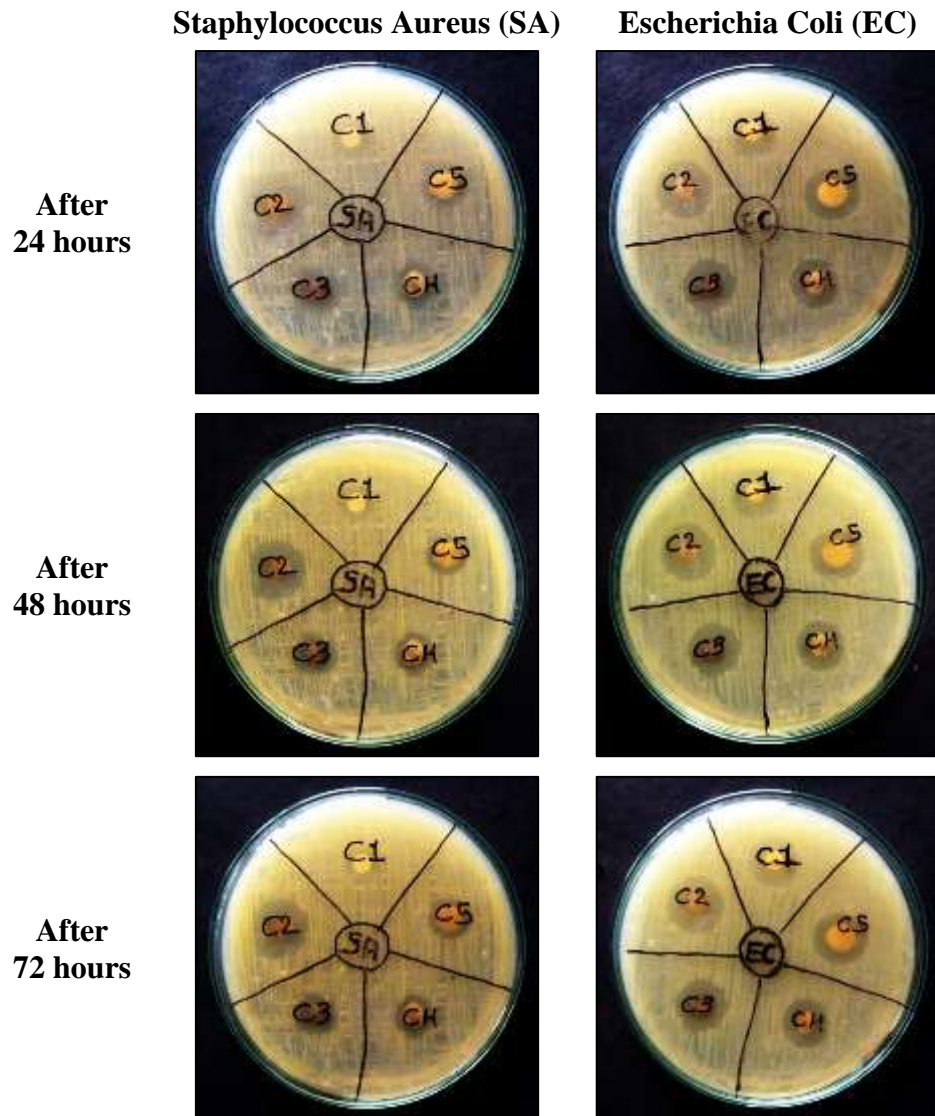


Figure 4.31: Antibacterial assessment (Set C)

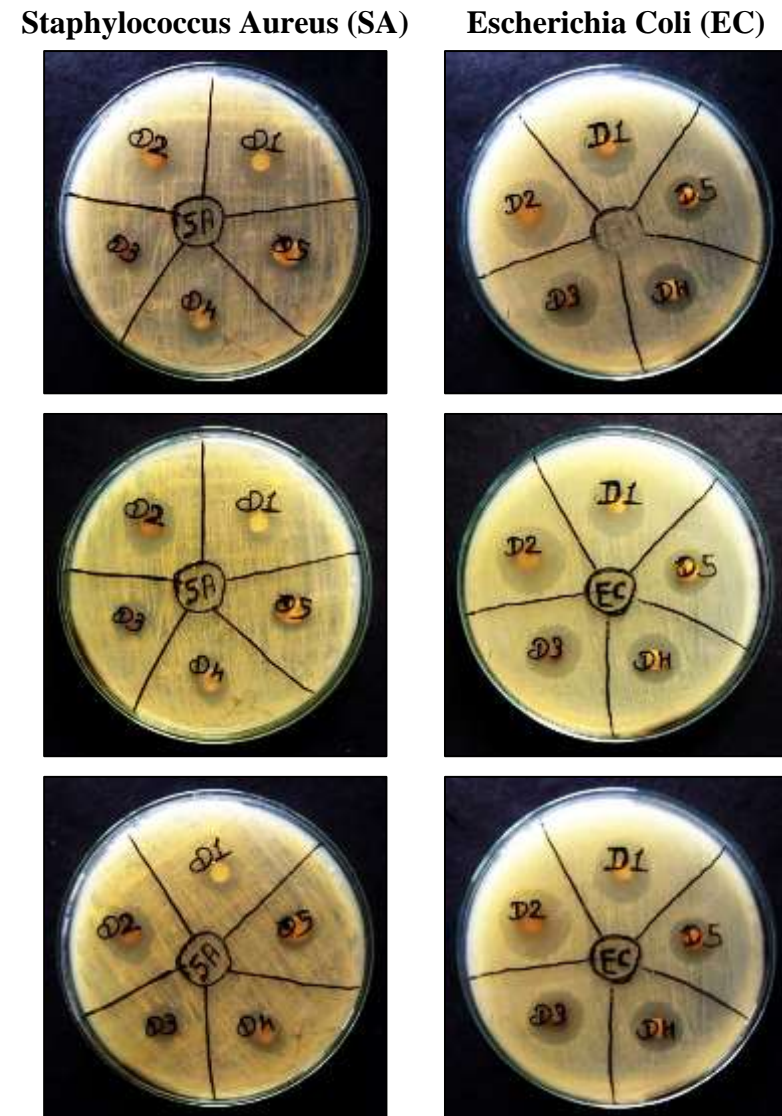


Figure 4.32: Antibacterial assessment (Set D)

4.3.1.1.3 Antibacterial assessment of the samples treated with AgNPs colloidal solutions

The antibacterial activities of samples made from PV-nonwoven (Set A, B, C, and D) were examined qualitatively to choose the optimal/best AgNPs colloidal solution. The test was carried out following the SN 195 920 (Disc diffusion technique) standard, using the bacterial cultures SA and EC. Stability for all the samples was evaluated at 24 hours, 48 hours, and 72 hours' time intervals. Table 4.9 and Figure 4.28 illustrates the zone of inhibition (ZOI in mm) measured at prescribed time intervals of 24 hours, 48 hours, and 72 hours for all the samples (Set A, B, C, and D) against both bacterial cultures (SA and EC), whereas, Figures 4.29 to 4.32 display their antibacterial activity.

The highest ZOI was observed after 72 hours against *Staphylococcus aureus* in samples B2, C2, and D2 (16mm), followed by B1 (15mm). Whereas, the maximum ZOI after 72 hours against *Escherichia coli* were observed in samples A2 and B1 (21mm), followed by B2 and D2 (20mm) respectively (Table 4.9). However, apart from the stated samples, all other samples ended with lower ZOI values.

a) Antibacterial Stability

Figures 4.33 to 4.36 depict the antibacterial activity stability for all sets of nano-composites (i.e. Set A, B, C, and D) against both bacterial cultures (SA and EC) during the selected time intervals; i.e. 24 hours, 48 hours, and 72 hours.

A little drop in antibacterial zone of inhibition of the order of 1mm to 3mm was noticed amongst all the samples after 24, 48, and 72 hours when tested against gram-positive bacteria (SA). The highest drop of 3mm in antibacterial effectiveness was seen with sample D1 against gram-positive bacteria (SA) after 72 hours' time-leap. Whereas, no change has been reported in antibacterial inhibition and thereby antibacterial activities up to 72 hours against gram-negative bacteria (EC) was observed. The extent of antibacterial efficacy detected was higher as well as consistent against *E. coli* rather than *S. aureus* bacteria for this innovative green-way synthesized AgNPs.

The nano-composite sample A1 (E05S00) prepared by treating only with the lowest CP extract concentration (5%) was failed in creating inhibition against comparatively stronger gram-positive SA bacteria at any level. But it has executed some bacterial inhibition against EC bacteria which was lasted only up to 24 hours, thence after the value was reduced to '0mm', indicating lost antibacterial efficacy or no inhibition. This behaviour is likely, as no

established antibacterial agent (AgNO_3) was used in the synthesis process and a very low concentration of natural medium (CP extract 5%) recognized for its antibacterial characteristics has participated. The argument gets substantiated by the increased ZOI noticed against both the bacterium species with increased CP extract concentrations even in the absence of AgNO_3 [samples B1, C1 & D1]. No doubt effectiveness of the antibacterial activities was found highest at 10% CP extract concentration (sample B1) which was dropped at 15% level (sample C1) and again raised for 20% (sample D1) but still remained lower than 10% concentration. This behaviour needs to be investigated in the absence as well as presence of AgNO_3 .

It can also be seen that all the groups have shown identical antibacterial inhibition changes against both the bacterium species with respect to participating constituents' concentration levels. The ZOI values noted were lower in the absence of AgNO_3 [samples A1-B1-C1-D1] and attained highest value at 100mM AgNO_3 concentration for all the samples (A2-B2-C2-D2), except sample B2 against E-coli bacteria. Thence after ZOI value was undergone down-up fluctuations with increased AgNO_3 concentrations but never touched the performance registered for 100mM concentration in each group (Figures 4.33 to 4.36). The best performance in terms of antibacterial inhabitation size and its stability against both the species under consideration has gone in the account of sample B2, prepared with colloidal synthesized with 100mM AgNO_3 and 10% CP leave extract concentrations (Table 4.9). This also supports the findings of visual judgment test about the nanoparticles formation.

b) Selection of the best AgNPs colloidal solution (Major scale)

The optimal concentrations for the components used in the synthesis of AgNPs colloidal solution was done as per its antibacterial activity in the nano-composites. An average ZOI for the set reported against both the bacterium types was taken into account. The set was formed by considering only the fixed concentration of the CP leave extract or the molarity of the AgNO_3 at a time. Accordingly, the plots given in Figure 4.37 represent the average ZOI values as per the extract concentrations and in Figure 4.38 as per the AgNO_3 molarity, against SA and EC, respectively.

It can be visible that the samples incorporated in set B (as per CP leave extract concentration only) when synthesized with 10% CP leave extract (E10) irrespective of AgNO_3 concentration achieved the highest average ZOI values; 14.8mm, 13mm, and 12.8mm against SA, and constant 17mm against EC after 24, 48, and 72 hours' time-leap (Figure 4.37).

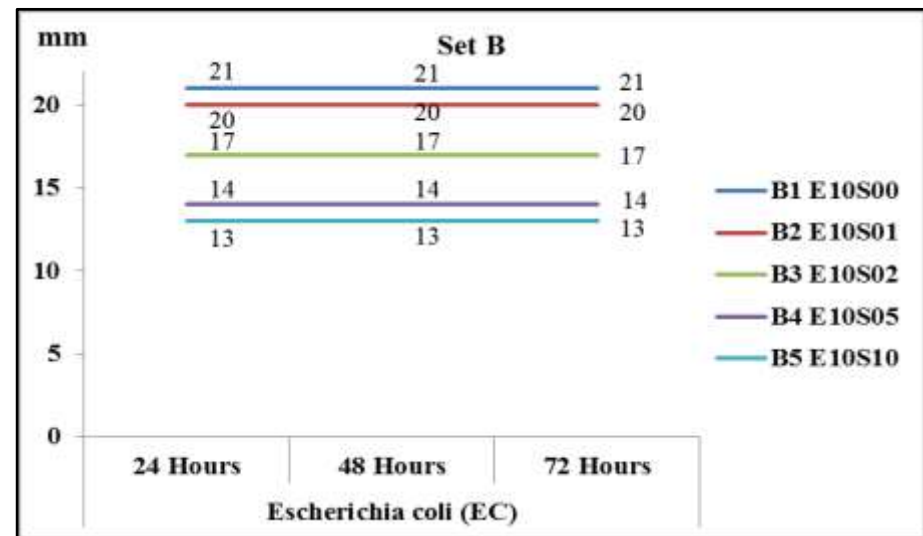
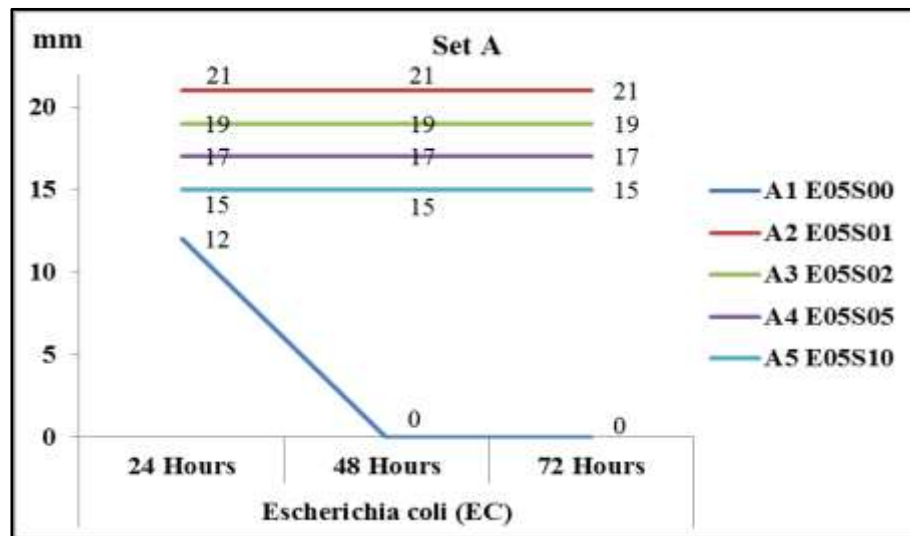
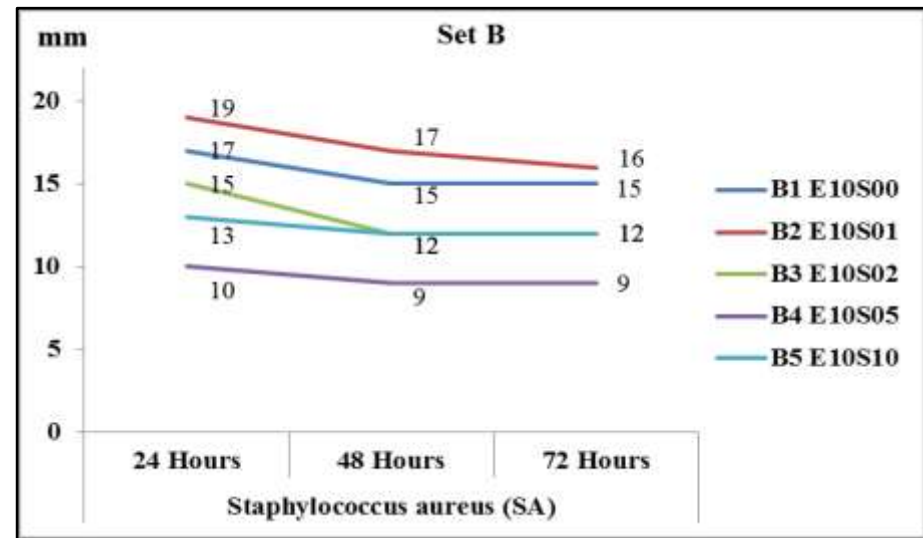
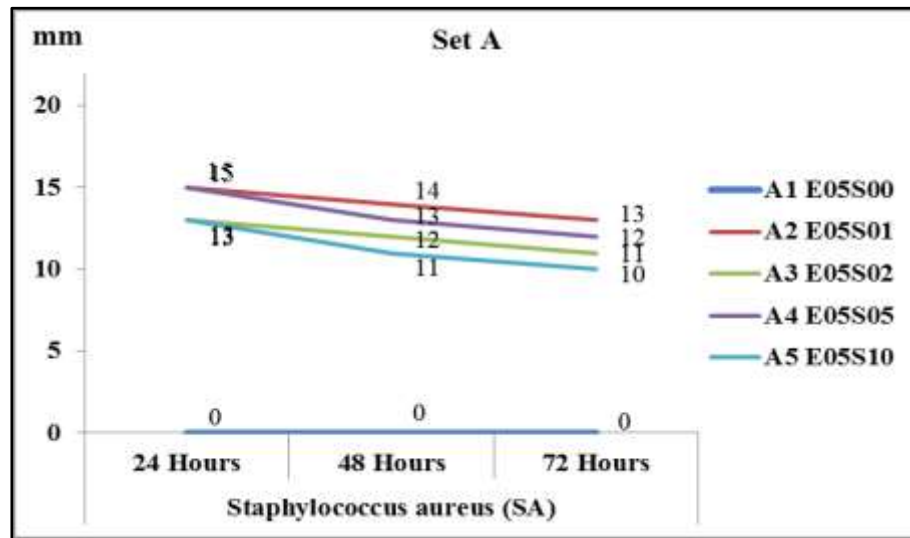


Figure 4.33: Antibacterial Stability (Set A)

Figure 4.34: Antibacterial Stability (Set B)

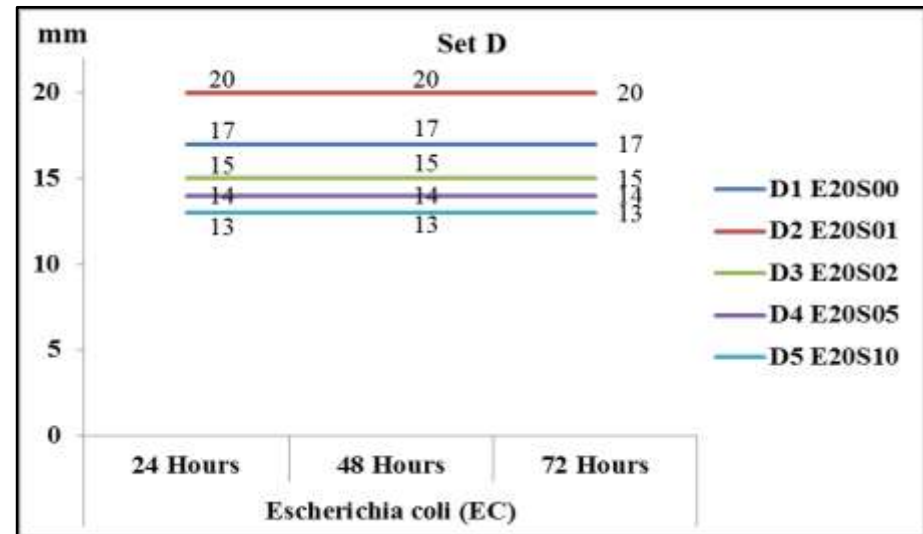
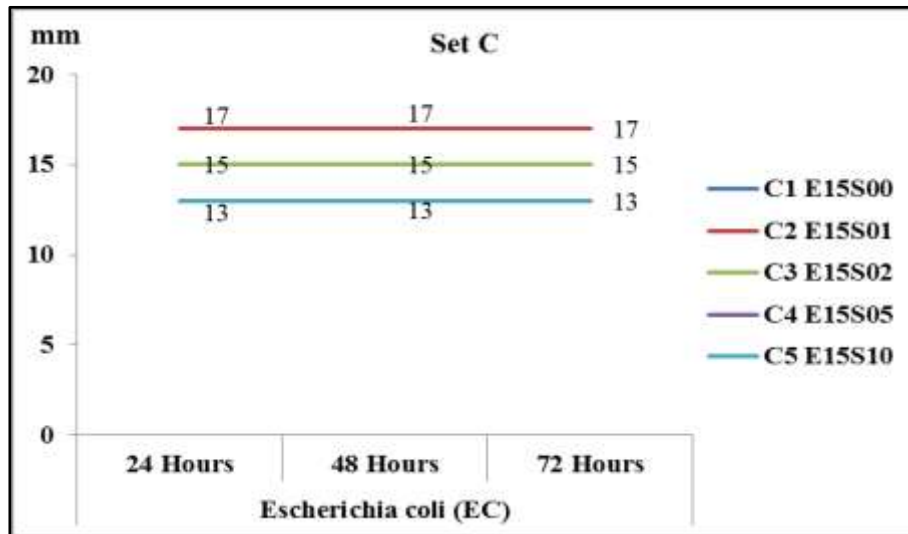
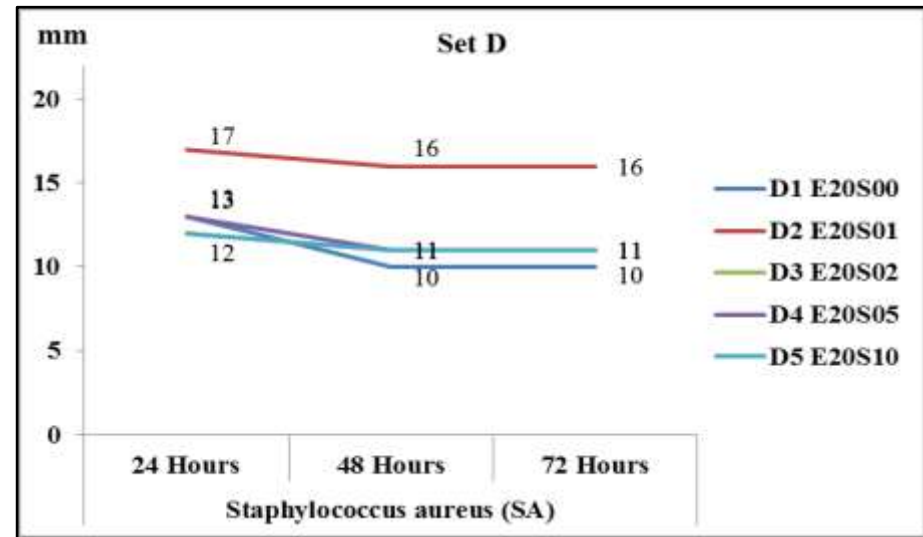
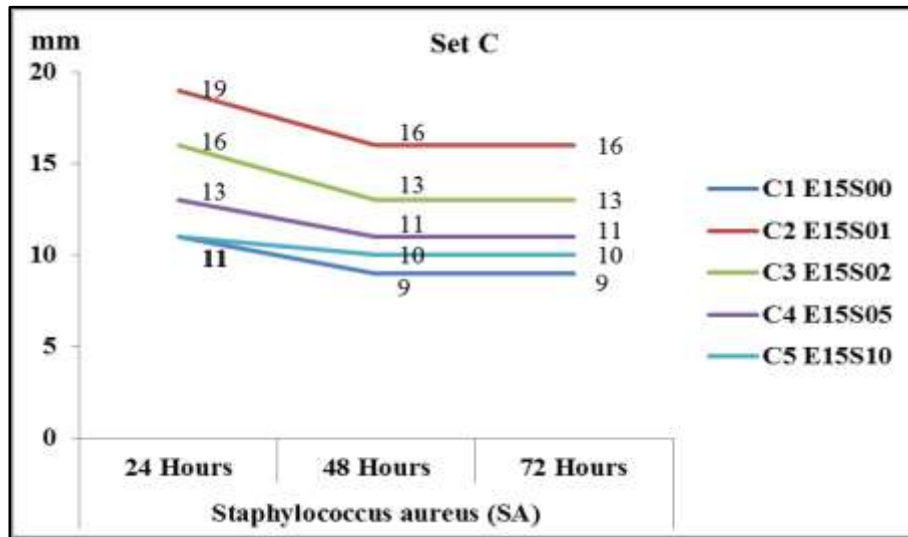


Figure 4.35: Antibacterial Stability (Set C)

Figure 4.36: Antibacterial Stability (Set D)

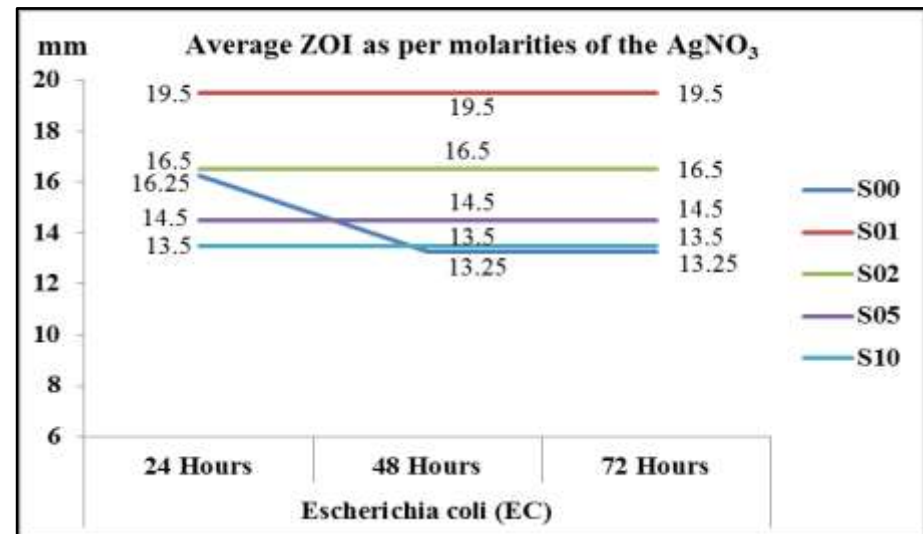
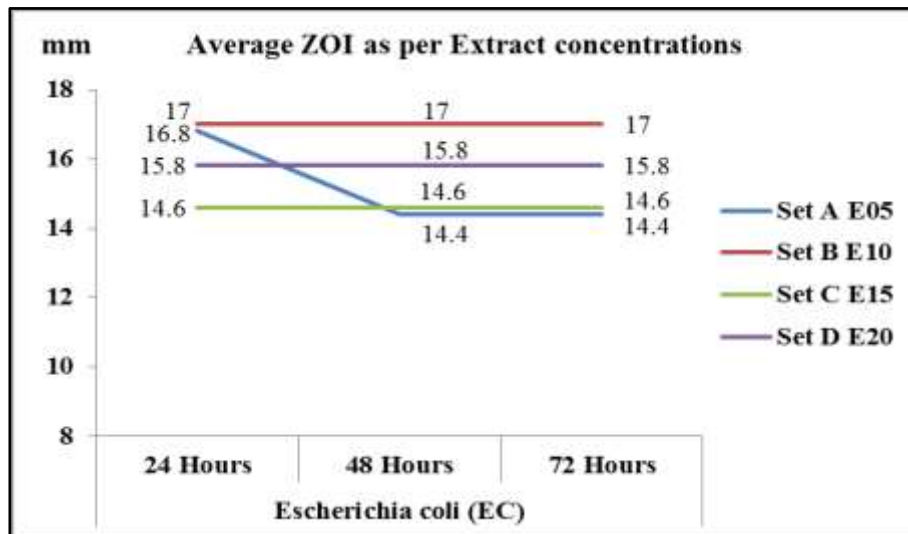
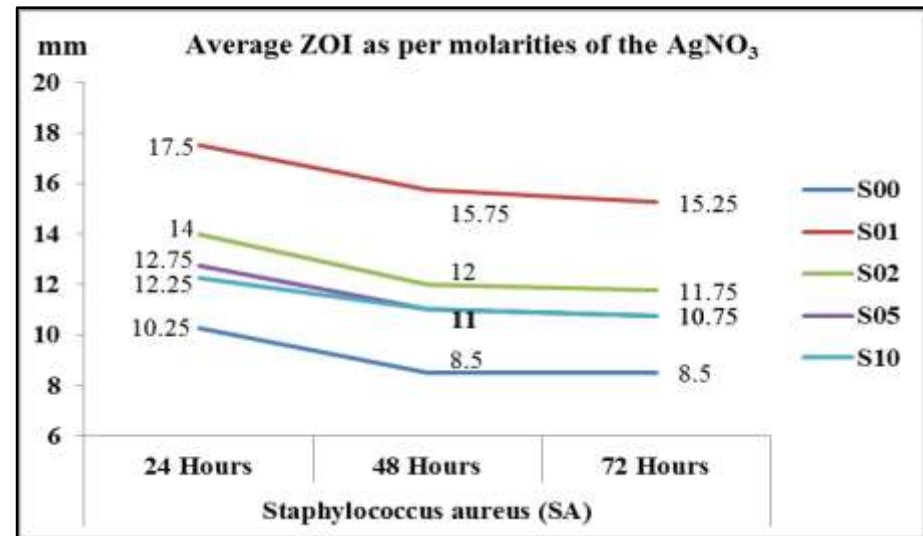
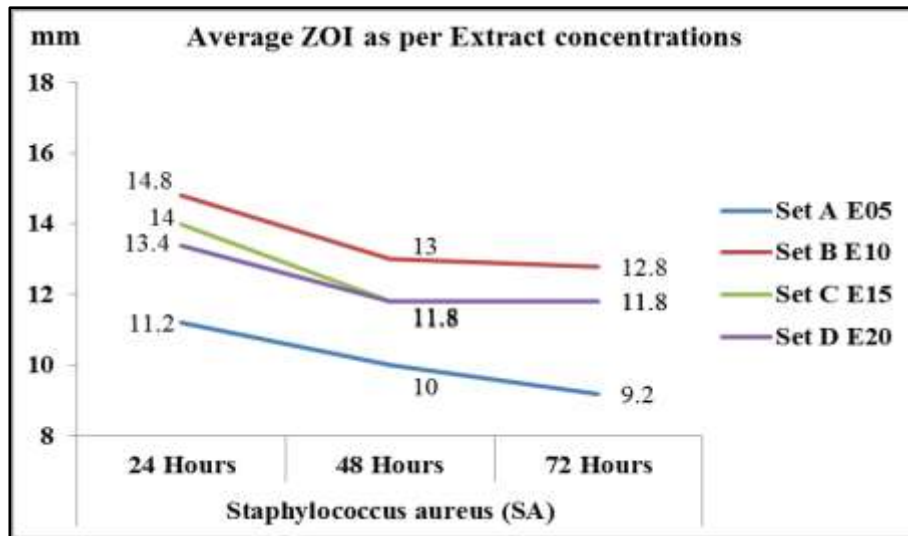


Figure 4.37: Average ZOI as per Extract concentrations

Figure 4.38: Average ZOI as per molarity of the AgNO₃

Eventually, the samples in the set as per AgNO_3 molarity produced with 100mM concentration (S01) demonstrated the highest average ZOI values; 17.5mm, 15.75mm, and 15.25mm against *Staphylococcus aureus*, and 19.5mm constant ZOI against *Escherichia coli* after 24, 48, and 72 hours, respectively. Thus, the average antibacterial activities have also supported outcome of individual antibacterial inhabitation measures. Accordingly, the colloidal sample B2 (E10S01) synthesized with combination of 10% CP leave extract concentration with 100mM molarity of AgNO_3 (S01) was emerged out with the highest average ZOI value in the major group study. Apart from this at 10% CP leave extract concentration second highest (92%) cell viability (non-toxic behaviour) was obtained during MTT analysis in the present study. Considering both these positive insights, 10% CP leave extract concentration value was regarded optimal for further downstream analysis of AgNO_3 molarity during minor scale study.

4.3.1.2 Conclusion: Major scale Pilot trials

All the colloidal have invariably shown a colour change from brownish to blackish after 24 to 48 hours of synthesis and revealed formation of unstable nanoparticles which were converted into macro/micro structure on agglomeration.

- ❖ The MTT assay cytotoxicity test has demonstrated comparatively much better; 73% – 98% viability of cell line at the selected concentrations of CP leave extract than 24% viability of CP pure latex. The cell line's viability has shown descend with the increase in concentration of the CP leave extract. Following the trend, the best value was noticed at the lowest concentration CP leave extract amongst the chosen cell lines.
- ❖ All the samples under study except sample A1 (E05S00) have demonstrated considerable bacterial inhibition against both bacterial cultures; SA and EC up to 72 hours. Supporting the precedents for green AgNPs synthesis, in the present study also, the highest average ZOI value while assessing antibacterial activity was observed for a colloidal solution 'E10S01 (B2)' produced with 10% CP extract (green medium) concentration and 100mM AgNO_3 . Sample A1 (E05S00) was unable to execute bacterial inhibition against SA bacteria at all the levels. However, it has shown ZOI of 12mm against EC bacteria in first 24 hours which was diminished to zero by next 24 hours.
- ❖ Although the CP extract E05 has exhibited highest 98% cell viability but impotent to antibacterial activity. On the contrary, E10, E15 and E20 have exhibited decrease order cell viability but emerged with effective antibacterial activity.

4.3.2 MINOR SCALE PILOT TRIALS

The objective behind this series of trials was to determine the best possible concentration combination for both the participants, in order to earn optimal AgNPs quality at an economical rate. The trials were conducted into two sequential sets; Set-I and Set-II, by small (20mM) to very small (5mM) scaling down respectively, for the molarities of the costlier component AgNO_3 so as to validate precisely its optimum level. The upper level in each case was the lowest one chosen in the previous set of trial (Table 3.8). However, the concentration of CP leave extract was kept constant; 10% (E10), because it has shown perpetually the best performance as an individual as well as in combo with the AgNO_3 , unrelatedly to its molarity values, during the major scale trials.

The colloidal obtained were evaluated for AgNPs formation and stability via, visual colour change observation, UV-VIS spectroscopy, particle size analysis, MTT assay cytotoxicity, and antibacterial activity analysis.

Hence, trials for both the sets were conducted consecutively, their results obtained and related analysis are also separated in this section.

MINOR SCALE TRAIL: SET-I

4.3.2.1 Result's Analysis

4.3.2.1.1 Visual colour change observation

Figure 4.39 shows the pictures taken for the colloidal solutions filled containers at the selected time periods of 0 hour, 24 hours, 48 hours, 1 week, 1 month, and 6 months, to assess initially formation of AgNPs and later their stability on the basis of visual colour change observations.

It can be observed from Figure 4.39 that almost all solutions turned to fuzzy milky brownish at the point of synthesis (0 hour), advocate formation of AgNPs. It can also be seen that the colloidal solutions E10S0060, E10S0080, and E10S0100 formed with upper range of AgNO_3 molarities in the group became blackish or fuzzy milky blackish after 24 hours. This colour change behaviour of these samples has corroborated very poor instability of the nanoparticles with higher AgNO_3 molarities used during synthesis. On the other hand, colloidal solutions E10S0020 and E10S0040 formed with lower range of AgNO_3 molarities in the group have retained their fuzzy milky brownish colour even after a week (1 week), but

they also turned to blackish or fuzzy milky blackish to some extent after 1 month interval. These observations have pointed towards AgNPs formation with better stability initially on synthesizing with reduced AgNO₃ molarities but still failed in preventing occurrence of macromolecules after one month [5,111]. Thus, visual decision-based colour change test results stresses for further scaling down of AgNO₃ molarity to define optima.

It should be noted that subjective mode of visual colour determination is hindered by the interaction of natural dark brownish tint of selected 10% concentration of CP leave extract (Figure 4.25). So, the confirmation for the formation of nanoparticles as well as their stability was thoroughly investigated using established objective test procedures, instead of relying solely on the observations of the colour change.

4.3.2.1.2 UV-VIS Spectroscopy

The presence, size and concentration of AgNPs in the colloidal solutions were investigated from the UV-Visible spectrum obtained for all the samples under study. Hence three substances have participated in colloidal formation, viz; DDW, CP leave extract and AgNO₃, the test was split into two parts to filter effect of minor participating matters; DDW and CP leave extract.

Figures 4.40 (a-e) illustrate the spectrums obtained in the Part-I, tested by placing DDW in the reference cuvette and AgNPs colloidal solution in the sample cuvette. It can be observed that all the spectrums recorded with DDW as reference are spread in the wavelength range of 190–1000 nm and characteristically can be divided into three sections; 190nm-400nm, 400nm-600nm & 600nm-1000nm. The progressively ascending magnitude-wise changes are perceived with the increased AgNO₃ molarity (from sample E10S0020 to E10S0100) in all the three characterized segments of the spectrums.

It can be noted that the magnitude of the frequency change and its clustering is higher before 400nm. The values are more prominent for the spectrums plotted for the colloidal formed with low AgNO₃ concentration. Later on, the frequency span gets broaden along with remarkable reduction in its magnitude of fluctuations in inverse proportion to AgNO₃ molarity during the wavelength range of 400–600 nm. Almost flatten but the broadest band has been realized for the sample E10S0100 in this region. Surprisingly, sample E10S0080 has deviated from the trend and shown reduction in band breadth, need further investigation.

All the spectrums have undergone a steep declination in the 600nm to 1000nm wavelength section and endorsed absence of any participating group in this assessment region. Thus, UV absorption wavelengths on filtering out the third element DDW are found coincided in the nearby nanometer (nm) range that is 190nm to 600nm for CP leave extracts and AgNPs in the present study, substantiated back stuff record [301]. In order to evaluate distinct AgNPs features on the ground of UV absorption bands, the CP extract characteristic bands were filtered out in Part-II. The spectrums were obtained by keeping 10% CP leave extract in reference cuvette and restricting their wavelength execution only for coinciding band; from 190nm to 600nm, as per Part-I outcome [Figure 4.40 (a-e)].

All the colloidal samples revealed typical spectrums having two distinct regions for two differently behaving investigation matters; CP leave and AgNO₃ for UV absorption. The initial region carrying the widely varying positive and negative intensity peaks spread over 190nm-400nm wavelength. This exemplifies subtraction of the CP leave extract particles with respect to the reference cuvette.

The usual range of absorption for silver (Ag) nanoparticles is 400nm to 500nm. If it extends beyond 500nm then it indicates agglomeration or presence of micro/macro molecules of silver [176,222]. Thus, the peaks fallen in 400nm to 600nm region of the UV spectrums have purely corresponded to the plasmon resonance of AgNO₃ and represented AgNPs behaviour in tested colloidal as per their size and frequency in the present study.

The continuously changing frequency band observed in the spectrum is generally pointing towards respective change in the particles size irrespective of type; nano/micro/macro. On the other hand, the band intensity value represents existing quantity of the analysed particles in the tested material. Accordingly, matter found with higher intensity relates a greater number for analysed particles in the sample irrespective of their size.

It can be observed that all the samples synthesized in minor set-I have executed identical trend in terms of intensity, frequency change and span of broadening of the spectrum beyond the limit of 500nm for the nanoparticles. This common behaviour witnessed unwanted larger AgNPs size on agglomeration, i.e. micro/macro particles incidence at all the selected AgNO₃ levels [302]. It can also be seen that intensity and broadening of the peak after 500nm has increased in direct proportion to AgNO₃ molarity. Accordingly, the most undesirable behaviour has been gone in the account of sample E10S0100 and better in the group but yet not satisfying need, with sample E10S0020.

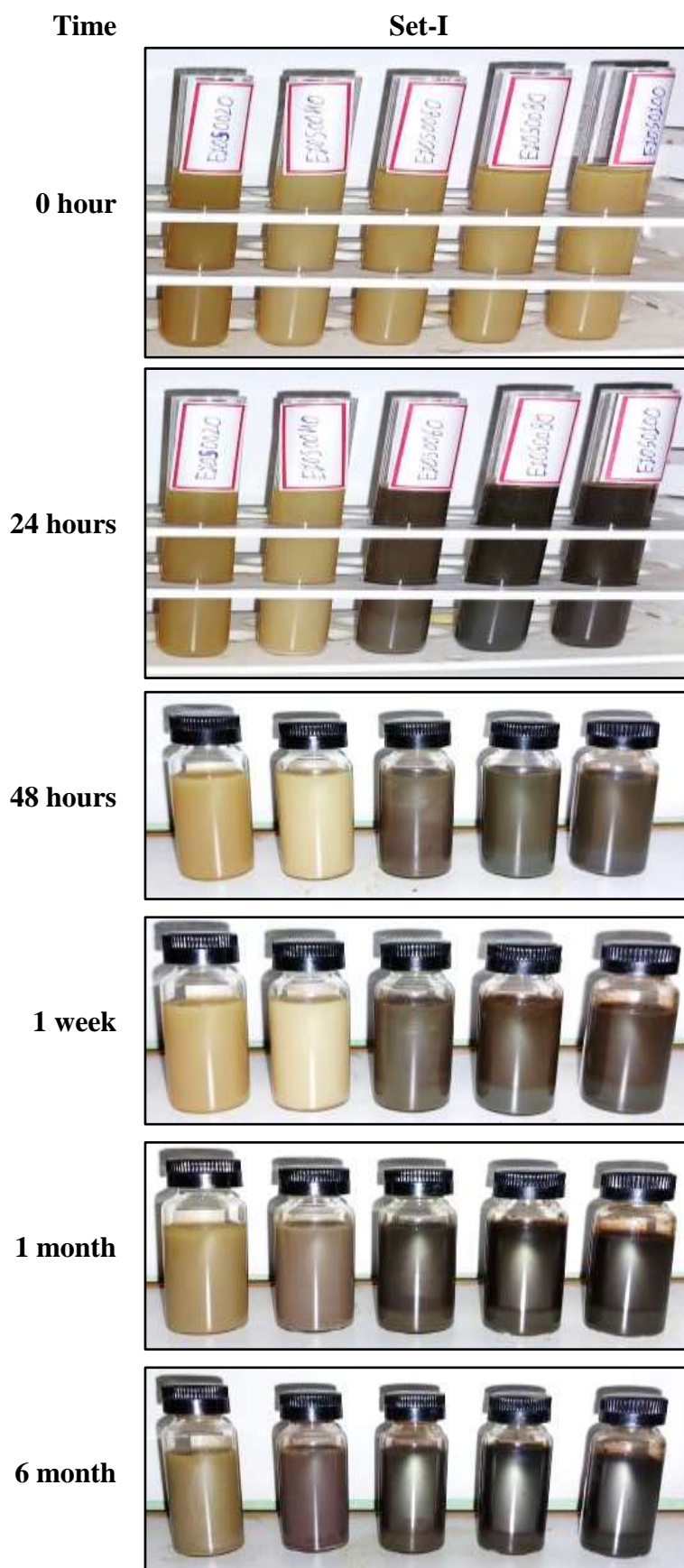


Figure 4.39: Colour change of the AgNPs colloidal solutions (Set-I)

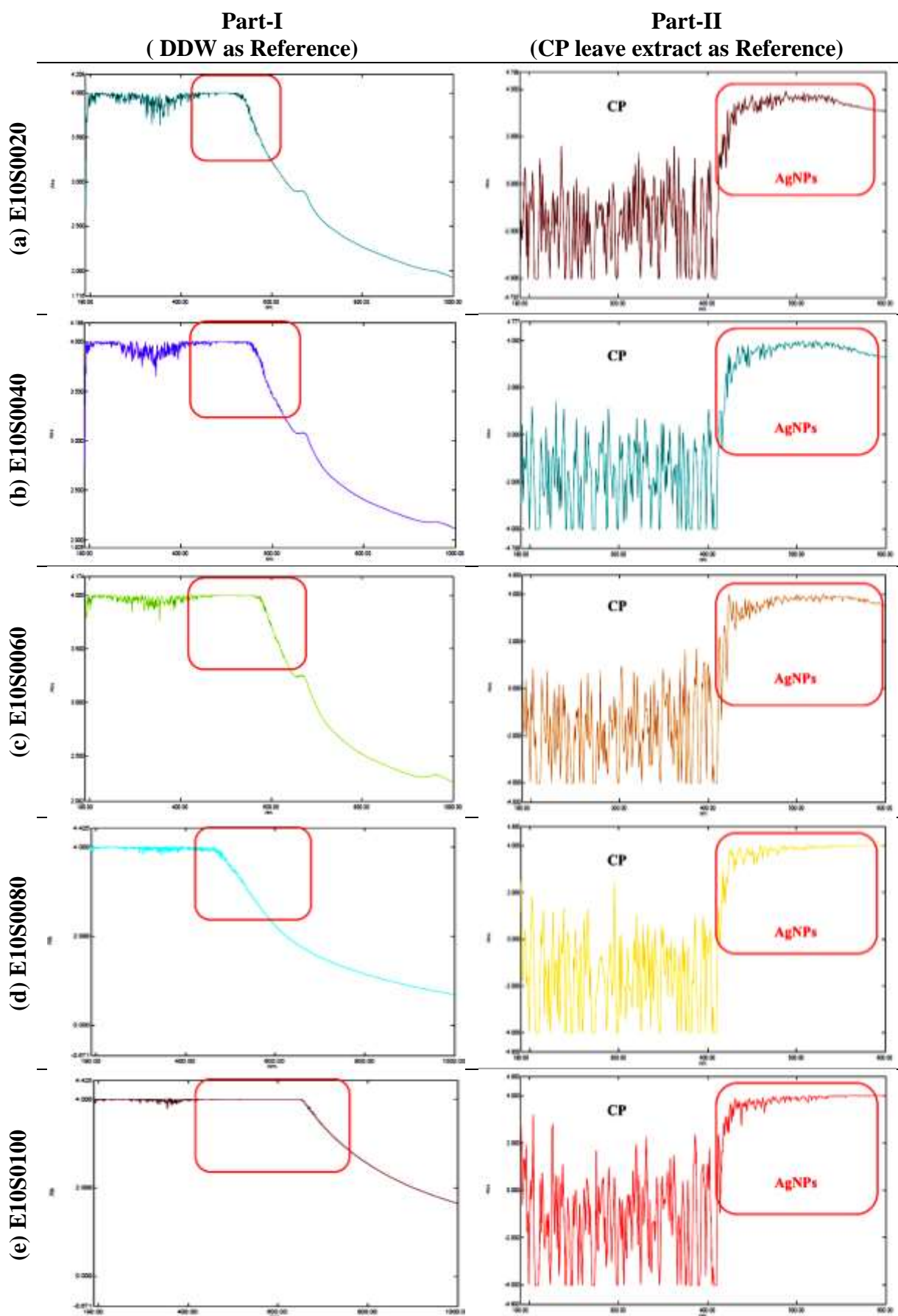


Figure 4.40: UV-Vis spectrum of the AgNPs colloidal solutions in Set-I (a-e)

4.3.2.1.3 Particle size analysis of AgNPs/CP colloidal solutions

The UV spectrum results resolved about micro/macro particle formation due to agglomeration of AgNPs at all the levels of AgNO₃ used in set-I, thereby particle size analysis was conducted for ensuring findings. Table 4.10 shows the particle size distributions and Figures 4.41 (a-e) illustrate the DLS spectrums obtained during particle size analysis.

It can be seen that the DLS spectrums obtained on accomplishing particle size analysis for the AgNPs colloidal solutions E10S0020 has executed two peaks, whereas E10S0040 to E10S0100 have executed three peaks. Parlinska-Wojtan et al. [303] while working on green AgNPs synthesis with Camomile (flower) extract also reported DLS spectrum with three peaks, and amongst which the highest intensity peak related plants leave extract, medium peak AgNPs and low peak other miscellaneous particles. The similar trend has been noted in the present study also, the peak magnitude has varied in proportion to the quantity of participants used during the course of synthesis [Figures 4.41 (a-e)]. Accordingly, for all colloidal higher intensity peak has gone on the account of the extract, the medium to the metal salt (i.e. AgNO₃) and low or no peak to the other foreign particles.

The strongest peaks indicating the CP leave extract particles have shown an average particle size of 247.5, 229.2, 354.0, 191.9 and 235.1 nm with an intensity of 86.1, 85.9, 77.3, 64.8, and 74.4% respectively in colloidal solutions from E10S0020 to E10S0100. Even though the concentration of CP leave extract used during synthesis was identical (10%) for all colloidal solutions, the intensity % has shown declination in an irregular pattern, as did the particle size. These consequences seen concerning to CP leave extract can be instigated by the particles' response towards the increasing quantity of AgNO₃ during synthesis [303].

The second strongest peaks representing AgNPs have shown an average particle size of 51.4, 33.2, 58.7, 28.8 and 49.2 nm with respective intensity of 13.9, 10.8, 17.2, 23.4 and 18.3% in colloidal solutions from E10S0020 to E10S0100. The increase pertaining to the AgNPs size and intensity are likely because the AgNO₃ molarity was increased at constant level during synthesis. But surprisingly the increment values observed for AgNPs have also not defined clear trend and followed irregular modus. However, the average size of the nanoparticles detected remain well within satisfactory level (<100nm) for all the colloidal solutions [303]. The favourable lowest size nanoparticles (28.8nm) with highest intensity in the group assessed has gone in the account of sample E10S0080.

Thus, the particle size and intensity observed for the activator CP extract was as per expectation higher in an aggregate compared to AgNPs. However, change in their values has not followed particular pattern for both, although rise in AgNO₃ molarity was consistent for chemical interaction with 10% concentration CP leave extract. Due to this random outcome of the chemical interaction, the solution E10S0080 observed the lowest and the solution E10S0060 observed the highest values in the selected parameters of the group. Such an imbalanced outcome in terms of intensity and particle size of the CP leave extracts and AgNO₃ should be investigated further.

The smallest intense peaks commonly represent other foreign particles while resourcing green agent even though with utmost care and thereby their percentage presence is never been treated compulsory in DST curves. Even their particle size is ever higher than the rest of two components used in the formation of the colloidal [303]. Going in accordance, no peak was observed for the solution E10S0020 and a very low intensity 3.3% and 5.5% respectively seen for the solution E10S0040 at 5166 nm, and E10S0060 at 5191 nm. However, the AgNPs colloidal solutions E10S0080 and E10S0100 were behaved differently and executed peaks at 7.591 nm and 6.225 nm respectively. Surprisingly, their size and intensity figures (11.7% and 7.3% respectively) have been fallen in the region of AgNPs more rather than other foreign particles need further investigation.

The Z-averages of the colloidal solutions represent overall particle size, i.e. combination of CP leave extract, AgNPs and other foreign matters, were 254.6, 155.6, 249.6, 409.1 and 394.7 nm respectively for the ascending order of AgNO₃ molarity. Such deviation in the values is likely owing to random track records noted for CP extract and AgNPs in this set of study.

The polydispersity (PDI) value determine success met in colloidal formation on amalgamation of participating components. PDI value of ≤ 0.1 indicates the solution is highly mono-disperse, 0.1-0.4 is moderately polydisperse, and greater than (>0.4) is a highly/broadly polydisperse type of distribution. In a broader sense polydisperse type of distribution is indicative for the presence of particle sizes with an undesirable large diversity and thereby a highly polydisperse solution. Similarly colloidal with highly mono-dispersity is also not viable due lack of or negligible interaction amongst participating matters. Thus, the colloidal with moderate polydispersity is highly inevitable [246,291].

It can be seen that the PDI values for AgNPs colloidal solutions E10S0020 to E10S0100 have followed irregular modus with respect to the increasing concentration of the AgNO₃. PDI values reported against increased AgNO₃ concentrations were 0.359 (moderately), 0.464 (broadly), 0.390 (moderately), 0.455 (broadly) and 1.000 (broadly) respectively. Except for the sample E10S0060 increase in the PDI value was observed with the increasing concentration of the AgNO₃. Even though particle size and intensity for CP extract as well as AgNPs were hiked from previous level this contradictory behaviour was happened, needs further investigation. It should also be noted that the colloidal E10S0080 having the most preferable lowest AgNPs size of 28.8nm with the highest intensity (23.4%) in the group was failed in terms of PDI and demonstrated non-preferable broadly polydisperse type (0.455) of distribution. Similarly, the colloidal solution E10S0060 which has shown necessary moderately polydisperse type of distribution (0.390, ≈0.4), by surpassing the colloidal solution E10S0040, but having the highest average AgNPs size of 58.7nm in the group. Going in line with visual judgment test and UV-VIS spectroscopy, the colloidal solution E10S0020 having preferable PDI of 0.359 with better nanoparticle size (51.4nm) formed with moderate intensity (13.9%) in the absence of foreign element has proven to be the best amongst all but yet not up to the mark. The values can expectedly get improved on providing better platform for interaction at further scale down molarity of AgNO₃.

4.3.2.1.4 Antibacterial assessment of the PV-AgNPs/CP composites

The qualitative changes in antibacterial activities of the AgNPs treated PV-nonwoven fabric samples (E1-E5) prepared at different AgNO₃ molarities were investigated. Apart from efficacy sustainability of antibacterial activities is also equally important for medical textile materials; thereby stability of this induced functional characteristic was also assessed at three different time intervals to the preparation; 24 hours, 48 hours, and 72 hours.

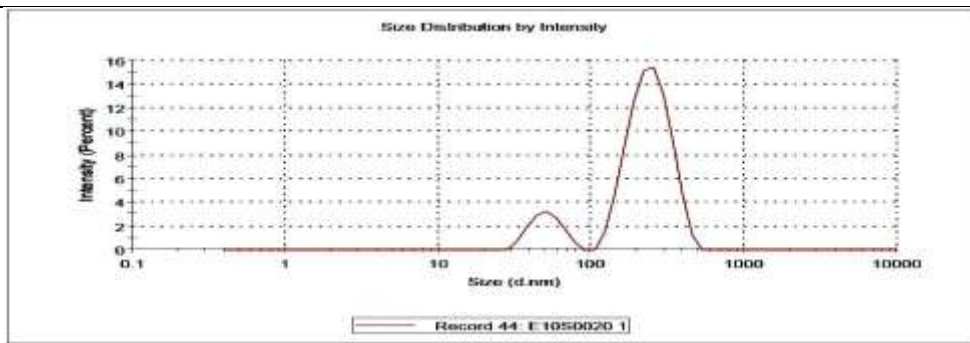
The antibacterial activity of the samples against both the bacterial cultures (i.e. SA and EC) at various time intervals of 24, 48 and 72 hours are summarized in Figures 4.42. The zone of inhibition (ZOI in mm) measured for these samples against both bacterial cultures (i.e. SA and EC) at the specified time intervals are given in Table 4.11.

Table 4.10: Particle size distribution of the AgNPs colloidal solutions (Set-I)

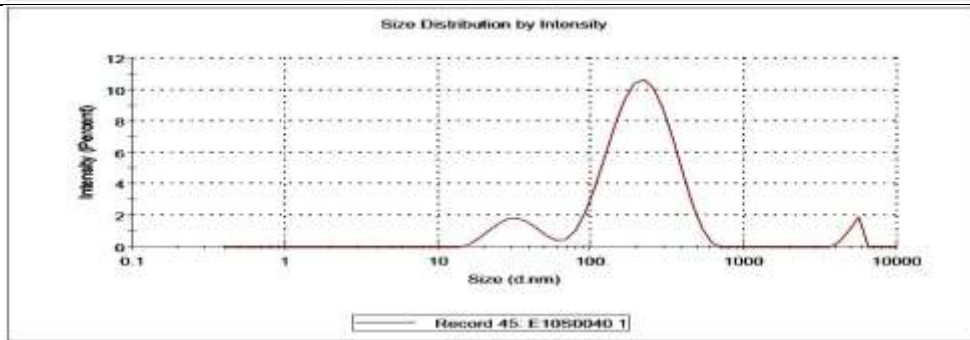
Sample Code	Particles size (d.nm)						Z-average (nm)	PDI	Distribution type
	Peak 1 (CP)		Peak 2 (AgNPs)		Peak 3 (Others/Misc.)				
	Size (d.nm)	% Intensity	Size (d.nm)	% Intensity	Size (d.nm)	% Intensity			
E10S0020	247.5	86.1	51.4	13.9	0	0	254.6	0.359	Moderately polydisperse
E10S0040	229.2	85.9	33.2	10.8	5166	3.3	155.6	0.464	Broadly polydisperse
E10S0060	354.0	77.3	58.7	17.2	5191	5.5	249.6	0.390	Moderately polydisperse
E10S0080	191.9	64.8	28.8	23.4	7.591	11.7	409.1	0.455	Broadly polydisperse
E10S0100	235.1	74.4	49.2	18.3	6.225	7.3	394.7	1.000	Broadly polydisperse

* d.nm = diameter in nanometer

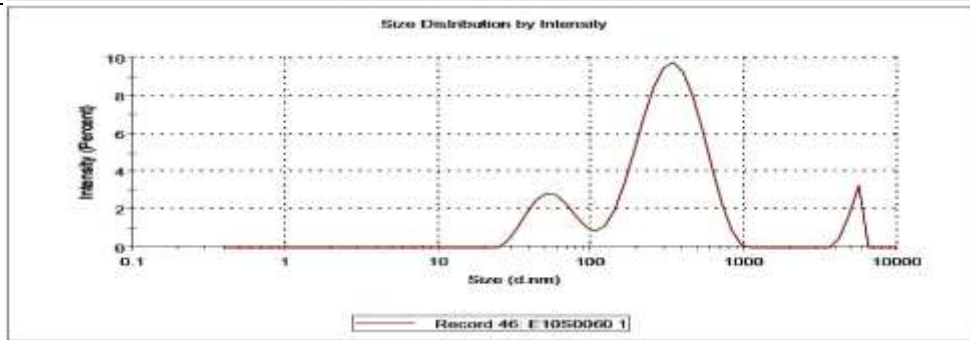
(a) E10S0020



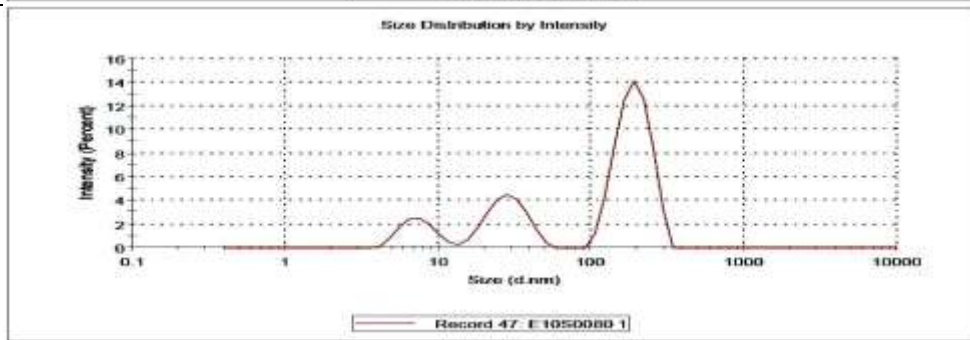
(b) E10S0040



(c) E10S0060



(d) E10S0080



(e) E10S0100

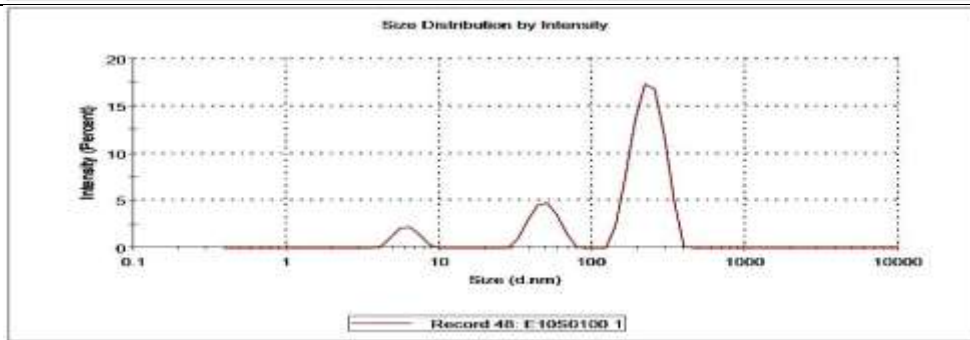


Figure 4.41: DLS spectrum for the particle size distribution of samples in Set-I (a–e)

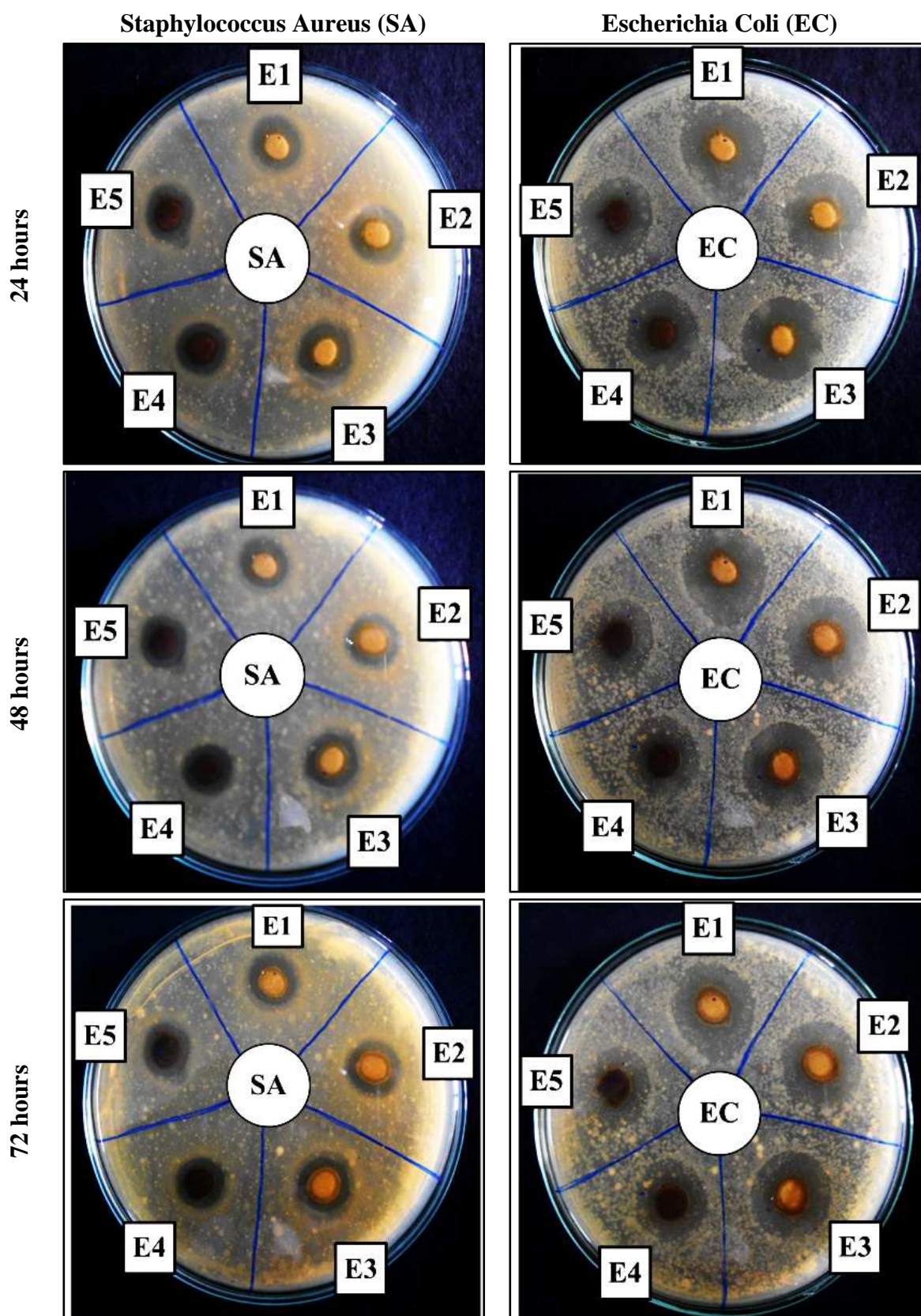


Figure 4.42: Antibacterial assessment (Set-I)

Table 4.11: Zone of Inhibition (ZOI) in (mm) of various samples (Set-I)

Sample Code	Colloidal solution (Code)	Staphylococcus aureus (SA)			Escherichia coli (EC)		
		24 Hours	48 Hours	72 Hours	24 Hours	48 Hours	72 Hours
E1	E10S0020	19	17	17	21	20	19
E2	E10S0040	19	17	17	21	20	19
E3	E10S0060	18	17	17	20	19	18
E4	E10S0080	17	16	16	19	18	17
E5	E10S0100	17	16	16	19	18	17

It can be seen that all the samples have invariably shown ZOI against both the bacterium culture and its value get declined with increase in resting time. The highest ZOI value was observed after 72 hours against Staphylococcus aureus in samples E1, E2, and E3 (17mm), followed by E4 and E5 (16mm), and against Escherichia coli in samples E1 and E2 (19mm), followed by E3 (18mm), and E4 and E5 (17mm) respectively [Table 4.11]. Thus, on an aggregate five to ten percentage change in ZOI was recorded in each category. It can also be noticed that antibacterial efficacy of the newly engineered nano-composite materials is far better against gram-negative EC bacterial culture than gram-positive SA bacterial culture irrespective of the colloidal and time. This behaviour goes in accordance with previous findings for green synthesized AgNPs treated textile materials [304].

According to ZOI value and its change with respect to time against both the bacterial cultures, samples E1 and E2 with 20mM (E10S0020) and 40mM (E10S0040) AgNO₃ concentrations have shown identical best performance in the group. Since, economy of the composite is mainly born by the costliest element; AgNO₃ used in the course of the manufacturing process. In the present study samples E1 and E2 were emerged with the identical qualitative performance but the composite E1 made with a least use of the AgNO₃ is preferred on the economical ground also.

4.3.2.1.5 Conclusion: Minor scale Pilot trails: Set-I

- ❖ All the colloidal solutions have visually confirmed formation of AgNPs by observing a fuzzy milky brownish colour at the point of synthesis. However, the stability of the colloidal solutions E10S0020 and E10S0040 was lasted till a week and rest up to a month only. The colloidal solution turned to blackish (fuzzy milky blackish) on becoming unstable.

- ❖ The broadness of the peak was increased with the molarity of the AgNO₃ during UV-VIS Spectroscopy study within the wavelength ranges of 400–600 nm (or <600 nm). All the samples have shown invariably a broad but less strong peak between 400–600 nm (or <600nm) indicating presence of poor quality AgNPs, i.e.; indicates small to medium sized nanoparticles with agglomeration.

- ❖ The DLS spectrum results have revealed a wide polydisperse kind of distribution with AgNPs of <100nm in size (ranges from 28.8nm to 58.7nm) for all the colloidal solutions under observation. However, the colloidal solution E10S0020 (0.359) has displayed a moderately polydisperse type of distribution with AgNPs measuring 51.4nm in size. The colloidal solution E10S0020 has also demonstrated better nanoparticle formation and dispersion, but resumed bit higher nano particle size (51.4nm).

- ❖ The Colloidal solutions, i.e.; E10S0020 (E1) and E10S0040 (E2), have reported higher antibacterial activity against SA and EC bacterial cultures in a group.

MINOR SCALE TRAIL: SET-II

The outcomes of first minor set trails have recommended the colloidal solution E10S0020 made with the lowest AgNO₃ molarities (20mM) over the other samples prepared in the group. The preference is decided on the account of better performance recorded during all the basic evaluation tests; visual colour change based confirmation about nanoparticles formation and their long-term stability, DLS spectrum-based particle size analysis values as well as the fundamental antibacterial activities against both the bacterium cultures. However, this better should not be regarded as an optimal because of its limiting behaviour noted during these evaluation process, viz; the colloidal resumed during visual analysis unwanted near about blackish tint due to agglomeration of AgNPs after 6 months' time stay and this finding was also supported by UV-spectra as well as DLS- spectra [Section 4.3.2.1]. Thereby, second minor set of experiments were conducted to work out qualitatively and quantitatively optimum by further scaling down of AgNO₃ from the better 20mM with miniscule gaps; 15mM, 10mM, 5mM, and 1 mM, and keeping the best suitable concentration 10% of the CP leave extract – a natural reducing and capping agent used in this study. Hence quantum of AgNO₃ has been reduced considerably in the group, characteristic behaviour of pure 10% CP leave extract (sample E10S0000) was also studied at all the point of evaluation.

4.3.2.2 Result's Analysis

4.1 Visual colour change observation of the AgNPs colloidal solutions

Figure 4.43 depicts the pictures of the colloidal solutions taken as a record for colour change observations and captured at different time periods; 0 hour, 24 hours, 48 hours, 1 week, 1 month, and 6 months.

It can be seen that the colour of the 10% pure extract (E10S0000) at the point of synthesis (0 hour) was deep brown. Progressively this deep brown colour shade was diminished to light brownish for the colloidal solutions starting from E10S0001 to E10S0015 at the point of completion of synthesis; 0 hour (Figure 4.43). This colour change has witnessed about occurrence of AgNPs at the point of synthesis for all the samples, and its pattern has endorsed intensity of AgNPs formation. The intensity was varied in direct proportion of AgNO₃ molarity and thereby sample E10S0015 has executed lightest shade in the group [5,111].

It can also be visualized that all the colloidal solutions have almost retained their initial colour (0 hour) for a period of week by showing negligible shade variation from the fuzzy light brownish. However, a major colour change was detected in the duration of 1 month to 6 months. A modest rise in the depth of the colour was caused not only for the colloidal but also for the CP leave extract tint which was shifted to dark brownish in this duration. Definitely it has impacted colour shade of the colloidal samples also in the presence of AgNPs. The colour change noticed for the colloidal solutions E10S0001 and E10S005 was stronger; darker brownish colour than rest of the two colloidal solutions E10S0010 and E10S0015 which were still holding bit darker but still favourable fuzzy light brownish colour tint. This visual judgment-based evaluation has substantiated the long-term stability up to 6 months of AgNPs is resumed for the colloidal solutions E10S0010 and E10S0015. But the strong colour change instigated towards darker brownish for the colloidal solution E10S0001 and E10S005 pointed towards micro/macro -molecules formation on agglomeration of instable AgNPs after 6 month [5,111].

4.3.2.2.2 UV-VIS Spectroscopy

The spectrums were obtained in two parts for Set-II in the similar way as done in Set-I. Initial phase testing was done by placing DDW in the reference cuvette and later phase by placing 10% CP leave extract in reference cuvette. The AgNPs colloidal solution to be evaluated was kept in the sample cuvette in both the parts of experimentation. Hence, sample E10S0000 was produced using only DDW and CP for relating characteristics of pure 10% CP leave extract, its spectrum was obtained in part-II also by keeping DDW in reference cuvette.

Figure 4.44 (a-e) illustrate the spectrums obtained in the Part-I. The sample E10S0000 consisted of CP leave extract (10%) only has exhibited as per expectation the board peak with high intensity between the wavelength range of 190–400 nm [Figure 4.44 (a)] [301]. Whereas, all the colloidal samples (E10S0001 to E10S0015) have shown the peak broadness progressively increasing almost with the same intensity as per the increase in the molarity of AgNO_3 between the wavelength range of 400–600 nm (or <600 nm).

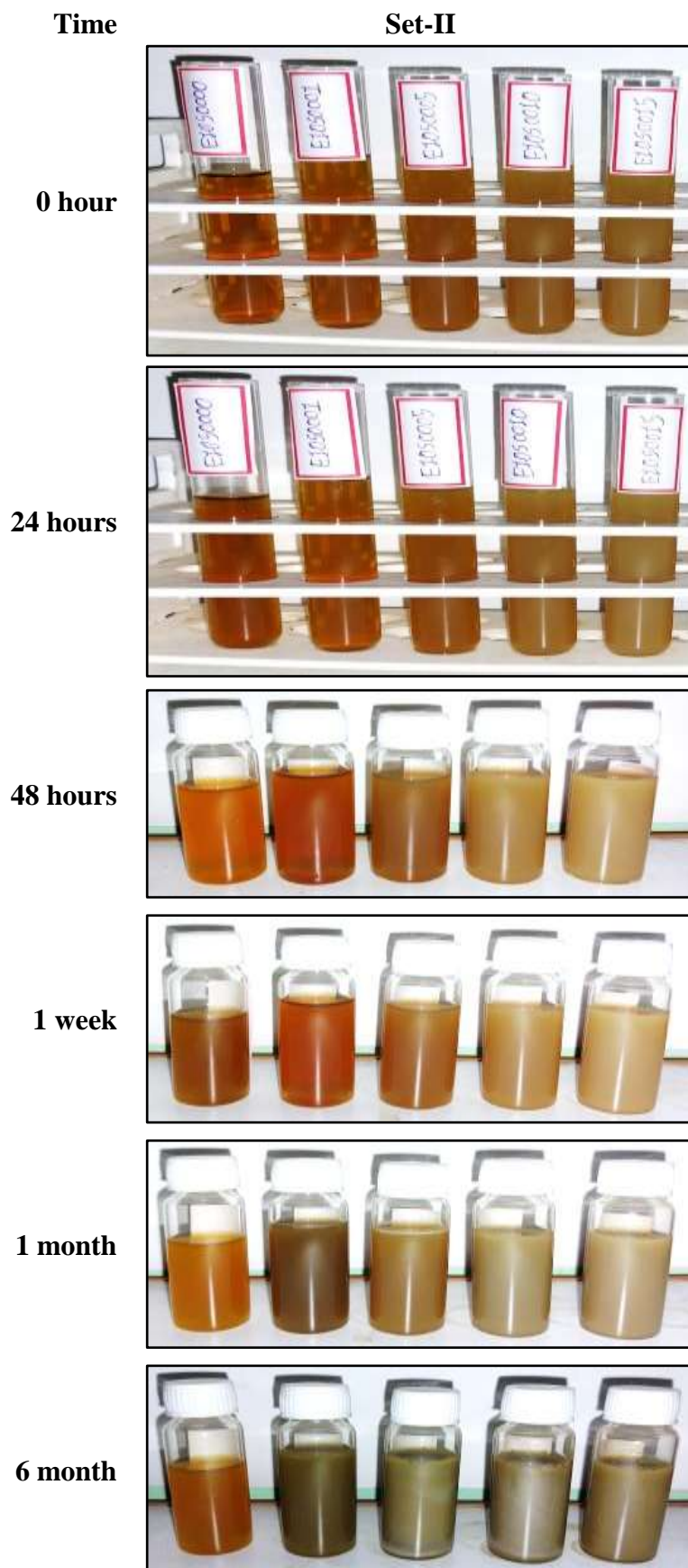


Figure 4.43: Colour change observation of the AgNPs colloidal solutions (Set-II)

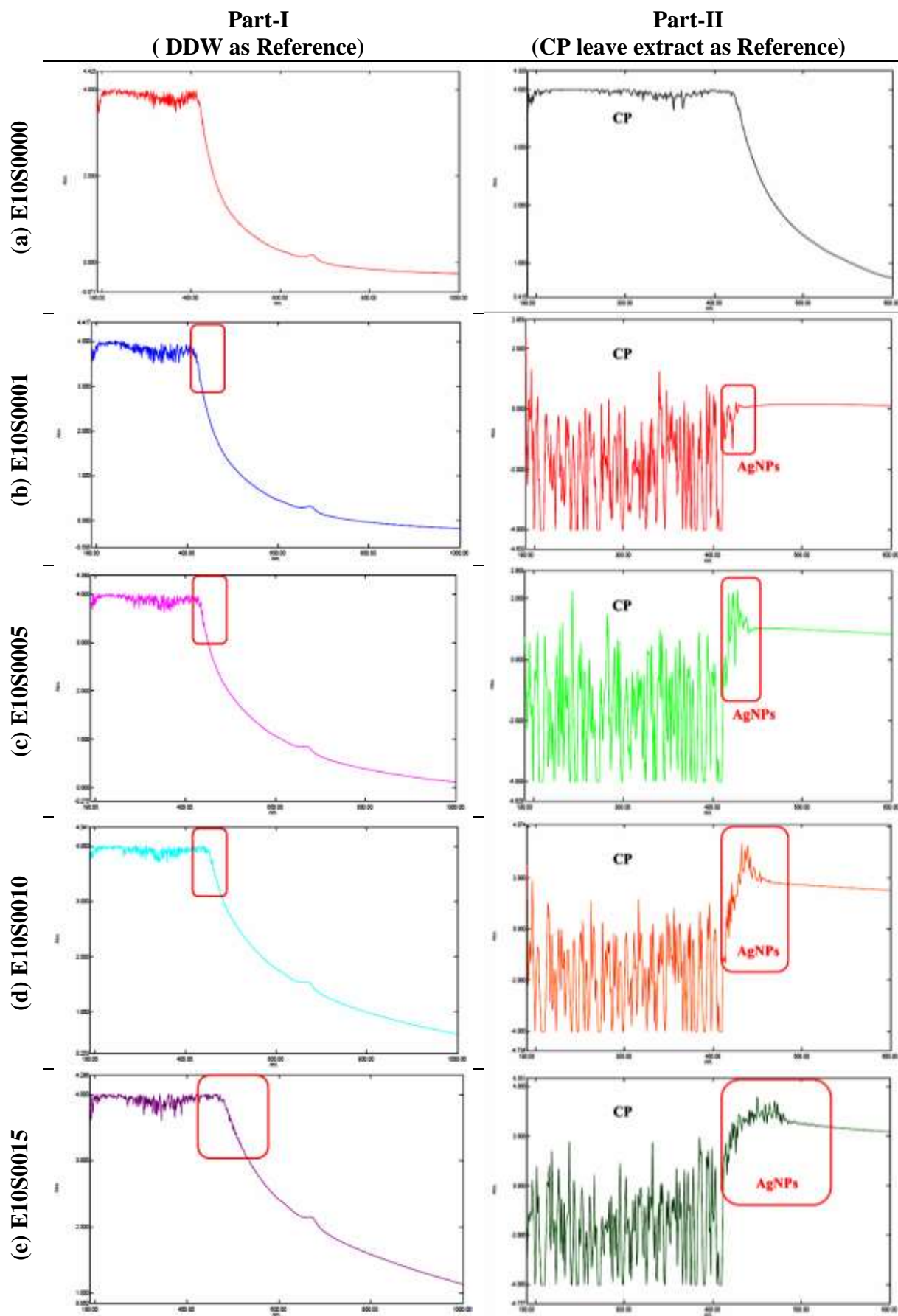


Figure 4.44: UV-Vis spectrum of the AgNPs colloidal solution in Set-II (a-e)

Figure 4.44 (a-e) illustrate the spectrums obtained in Part-II, by restricting the wavelength range to 190–600 nm. The sample E10S0000 [Figure 4.44 (a)] displayed identical spectrum being tested under the same test conditions to Part-I but with board and more intense peaks execution between narrowed range of 190–400 nm. The spectrum has shown a slanting down curve after 400nm and certified the absence of AgNO₃. The pigeon-holed UV spectrum in 190-400nm unrevealing presence of CP extract was same for all the colloidal solutions [E10S0001 to E10S0015], but thence after an elevating band width and intensity was noticed in direct relation to the rise in molarity of the AgNO₃ between 400–500 nm wavelength [Figure 4.44 (b-e)]. These peaks falling in 400-500nm wavelength of UV spectrum resembled to the plasmon resonance of AgNO₃ and characterized AgNPs in the colloidal [176,222].

The narrowest and least strong peak for the plasmon resonance of AgNO₃ (400–450 nm) was gone obviously on the account of colloidal solution E10S0001 synthesized with a very low concentration of AgNO₃ due to lowest UV absorption [Figure 4.44 (b)]. This behaviour demonstrated formation of the relatively miniscule AgNPs on interaction of less quantum of AgNO₃ with CP extract in the group [302]. Similarly, the widest and strongest peak for the plasmon resonance of AgNO₃ (400–450 nm) was gone obviously on the account of colloidal solution E10S0015 synthesized with a highest concentration of AgNO₃ due to highest UV absorption [Figures 4.44 (e)]. However, broadening of the peak beyond 500nm was also observed for the same substantiating phenomenon of bigger particles development on agglomeration of AgNPs. On the contrary second highest AgNPs holder sample E10S0010 displayed a narrow and more (sharp) intense peak with maximum absorption in the preferential wavelength region of 400–450 nm [Figures 4.44 (d)]. This limited broadness and higher strength of the absorbance peak has interpreted about the synthesis quality that it ensued with comparatively smaller-sized AgNPs but low quantum and without undergoing agglomeration [302].

4.3.2.2.3 Particle size analysis of AgNPs/CP colloidal solutions

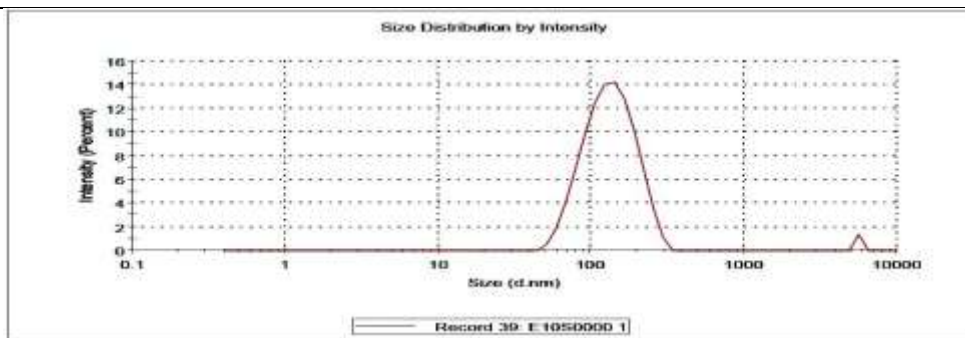
The DLS spectrum [Figure 4.45 (a)] of the colloidal solution E10S0000 (F1), composed of only CP leave extract has shown two peaks with an average particle size of 139.0 and 5560 nm, respectively. Even though the solution was formulated with only CP leave extract still intensity of its peak realized was 98.6%, because the second peak at 5560 nm representing presence of foreign matter has seized a very small but remaining 1.4% intensity out of hundred. This behaviour is usual for the colloidal being synthesised from green resource even with due precautions [114,162].

Table 4.12: Particle size distribution of the AgNPs colloidal solutions (Minor Set-II)

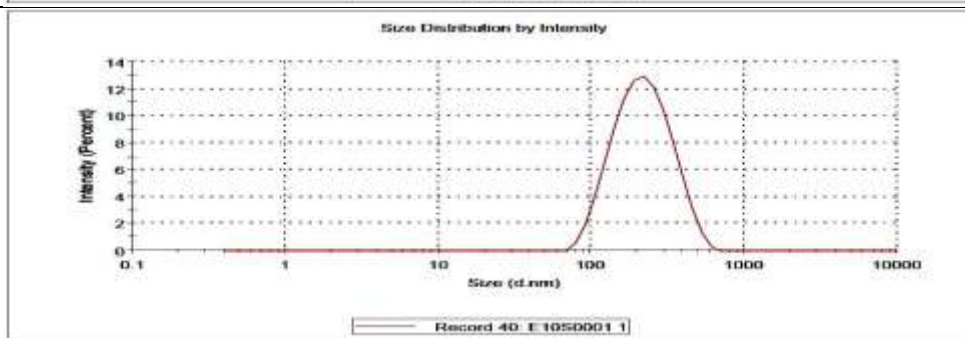
Sample Code	Particles size (d.nm)						Z-average (nm)	PDI	Distribution type
	Peak 1 (CP)		Peak 2 (AgNPs)		Peak 3 (Others/Misc.)				
	Size (d.nm)	% Intensity	Size (d.nm)	% Intensity	Size (d.nm)	% Intensity			
E10S0000	139.0	98.6	NA	NA	5560	1.4	138.4	0.343	Moderately polydisperse
E10S0001	232.5	100.0	0	0	0	0	177.5	0.225	Moderately polydisperse
E10S0005	183.7	95.7	0	0	5224	4.3	203.4	0.212	Moderately polydisperse
E10S0010	201.9	88.8	25.8	6.4	5019	4.8	163.4	0.254	Moderately polydisperse
E10S0015	186.7	87.5	22.6	10.4	4467	2.1	107.6	0.457	Broadly polydisperse

* d.nm = diameter in nanometer

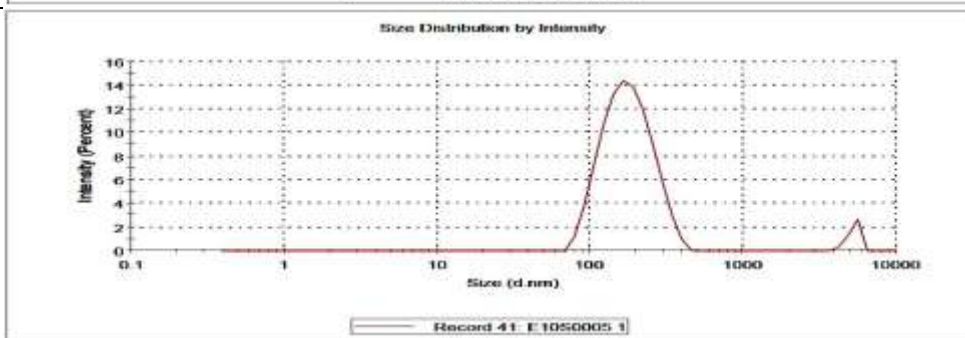
(a) E10S0000



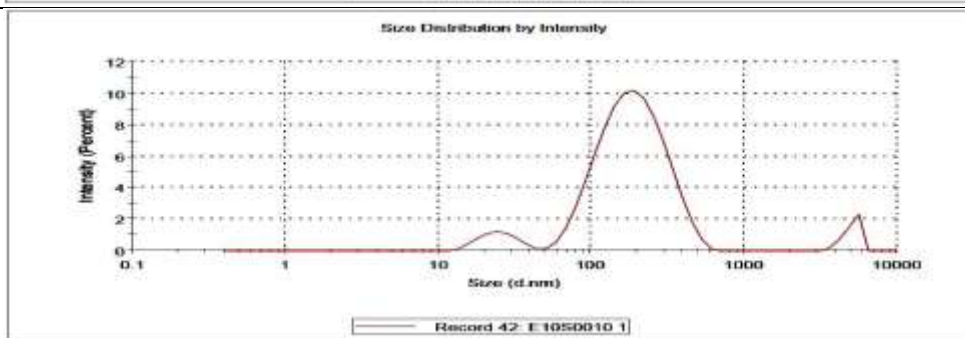
(b) E10S0001



(c) E10S0005



(d) E10S0010



(e) E10S0015

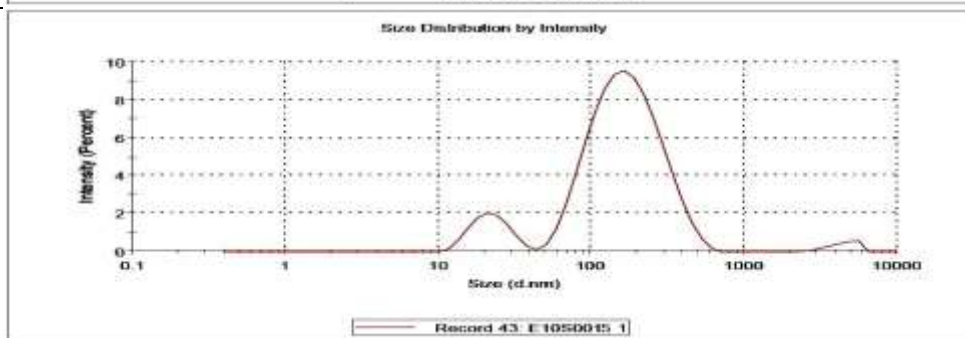


Figure 4.45: DLS spectrum for the particle size distribution of samples in Set-II (a–e)

The Z-average and PDI value of the colloidal solution observed are 138.4 nm and 0.343 respectively, and accordingly categorizing it as a moderately polydisperse type of distribution. These characteristic behaviours analyzed for the pure 10% CP leave extract provides strong ground in discriminating particular CP extract peak from all observed during spectrum analysis of AgNPs colloidal solution. Even deviation in Z-average and PDI values of the AgNPs colloidal from reference CP extract values distinguish extent of successful chemical interaction took place during the course of synthesis.

Figure 4.45 (b–e) illustrate the DLS spectrums and Table 4.12 shows particle size distribution for the minor set-II AgNPs colloidal solutions starting from E10S0001 to E10S0015. It can be noticed that the sample E10S0001 has illustrated single peak, E10S0005 has two peaks and rest two solutions: E10S0010 & E10S0015, have three peaks in their respective DLS spectrums. Further noting should be made about a single peak with 100% intensity for sample E10S0001 and the larger peak with 95.7% intensity for sample E10S0005 that they are going in good simulation with CP leave extract spectrum [Figure 4.45 (a-c)]. Even the second peak observed at 5224 d-nm is covering residual 4.3% intensity for the sample E10S0005 and no more falling in the characteristic region of AgNPs but rather lies in foreign element section. These analytical remarks are clearly substantiating failure of AgNPs formation at the selected very low AgNO_3 molarities and resulted in DLS spectrums almost identical to 10% CP extract.

It can be seen that the colloidal solutions E10S0010 and E10S0015 have executed AgNPs peaks with increased % intensity in relation to the concentration of AgNO_3 during the course of synthesis. The best AgNPs formation with the average particle size of 22.6 nm at the highest 10.4% intensity in the group has been reported for the sample E10S0015. Even, this favourable interaction has caused proportionate reduction in the size as well as intensity recorded for the CP leave extract and other foreign matter, also reflected from its lower Z-average value (107.6 nm). However, its PDI value recorded was 0.457; revealed that the colloidal has a broadly polydisperse type of nanoparticle distribution (\therefore PDI >0.4) which is qualitatively undesirable.

Conversely, the 'E10S0010 (F4)' AgNPs colloidal solution holding PDI value of 0.254 has validated occurrence of a moderately polydisperse type of nanoparticle distribution, an utmost necessary qualitative condition. Thereby, the 'E10S0010 (F4)' AgNPs colloidal solution finished closer to the E10S0015 with a formation of a bit bigger size nanoparticles

(25.8 nm) at comparatively lower intensity of 6.4% and having higher Z-average of 163.4 nm was regarded as an optimum qualitatively. Additionally, its synthesis included less quantum (10 mM) of the costliest participant AgNO_3 than the E10S0015 (15 mM) colloidal solution, sufficient enough to be advocated as an optimum at an economical front also.

4.3.2.2.4 Antibacterial assessment of the PV-AgNPs/CP composites

Figures 4.46 describe the antibacterial activity photographed for all the samples against both the bacterial cultures (i.e. SA and EC) at selected test intervals of 24, 48 and 72 hours.

The zone of inhibition (ZOI in mm) for all the PV-AgNPs/CP composite samples (F1-F5) mapped against both bacterial cultures (SA and EC) at selected three time intervals: 24 hours, 48 hours, and 72 hours are given in Table 4.13 and illustrated graphically in Figure 4.47.

Table 4.13: Zone of Inhibition (ZOI) in (mm) of various samples (Set-II)

Sample Code	Colloidal solution (Code)	Staphylococcus aureus (SA)			Escherichia coli (EC)		
		24 Hours	48 Hours	72 Hours	24 Hours	48 Hours	72 Hours
F1	E10S0000 [©]	18	15	15	20	19	19
F2	E10S0001	16	11	11	19	18	18
F3	E10S0005	19	16	16	20	18	18
F4	E10S0010	20	17	17	23	21	21
F5	E10S0015	19	17	17	21	20	20

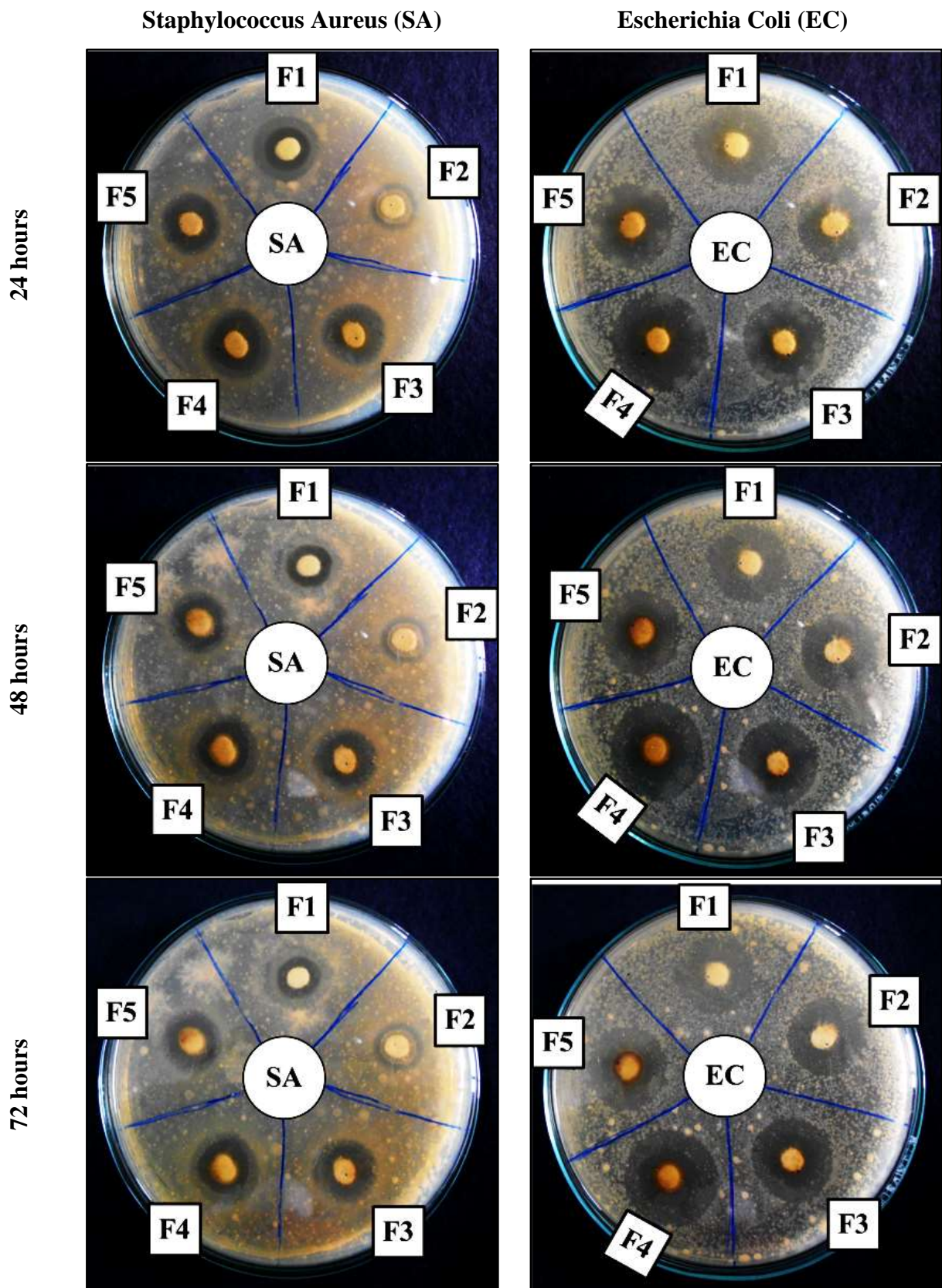


Figure 4.46: Antibacterial assessment (Set-II)

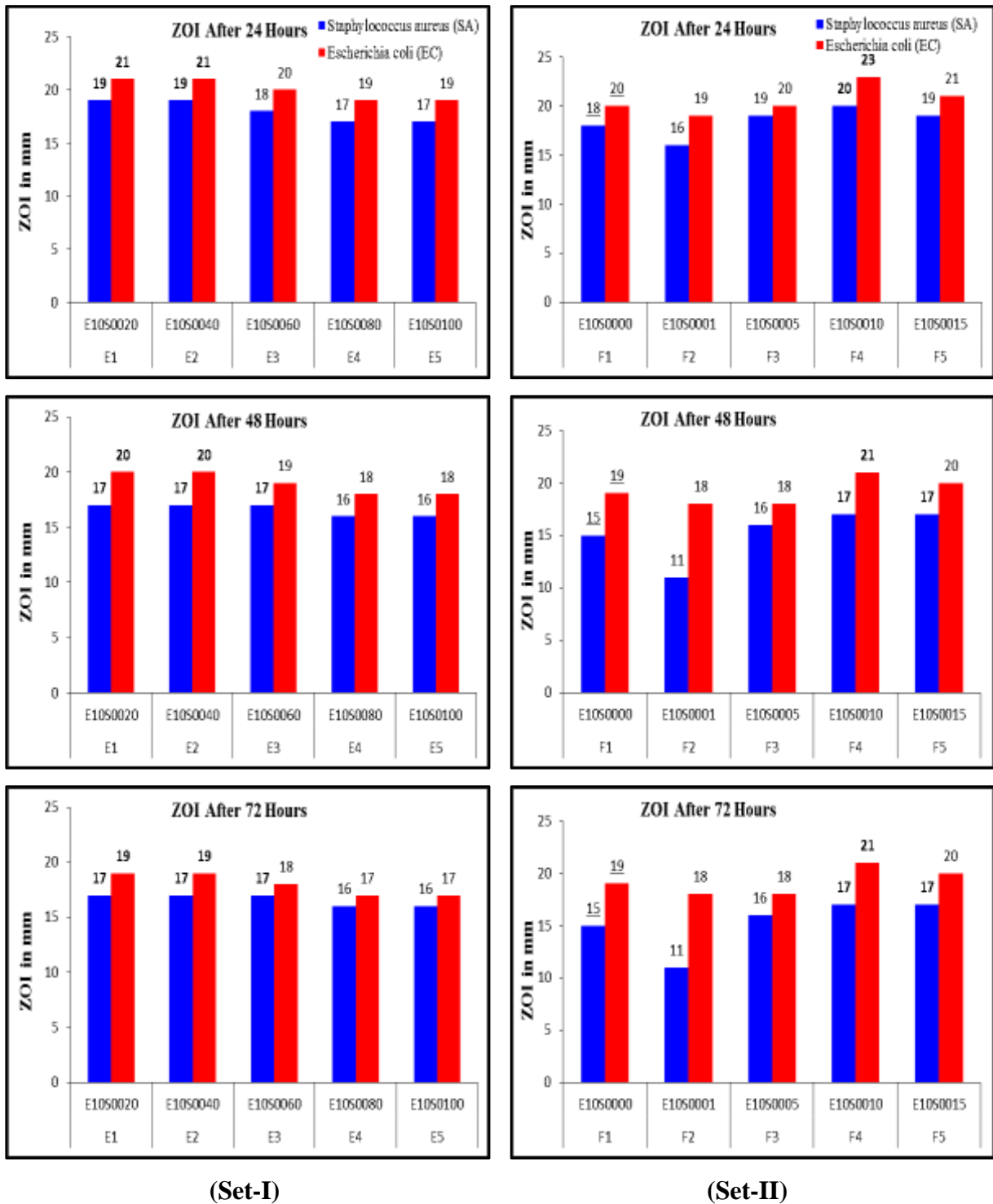


Figure 4.47: Zone of Inhibition (ZOI in mm) of all samples (Set-I & II)

It can be seen from the results that the efficacy and stability of the antibacterial activities mapped against gram-positive and gram-negative bacterium were get enhanced with increased amount of AgNO_3 in the colloidal, except sample F5 which has behaved differently. This adverse behaviour of sample F5 may be attributed to its broadly polydisperse type of nanoparticle distribution usually attained on agglomeration [Section 4.3.2.2.3].

The highest ZOI was registered on the account of sample F4 after first 24 hours against both the bacterium cultures. The ZOI values dropped by 3mm against SA and 2mm against EC after next 24 hours (48 hours observation) and thence after became constant (at 72 hours) but yet remain highest in the group, authenticated its better efficiency irrespective of time gap. These strong antibacterial capabilities of the sample F4 are attributed to the presence of the higher number of small size (25.8 nm) AgNPs without getting aggregated in a moderately polydisperse distribution as revealed from the particle size analysis results and supported by UV-VIS spectrum also [Section 4.3.2.2.2 & 4.3.2.2.3].

A drop in antibacterial inhibition after 24, 48, and 72 hours was observed similar to minor set-I experiments. No doubt, drop in the ZOI value recorded against gram-positive bacteria (SA) with respect to time lag has been increased from 1mm - 2mm scale to 2mm - 5 mm scale, but 1mm - 2mm scale drop was remained identical against gram-negative bacteria (EC) (Table 4.17 and Table 4.13). This big decline in ZOI observed for Sample F2 (E10S0001) for the lowest concentration of functional AgNO_3 group is usual.

It should be noted that sample F4 (E10S0010) worked out with two times lower AgNO_3 molarity of set-I best sample E10S0020, has shown better antibacterial performance against gram-negative bacteria (EC) and equivalent against gram-positive bacteria (SA). Such, a boosted antibacterial activities of AgNPs colloidal treated PV composite can only be earned by the higher functional specific surface availed from a large number of nanoparticles [46,48]. These observations substantiate the best qualitative as well as quantitative antibacterial efficacy of sample F4 amongst all investigated in both the minor sets.

It can be seen that Sample F1 (E10S0000[®]), which was produced only from CP leave extract has shown better ZOI value than lowest AgNO_3 molarity based colloidal solution E10S0001 and very close to second lowest AgNO_3 molarity colloidal solution E10S0005 in the set-II against both the bacterial cultures. A marginal drop in ZOI value of 3 mm and 1 mm against SA and EC respectively, were observed in its antibacterial activities after 48 hours. There was no change in ZOI value was noticed for either of bacterial cultures during

48 hours to 72 hours exposure (Table 4.13). Thus, medicinally enriched CP leave extract [201], selected as an innovative green medium for capping and reducing AgNPs in the present study itself was emerged out as a self-sufficient antibacterial agent along with good stability against both bacterial cultures up to 72 hours.

According to these findings, CP leave extract which is well recognized from age-old medicinal therapy has contributed positively in enhancing antibacterial capacity of innovative green-way synthesized AgNPs and provided a platform to set out optimum antibacterial activities at an economical rate due to lower level AgNO₃ consumption. Thereby, samples F4 (E10S0010), emerged out as an optimum new green-way synthesized colloidal and F1 (E10S0000[®]) for defining CP extract contribution in its performance (Figure 4.47), were selected for further investigation with respect to targeted bio medical application material.

4.3.2.2.5 MTT assay cytotoxicity test of AgNPs/CP colloidal solution and pure AgNO₃

The amount of toxicity caused in cells usually determines the rate of success for any antibacterial drug in medical/clinical usage. Thereby, the cytotoxicity of green synthesised AgNPs/CP colloidal solution and pure AgNO₃ against Hep-G2 epithelial cell line was investigated using the MTT assay in the similar manner to the major trial. The green synthesised AgNPs/CP colloidal solutions (as mentioned before in chapter-III, Section 3.3.2.2.1) were tested against the toxicity of pure AgNO₃ and positive control of 2,4-dinitrophenol produced in DMSO (Figure 4.48).

The viability (non-toxic behaviour) of the cell line casted is substantially superior for prepared AgNPs/CP colloidal solutions compared to pure AgNO₃ as well as the value of 24% noted for CP pure latex (Figure 4.48 & 4.27). A good cell viability of 92% was obtained at the selected 10% concentration of CP leave extract (E10 extract) for AgNPs synthesis throughout the study. It is interesting to note that toxic nature of the colloidal gets declined with the decreased concentration (molarity in mM) of the AgNO₃ for a fixed 10% CP concentration in the AgNPs/CP colloidal solution, i.e. E10S0001 (90%), E10S0005 (88%), E10S0010 (84%), E10S0015 (80%), and E10S0020 (73%) respectively. This is customary because of increased sharing of toxic element AgNO₃ in the course of colloidal synthesis [305].

Results for the viability of the cell line mapped against pure AgNO_3 , have gone in line with AgNPs, and shown amplified toxicity with increase in its concentration, viz; S0001 (73%), S0005 (67%), S0010 (61%), S0015 (57%), and S0020 (49%). Nevertheless, the toxicity has been reduced on green synthesis of AgNO_3 with CP leave extract rather than treating individual traits (AgNO_3 & CP extract) in their root forms for the test at all the selected molarity values (Figure 4.48). This condensed toxicity is mainly attributed to the drop in AgNO_3 & CP leave extract concentrations on transforming to polydisperse colloidal solution in proportion to the AgNO_3 add-on values for the fixed 10% CP leave extract [206].

Consequently, the cell line viability point of view sample E10S0010 with 84% value have sustained superiority on close finisher sample E10S0015 with 80% value, and ensured better safety for the wearer using next to the skin.

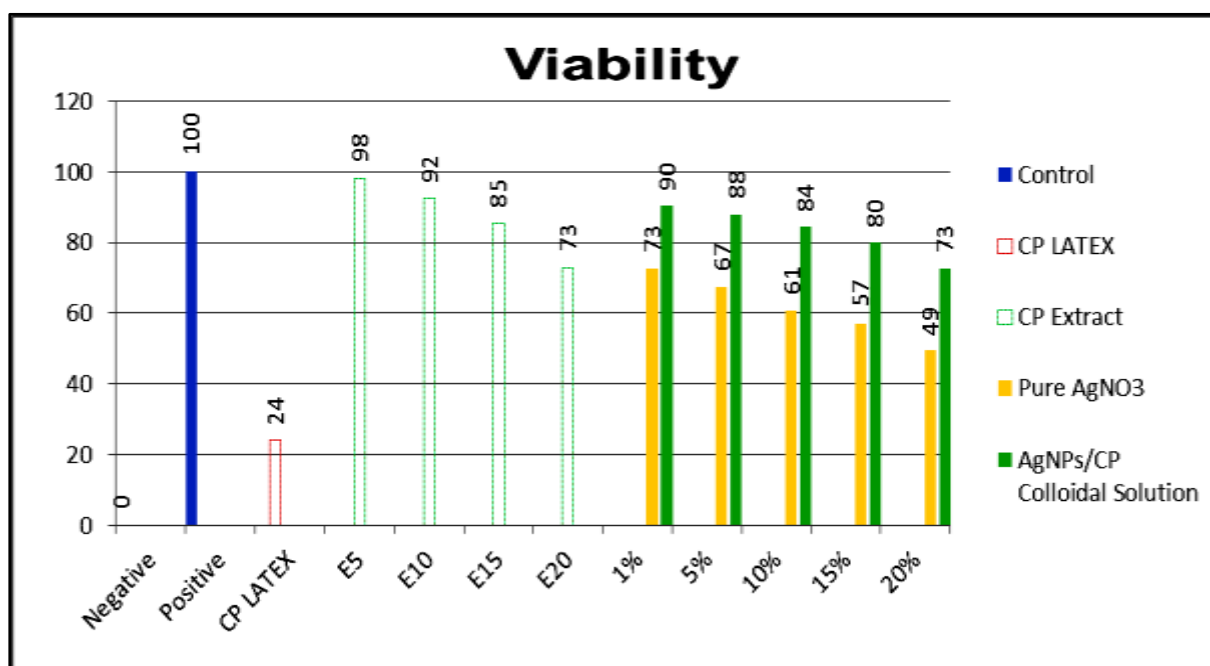


Figure 4.48: Cytotoxicity effects of pure AgNO_3 and AgNPs colloidal solutions

4.3.2.2.6 GC-MS analysis of CP leaves extract

Table 4.14 shows the major peaks of phytochemical constituents found during GC-MS analysis, along with retention time (RT) and % area. Figure 4.51 depicts the GC-MS chromatogram of CP leave extract. Table 4.15 to 4.20 lists the phytochemical constituents found in CP leave extract at 9.41, 18.705, 19.78, 20.33, 25.81, and 39.29 RT, whereas Figure 4.52 to 4.57 shows the mass spectra for particular RT respectively.

As seen from the Table 4.14, compounds at 20.33 RT have the highest % area (31.94%), followed by compounds at 18.71, 19.78, 39.29, 25.813, and 9.411 RT, which have 25.23%, 15.40%, 10.14%, 8.93%, and 8.37% area respectively. The peak showing maximum % area at RT 20.33, 18.71, and 19.78 in the chromatogram, revealed the presence of phytochemical compounds such as terpenoids, flavonoids, cardenolides, alkaloids, phenolics, etc.

Table 4.14:

GC-MS retention time (RT) and % area of the phytoconstituents major peaks

Peak#	RT	Area	Area %
1	9.411	649,05,500.00	8.37
2	18.705	1957,03,168.00	25.23
3	19.780	1194,74,688.00	15.40
4	20.330	2477,43,040.00	31.94
5	25.813	692,47,952.00	8.93
6	39.298	786,32,176.00	10.14

The peak at RT 18.07 in GC–MS analysis (Table 4.16 and Figure 4.51), revealed the presence of N-Decanoic Acid ($C_{10}H_{20}O_2$), have a molecular weight of 172. The compound identified is a saturated fatty acid. It has been found that CP extract includes seven different forms of saturated fatty acids and eleven different types of unsaturated fatty acids [306]. N-Decanoic Acid ($C_{10}H_{20}O_2$), which was discovered in the current work, has also been reported by Khanzada et al. (2008) from CP [306]. This saturated fatty acid is the main constituent responsible for antibacterial activity [293]. Figure 4.49 depicts the chemical structure of N-Decanoic Acid.

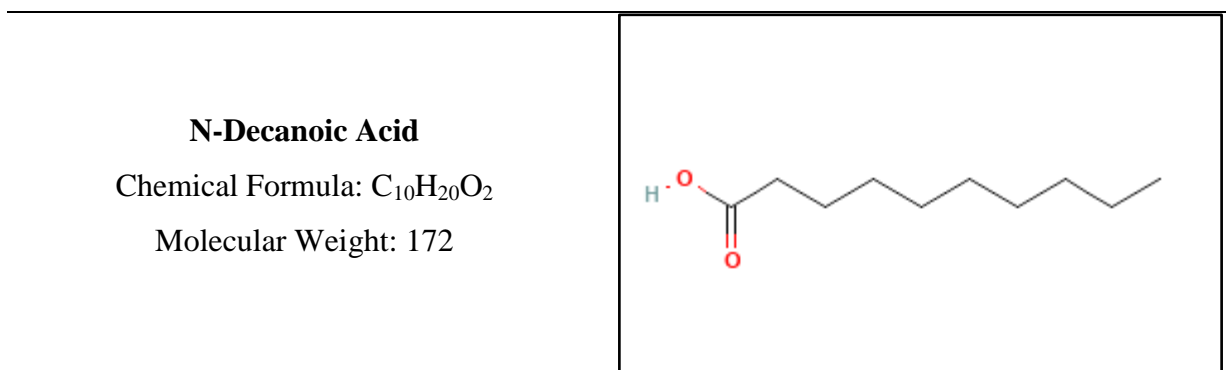


Figure 4.49: Structure of the antibacterial compound N-Decanoic Acid [307]

This analysis also revealed the presence of the flavonoid glycoside [D-Glucopyranoside, 4-O-Decyl-, ($C_{16}H_{32}O_6$)] at 25.23% area and 18.07 RT, having a molecular weight of 320, which is likewise responsible for the antimicrobial activity [308]. Previous investigations about the CP plants reported that the flavonoid glycoside D-Glucopyranoside, 4-O-Decyl- is existing in the aerial parts of the plant [309]. The chemical structure of flavonoid glycosides D-Glucopyranoside, 4-O-Decyl- is shown in Figure 4.50.

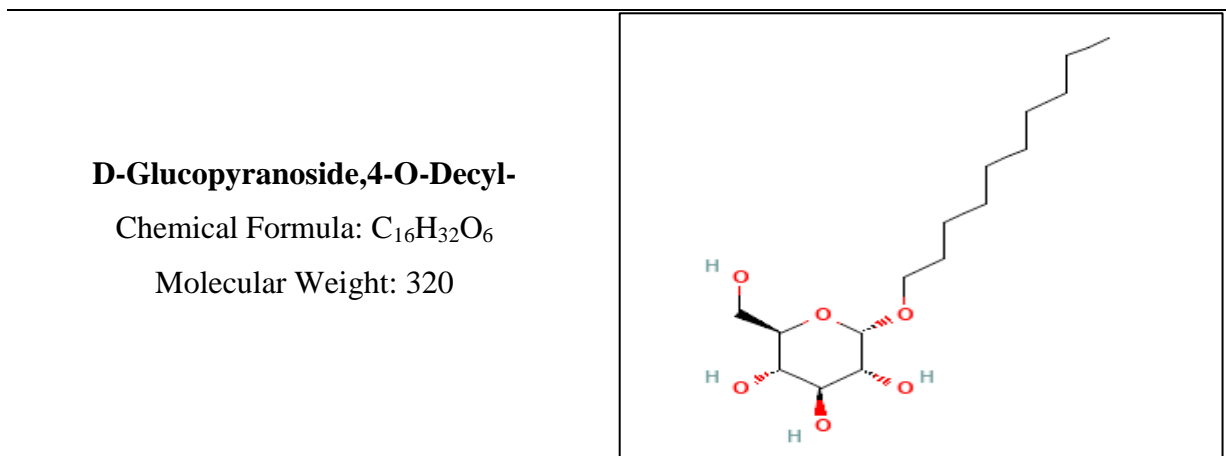


Figure 4.50: Structure of the antibacterial compound D-Glucopyranoside,4-O-Decyl- [310]

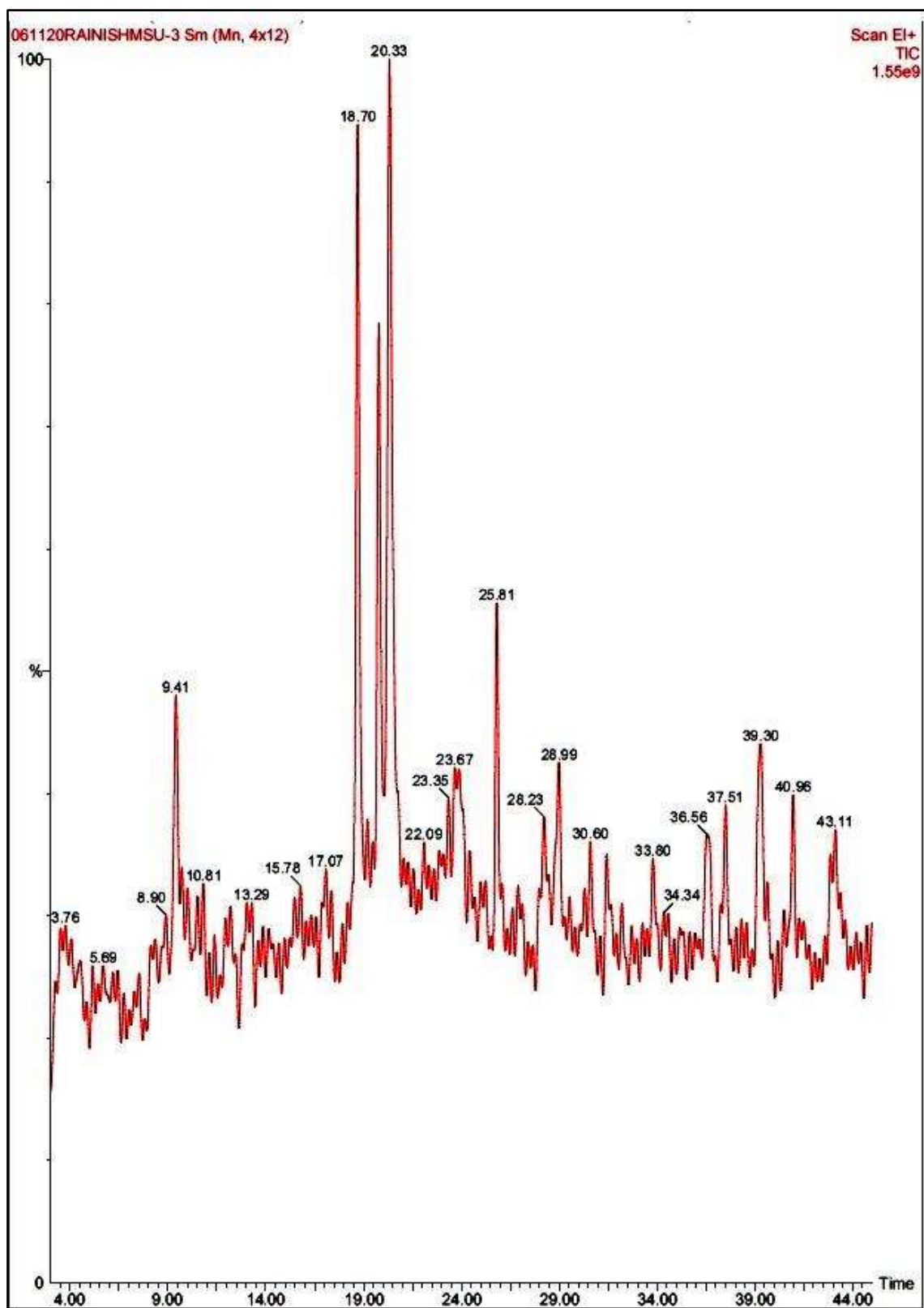


Figure 4.51: Chromatogram of CP leaf extract

Table 4.15: Phytochemical constituents present at 9.4 RT

Hit	Compound Name	M.W.	Formula
1	ACETONITRILE, 2,2'-IMINOBIS-	95	C ₄ H ₅ N ₃
2	9-BORABICYCLO[3.3.1]NONANE, 9-METHYL-	136	C ₉ H ₁₇ B
3	8-NONENE-1-NITRILE	137	C ₉ H ₁₅ N
4	9-DECENE-1-NITRILE	151	C ₁₀ H ₁₇ N
5	1-(PYRROLIDIN-1-YL)CYCLOPENTANE-1-CARBONITRILE	164	C ₁₀ H ₁₆ N ₂
6	PROPANENITRILE, 2,2'-AZOBIS[2-METHYL-	164	C ₈ H ₁₂ N ₄
7	2-CYCLOOCTENE-1-CARBOXYLIC ACID	154	C ₉ H ₁₄ O ₂
8	ISO-BORNYL METHACRYLATE	222	C ₁₄ H ₂₂ O ₂
9	[1,1'-BICYCLOPENTYL]-2-OL	154	C ₁₀ H ₁₈ O
10	10-UNDECENENITRILE	165	C ₁₁ H ₁₉ N
11	.BETA.-MYRCENE	136	C ₁₀ H ₁₆
12	[1,1'-BICYCLOPENTYL]-2-OL	154	C ₁₀ H ₁₈ O
13	3-BUTENOIC ACID, 3-METHYL-, (3-METHYL-3-BUTENYL) ESTER	168	C ₁₀ H ₁₆ O ₂
14	4-METHYL-6-NITRO-7-OXO-4,7-DIHYDRO-1,2,4-TRIAZOLO[5,1-C][1,2,4]TRIAZINE	196	C ₅ H ₄ O ₃ N ₆
15	ISOBORNEOL, TRIFLUOROACETATE (ESTER)	250	C ₁₂ H ₁₇ O ₂ F ₃
16	(2S)-BORNANE-10,2-SULTAM	215	C ₁₀ H ₁₇ O ₂ NS
17	BICYCLO[2.2.1]HEPTANE-2,3-DIONE, 1,7,7-TRIMETHYL-, 3-OXIME	181	C ₁₀ H ₁₅ O ₂ N
18	2-METHYL-3-PROPYLPYRAZINE	136	C ₈ H ₁₂ N ₂
19	2H-INDEN-2-ONE, 1,3,3A,4,5,7A-HEXAHYDRO-, TRANS-	136	C ₉ H ₁₂ O

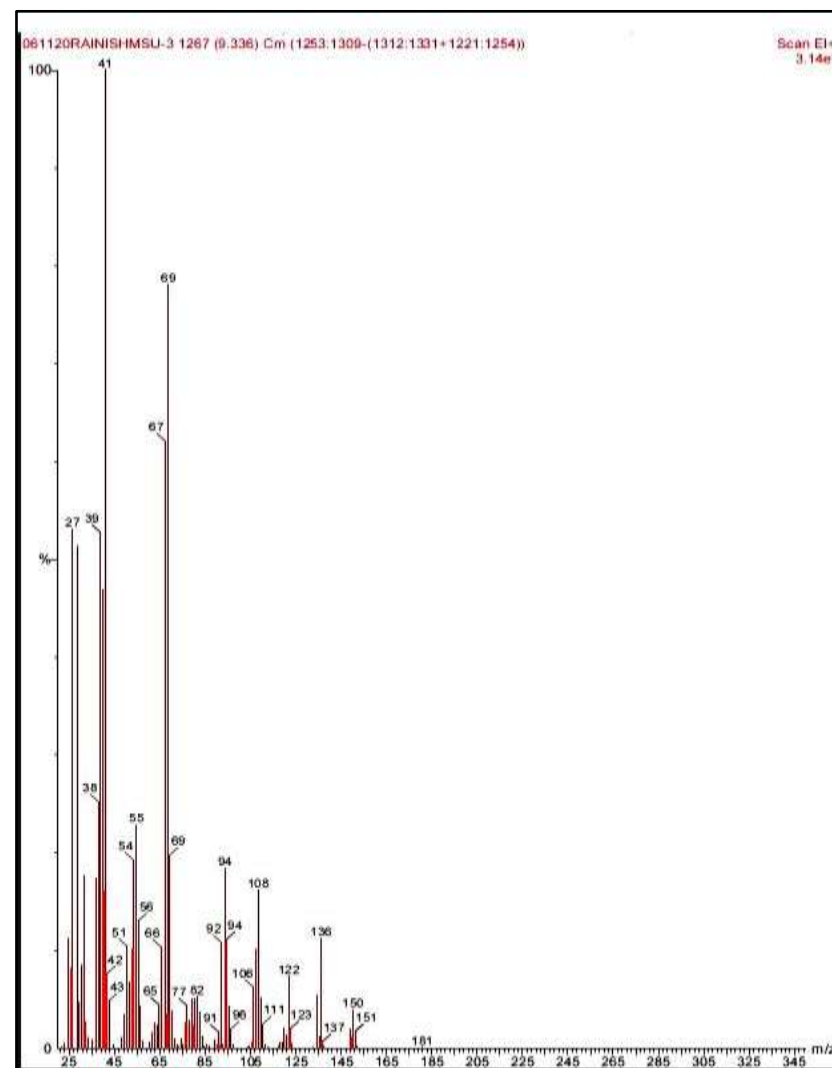
**Figure 4.52: Mass spectra of CP leave extract at 9.4 RT**

Table 4.16: Phytochemical constituents present at 18.71 RT

Hit	Compound Name	M.W.	Formula
1	NONADECANOIC ACID	298	C ₁₉ H ₃₈ O ₂
2	N-HEXADECANOIC ACID	256	C ₁₆ H ₃₂ O ₂
3	N-DECANOIC ACID	172	C ₁₀ H ₂₀ O ₂
4	N-HEXADECANOIC ACID	256	C ₁₆ H ₃₂ O ₂
5	EICOSANOIC ACID	312	C ₂₀ H ₄₀ O ₂
6	OCTADECANOIC ACID	284	C ₁₈ H ₃₆ O ₂
7	PENTADECANOIC ACID	242	C ₁₅ H ₃₀ O ₂
8	NONADECANOIC ACID	298	C ₁₉ H ₃₈ O ₂
9	UNDECANOIC ACID	186	C ₁₁ H ₂₂ O ₂
10	HEPTADECANOIC ACID	270	C ₁₇ H ₃₄ O ₂
11	UNDECANOIC ACID	186	C ₁₁ H ₂₂ O ₂
12	OCTADECANOIC ACID	284	C ₁₈ H ₃₆ O ₂
13	TRIDECANOIC ACID	214	C ₁₃ H ₂₆ O ₂
14	EICOSANOIC ACID	312	C ₂₀ H ₄₀ O ₂
15	PENTADECANOIC ACID	242	C ₁₅ H ₃₀ O ₂
16	D-GLUCOPYRANOSIDE, 4-O-DECYL-	320	C ₁₆ H ₃₂ O ₆
17	DOCOSANOIC ACID	340	C ₂₂ H ₄₄ O ₂
18	UNDECANOIC ACID	186	C ₁₁ H ₂₂ O ₂
19	N-CAPRIC ACID ISOPROPYL ESTER	214	C ₁₃ H ₂₆ O ₂

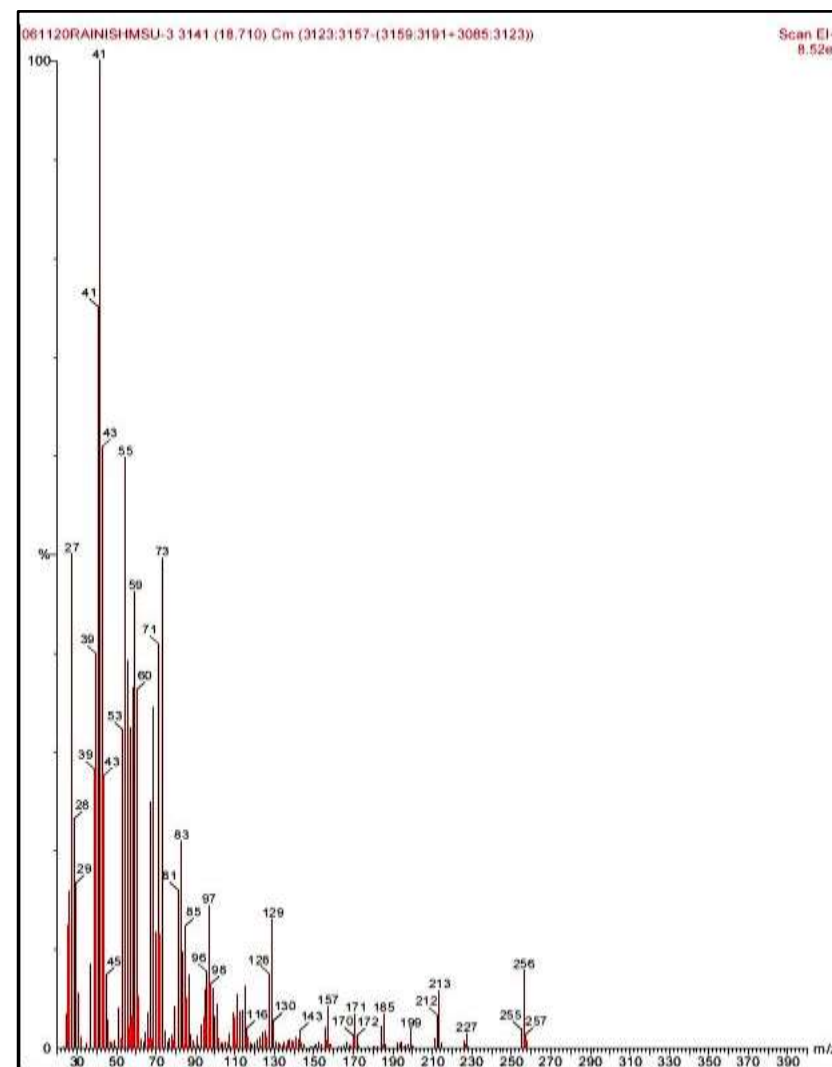


Figure 4.53: Mass spectra of CP leave extract at 18.71 RT

Table 4.17: Phytochemical constituents present at 19.78 RT

Hit	Compound Name	M.W.	Formula
1	2-METHYL-6-METHYLENE-OCTA-1,7-DIEN-3-OL	152	C ₁₀ H ₁₆ O
2	3,7,11,15-TETRAMETHYL-2-HEXADECEN-1-OL	296	C ₂₀ H ₄₀ O
3	PHYTOL	296	C ₂₀ H ₄₀ O
4	CITRONELLOL	156	C ₁₀ H ₂₀ O
5	2,11-DODECADIENE, 4-ACETOXY-	224	C ₁₄ H ₂₄ O ₂
6	1,7-OCTADIENE-3,6-DIOL, 2,6-DIMETHYL-	170	C ₁₀ H ₁₈ O ₂
7	CITRONELLYL BUTYRATE	226	C ₁₄ H ₂₆ O ₂
8	2,6,10-TRIMETHYLUUNDECA-1,3-DIENE	194	C ₁₄ H ₂₆
9	10-METHYL-E-11-TRIDECE-1-OL ACETATE	254	C ₁₆ H ₃₀ O ₂
10	7-DECEN-1-OL ACETATE	198	C ₁₂ H ₂₂ O ₂
11	TETRACOSANAL	352	C ₂₄ H ₄₈ O
12	OXIRANE, TETRADECYL-	240	C ₁₆ H ₃₂ O
13	OXIRANE, DECYL-	184	C ₁₂ H ₂₄ O
14	2-OCTEN-1-OL, 3,7-DIMETHYL-	156	C ₁₀ H ₂₀ O

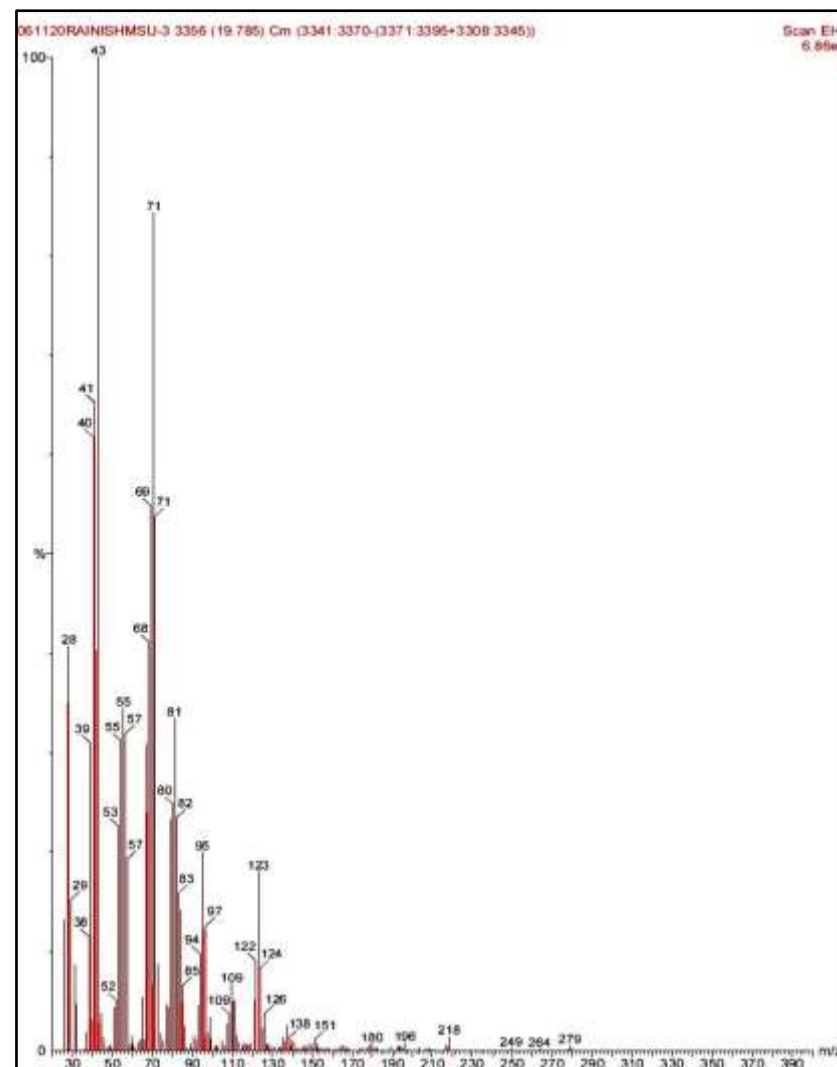
**Figure 4.54: Mass spectra of CP leaf extract at 19.78 RT**

Table 4.18: Phytochemical constituents present at 20.33 RT

Hit	Compound Name	M.W.	Formula
1	1,4,9-DECATRIENE, (E)-	136	C ₁₀ H ₁₆
2	1,3(Z),13-TETRADECATRIENE	192	C ₁₄ H ₂₄
3	PENTANAL, 5-(METHYLENECYCLOPROPYL)-	138	C ₉ H ₁₄ O
4	10-UNDECYN-1-OL	168	C ₁₁ H ₂₀ O
5	10-DODECYN-1-OL	182	C ₁₂ H ₂₂ O
6	8-NONYNOIC ACID	154	C ₉ H ₁₄ O ₂
7	7-OXABICYCLO[4.1.0]HEPTANE, 3-OXIRANYL-	140	C ₈ H ₁₂ O ₂
8	8-HEPTADECYNE, 1-BROMO-	314	C ₁₇ H ₃₁ Br
9	CYCLOPROPANE, (3-CHLOROPROPYL)METHYLENE-	130	C ₇ H ₁₁ Cl
10	9-OCTADECYNOIC ACID	280	C ₁₈ H ₃₂ O ₂
11	13-TETRADECE-11-YN-1-OL	208	C ₁₄ H ₂₄ O
12	9,12-OCTADECADIENOIC ACID, METHYL ESTER, (E,E)-	294	C ₁₉ H ₃₄ O ₂
13	10-UNDECYN-1-OL	168	C ₁₁ H ₂₀ O
14	11-TRIDECYN-1-OL	196	C ₁₃ H ₂₄ O
15	9,12-OCTADECADIEN-1-OL, (Z,Z)-	266	C ₁₈ H ₃₄ O
16	2-NONYNE	124	C ₉ H ₁₆
17	SPIROPENTANE, BUTYL-	124	C ₉ H ₁₆
18	7-OXABICYCLO[4.1.0]HEPTANE, 2-METHYLENE-	110	C ₇ H ₁₀ O
19	(Z)6,(Z)9-PENTADECADIEN-1-OL	224	C ₁₅ H ₂₈ O

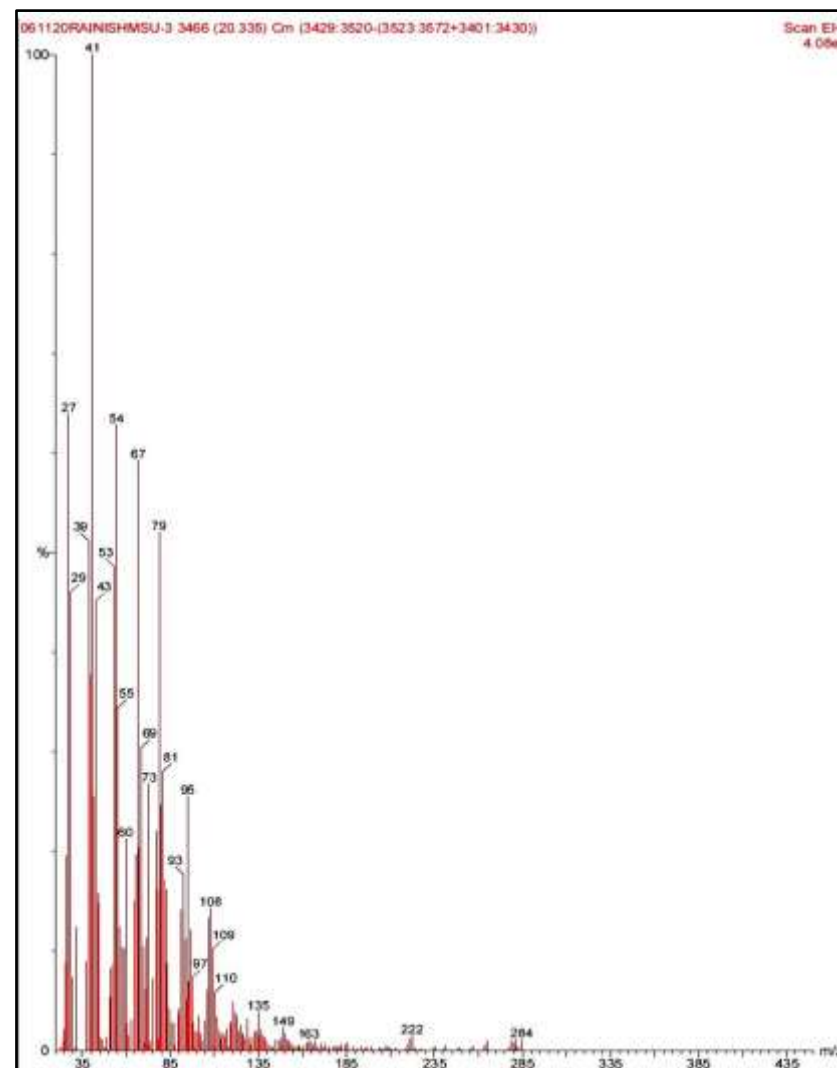
**Figure 4.55: Mass spectra of CP leave extract at 20.33 RT**

Table 4.19: Phytochemical constituents present at 25.81 RT

Hit	Compound Name	M.W.	Formula
1	(3E,7E)-4,8,12-TRIMETHYLTRIDECA-1,3,7,11-TETRAENE	218	C ₁₆ H ₂₆
2	SQUALENE	410	C ₃₀ H ₅₀
3	SUPRAENE	410	C ₃₀ H ₅₀
4	1-(3,5-DINITROPHENOXY)-3,7,11-TRIMETHYL-DODECA-2,6,10-TRIENE	388	C ₂₁ H ₂₈ O ₅ N ₂
5	3,7,11-TRIDECATRIENENITRILE, 4,8,12-TRIMETHYL-	231	C ₁₆ H ₂₅ N
6	SUPRAENE	410	C ₃₀ H ₅₀
7	2,6,10-DODECATRIEN-1-OL, 3,7,11-TRIMETHYL-	222	C ₁₅ H ₂₆ O
8	7,11-DIMETHYLDODECA-2,6,10-TRIEN-1-OL	208	C ₁₄ H ₂₄ O
9	2-BROMOMETHYL-1-ISOPROPENYL-3-METHYL-CYCLOPENTANE	216	C ₁₀ H ₁₇ Br
10	SQUALENE	410	C ₃₀ H ₅₀
11	(E,E)-7,11,15-TRIMETHYL-3-METHYLENE-HEXADECA-1,6,10,14-TETRAENE	272	C ₂₀ H ₃₂
12	4,8,12-TETRADECATRIENENITRILE, 5,9,13-TRIMETHYL-	245	C ₁₇ H ₂₇ N
13	CARBONIC ACID, METHYL ESTER, [(E,E)-3,7,11-TRIMETHYL-2,6,10-DODECATRIEN-1	280	C ₁₇ H ₂₈ O ₃
14	4,9,13,17-TETRAMETHYL-4,8,12,16-OCTADECATETRAENAL	316	C ₂₂ H ₃₆ O
15	DOCOSA-2,6,10,14,18-PENTAEN-22-AL, 2,6,10,15,18-PENTAMETHYL-, ALL-TRANS	384	C ₂₇ H ₄₄ O
16	6,10,14-HEXADECATRIEN-1-OL, 3,7,11,15-TETRAMETHYL-, [R-(E,E)]-	292	C ₂₀ H ₃₆ O

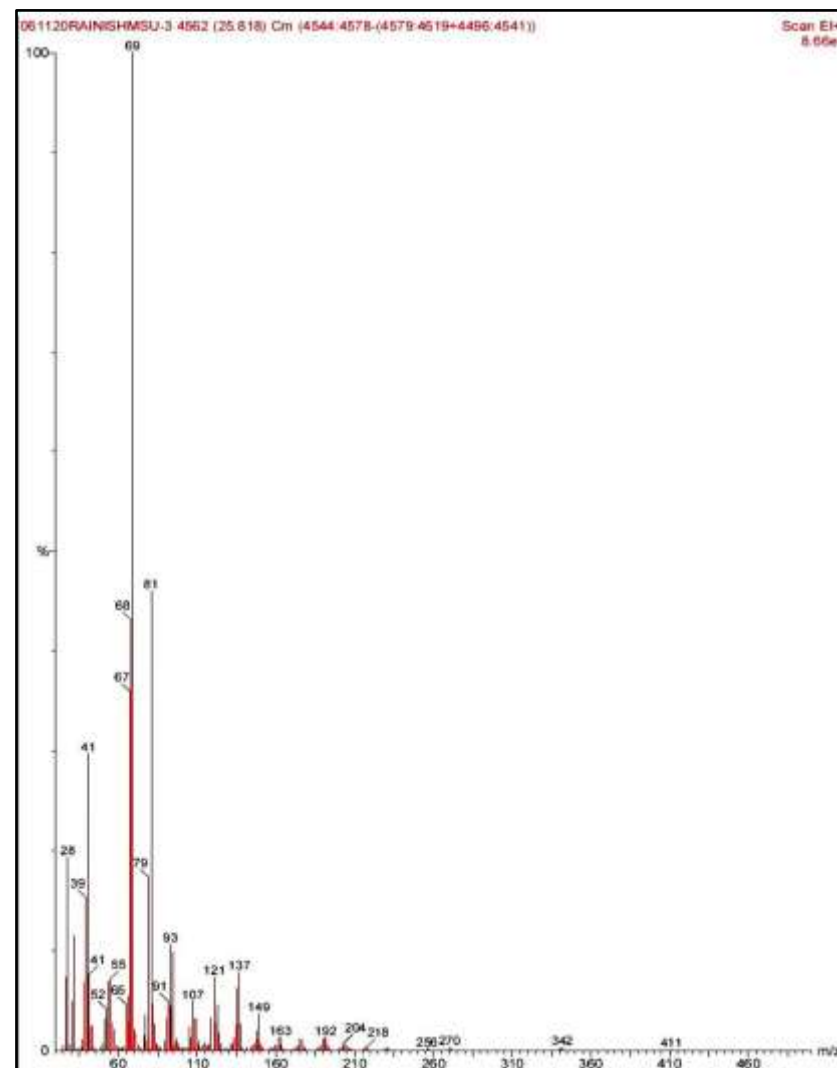
**Figure 4.56: Mass spectra of CP leaf extract at 25.81 RT**

Table 4.20: Phytochemical constituents present at 39.29 RT

Hit	Compound Name	M.W.	Formula
1	.ALPHA.-AMYRIN	426	C ₃₀ H ₅₀ O
2	24-NOROLEANA-3,12-DIENE	394	C ₂₉ H ₄₆
3	OLEAN-12-EN-3-OL, ACETATE, (3.BETA.)-	468	C ₃₂ H ₅₂ O ₂
4	24-NORURSA-3,12-DIENE	394	C ₂₉ H ₄₆
5	.BETA.-AMYRIN	426	C ₃₀ H ₅₀ O
6	.BETA.-AMYRONE	424	C ₃₀ H ₄₈ O
7	URS-12-EN-3-OL, ACETATE, (3.BETA.)-	468	C ₃₂ H ₅₂ O ₂
8	URS-12-EN-24-OIC ACID, 3-OXO-, METHYL ESTER, (+)-	468	C ₃₁ H ₄₈ O ₃
9	4,4,6A,6B,8A,11,12,14B-OCTAMETHYL-1,4,4A,5,6,6A,6B,7,8,8A,9,10,11,12,12A,14,14A,	424	C ₃₀ H ₄₈ O
10	7-OXABICYCLO[4.1.0]HEPTANE, 2,2,6-TRIMETHYL-1-(3-METHYL-1,3-BUTADIENYL)-5-	218	C ₁₅ H ₂₂ O
11	1H-BENZOCYCLOHEPTENE, 2,4A,5,6,7,8,9,9A-OCTAHYDRO-3,5,5-TRIMETHYL-9-ME	204	C ₁₅ H ₂₄
12	URS-12-EN-3-OL, ACETATE, (3.BETA.)-	468	C ₃₂ H ₅₂ O ₂
13	6-ISOPROPENYL-4,8A-DIMETHYL-4A,5,6,7,8,8A-HEXAHYDRO-1H-NAPHTHALEN-2-O	218	C ₁₅ H ₂₂ O
14	BETULIN	442	C ₃₀ H ₅₀ O ₂
	2,3,3-TRIMETHYL-2-(3-METHYLBUTA-1,3-DIENYL)-6-METHYLENECYCLOHEXANONE	218	C ₁₅ H ₂₂ O
16	HIBAENE	272	C ₂₀ H ₃₂
17	AZULENE, 1,2,3,3A,4,5,6,7-OCTAHYDRO-1,4-DIMETHYL-7-(1-METHYLETHENYL)-, [1R	204	C ₁₅ H ₂₄

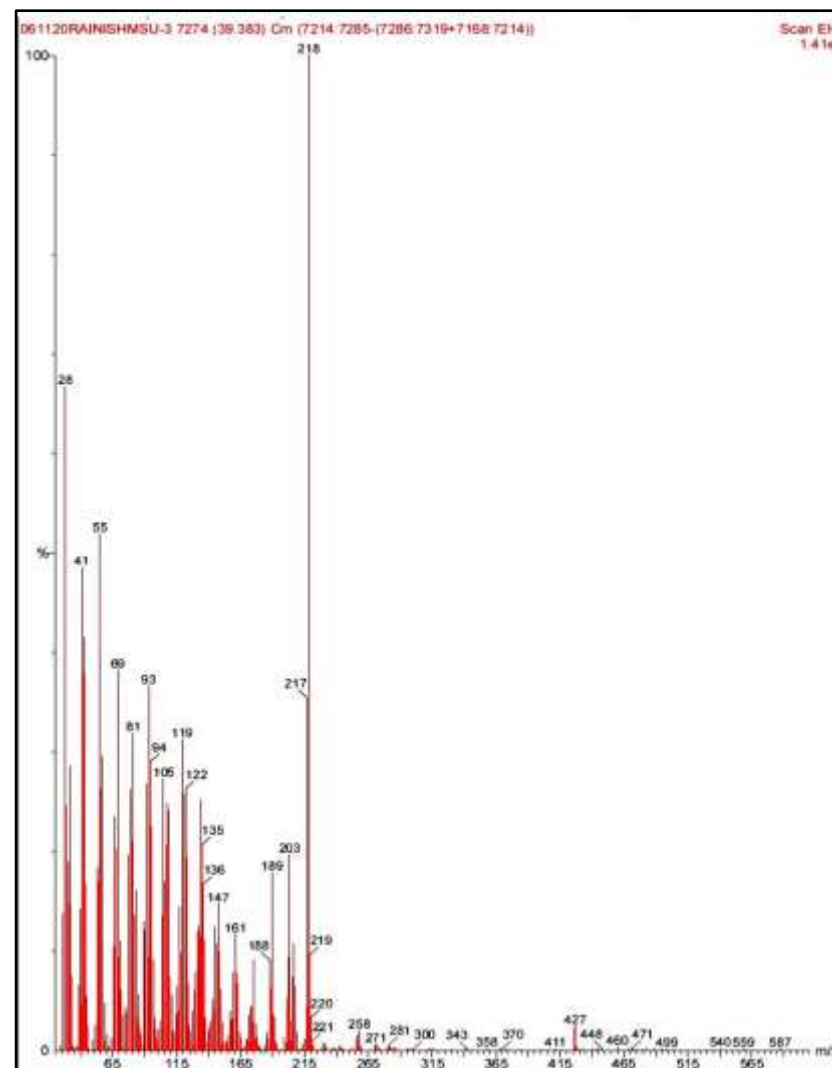


Figure 4.57: Mass spectra of CP leaf extract at 39.29 RT

By various investigators, it has been reported that phytochemicals were responsible for the inhibition of bacteria growth [292,311-314]. According to Sodipo et al. [312], tannins inhibit the growth of microbes by rendering beneficial proteins inaccessible to the organism and facilitating the precipitation of microbial protein. In separate studies, Ogbulie et al. [313], and Banso [292], discovered that phytochemicals had antibacterial action against a variety of microbes. Plant extracts have been shown to exhibit antibacterial activity against both gram-positive and gram-negative bacteria [314]. This can be easily seen from the antibacterial test reports for CP extract (Table 4.9 and Table 4.13)

Many studies, on the other hand, have indicated that phytochemicals are equally responsible for the reduction and capping of nanoparticles [1,141,277]. According to Sharma et al., phytochemicals fulfil the combined roles of capping agent and reducing agent in green synthesis; they are generally present in the natural components used so far. Hoag et al. [315], discovered that polyphenols are the active components in the plant extract, had both reducing and capping agents properties.

Proteins and carbohydrates are significant elements of plant extracts that function as reducing agents and are responsible for the creation of MNPs (Metal Nanoparticles) and metal ion reduction, according to Richardson et al. [316]. Shafey Asmaa et al. [317], in their review, stated that the primary compounds of plants such as amino acids, citric acid, flavonoids, phenolic compounds, terpenoids, heterocyclic compounds, enzymes, peptides, polysaccharides, saponins, and tannins are responsible for metal ion reduction due to the presence of metallic counterparts and the stabilisation of the surface of the MNPs and MONPs. Kesharwani et al. [318], discovered that plant extract phytochemicals are responsible for the metal reduction. The reduced metal ions are linked by oxygen generated by either the environment or phytochemical degradation. The electrostatic attraction will connect metal oxide ions, resulting in the production of nanoparticles. They are stabilised by phytochemicals, which prevent the agglomeration of nanoparticles.

As a result, the antibacterial activity of CP leave extract against SA and EC bacterium pathogens can be attributed to the extract's bioactive constituents [319]. As well as, the reduction of the AgNO_3 was also due to the feasibility of replacing chemical reducing agents (i.e. sodium borohydride) with CP leave extract, which serves as both a reducing agent and a capping agent [320].

Conclusion: Minor scale Pilot trails: Set-II

- ❖ All the colloidal solutions have confirmed formation of AgNPs via a fuzzy milky brownish colour shown at the point of synthesis. All the colloidal solutions have retained their colour for more than a week, with just a slight variation in the strength of the fuzzy light brownish hue. Even after 6 months, colloidal solutions E10S0010 and E10S0015 have shown a little bit but non objectionable colour change indicative of good stability.

- ❖ The sample E10S0010 has exhibited a narrower but much sharper and stronger peak with a maximum absorption in the 400–450nm wavelength region. Construed good quality of the synthesis with the smaller sized nanoparticles without agglomeration. All other AgNPs colloidal solution have displayed a narrow - to - broad and less - to - more intense peak between the wavelength ranges of 400–500 nm (or <500 nm). The sample E10S0000 has a broader and more intense peak between 190 – 400 nm, indicative for CP leave extract particles.

- ❖ The DLS spectra of the AgNPs colloidal solutions revealed that the 'E10S0010 (F4)' AgNPs colloidal solution possessed the most desirable nanoparticle size distribution with 25.8nm AgNPs size in a group.

- ❖ The Colloidal solution E10S0010 (F4) has the greatest average ZOI value, with 18.0mm against SA and 21.7mm against EC bacterial culture, respectively. Furthermore, the samples E10S0000 (F1) produced using only CP leave extract (10%) has also revealed a very good average ZOI value of 16.0mm against SA and 19.3mm against EC bacterial cultures respectively. A virtuous antibacterial activity of the

produced AgNPs colloidal solution (E10S0010) as well as only CP leave extract (E10) was verified.

- ❖ E10S0010 colloidal solution has shown 84% cell viability, considered as non-toxic in nature (>80% is significant). The colloidal solutions E10S0001 and E10S0005 have also exhibited very good cell viability (90% and 88%, respectively). However, there was no AgNPs peak was observed during particle size measurement and also reported with less antibacterial activity than other colloidal solutions in the group attributed to very low quantity of AgNO₃. The CP leave extract (E10) has shown 92% cell viability; considered to be a very significant, hence non-toxic.

- ❖ The GC-MS analysis of the 10% concentrated CP leave extract has revealed the presence of N-Decanoic Acid (C₁₀H₂₀O₂) identified as saturated fatty acids and flavonoid glycoside [D-Glucopyranoside, 4-O-Decyl-, (C₁₆H₃₂O₆)], these are the main constituents responsible for antibacterial activity. Other phytochemicals included in the extract, such as amino acids, citric acid, flavonoids, phenolic compounds, terpenoids, heterocyclic compounds, enzymes, peptides, polysaccharides, saponins, tannins, and so on, are also responsible in the reduction and capping of nanoparticles.

4.4 PHASE-IV:

DEVELOPMENT OF NANO-COMPOSITES BY TREATING COMMONLY USED BIO-MEDICAL NONWOVEN TEXTILE WITH OPTIMAL AgNPs/CP COLLOIDAL & EVALUATING THEIR PHYSICAL AND FUNCTIONAL CHARACTERISTICS AS PER ASTM STANDARDS

This phase was designed to develop various nano-composites which can be used for various medical and health care applications. The antibacterial efficacy of synthesised AgNPs/CP as well as CP extract has already been assessed in previous phases of research. Thereby, retention of their active functionality while reinforcing into the most commonly used bio-medical textile materials; PP (Polypropylene) and PV (Polyester-Viscose) nonwoven fabric was measured.

4.4.1 RESULT'S ANALYSIS

4.4.1.1 Antibacterial assessment of the Nano-composites

The antibacterial activity of CP treated and AgNPs/CP treated nano-composite samples were evaluated against respective untreated non-woven fabric. The test was carried out using the same approach as outlined in Phase II (Section 3.2.3.1), against the bacterial cultures *Staphylococcus Aureus* (SA) and *Escherichia Coli* (EC). The average Zone of Inhibition (ZOI) for all the samples casted against both organisms SA and EC and are given in Table 4.21 and graphically depicted in Figure 4.58.

All parent nonwoven samples have not shown any bacterial inhibition against any of the bacterial cultures. This behaviour was as per expectation. But the efficacy and stability of the antibacterial activities mapped against SA and EC bacteria have shown very promising results for CP treated and AgNPs/CP treated samples. This behaviour has witnessed extent of functionality induced into the fabric structure on the respective treatments.

It can also be seen that the highest antibacterial efficacy as well as stability against both the tested cultures has gone on the account of the PV nano-composite (PV40-AgNPs/CP) in the group. This has substantiated ease of receptibility and retention of hydrophilic PV material on the resistant hydrophobic PP matter irrespective of its size and

structure. They also supported previous findings about surface deposition of AgNPs on treatment, which did not allow long term stability under wear or wash cycles [299].

The ZOI value of all the samples were analysed statistically to find out the effect of CP extract and AgNPs/CP through the sample mean paired 't-test'. The statistical analysis has shown higher calculated ' t_{cal} ' values at 95% confidence level and degrees of freedom of '3' ($\therefore \eta = 4-1$) [Table 4.22 and Figure 4.59 (a & b respectively)]. Hence, it is statistically proved that after application of the CP leave extract and AgNPs/CP, have a significant effect on the ZOI, hence antibacterial activities of the respective nonwoven textile materials.

Table 4.21: Zone of Inhibition (ZOI) in (mm)

Sample Code	Staphylococcus aureus (SA)			Escherichia coli (EC)		
	24 Hours	48 Hours	72 Hours	24 Hours	48 Hours	72 Hours
PP30 (SMS)	0	0	0	0	0	0
PP30-CP	15.50	13.75	12.75	16.75	14.75	14.25
PP30-AgNPs/CP	16.75	14.75	14.00	18.75	16.25	15.50
PV40 (SMS)	0	0	0	0	0	0
PV40-CP	22.50	20.75	20.00	26.75	24.00	23.25
PV40-AgNPs/CP	26.25	24.25	23.75	27.00	25.00	24.50
PP50 (SMS)	0	0	0	0	0	0
PP50-CP	17.00	15.00	14.50	19.00	17.00	16.5
PP50-AgNPs/CP	19.00	16.50	16.00	20.00	17.50	17.00
PP45 (SMMMS)	0	0	0	0	0	0
PP45-CP	18.25	16.5	16.00	19.75	17.50	17.25
PP45-AgNPs/CP	20.75	18.5	17.25	21.00	18.75	18.25

SMS = Spunbond-Meltblown-Spunbond nonwoven
SMMMS = Spunbond-Meltblown-Meltblown-Meltblown-Spunbond nonwoven

Table 4.22: 't'-Test (Zone of Inhibition)

Parameters	Staphylococcus aureus (SA)		Escherichia Coli (EC)	
	Mean	('t _{cal} ')	Mean	('t _{cal} ')
PP30 (SMS)	0	--	0	--
PP30-CP	12.750	26.634	14.25	19.000
PP30-AgNPs/CP	14.000	15.336	15.5	24.012
PV40 (SMS)	0	--	0	--
PV40-CP	20.000	13.5873	23.25	14.074
PV40-AgNPs/CP	23.750	16.5374	24.5	11.884
PP50 (SMS)	0	--	0	--
PP50-CP	14.500	12.182	16.5	13.863
PP50-AgNPs/CP	16.000	17.527	17	13.880
PP45 (SMMMS)	0	--	0	--
PP45-CP	16.000	13.064	17.25	10.442
PP45-AgNPs/CP	17.250	10.442	18.25	16.461

('t_{cal}') = Calculated 't' value

('t_{.95}') = 2.353

('t_{.99}') = 4.541

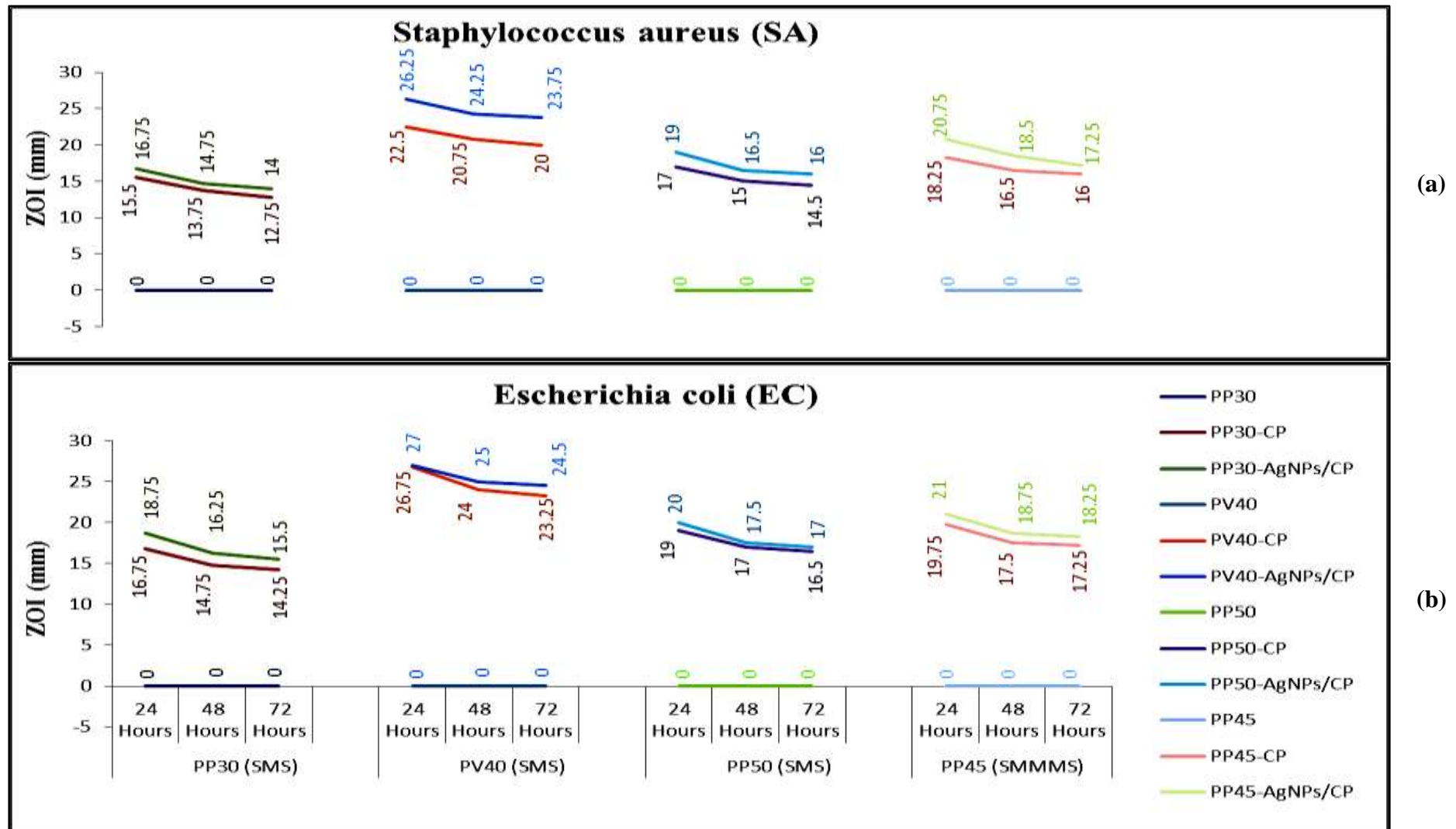
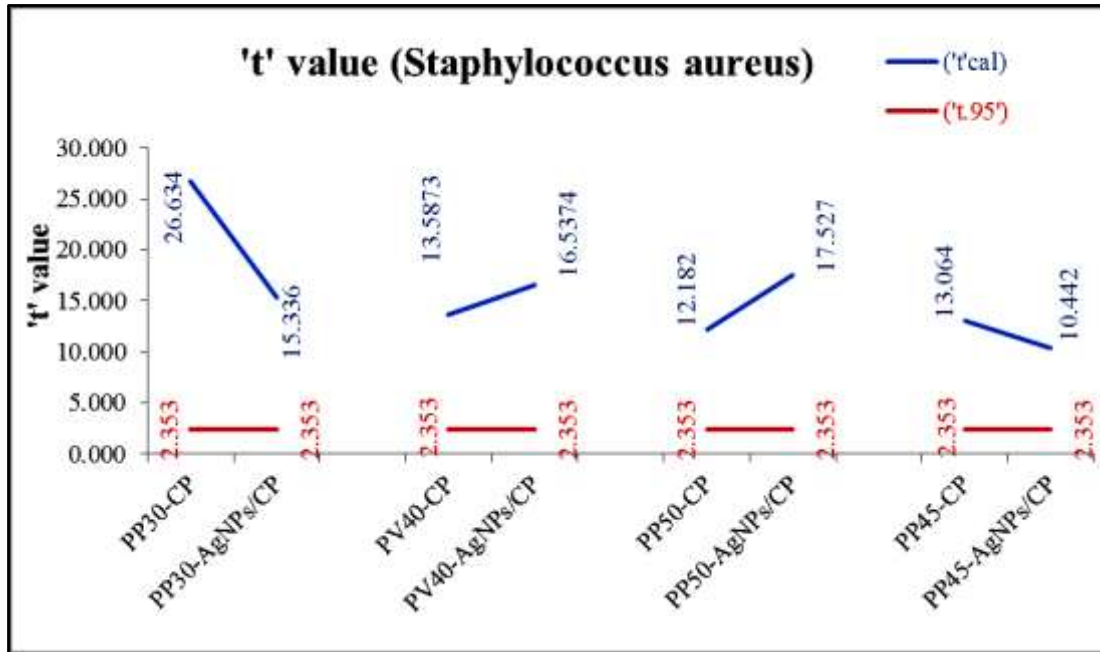
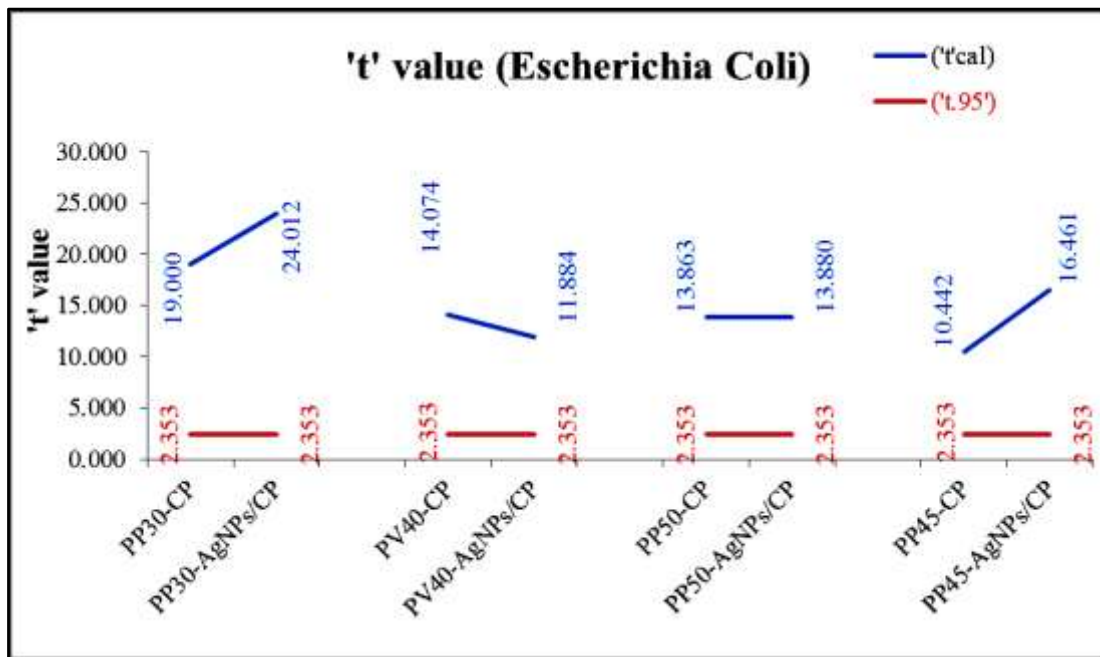


Figure 4.58: Zone of Inhibition (ZOI) in (mm) of all the samples for a) SA and b) EC



(a)



(b)

Figure 4.59: 't'-Test value [Zone of Inhibition for a) SA, and b) EC]

4.4.1.2 Structural assessment of the Nano-Composite

4.4.1.2.1 Morphological assessment by Environmental Scanning Electron Microscopy (ESEM)

The structural changes undergone by all the selected bio-medical materials on CP treatment as well as AgNPs/CP loading were analysed using ESEM. The micrographs for the untreated and CP extract treated samples were captured at 1000X and AgNPs/CP loaded samples at 2000X and illustrated in Figures 4.60 (a–c) respectively.

The surface morphology, structure, and orientation of the constituent fibres in the base materials have been well revealed by ESEM micrographs [Figures 4.60(a)]. Similarly, CP particles good penetration, well deposition and adherence on the fiber surface have been confirmed by the ESEM images [Figures 4.60 (b)]. Whereas, ESEM images [Figures 4.60(c)] have endorsed consistent distribution of nanoparticles @AgNPs/CP on the fibres surface for the selected deposition approach. This was indeed attained with certain tiny aggregates of very small nanoparticles. Thus, method adopted in the present study was found satisfactory for a virtuous deposition of AgNPs on the PP and PV non-woven fabric.

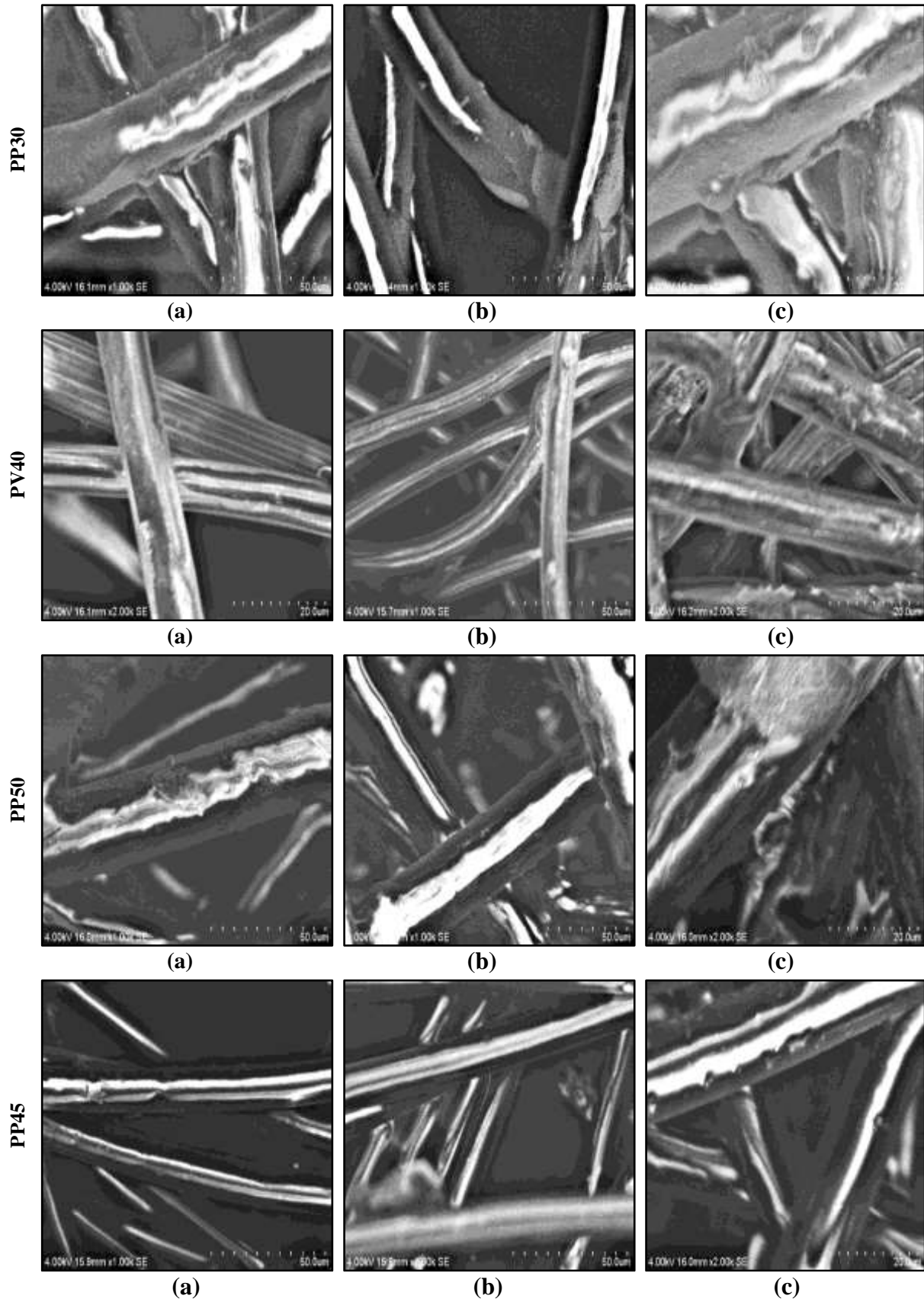


**Figure 4.60: ESEM Images: a) untreated nonwovens (1000X),
b) CP treated (1000X), and
c) AgNPs/CP treated composites (2000X)**

4.4.1.2.2 FTIR analysis of the Nano-composites

Fourier transform infrared spectroscopy was used to assess changes took place in the chemical structure of the parent non-wovens on treatment. The FTIR spectral characterization peaks of respective untreated, CP treated and AgNPs/CP treated samples are depicted in Figures 4.61 to Figures 4.64 (a–c) and listed in Table 4.23 to 4.26 respectively.

The corresponding spectrums were appeared same with respect to the parent nonwoven irrespective of material type. This was due to identical base material major content in the specimen structure under observation.

PP based samples:

Maximal composition of the polypropylene (PP) is evidenced by the characterisation peaks in the FTIR bands for all the untreated, CP treated and AgNPs/CP treated PP based samples respectively. They have shown a medium peak around 2915.02, 2914.86, 2914.88, 2910.56, 2908.08, 2912.38, 2910.2 and 2952.5 cm^{-1} associated with C-H stretching vibration of alkene. The medium peaks observed around 2839.01, 2839.05, 2839.03, 2839.39, 2839.24, 2839.17, 2838.7, 2840.8 and 2839.09 cm^{-1} have related C–H stretching vibrations of aldehyde. The weak peaks observed around 2722.4, 2722.43, 2722.41, 2722.4, 2722.37, 2722.38, 2722.43, 2722.44 and 2722.54 cm^{-1} are related with intra-molecular bonded O-H stretching vibration of the alcohol. All these peaks formation were seen in the range of 2500 to 3000 cm^{-1} due to the stretching vibration of group CH_2 , NH_2 and OH , and represented overlapping of the stretching vibration caused on the account of distilled water and CP leave extract molecules [176].

Medium peaks observed around 1376.44, 1376.69, 1376.53, 1376.25, 1376.23, 1376.71, 1376.39, 1376.39 and 1376.36 cm^{-1} were associated with C-H stretching vibration (gem dimethyl) of alkene. Further medium peaks seen around 1166.98, 1166.77, 1166.94, 1167.04, 1167.02, 1167.05, 1166.97, 1166.96 and 1166.95 cm^{-1} were associated with C-O stretching vibration of ester group. These peaks were observed in the ranges from 1000 to 1400 cm^{-1} and endorsed an excess presence of flavonoids and terpenoids in the CP leave extract [207].

Various other peaks were detected in the range of 650.00 to 1000.00 cm^{-1} and associated with C=C bending vibration of alkene with mono-substituted, vinylidene and tri-substituted in subsiding order. The strong peaks noted around 729, 729.1, 728.95, 712.53,

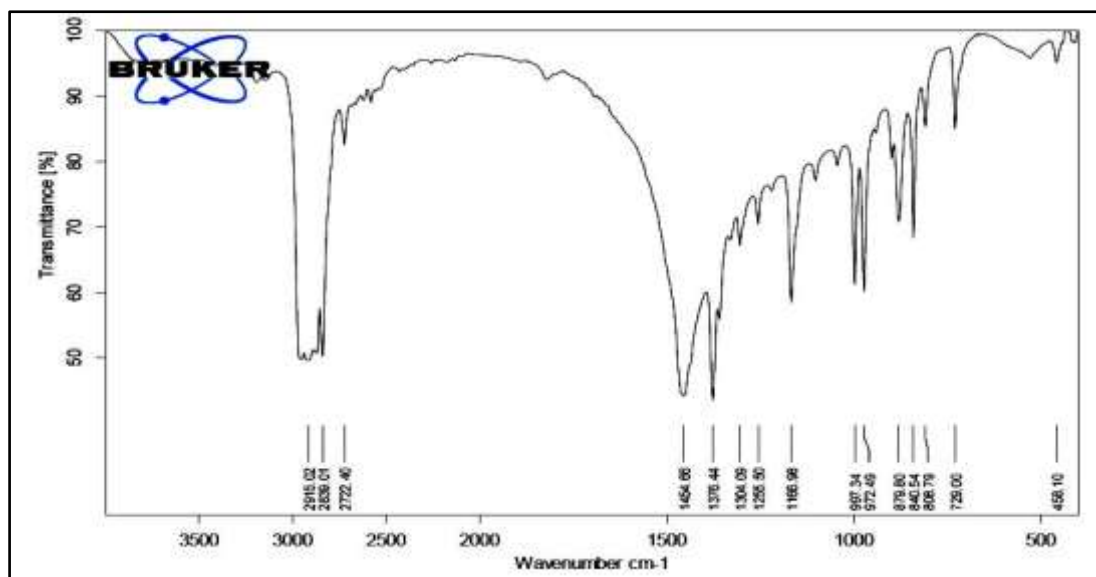
712.52, 712.51, 730.9, 730.89 and 730.98 cm^{-1} were associated with C-H bending vibration of alkene (1,2,3-Tri-substituted).

Additionally, all the spectrums of AgNPs/CP nano-composites (i.e. PP30-AgNPs/CP, PP50-AgNPs/CP, PP45-AgNPs/CP) have demonstrated the peaks at 1382.6, 1382.24, and 1382.66 cm^{-1} have related to phenolic (O-H) bending vibration. The strong peaks realized at 1263.41, 1262.98, and 1263.66 cm^{-1} have represented aromatic amine (C-N) stretching vibration. These spectrum peaks associated with phenolic and aromatic amine groups have indicated about the incorporation of AgNPs into the AgNPs/CP nano-composites [225].

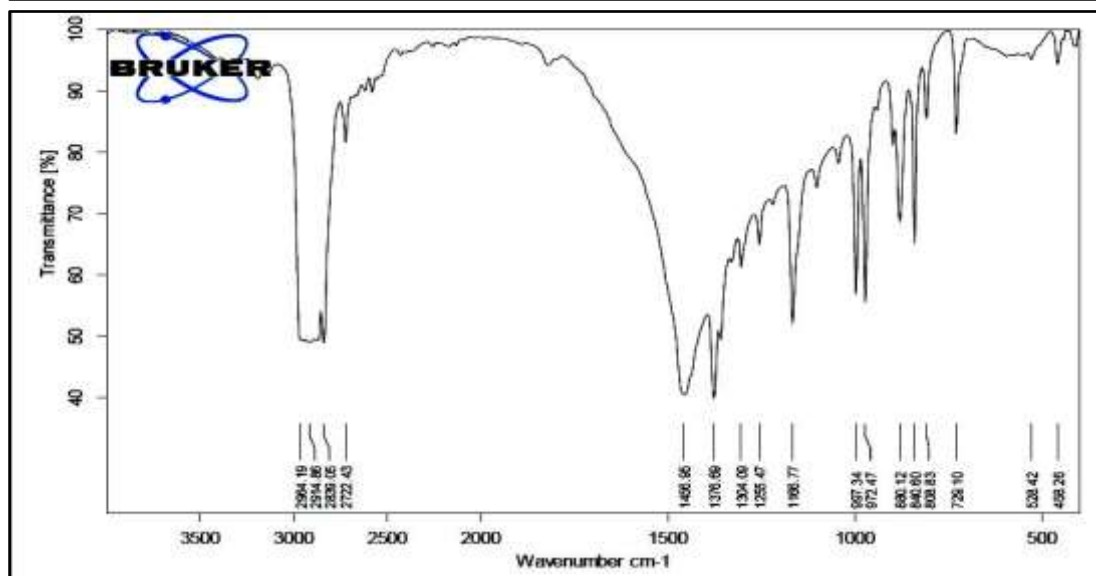
PV based sample:

Highest composition of the polyester and viscose are evidenced from the characterisation peaks in the FTIR bands in all three samples (i.e. PV40, PV40-CP and PV40-AgNPs/CP) at around 3432.49, 3431.48 and 3432.94 cm^{-1} associated with the N-H stretching vibration of primary amines. The peaks observed around 2969.29, 2967.59 and 2966.53 cm^{-1} to 2907.62, 2907.5 and 2907.54 cm^{-1} were related to symmetric stretching vibrations of hydrogen bond (C-H stretching) respectively. The polyester profile has a strong peak around 1714.2, 1711.94 and 1714.66 cm^{-1} related with carboxyl groups (C=O stretching), and a weak peak at 1577.58, 1577.98 and 1577.6 cm^{-1} associated with cyclic alkene (C=C) stretching vibration. The peaks seen around 1454.64, 1458.68, 1455.95 cm^{-1} and 1371.63, 1371.18, 1372.83 cm^{-1} were related with the bending vibration of alkanic hydrogen bond (C-H), and at 1408.96, 1409.55, 1409.64 cm^{-1} and 1339.91, 1340.69, 1340.21 cm^{-1} were associated with alcoholic (O-H) bending vibrations respectively. Various other bands observed within the range of 1250 to 1000 cm^{-1} were accompanied with (C-O) stretching vibration of alkyl ether, ester, aliphatic ether, and vinyl ether, respectively.

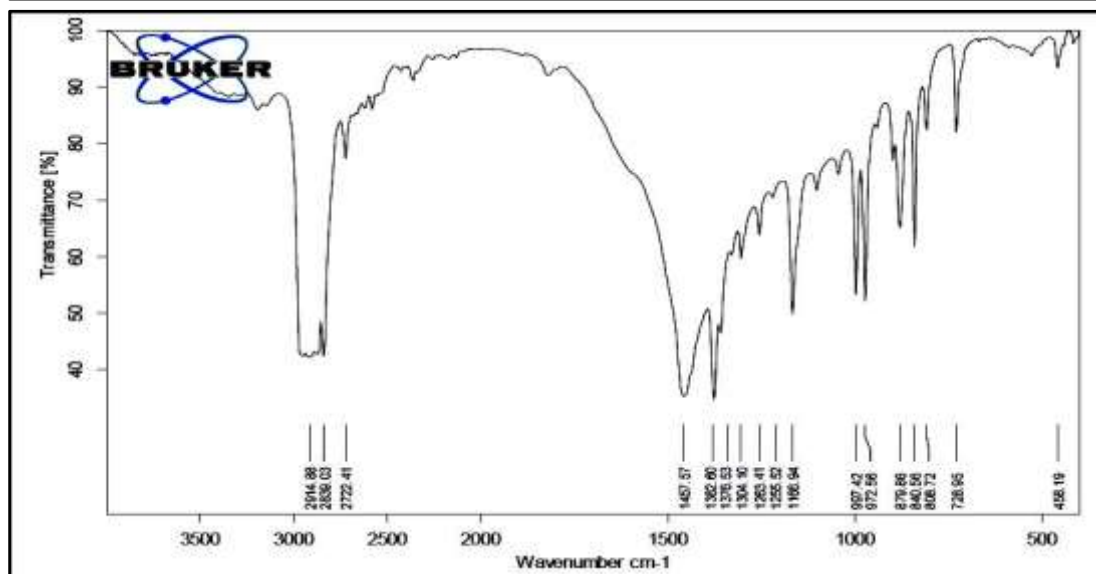
Here also, in addition, the spectrum for PV-AgNPs/CP nano-composite has demonstrated a peak at 1382.76 cm^{-1} related to phenolic (O-H) bending vibration, and at 1263.74 cm^{-1} associated with aromatic amine (C-N) stretching vibration.



(a)

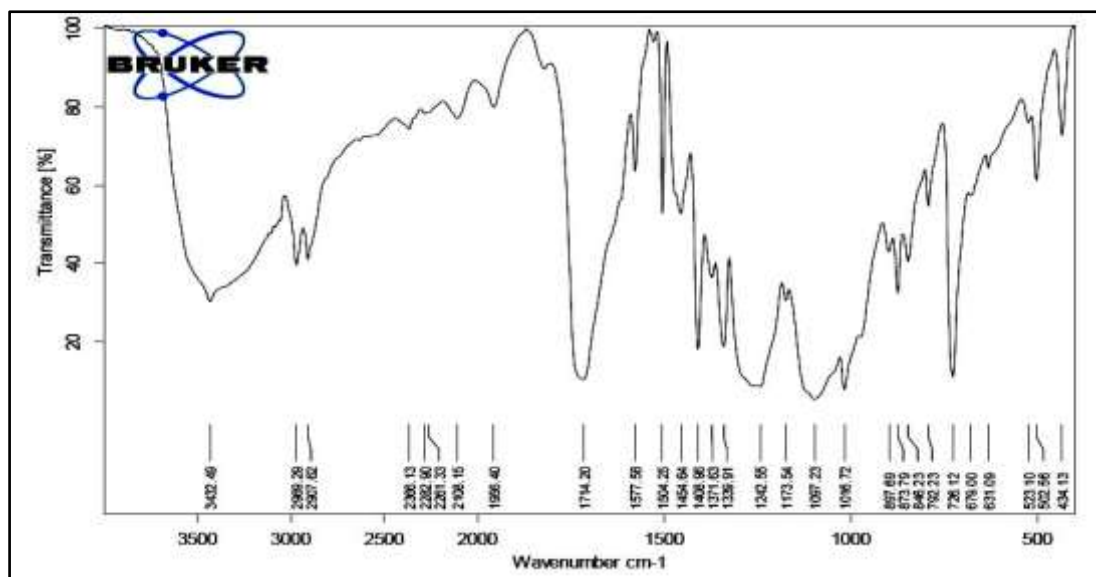


(b)

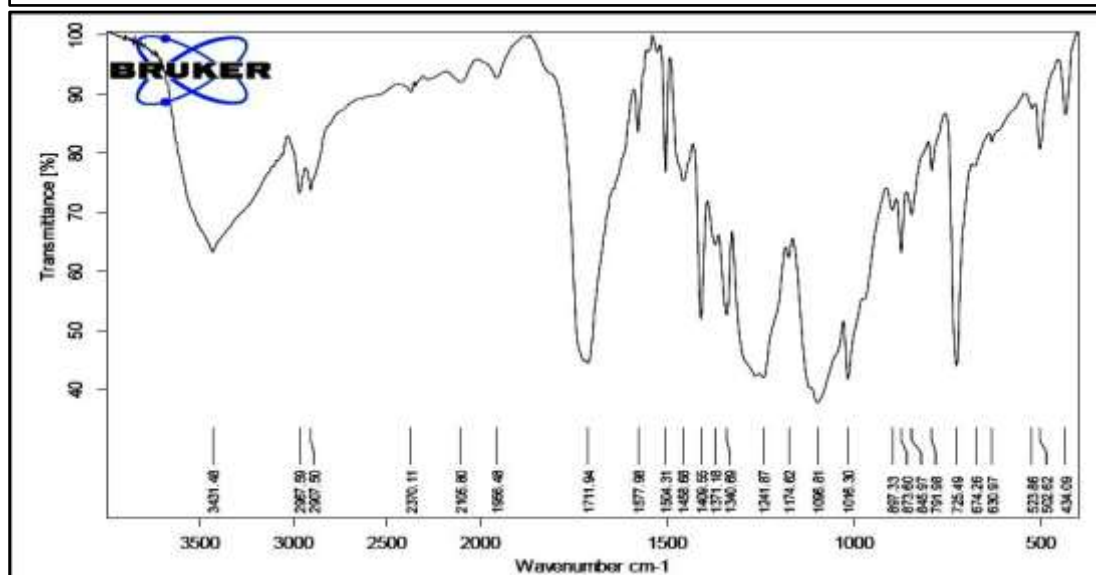


(c)

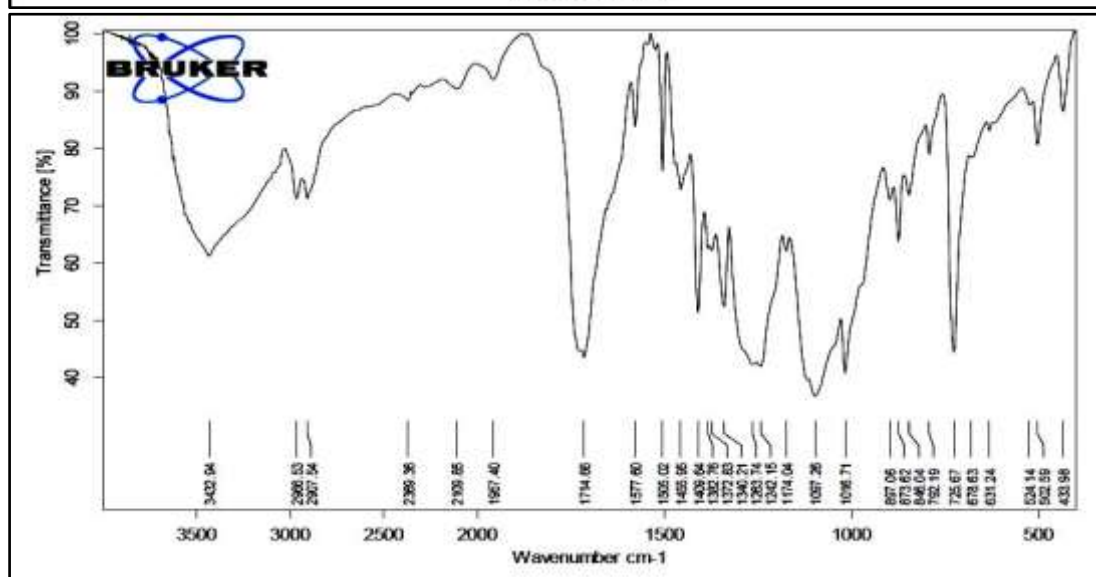
Figure 4.61: FTIR spectra of the a) PP30, b) PP30-CP, and c) PP30-AgNPs/CP



(a)

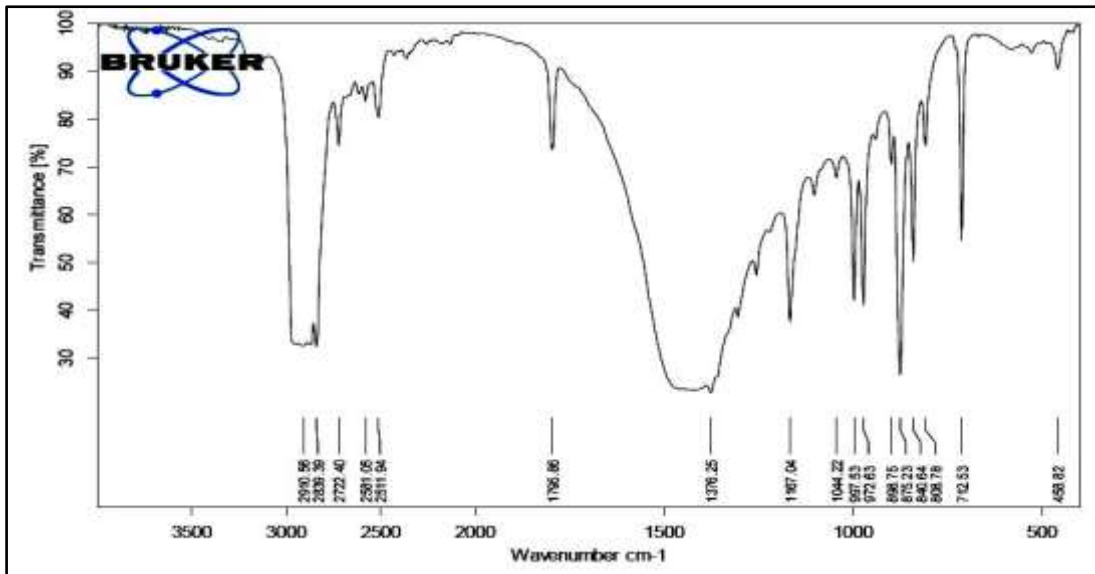


(b)

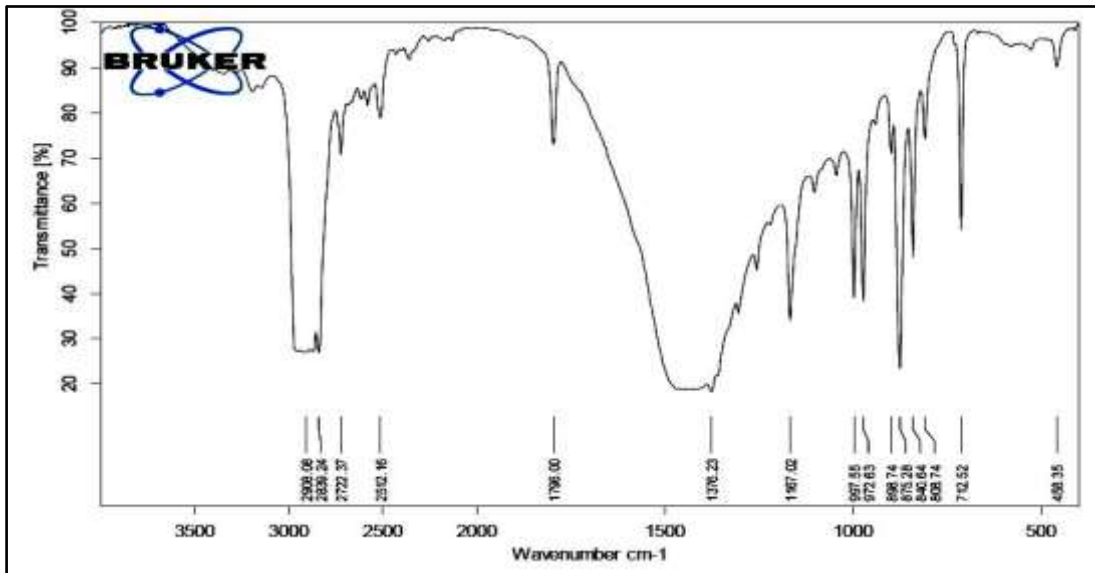


(c)

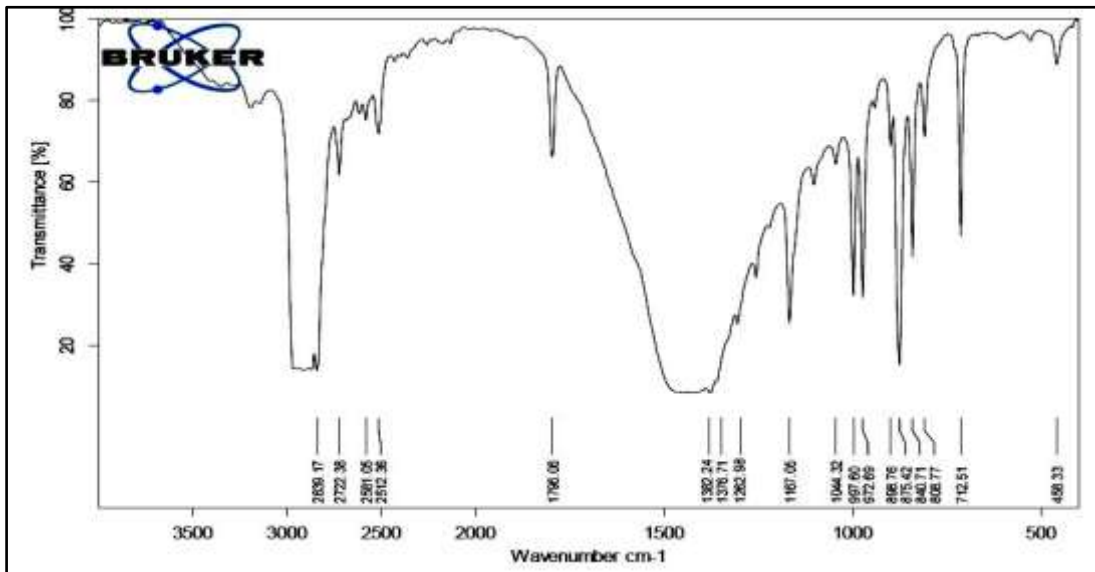
Figure 4.62: FTIR spectra of the a) PV40, b) PV40-CP, and c) PV40-AgNPs/CP



(a)

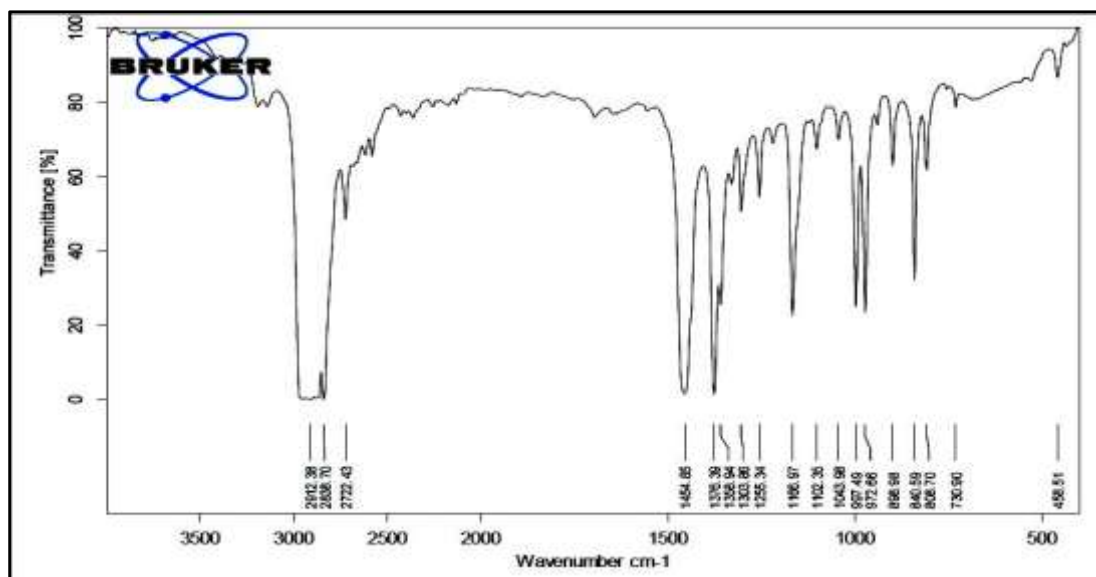


(b)

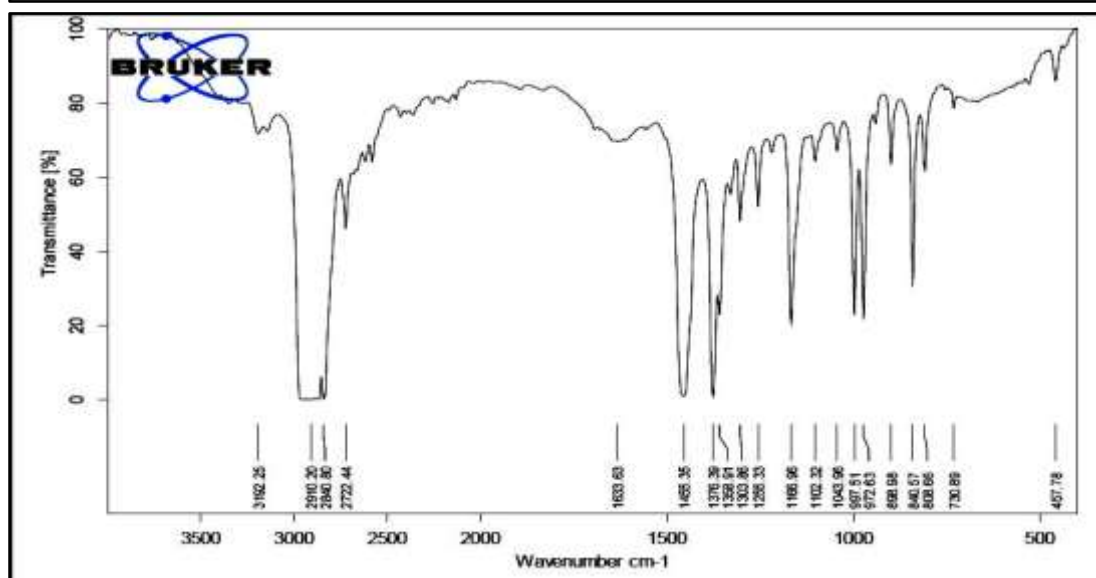


(c)

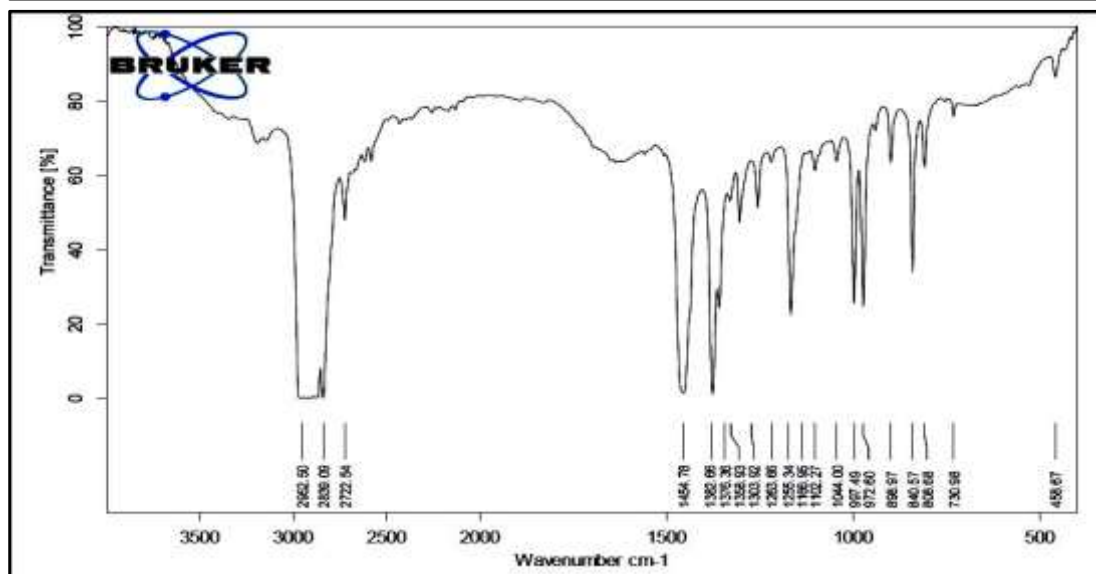
Figure 4.63: FTIR spectra of the a) PP50, b) PP50-CP, and c) PP50-AgNPs/CP



(a)



(b)



(c)

Figure 4.64: FTIR spectra of the a) PP45, b) PP45-CP, and c) PP45-AgNPs/CP

Table 4.23: FTIR characterization peaks of PP30 (SMS)

Wavenumber (cm ⁻¹)			Appearance	Group	Compound Class	Comments
PP30 (SMS)	PP30-CP	PP30-AgNPs/CP				
2915.02	2914.86	2914.88	Medium	C-H stretching	Alkane	
2839.01	2839.05	2839.03	Medium	C-H stretching	Aldehyde	
2722.4	2722.43	2722.41	Weak	O-H stretching	Alcohol	Intramolecular bonded
1454.66	1456.95	1457.57	Medium	C-H bending	Alkane	
---	---	1382.6	Medium	O-H bending	Phenol	
1376.44	1376.69	1376.53	Medium	C-H bending	Alkane	gem dimethyl
1304.09	1304.09	1304.1	Medium	O-H bending	Alcohol	
---	---	1263.41	Strong	C-N stretching	Aromatic amine	
1255.5	1255.47	1255.52	Medium	C-O stretching	Alkyl aryl ether	
1166.98	1166.77	1166.94	Medium	C-O stretching	Ester	
997.34	997.34	997.42	Medium	C=C bending	Alkene	Monosubstituted
972.49	972.47	972.56	Medium	C=C bending	Alkene	Monosubstituted
840.54	840.6	840.56	Medium	C=C bending	Alkene	Trisubstituted
729	729.1	728.95	Strong	C-H bending	Alkene	1,2,3-Trisubstituted

* --- = No peak found

Table 4.24: FTIR characterization peaks of PV40 (SMS)

Wavenumber (cm ⁻¹)			Appearance	Group	Compound Class	Comments
PV40 (SMS)	PV40-CP	PV40-AgNPs/CP				
3432.49	3431.48	3432.94	Medium, Broad	N-H stretching	Primary amine	
2969.29	2967.59	2966.53	Medium	C-H stretching	Alkane	
2907.62	2907.5	2907.54	Medium	C-H stretching	Alkane	
2366.13	2370.11	2369.36	Weak	O=C=O stretching	Carbon dioxide	
2108.15	2105.8	2109.85	Weak	C≡C stretching	Alkane	Monosubstituted
1956.4	1956.48	1957.4	Weak	C-H bending	Aromatic compound	Overtone
1714.2	1711.94	1714.66	Strong	C=O stretching	Carboxylic acid	Dimer
1577.58	1577.98	1577.6	Medium	C=C stretching	Cyclic alkene	
1504.25	1504.31	1505.02	Weak	N-O stretching	Nitro compound	
1454.64	1458.68	1455.95	Medium	C-H bending	Alkane	
1408.96	1409.55	1409.64	Medium	O-H bending	Alcohol	
---	---	1382.76	Medium	O-H bending	Phenol	
1371.63	1371.18	1372.83	Medium	C-H bending	Alkane	gem dimethyl
1339.91	1340.69	1340.21	Medium	O-H bending	Alcohol	
---	---	1263.74	Strong	C-N stretching	Aromatic amine	
1242.55	1241.87	1242.15	Strong	C-O stretching	Alkyl aryl ether	
1173.54	1174.62	1174.04	Medium	C-O stretching	Ester	
1097.23	1096.81	1097.26	Strong	C-O stretching	Aliphatic ether	
1016.72	1016.3	1016.71	Strong	C-O stretching	Vinyl ether	
846.23	845.97	846.04	Medium	C=C bending	Alkene	Trisubstituted
726.12	725.49	725.67	Strong	C-H bending	Alkene	1,2,3-Trisubstituted

* --- = No peak found

Table 4.25: FTIR characterization peaks of PP50 (SMS)

Wavenumber (cm ⁻¹)			Appearance	Group	Compound Class	Comments
PP50 (SMS)	PP50-CP	PP50-AgNPs/CP				
2910.56	2908.08		Medium	C-H stretching	Alkane	
2839.39	2839.24	2839.17	Medium	C-H stretching	Aldehyde	
2722.4	2722.37	2722.38	Weak	O-H stretching	Alcohol	Intramolecular bonded
2511.94	2512.16	2512.36	Weak	S-H stretching	Thiol	
1795.86	1796	1796.06	Weak	C-H bending	Aromatic compound	Overtone
---	---	1382.24	Medium	O-H bending	Phenol	
1376.25	1376.23	1376.71	Medium	C-H bending	Alkane	gem dimethyl
---	---	1262.98	Strong	C-N stretching	Aromatic amine	
1167.04	1167.02	1167.05	Medium	C-O stretching	Ester	
997.53	997.55	997.6	Medium	C=C bending	Alkene	Monosubstituted
972.63	972.63	972.69	Medium	C=C bending	Alkene	Monosubstituted
840.64	840.64	840.71	Medium	C=C bending	Alkene	Trisubstituted
712.53	712.52	712.51	Strong	C-H bending	Alkene	1,2,3-Trisubstituted

* --- = No peak found

Table 4.26: FTIR characterization peaks of PP45 (SMMMS)

Wavenumber (cm ⁻¹)			Appearance	Group	Compound Class	Comments
PP45 (SMMMS)	PP45-CP	PP45-AgNPs/CP				
2912.38	2910.2	2952.5	Medium	C-H stretching	Alkane	
2838.7	2840.8	2839.09	Medium	C-H stretching	Aldehyde	
2722.43	2722.44	2722.54	Weak	O-H stretching	Alcohol	Intramolecular bonded
1454.85	1455.35	1454.78	Medium	C-H bending	Alkane	
---	---	1382.66	Medium	O-H bending	Phenol	
1376.39	1376.39	1376.36	Medium	C-H bending	Alkane	gem dimethyl
1358.94	1358.91	1358.93	Medium	O-H bending	Alcohol	
1303.86	1303.86	1303.92	Medium	O-H bending	Alcohol	
---	---	1263.66	Strong	C-N stretching	Aromatic amine	
1255.34	1255.33	1255.34	Medium	C-O stretching	Alkyl aryl ether	
1166.97	1166.96	1166.95	Medium	C-O stretching	Ester	
1102.35	1102.32	1102.27	Strong	C-O stretching	Aliphatic ether	
1043.98	1043.96	1044	Strong	C-O stretching	Vinyl ether	
997.49	997.51	997.49	Medium	C=C bending	Alkene	Monosubstituted
972.66	972.63	972.6	Medium	C=C bending	Alkene	Monosubstituted
840.59	840.57	840.57	Medium	C=C bending	Alkene	Trisubstituted
730.9	730.89	730.98	Strong	C-H bending	Alkene	1,2,3-Trisubstituted

* --- = No peak found

4.4.1.3 Physical and comfort-related properties

The physical properties, low-stress properties, and comfort-related properties are equally important to that of functional properties for any bio-medical textile material. Changes occurred in these characteristics on AgNPs/CP loading and CP extract treatment on the selected base PP nonwoven and PV-nonwoven were worked out. Accordingly, these parameters of prepared prototype AgNPs/CP nano-composites (i.e. PP30-AgNPs/CP, PV40-AgNPs/CP, PP50-AgNPs/CP, and PP45-AgNPs/CP) and CP leave extract treated samples (i.e. PP30-CP, PV40-CP, PP50-CP, and PP45-CP) were investigated and compared with respective values of untreated samples (i.e. PP30, PV40, PP50 and PP45).

4.4.1.3.1 Physical properties

Test results for the GSM and Thickness for the reference as well as treated samples are reported in (Table 4.27) and graphically illustrated in Figure 4.65 and Figure 4.66. All the AgNPs/CP loaded samples have invariably shown more rise in GSM value compared to CP extract treated. The same behaviour was noted for thickness measurement also. This behaviour is attributed to the added component density mainly. The lighter CP extract has caused smaller change in resultant composite values compared to when it was loaded along with AgNPs [282]. However, percent changes noted in the values were much lower in each case.

In order to judge changes occurred on CP treatment/loading AgNPs/CP were really significant or not, both the test results were statistically analysed. The t-test for sample mean in pair was done for GSM as well as thickness properties, where base fabric value was regarded as reference. The calculated ' t_{cal} ' values along with ' t_{95} ' obtained from t-table at degree of freedom '9' ($\therefore \eta = 10-1$) are given in Table 4.28 and illustrated graphically in (Figure 4.67) and (Figure 4.68).

It can be observed that on AgNPs/CP treatment majority of the samples have shown more or less significant difference at 95% level but the parent as well as only CP treated samples physical test values were remain well below the warning limit [(Figure 4.67) and (Figure 4.68) & Table 4.28]. This behaviour is likely to be attributed to the higher density of the silver (10.5gm/cc) even though deposited in the nano state against PP (0.9gm/cc), PV (1.43 gm/cc) and CP extract (\cong 1.3 gm/cc).

Table 4.27: Physical characteristics of Nano-composites

Properties	PP30 (SMS)	PV40 (SMS)	PP50 (SMS)	PP45 (SMMMS)
Mean (\bar{x})	30.07	40.90	50.39	45.24
CV %	3.88	1.48	1.22	0.89
	PP30-CP	PV40-CP	PP50-CP	PP45-CP
Mean (\bar{x})	30.44	41.40	51.20	45.64
CV %	2.29	1.42	1.12	0.67
% Change	1.23	1.22	1.61	0.88
	PP30-AgNPs/CP	PV40-AgNPs/CP	PP50-AgNPs/CP	PP45-AgNPs/CP
Mean (\bar{x})	30.67	42.04	51.70	45.90
CV %	1.82	1.82	1.42	0.53
% Change	2.00	2.78	2.60	1.46
	PP30 (SMS)	PV40 (SMS)	PP50 (SMS)	PP45 (SMMMS)
Mean (\bar{x})	0.273	0.415	0.434	0.311
CV %	10.51	5.24	6.62	5.13
	PP30-CP	PV40-CP	PP50-CP	PP45-CP
Mean (\bar{x})	0.289	0.416	0.444	0.322
CV %	6.41	5.09	5.00	5.44
% Change	5.86	0.24	2.30	3.54
	PP30-AgNPs/CP	PV40-AgNPs/CP	PP50-AgNPs/CP	PP45-AgNPs/CP
Mean (\bar{x})	0.301	0.418	0.452	0.329
CV %	7.08	6.75	4.01	4.40
% Change	10.26	0.72	4.15	5.79

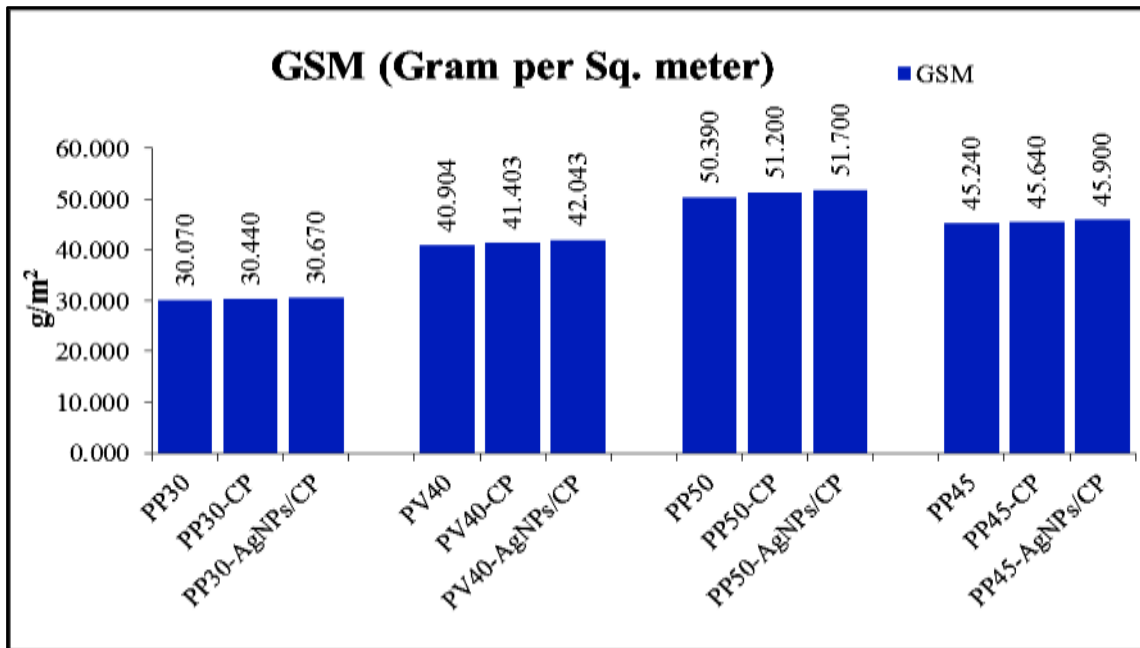


Figure 4.65: GSM (Gram per Sq. meter)

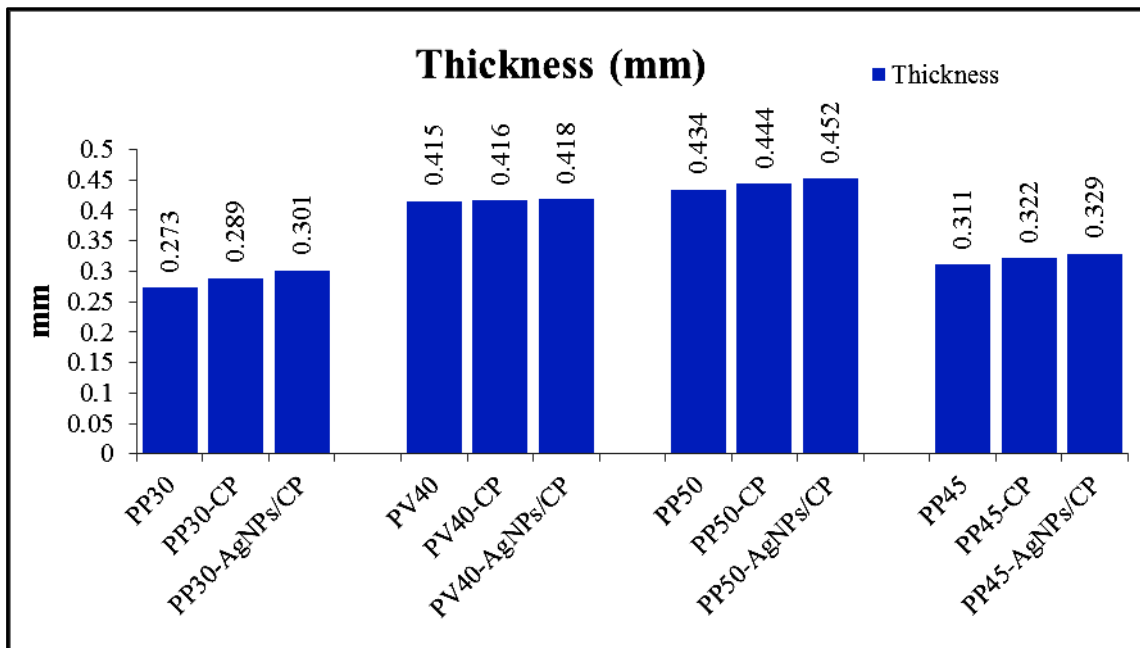


Figure 4.66: Thickness (mm)

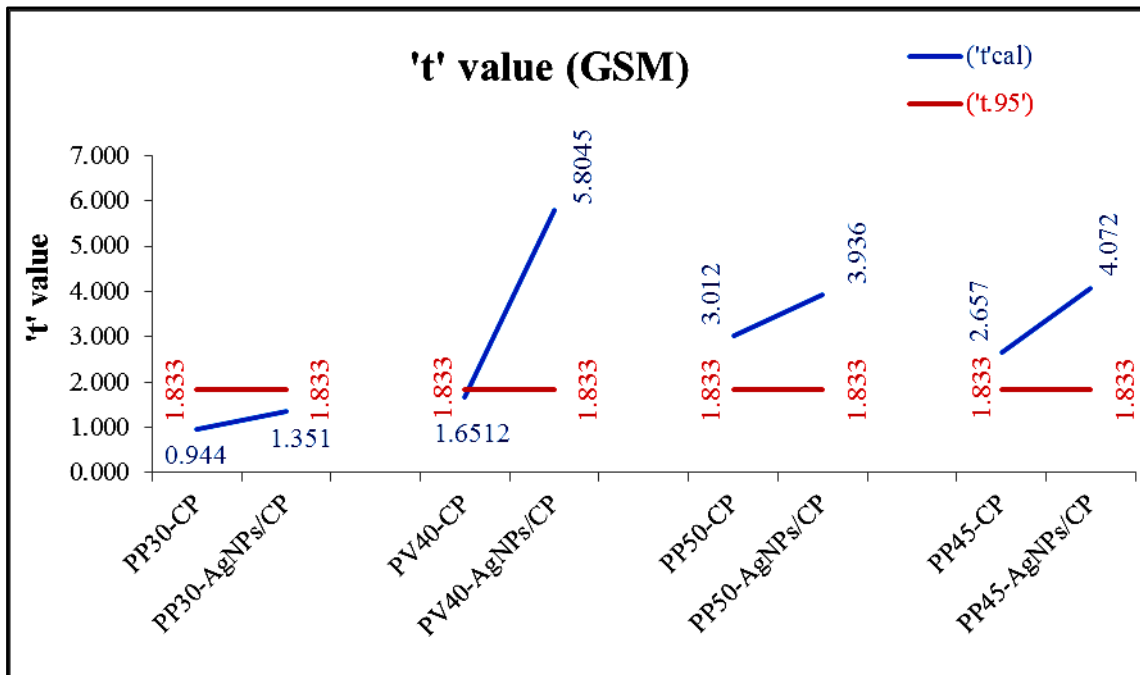


Figure 4.67: 't'-Test value (GSM)

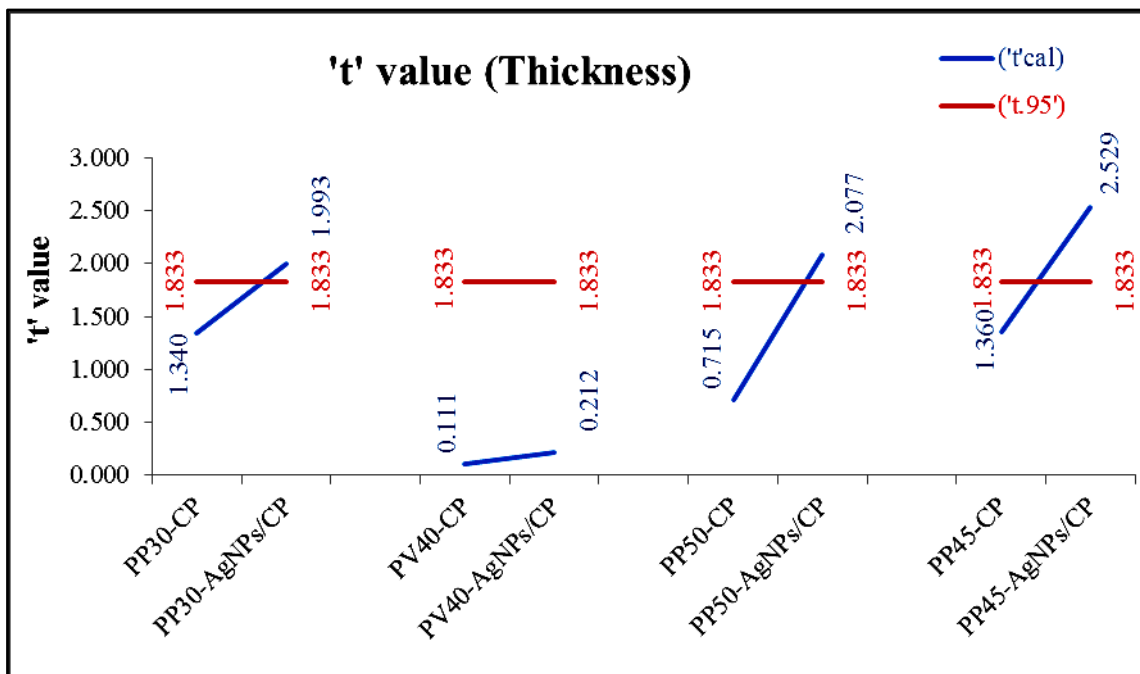


Figure 4.68: 't'-Test value (Thickness)

Table 4.28: 't'-Test (GSM and Thickness)

Parameters	GSM		Thickness	
	Mean	('t _{cal} ')	Mean	('t _{cal} ')
PP30 (SMS)	30.1	--	0.273	--
PP30-CP	30.4	0.944	0.289	1.340
PP30-AgNPs/CP	30.7	1.351	0.301	1.993
PV40 (SMS)	40.9	--	0.415	--
PV40-CP	41.4	1.6512	0.416	0.111
PV40-AgNPs/CP	42.0	5.8045	0.418	0.212
PP50 (SMS)	50.4	--	0.434	--
PP50-CP	51.2	3.012	0.444	0.715
PP50-AgNPs/CP	51.7	3.936	0.452	2.077
PP45 (SMMMMS)	45.2	--	0.311	--
PP45-CP	45.6	2.657	0.322	1.360
PP45-AgNPs/CP	45.9	4.072	0.329	2.529

('t_{cal}') = Calculated 't' value

('t₉₅') = 1.833

('t₉₉') = 2.821

Thus, it is statistically proven that application of AgNPs/CP has caused a significant improvement in the GSM and Thickness values of the particular bio-medical textile materials in the present study. But these changes were not found statistically significant for 1% level ('t₉₉') = 2.821 for thickness measures. However, the value yet remained significant for the GSM values of the samples PV40-AgNPs/CP, PP50-CP, PP50-AgNPs/CP, PP45-CP and PP45-AgNPs/CP. It should be noted that such physical changes alone are not going to affect anymore performance of these textile material in the targeted bio-medical field.

4.4.1.3.2 Low-stress properties

The low-stress parameters; bending modulus and crease recovery angle ($^{\circ}$) of the selected materials were examined before and after treatment. They are reported in (Table 4.29) and graphically defined in Figure 4.69 and Figure 4.70.

Increase in the bending modulus (BM) was noticed in machine-direction as well as cross-direction as per expectations for all the samples, except for the machine-direction (MD) measure of sample PV-40. It has shown drop in the value regardless of all other samples as well as its cross-direction (CD) BM value. This may be attributed to its inbuilt higher structural variations (BM CV%: MD = 20.01% & CD = 19.14%) compared to other samples in consideration (Table 4.29 and Figure 4.62).

The increase in the bending resistance is likely with the slight increase in GSM and thickness values on treatment. The statistical analysis also showed their ' t_{cal} ' values similar to thickness and GSM, more than the warning limits ' $t_{.95}$ ' value (Table 4.30 and Figure 4.71). Apart from this the crease recovery angles for all the samples shown descend of around 2% in case of CP treatment and around 5% in case of AgNPs/CP treatment (Table 4.29 and Figure 4.70). However, the statistical analysis showed their overall ' t_{cal} ' values below the warning limit ' $t_{.95}$ ' values (Table 4.30 and Figure 4.72). Hence, the treatments do not have statistically significant effect in case of the CP extract and AgNPs/CP treatment in both the directions MD and CD.

Similar to the physical characteristic's fabric bending modulus (intrinsic stiffness) and crease recovery angle ($^{\circ}$) especially for PP on the AgNPs/CP treatment has shown a remarkable rise at $t_{5\%}$ as well as $t_{1\%}$ levels. However, in PV fabric the effect has noticed only in machine-direction. Hence, the targeted bio-medical application areas for these materials are surgical aprons, surgical gowns, surgical caps, medical bed sheets, etc. where the fabric BM and crease recovery angle range normally adopted are $<100\text{--}120\text{ g/cm}^2$ and $<150^{\circ}$. Accordingly the changes noted were ignored in the present study.

Table 4.29: Low-stress characteristics of Nano-composites

Properties	PP30 (SMS)		PV40 (SMS)		PP50 (SMS)		PP45 (SMMMS)		
	MD	CD	MD	CD	MD	CD	MD	CD	
Mean (\bar{x})	19.07	15.94	9.55	0.88	46.61	46.36	37.52	37.04	
CV %	10.72	9.36	20.01	19.14	9.20	5.56	9.86	11.87	
Bending Modulus (g/cm ²)	PP30-CP		PV40-CP		PP50-CP		PP45-CP		
	Mean (\bar{x})	21.66	17.07	7.40	1.00	48.68	47.08	39.21	38.39
	CV %	5.83	11.36	15.35	22.21	16.70	6.54	7.16	6.63
	% Change	13.59	7.10	-22.53	13.85	4.44	1.56	4.50	3.64
	PP30-AgNPs/CP		PV40-AgNPs/CP		PP50-AgNPs/CP		PP45-AgNPs/CP		
	Mean (\bar{x})	27.49	25.06	6.71	1.30	49.75	48.26	42.46	41.75
CV %	16.85	17.51	9.08	25.84	4.45	6.53	10.39	10.30	
% Change	44.13	57.25	-29.69	48.07	6.75	4.11	13.15	12.72	
Crease Recovery angle (°)	PP30 (SMS)		PV40 (SMS)		PP50 (SMS)		PP45 (SMMMS)		
	MD	CD	MD	CD	MD	CD	MD	CD	
	Mean (\bar{x})	107.80	104.30	116.40	111.00	114.90	109.70	109.40	103.90
	CV %	2.04	2.07	3.01	2.72	3.56	3.77	2.73	2.46
	PP30-CP		PV40-CP		PP50-CP		PP45-CP		
	Mean (\bar{x})	107.50	104.10	114.40	110.30	114.20	109.60	109.20	103.50
	CV %	1.66	1.78	3.30	3.37	3.30	3.39	2.28	2.24
	% Change	-0.28	-0.19	-1.72	-0.63	-0.61	-0.09	-0.18	-0.38
	PP30-AgNPs/CP		PV40-AgNPs/CP		PP50-AgNPs/CP		PP45-AgNPs/CP		
	Mean (\bar{x})	106.70	101.40	112.30	107.70	108.90	104.10	108.20	103.10
	CV %	1.98	1.81	3.03	2.94	3.98	3.64	2.13	1.85
	% Change	-1.02	-2.78	-3.52	-2.97	-5.22	-5.10	-1.10	-0.77

* MD = Machine-direction, CD = Cross-direction

Table 4.30: 't'-Test (Bending modulus and Crease recovery)

Parameters		Bending Modulus (g/cm ²)		Crease Recovery angle (°)	
		Mean	('t _{cal} ')	Mean	('t _{cal} ')
PP30 (SMS)		19.07	--	107.80	--
PP30-CP	Machine-direction (MD)	21.66	2.96527	107.50	0.537
PP30-AgNPs/CP		27.49	6.76478	106.70	1.383
PP30 (SMS)		15.94	--	104.30	--
PP30-CP	Cross-direction (CD)	17.07	1.3071	104.10	0.242
PP30-AgNPs/CP		25.06	5.2414	101.40	3.364
PV40 (SMS)		9.55	--	116.40	--
PV40-CP	Machine-direction (MD)	7.40	3.554	114.40	1.335
PV40-AgNPs/CP		6.71	4.752	112.30	3.231
PV40 (SMS)		0.88	--	111.00	--
PV40-CP	Cross-direction (CD)	1.00	1.517	110.30	0.500
PV40-AgNPs/CP		1.30	3.002	107.70	2.810
PP50 (SMS)		46.61	--	114.90	--
PP50-CP	Machine-direction (MD)	48.68	0.850	114.20	0.542
PP50-AgNPs/CP		49.75	2.141	108.90	3.544
PP50 (SMS)		46.36	--	109.70	--
PP50-CP	Cross-direction (CD)	47.08	0.741	109.60	0.067
PP50-AgNPs/CP		48.26	1.520	104.10	3.515
PP45 (SMMMS)		37.52	--	109.40	--
PP45-CP	Machine-direction (MD)	39.21	1.095	109.20	0.149
PP45-AgNPs/CP		42.46	2.528	108.20	0.957
PP45 (SMMMS)		37.04	--	103.90	--
PP45-CP	Cross-direction (CD)	38.39	0.883	103.50	0.349
PP45-AgNPs/CP		41.75	3.984	103.10	0.760

('t_{cal}') = Calculated 't' value

('t₉₅') = 1.833

('t₉₉') = 2.821

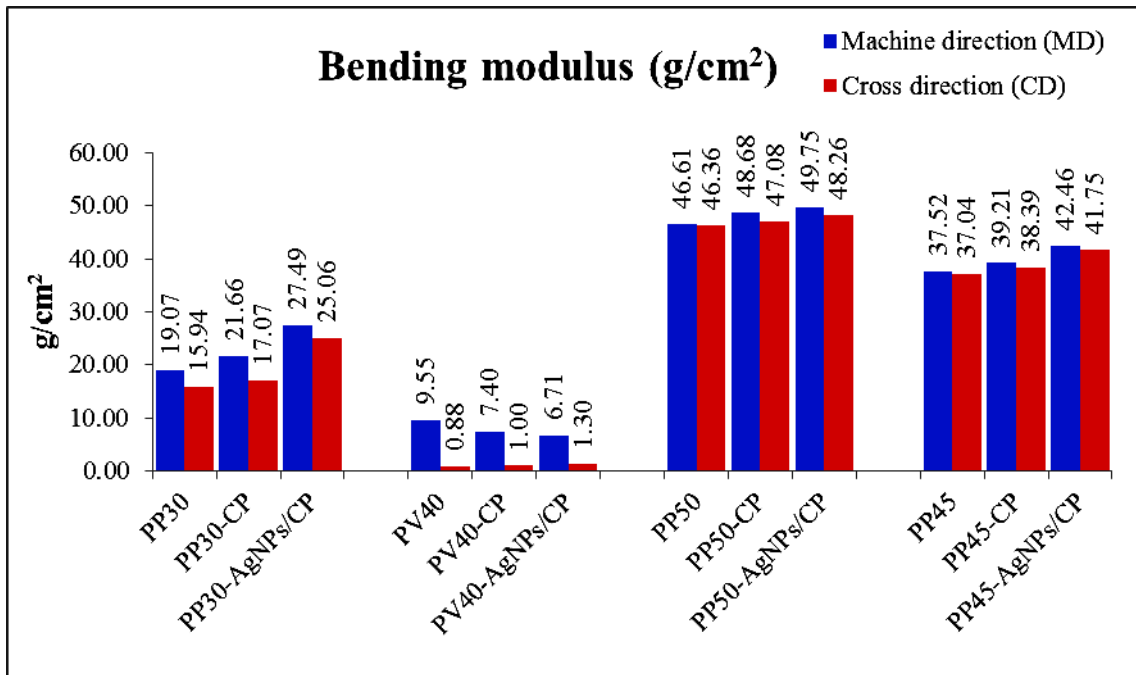


Figure 4.69: Bending modulus (g/cm²)

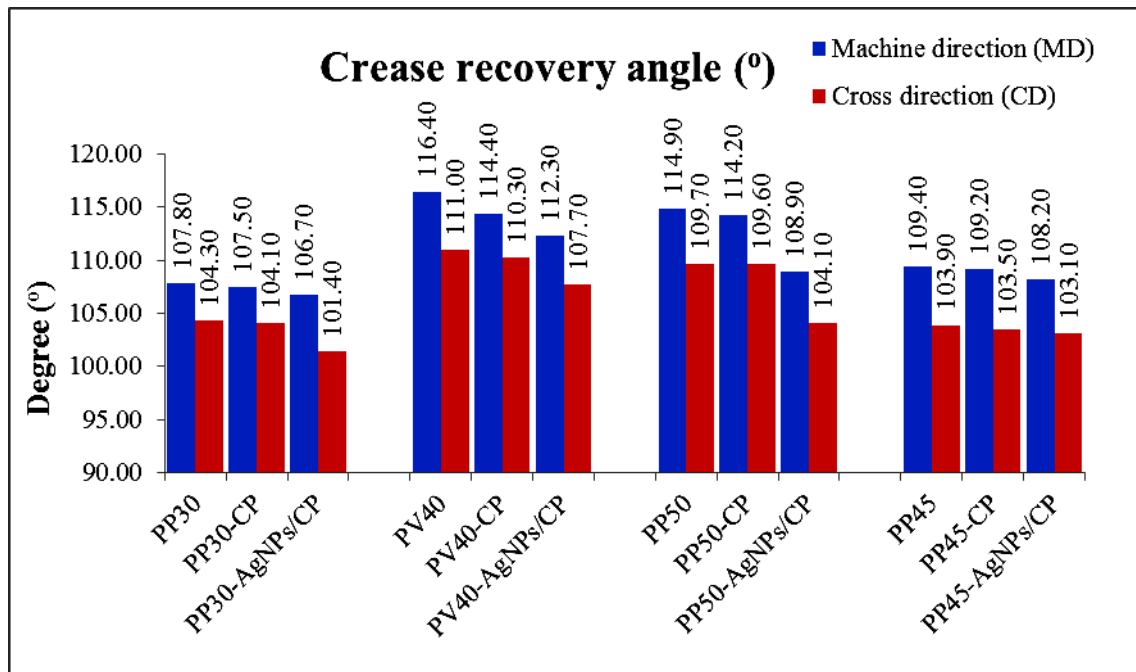


Figure 4.70: Crease recovery angle (°)

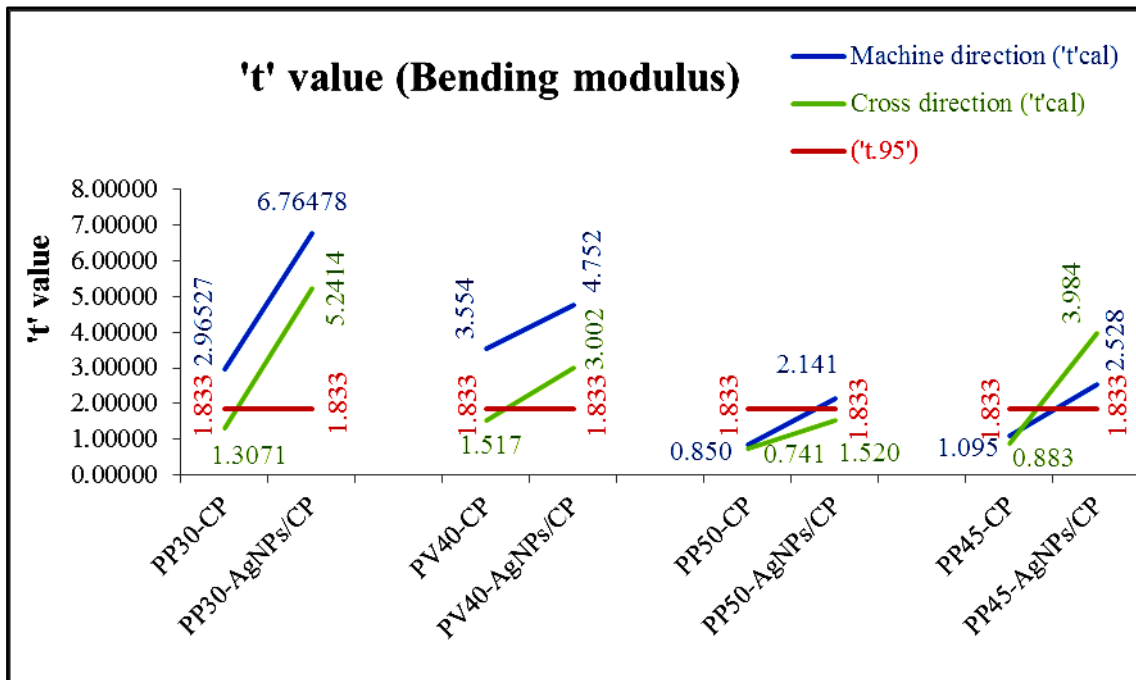


Figure 4.71: 't'-Test value (Bending modulus)

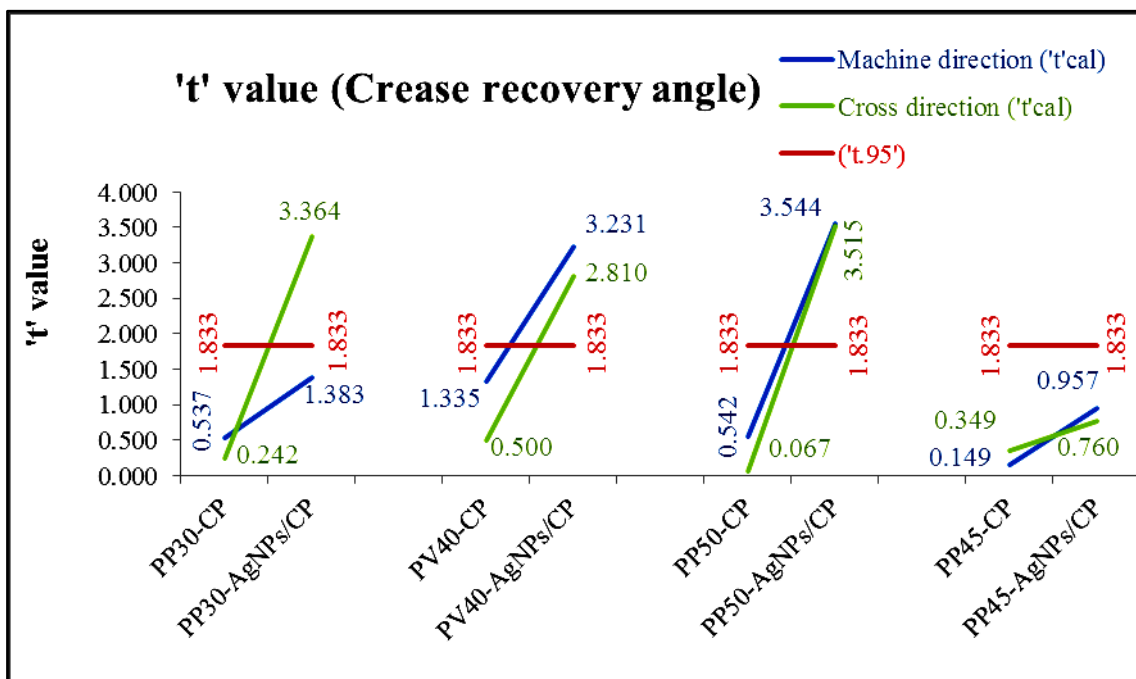


Figure 4.72: 't'-Test value (Crease recovery angle)

4.4.1.3.3 Comfort-associated properties

Air permeability and overall moisture management capabilities (OMMC) were measured and compared for any change took place with respect to the untreated nonwoven textile material.

I) Air permeability

Test results of the air permeability test are given in Table 4.31 and illustrated graphically in Figure 4.73.

Table 4.31: Air permeability (NI/m²/h or m³/m²/h) of Nano-composites

Properties	PP30 (SMS)	PV40 (SMS)	PP50 (SMS)	PP45 (SMSMM)
Mean (\bar{x})	4765.00	4752.50	4225.00	667.50
CV %	1.00	1.15	1.50	3.08
	PP30-CP	PV40-CP	PP50-CP	PP45-CP
Mean (\bar{x})	4715.00	4705.00	4130.00	542.50
CV %	1.23	1.20	1.42	7.85
% Change	-1.05	-1.00	-2.25	-18.73
	PP30- AgNPs/CP	PV40- AgNPs/CP	PP50- AgNPs/CP	PP45- AgNPs/CP
Mean (\bar{x})	4660.00	4657.50	4105.00	502.50
CV %	1.32	1.19	1.21	9.22
% Change	-2.20	-2.00	-2.84	-24.72

* (NI/m²/h) = Normal liter/meter²/hour = m³/m²/h = meter³/meter²/hour

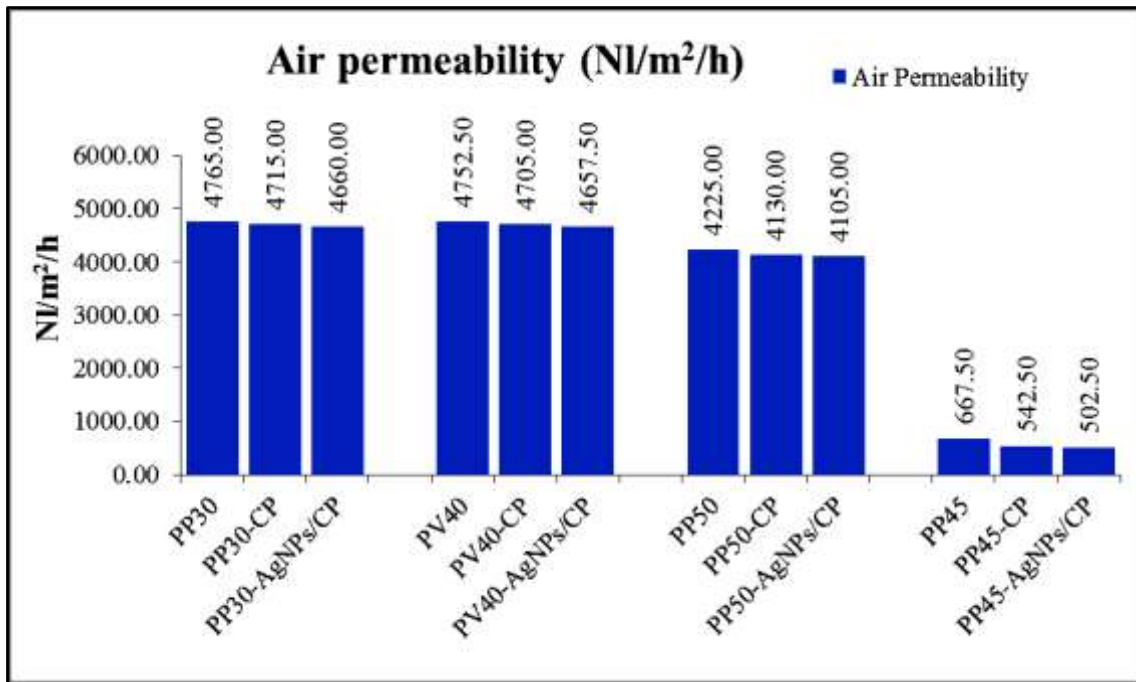


Figure 4.73: Air permeability (NI/m²/h)

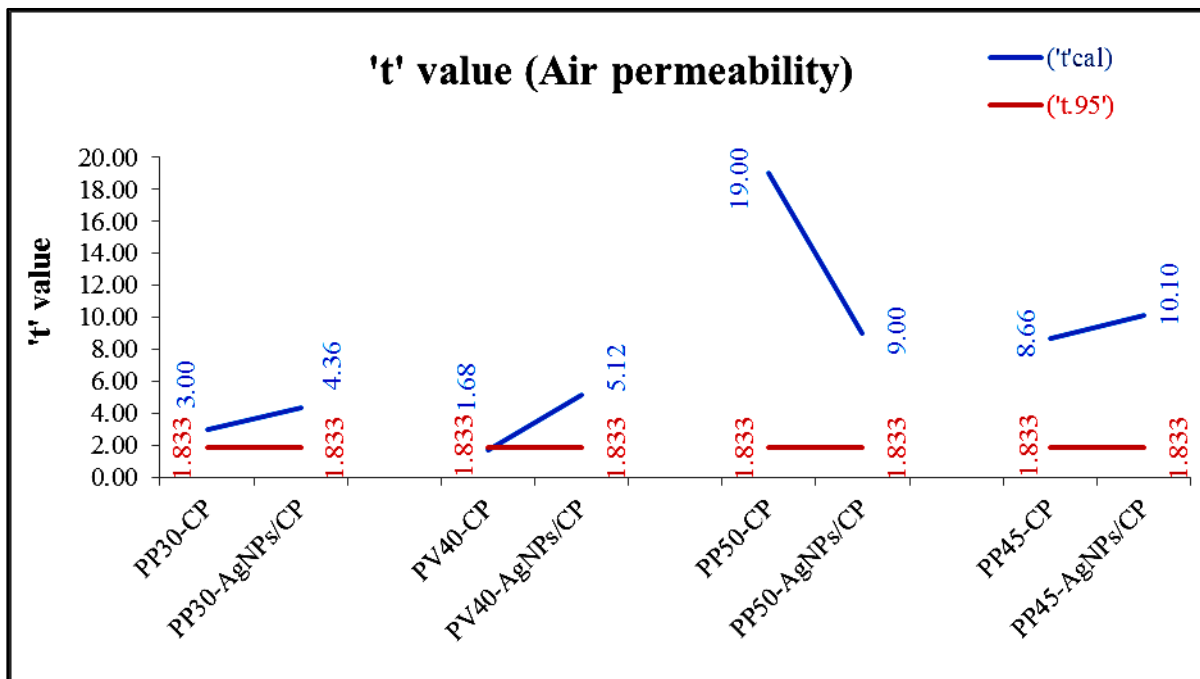


Figure 4.74: 't'-Test value (Air permeability)

Table 4.32: 't'-Test (Air permeability)

Parameters	Air Permeability	
	Mean	('t _{cal} ')
PP30 (SMS)	4765.00	--
PP30-CP	4715.00	3.00
PP30-AgNPs/CP	4660.00	4.36
PV40 (SMS)	4752.50	--
PV40-CP	4705.00	1.68
PV40-AgNPs/CP	4657.50	5.12
PP50 (SMS)	4225.00	--
PP50-CP	4130.00	19.00
PP50-AgNPs/CP	4105.00	9.00
PP45 (SMMMS)	667.50	--
PP45-CP	542.50	8.66
PP45-AgNPs/CP	502.50	10.10

('t_{cal}') = Calculated 't' value

('t₉₅') = 1.833

('t₉₉') = 2.821

Evidently a minor decrease in the air permeability ($\text{m}^3/\text{m}^2/\text{hr}$) with the application of the CP extract and the value has shown further reduction on loading AgNPs/CP invariably for all the nonwoven fabrics (Table 4.31). This trend witnessed increase in fabric covering area on the introduction of CP extract as well as AgNPs/CP colloidal into the fabric structure, which resisted air flow. Higher specific surface is offered by the nanoparticles, and that's why open gap for the air passage was reduced further [255]. A much higher drop in air permeability values was observed with PP45 sample in the group, can be due to the different structure of the nonwoven fabric (SMMMS), needs further investigation (Figure 4.73). The statistical analysis (Table 4.32) showed 't_{cal}' values are higher than warning limit 't₉₅' values, thus it can be concluded that the treatment by CP extract and AgNPs/CP can resulted in significant effect in the form of reduction in air permeability value for all the nonwoven textile materials, except PV40-CP composite (Figure 4.74).

II) Overall moisture management capability (OMMC)

The moisture management test results for all the samples are summarized in Table 4.33. Various entities; Overall moisture management capability (OMMC), Accumulative one-way transport index (%), wetting time (sec), absorption rate (%/sec), max wetted radius (mm) and spreading speed (mm/sec) mapped during the test are given in Figure 4.75 to Figure 4.80. The untreated sample was considered as a control sample during the entire evaluation.

It can be seen from the OMMC test findings that, almost all samples including control have attained 'very poor' (0–0.4) OMMC grade. Going in accordance, negative (< -50) value for the one-way transport index percentage (%) has been observed for all the samples. All together qualifies the base material as of 'very poor' grade with inadequate moisture management qualities and put them into the category of 'water proof fabrics'.

The only exception observed was PV40, which was originally having 'poor' OMMC grade but on CP extract treatment it also behaved as plastic. However, its nano-composite sample @PV-AgNPs/CP has shown 'Good' (0.4132) OMMC value (Table 4.33 and Figure 4.75). Its 'Good' (166.1951) accumulative one-way transport index percentage (%) also substantiate improvement in water handling characteristics and categorized as 'moisture management fabric' (Figure 4.76).

The water proof behaviour is likely for all the parent samples constituted of hydrophobic PP fibers as well as their treated samples having very low or nano-level add-on of CP extract and AgNPs/CP respectively [95]. Similarly, presence of higher water affinity viscose fibers along with water resistant polyester fibers in the selected PV40 nonwoven matrix allowed it to record better OMMC value in the group [5,254]. However, its -CP treated sample has shown shift towards water-proof group but enhancement in OMMC value has been reported on -AgNPs/CP treatment. The common point should be noted that, all the samples in the group irrespective of PP-based or PV-based have shown very minute improvement on AgNPs/CP reinforcement. This must be attributed to silver characteristics even though induced at the nano-scale [46].

Thus, no significant changes have been noted, especially in all PP nonwoven fabrics even after the application of the AgNPs/CP and CP extract. But, OMMC value and one-way transport index percentage (%) of the PV-based material have registered favourable change on the application of the AgNPs/CP.

Table 4.33: Moisture management properties of Nano-composites

	Wetting Time Top(sec)	Wetting Time Bottom(sec)	Top Absorption Rate (%/sec)	Bottom Absorption Rate (%/sec)	Top Max Wetted Radius (mm)	Bottom Max Wetted Radius (mm)	Top Spreading Speed (mm/sec)	Bottom Spreading Speed (mm/sec)	Accumulative one-way transport index(%)	OMMC	Fabric Type
PP30 (SMS)	1.591 (Very Fast)	120 (No Wetting)	12.447 (Slow)	0 (Very Slow)	5 (No Wetting)	0 (No Wetting)	2.8121 (Medium)	0 (Very Slow)	-548.7142 (Very Poor)	0 (Very Poor)	This is water proof fabric
PP30-CP	1.779 (Very Fast)	120 (No Wetting)	12.1 (Slow)	0 (Very Slow)	5 (No Wetting)	0 (No Wetting)	2.5432 (Medium)	0 (Very Slow)	-468.7614 (Very Poor)	0 (Very Poor)	This is water proof fabric
PP30-AgNPs/CP	1.591 (Very Fast)	91.822 (Slow)	15.1581 (Slow)	30.4894 (Medium)	5 (No Wetting)	0 (No Wetting)	2.8121 (Medium)	0 (Very Slow)	-390.6393 (Very Poor)	0.0569 (Very Poor)	This is water proof fabric
PV40 (SMS)	1.217 (Very Fast)	5.335 (Medium)	71.6256 (Fast)	29.486 (Slow)	30 (Very Fast)	25 (Very Fast)	13.0363 (Very Fast)	7.4152 (Very Fast)	-1117.0243 (Very Poor)	0.3041 (Poor)	This is fast absorbing and quick drying fabric
PV40-CP	21.341 (Slow)	5.616 (Medium)	14.7385 (Slow)	16.5701 (Slow)	10 (Small)	0 (No Wetting)	0.3321 (Very Slow)	0 (Very Slow)	-82.6629 (Very Poor)	0.0183 (Very Poor)	This is water proof fabric
PV40-AgNPs/CP	120 (No Wetting)	16.38 (Medium)	0 (Very Slow)	5.4189 (Very Slow)	0 (No Wetting)	15 (Medium)	0 (Very Slow)	3.0762 (Fast)	166.1951 (Good)	0.4132 (Good)	This is moisture management fabric
PP50 (SMS)	1.591 (Very Fast)	120 (No Wetting)	20.3884 (Slow)	0 (Very Slow)	5 (No Wetting)	0 (No Wetting)	2.8121 (Medium)	0 (Very Slow)	-519.0043 (Very Poor)	0 (Very Poor)	This is water proof fabric
PP50-CP	1.684 (Very Fast)	120 (No Wetting)	16.3891 (Slow)	0 (Very Slow)	5 (No Wetting)	0 (No Wetting)	2.6709 (Medium)	0 (Very Slow)	-833.5358 (Very Poor)	0 (Very Poor)	This is water proof fabric
PP50-AgNPs/CP	1.684 (Very Fast)	79.935 (Slow)	14.0018 (Slow)	17.549 (Slow)	25 (Very Fast)	0 (No Wetting)	3.1702 (Fast)	0 (Very Slow)	-834.8659 (Very Poor)	0.021 (Very Poor)	This is water proof fabric
PP45 (SMMMMS)	1.779 (Very Fast)	120 (No Wetting)	12.9075 (Slow)	0 (Very Slow)	5 (No Wetting)	0 (No Wetting)	2.5432 (Medium)	0 (Very Slow)	-510.7046 (Very Poor)	0 (Very Poor)	This is water proof fabric
PP45-CP	1.685 (Very Fast)	86.955 (Slow)	8.0789 (Very Slow)	4.4665 (Very Slow)	5 (No Wetting)	0 (No Wetting)	2.6709 (Medium)	0 (Very Slow)	-609.4548 (Very Poor)	0 (Very Poor)	This is water proof fabric
PP45-AgNPs/CP	1.592 (Very Fast)	120 (No Wetting)	13.0402 (Slow)	0 (Very Slow)	5 (No Wetting)	0 (No Wetting)	2.8106 (Medium)	0 (Very Slow)	-278.7221 (Very Poor)	0 (Very Poor)	This is water proof fabric

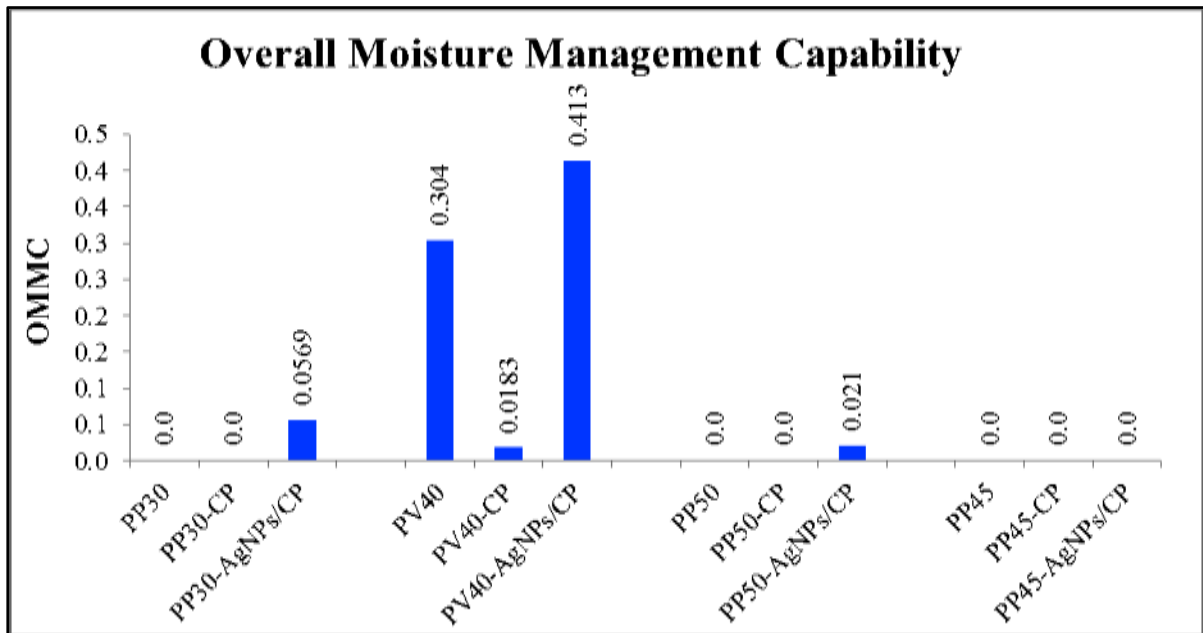


Figure 4.75: Overall moisture management capability

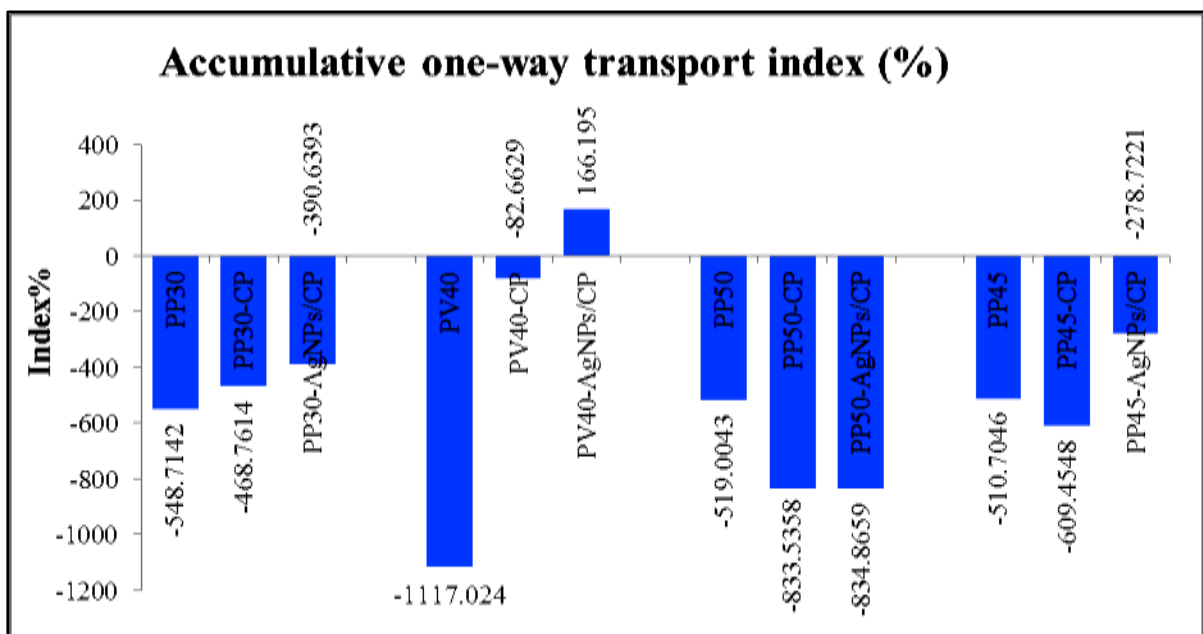


Figure 4.76: Accumulative one-way transport index (%)

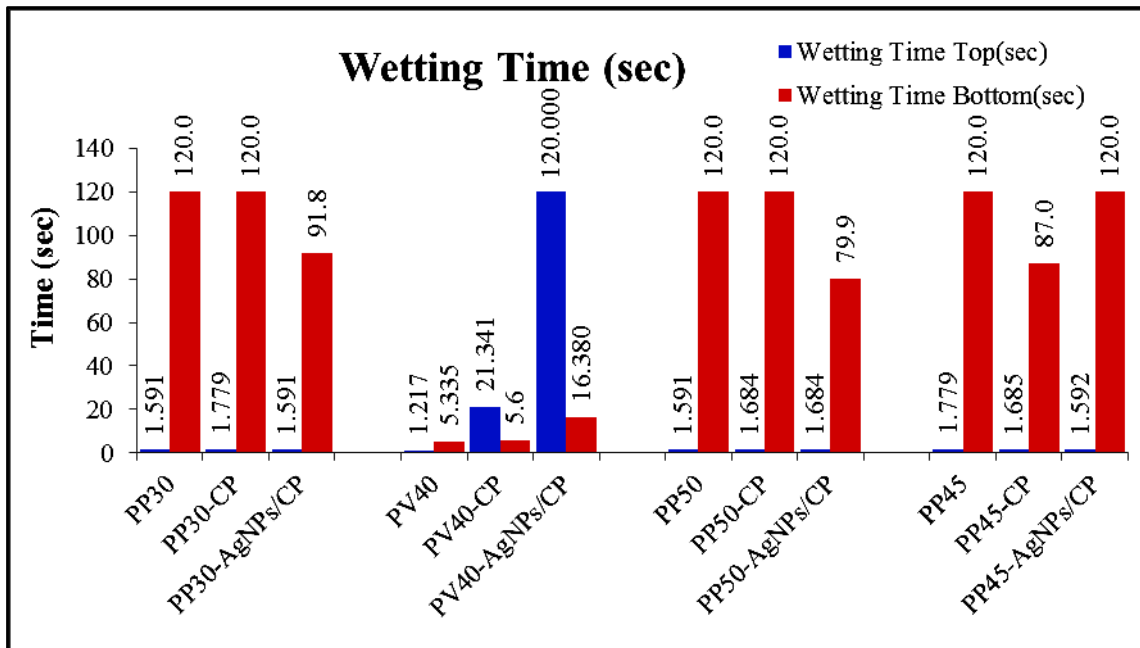


Figure 4.77: Wetting time (sec) for top and bottom surface

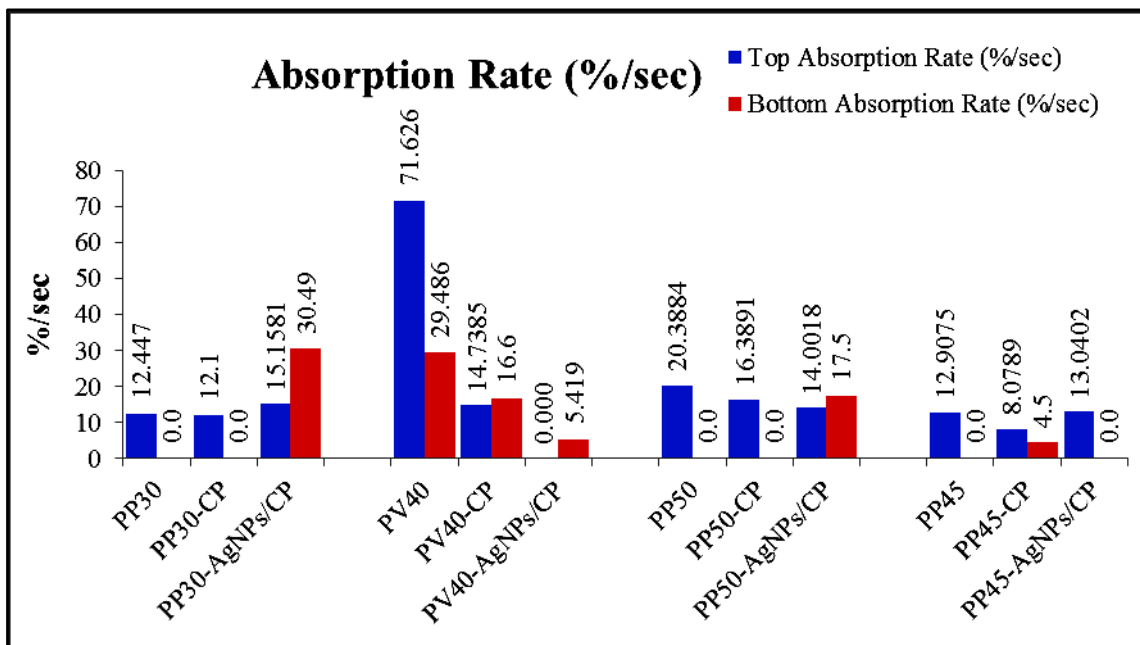


Figure 4.78: Absorption rate (%/sec) for top and bottom surface

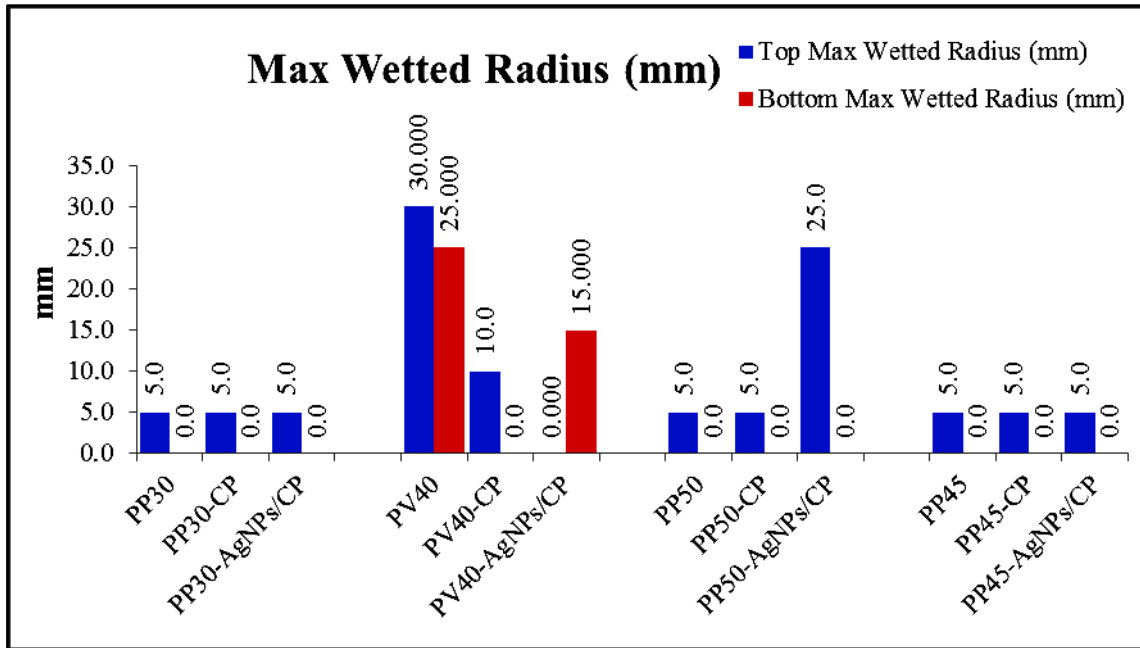


Figure 4.79: Max wetted radius (mm) for top and bottom surface

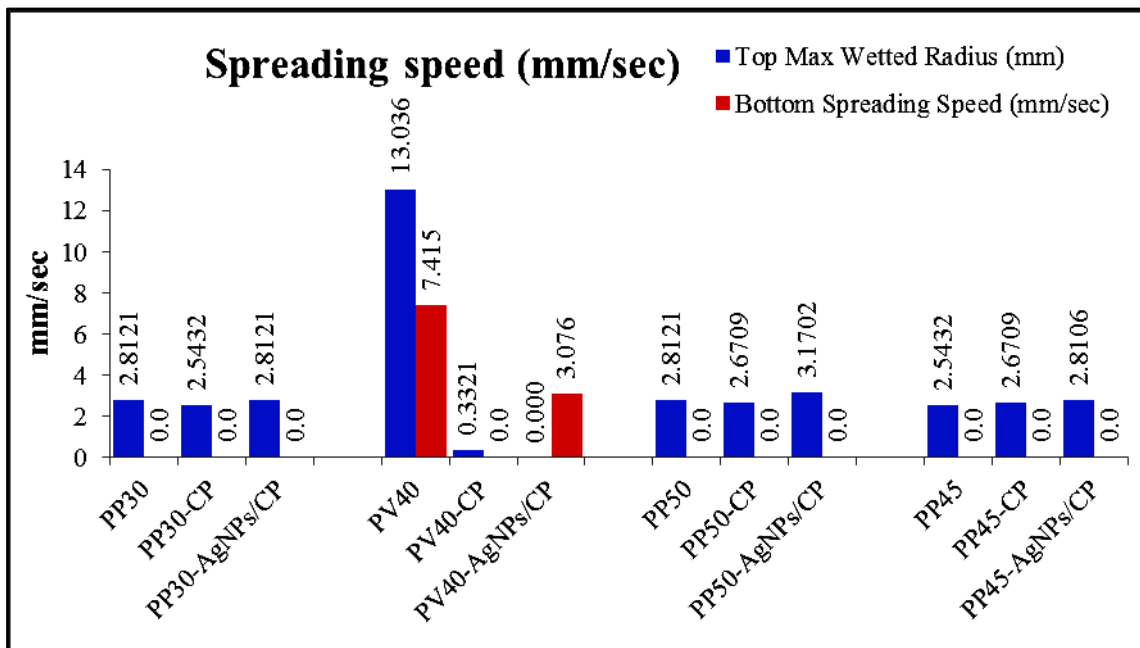


Figure 4.80: Spreading speed (mm/sec) for top and bottom surface

Figures (4.75 to 4.80) illustrate the graphical analysis and Figure 4.81 to Figure 4.92 show resultant maps of the moisture management test for all the samples respectively.

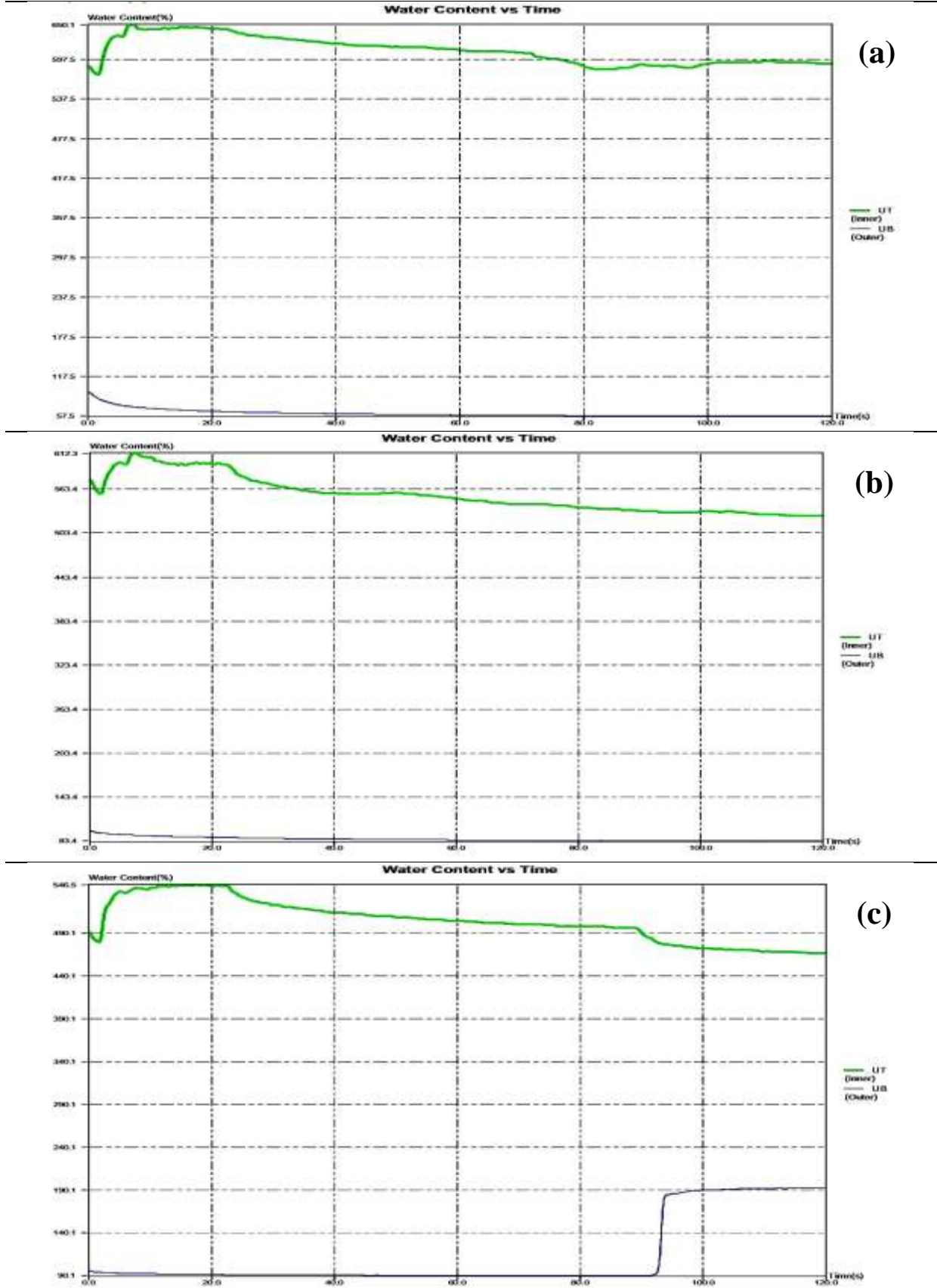


Figure 4.81: Water content vs Time
a) PP30, b) PP30-CP, and c) PP30-AgNPs/CP respectively

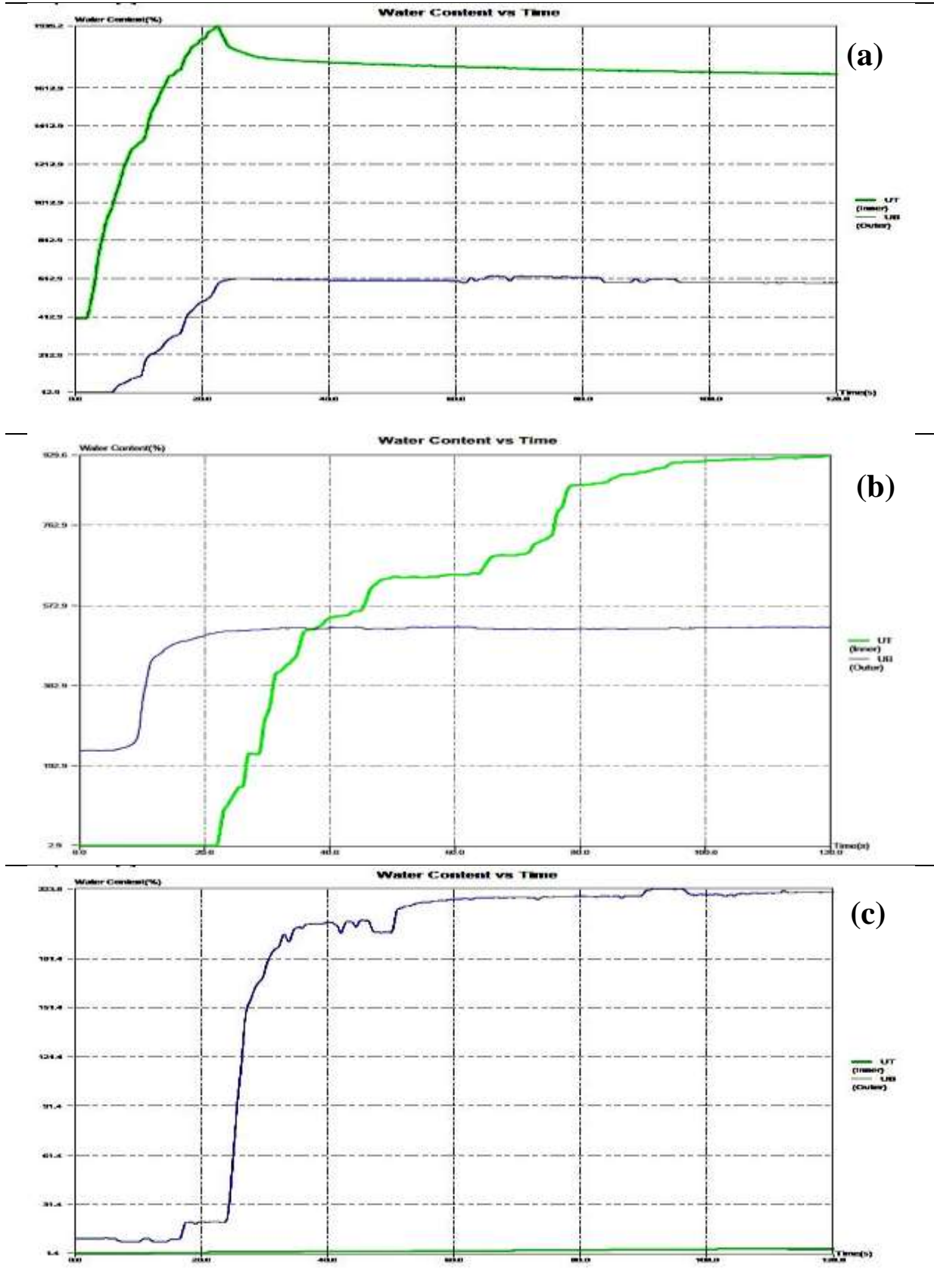


Figure 4.82: Water content vs Time
a) PV40, b) PV40-CP, and c) PV40-AgNPs/CP respectively

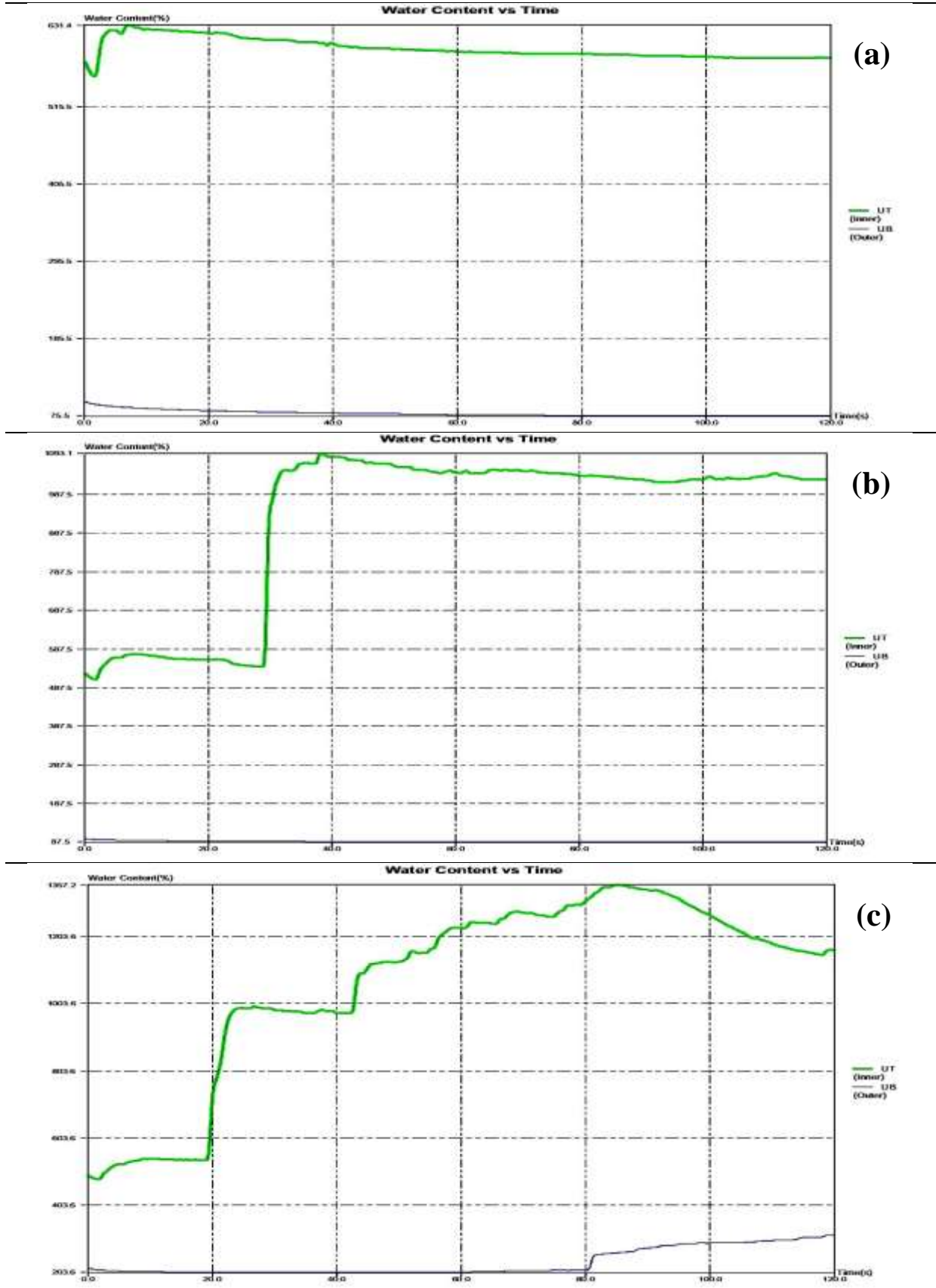


Figure 4.83: Water content vs Time
 a) PP50, b) PP50-CP, and c) PP50-AgNPs/CP respectively

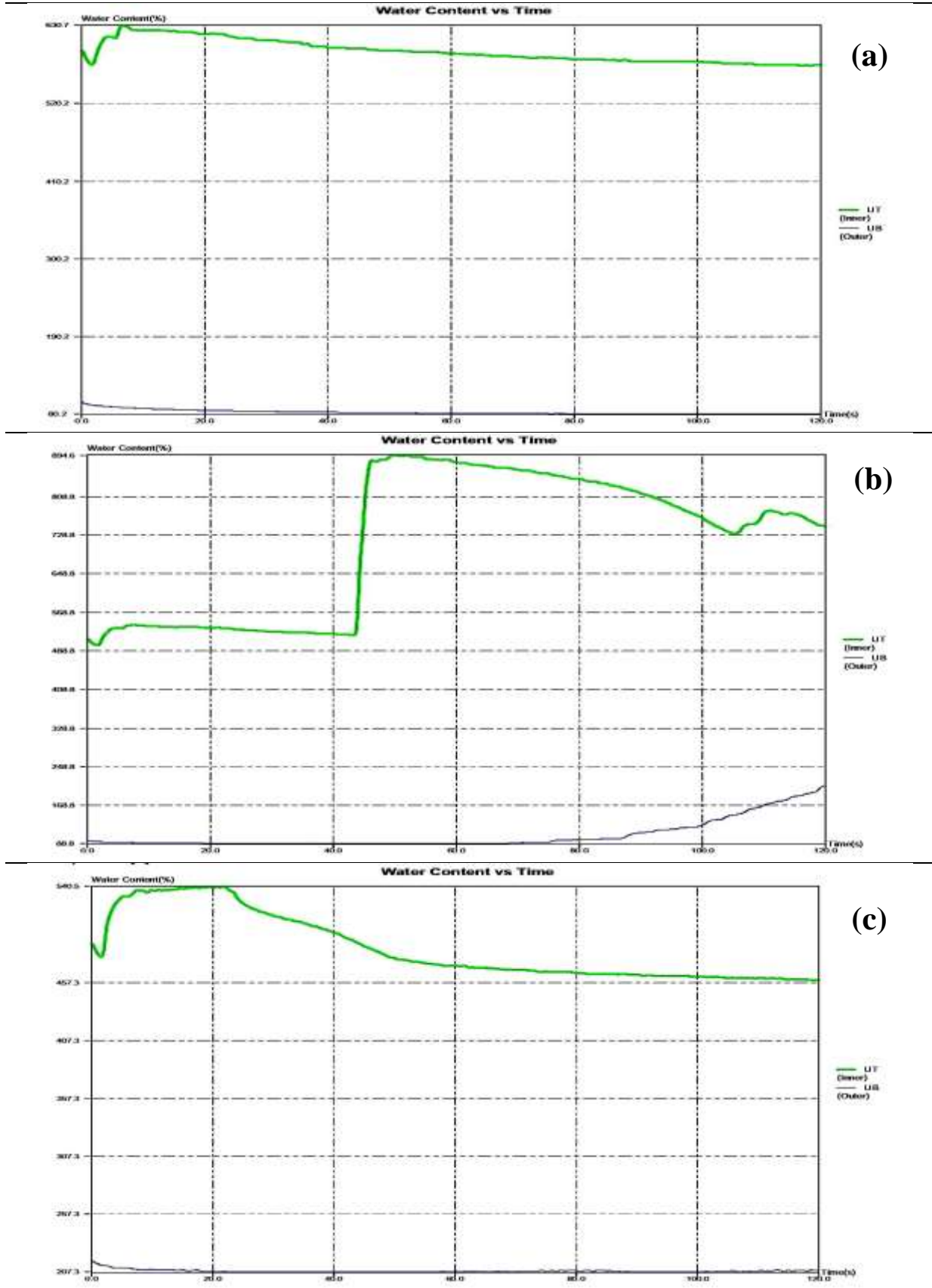


Figure 4.84: Water content vs Time
 a) PP45, b) PP45-CP, and c) PP45-AgNPs/CP respectively

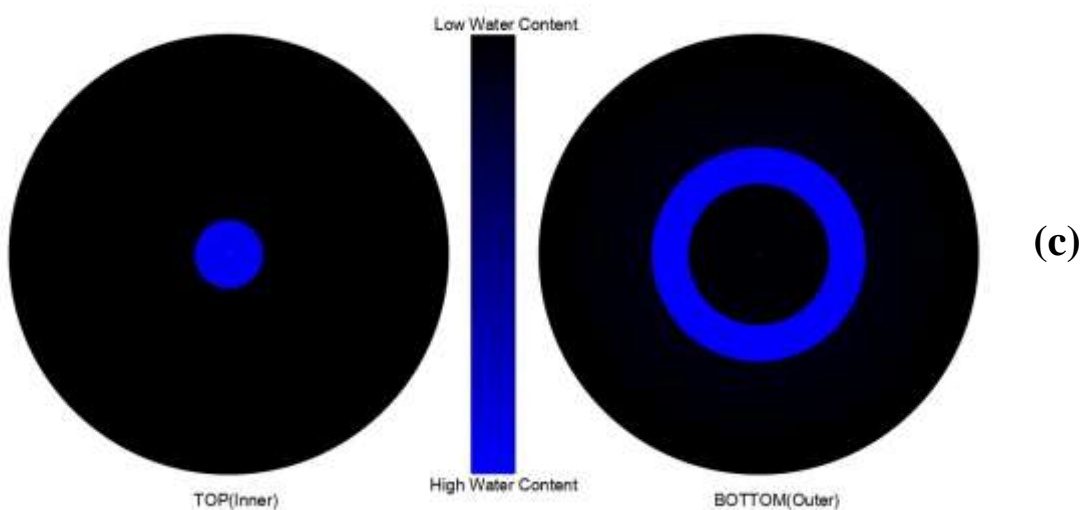
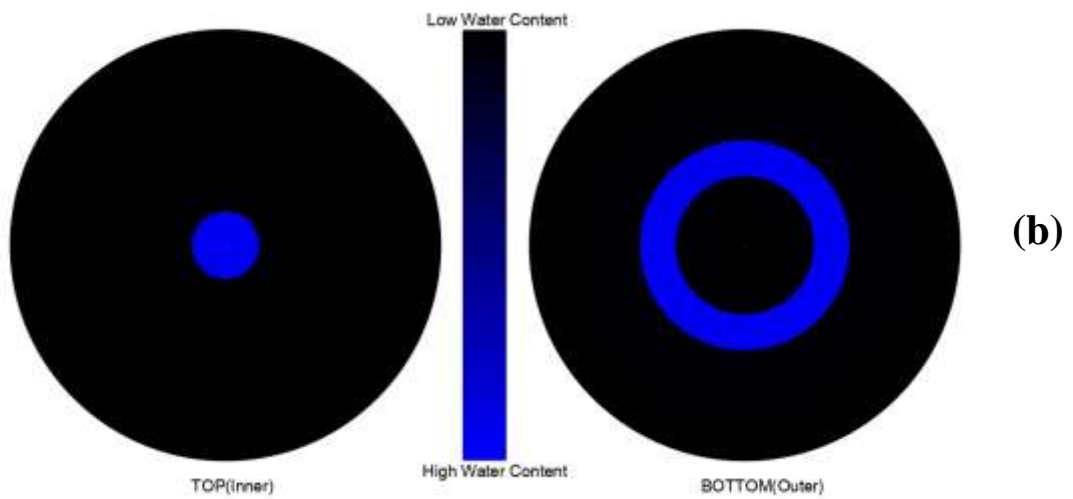
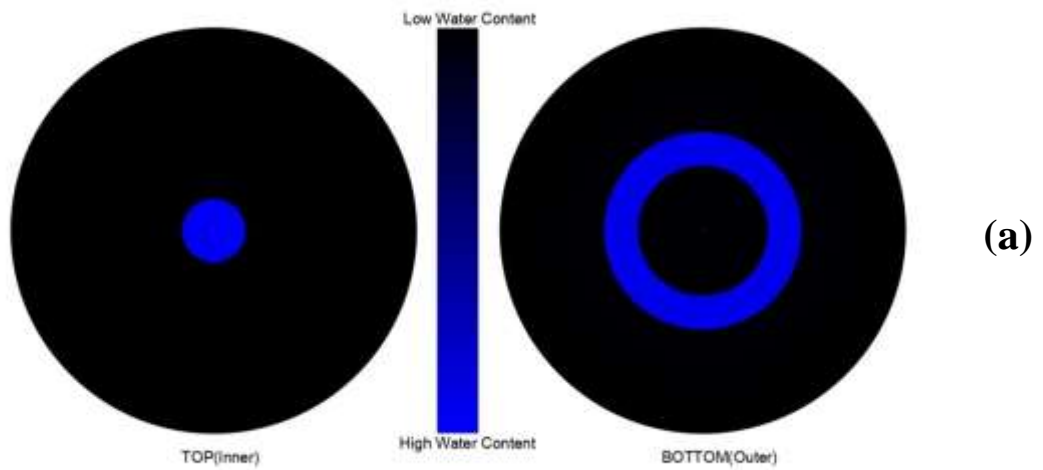


Figure 4.85: Water location vs Time
 a) PP30, b) PP30-CP, and c) PP30-AgNPs/CP respectively

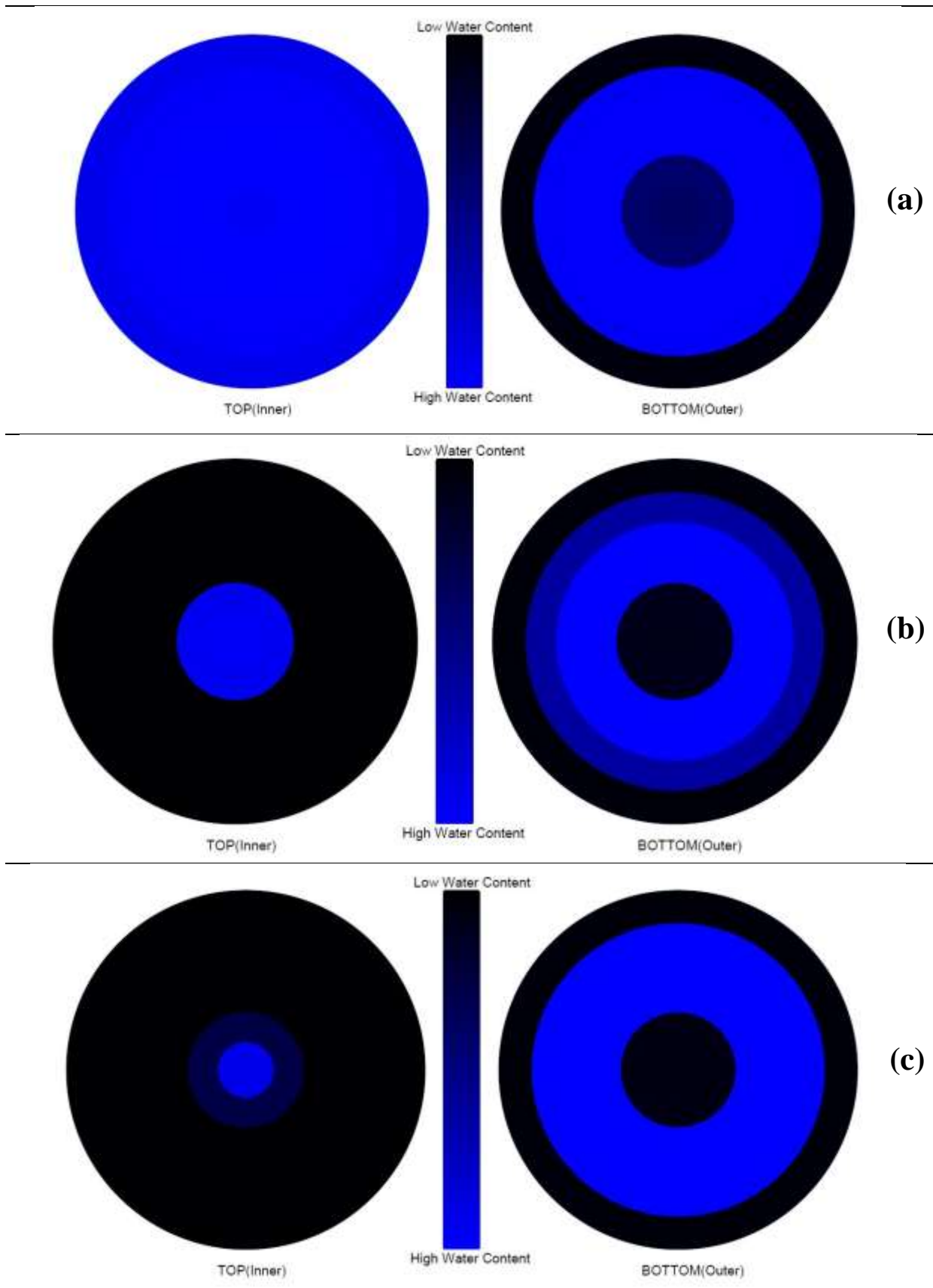


Figure 4.86: Water location vs Time
a) PV40, b) PV40-CP, and c) PV40-AgNPs/CP respectively

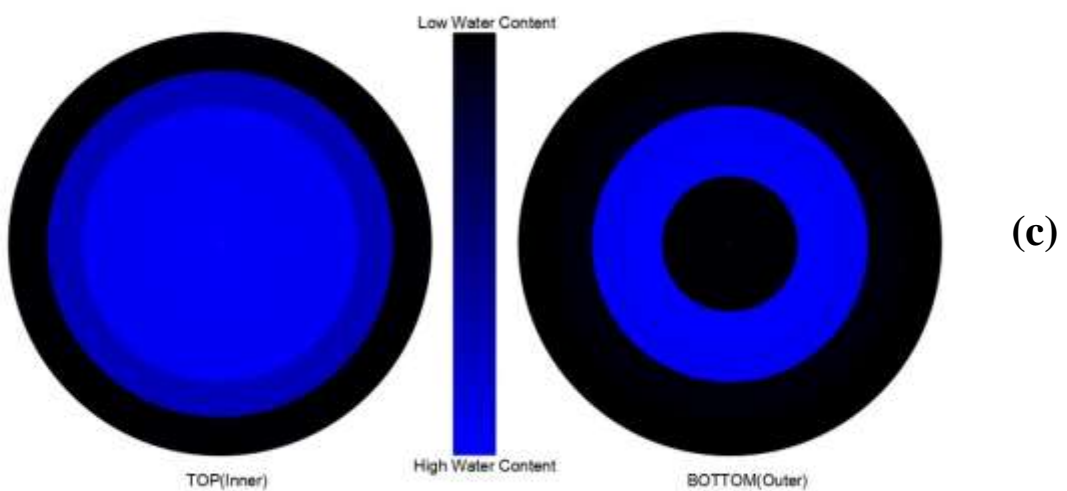
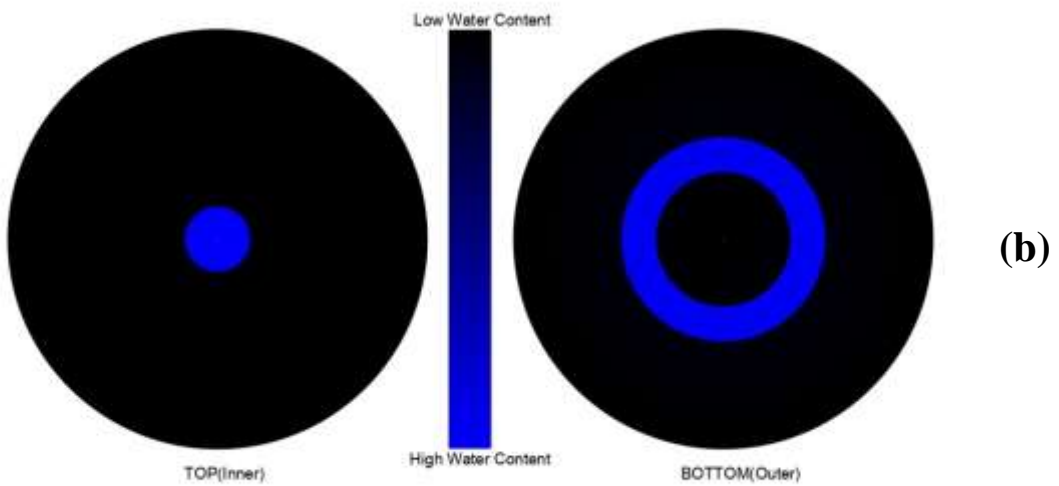
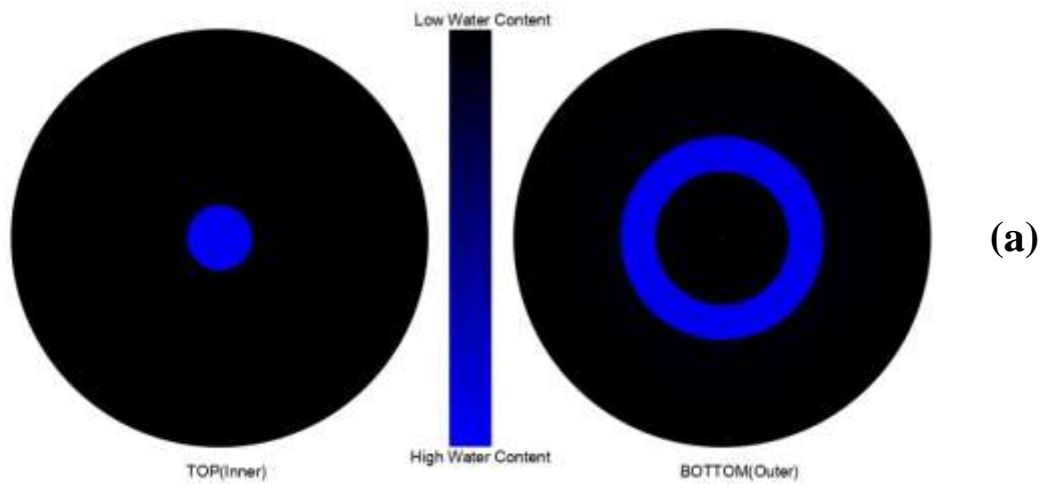


Figure 4.87: Water location vs Time
a) PP50, b) PP50-CP, and c) PP50-AgNPs/CP respectively

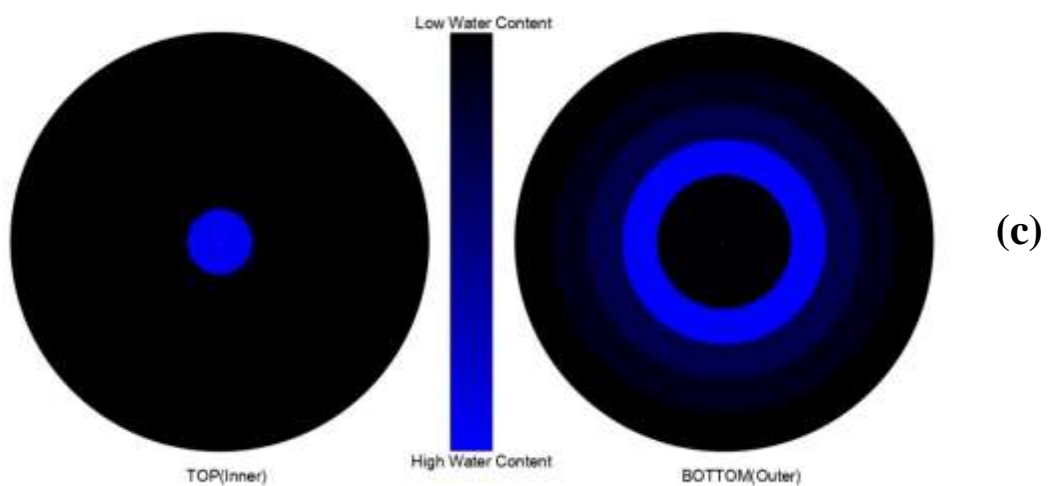
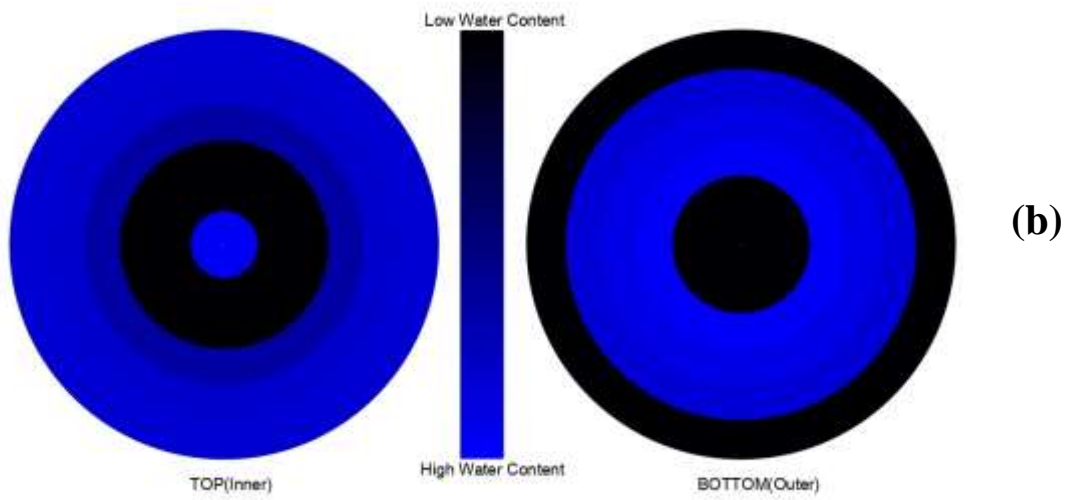
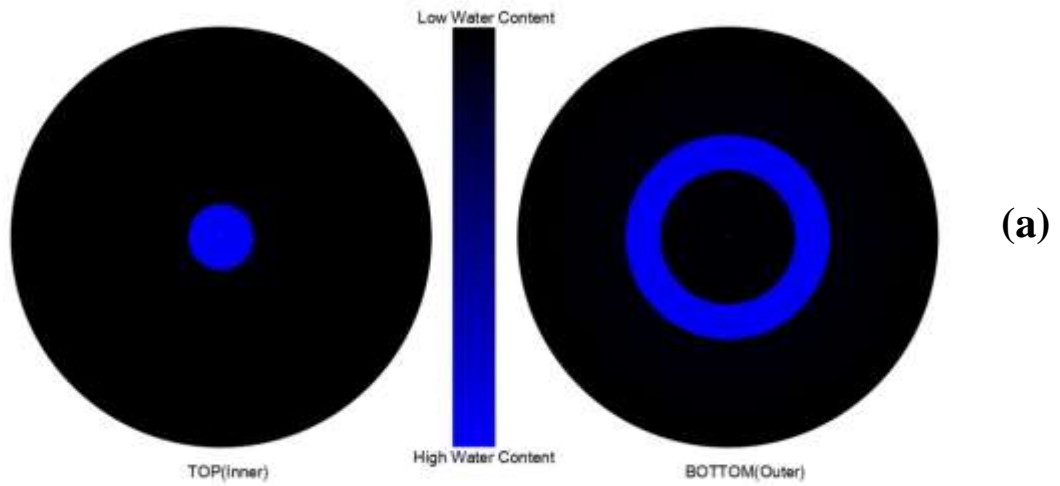


Figure 4.88: Water location vs Time
a) PP45, b) PP45-CP, and c) PP45-AgNPs/CP respectively

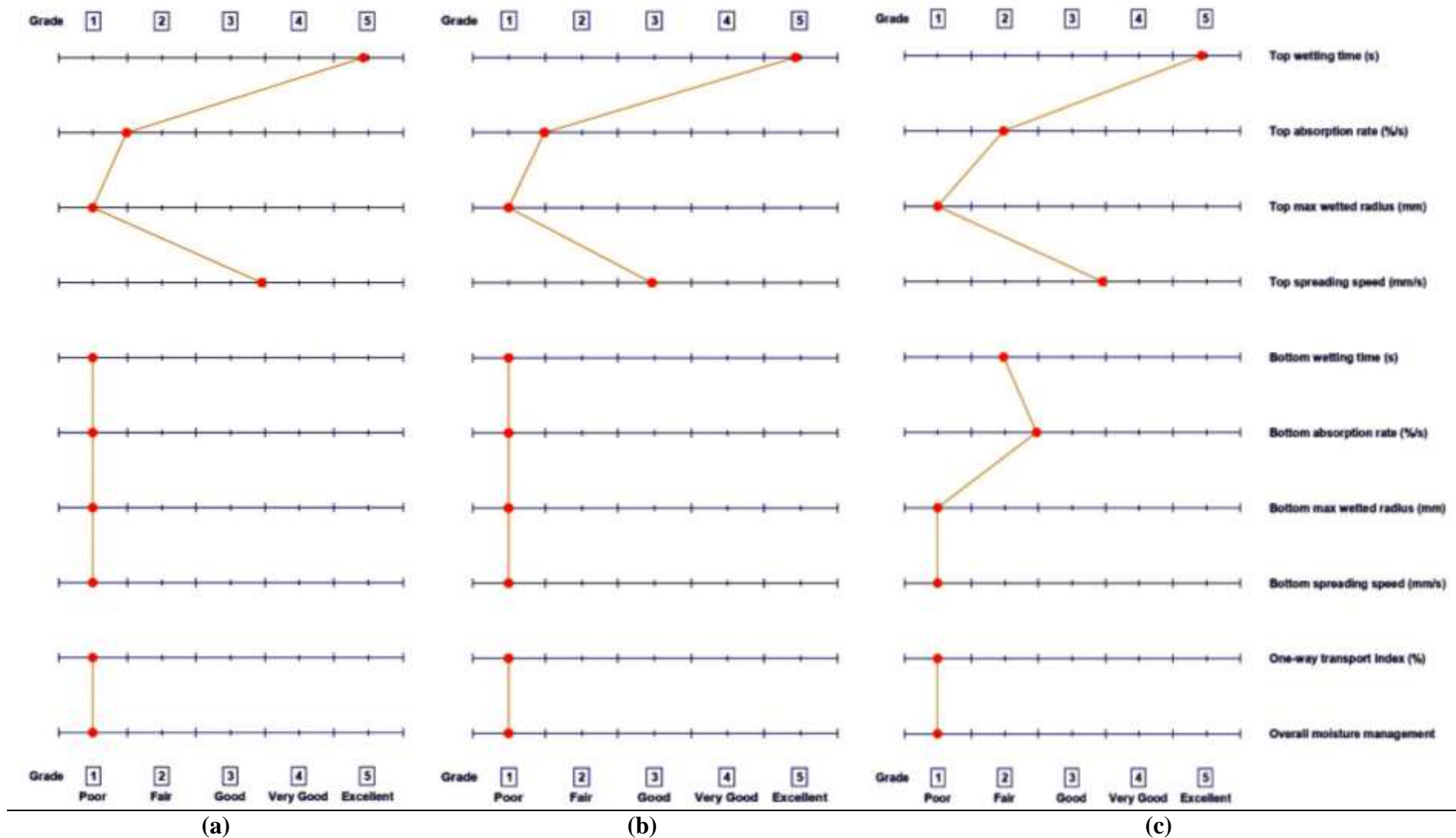


Figure 4.89: Finger print of moisture management properties for a) PP30, b) PP30-CP, and c) PP30-AgNPs/CP respectively

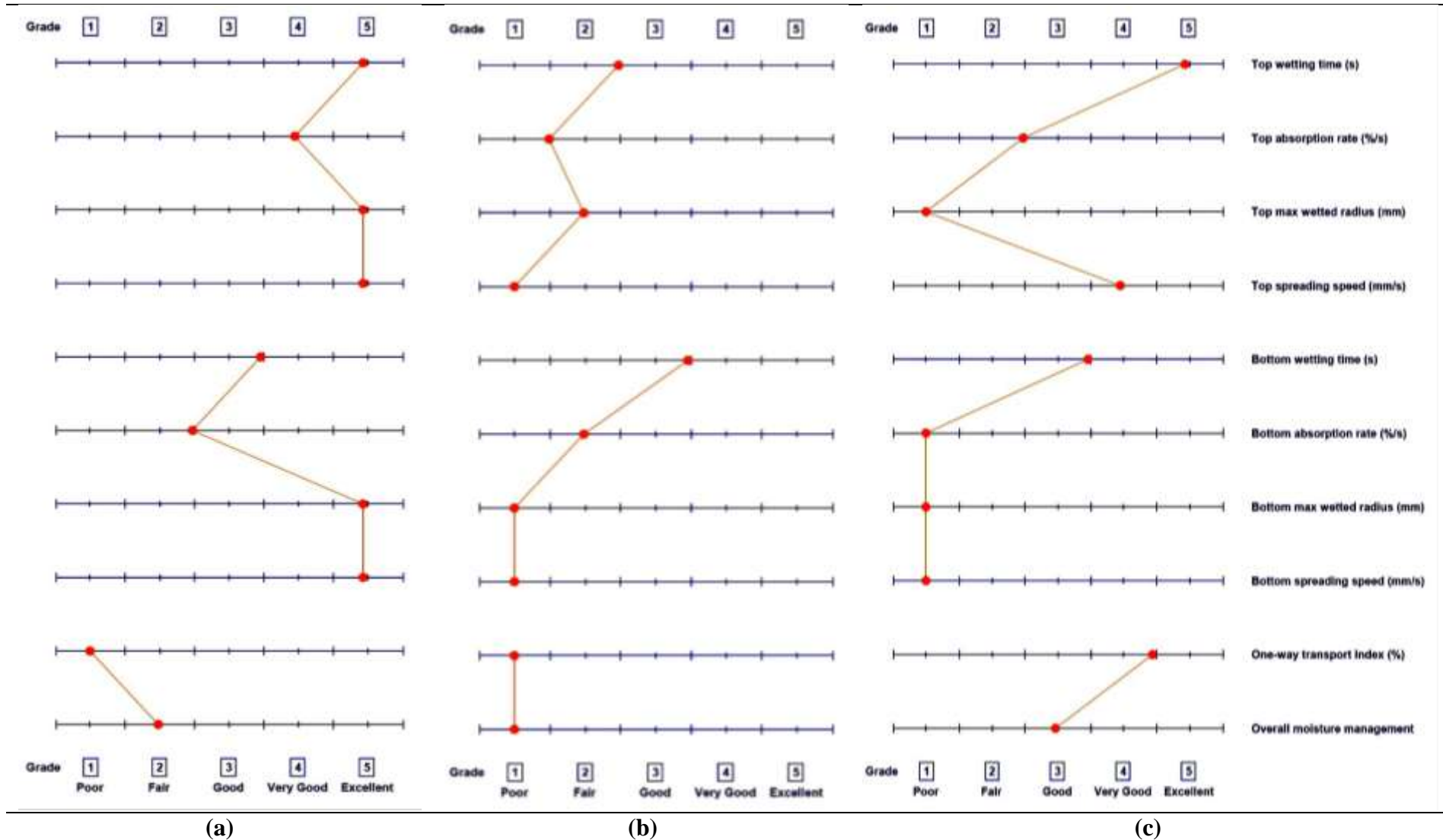


Figure 4.90: Finger print of moisture management properties for a) PV40, b) PV40-CP, and c) PV40-AgNPs/CP respectively

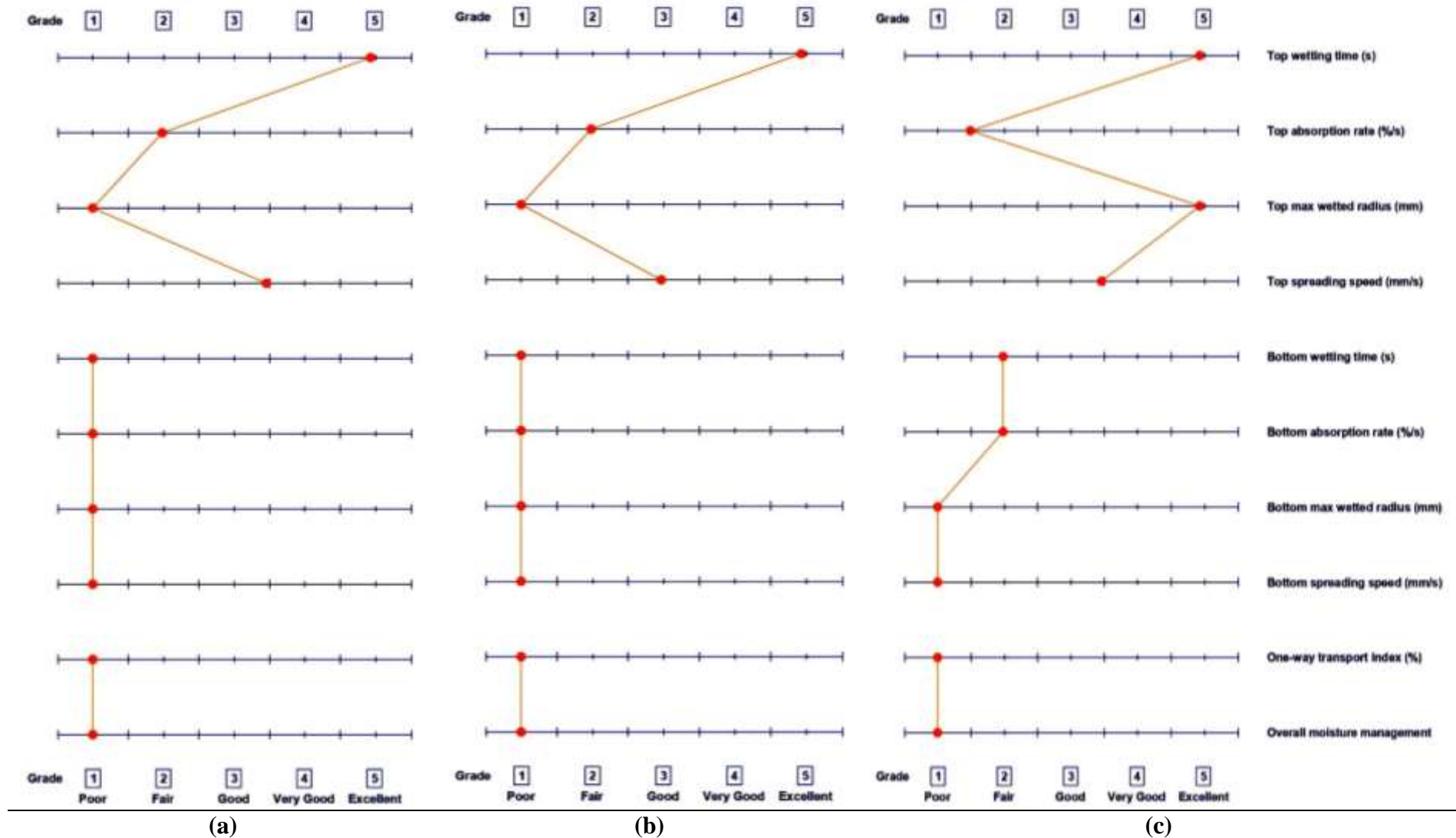


Figure 4.91: Finger print of moisture management properties for a) PP50, b) PP50-CP, and c) PP50-AgNPs/CP respectively

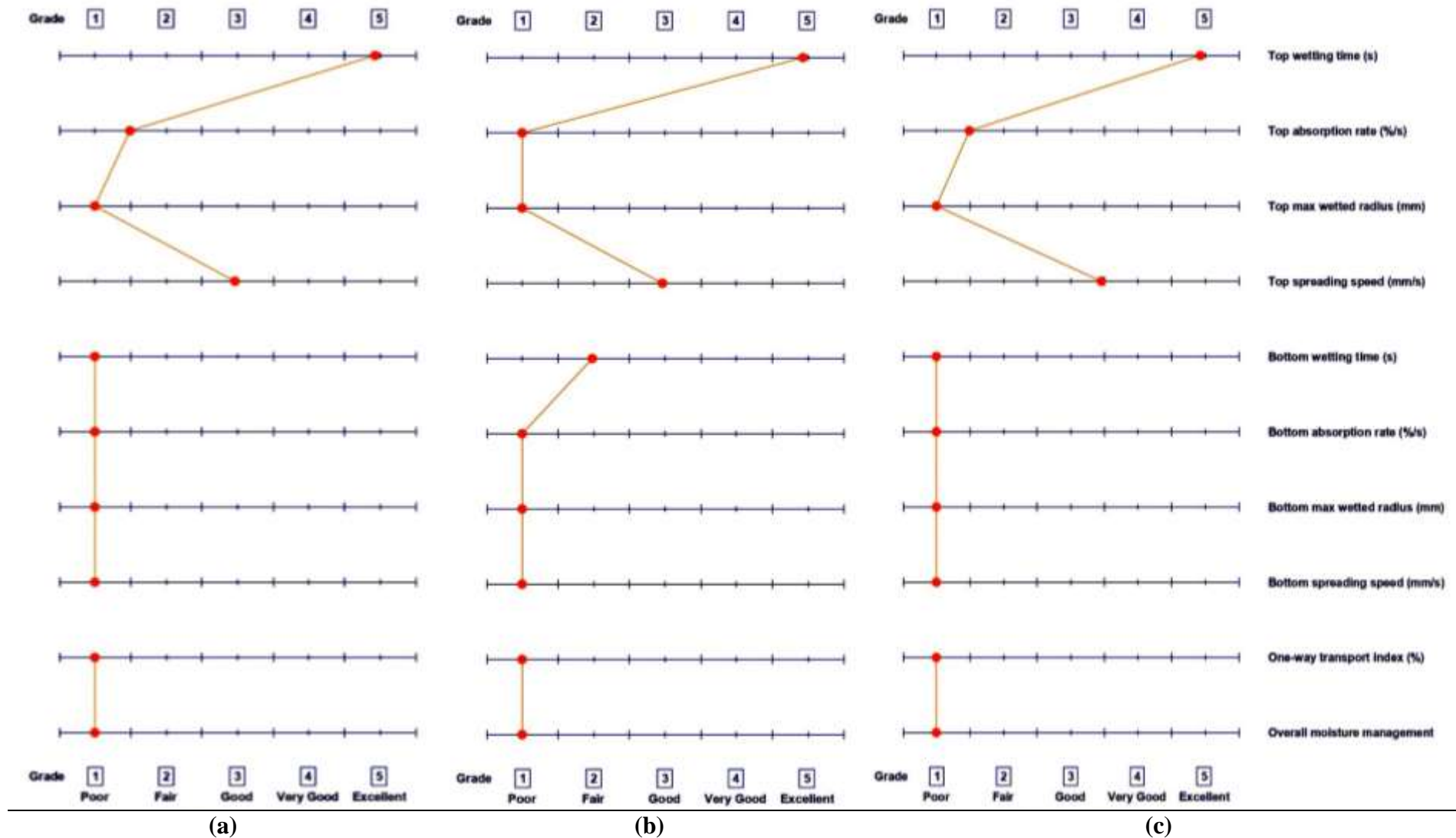


Figure 4.92: Finger print of moisture management properties for a) PP45, b) PP45-CP, and c) PP45-AgNPs/CP respectively

4.4.1.4 UV Transmission properties

The UV protection profiles of the nano-composites (respective-AgNPs/CP) and samples treated with CP leave extract (respective -CP) were assessed and compared with their respective untreated nonwoven textile materials.

The UV transmittance characteristics of all samples are demonstrations in Table 4.34. It can be seen that the UPF rating recorded for the untreated PP30, PV40 and PP50 SMS non-woven textile material are quite on a lower side, viz; 2, 5 and 3 respectively. Whereas, the moderate UPF rating of '14' has been executed by the PP45 SMMMS non-woven textile material. However, all the non-woven materials with their measured UPF rating values are categorized under the tag of 'Poor protection' for the tested UV radiations at 390, 384, 389 and 386 critical wavelengths. This trend is obvious for the selected low UPF manufactured fibers; PP, polyester and viscose rayon [7,95,298].

The UPF ratings of the untreated non-woven material got enhanced on treating with CP leave extract as well as AgNPs/CP almost in each category of base material (Table 4.34 and Figure 4.93).

The UVA transmittance (%) reported are 43.19, 34.12, 25.37 and 6.95, while the UVB transmittances (%) are 51.07, 11.54, 33.23 and 6.45 for the selected base materials. However, the UVA transmittance % was reduced to 35.00, 23.39, 20.79 and 4.90 on CP leave extract loading and 30.71, 20.75, 21.50 and 3.82 on AgNPs/CP loading. In the similar way UVB transmittance % has shown reduction to 38.68, 9.25, 23.10 and 4.43 on CP leave extract loading and 32.46, 9.18, 22.14 and 3.41 on AgNPs/CP loading. The results have indicated that the materials were became more protective against UVA and UVB type of radiations at around 389, 385, 389 and 387 critical wavelengths with CP leave extract, and 389, 386, 388, and 387 critical wavelengths with AgNPs/CP. This behaviour can be attributed to the deposited CP leave extract particles or AgNPs/CP on non-woven materials, which have dispersed or absorbed the radiations and reduced the UV transmittance [220,320].

Table 4.34: UV transmittance profile of Nano-composites

Sample	UPF Rating	Average UPF	CV %	T (UVA) %	CV %	T (UVB) %	CV %	Critical Wavelength
PP30 (SMS)	2	2.00	5.79%	43.19%	6.75%	51.07%	5.71%	390
PP30-CP	2	2.64	11.04%	35.00%	11.38%	38.68%	10.46%	389
PP30-AgNPs/CP	3	3.1	9.15%	30.71%	9.66%	32.46%	9.79%	389
PV40 (SMS)	5	6.48	14.75%	34.12%	9.80%	11.54%	17.35%	384
PV40-CP	7	8.69	17.84%	23.39%	12.48%	9.25%	24.82%	385
PV40-AgNPs/CP	8	8.97	12.93%	20.75%	14.85%	9.18%	15.12%	386
PP50 (SMS)	3	3.14	9.41%	25.37%	13.33%	33.23%	9.74%	389
PP50-CP	4	4.4	9.39%	20.79%	8.77%	23.10%	9.12%	389
PP50-AgNPs/CP	4	4.62	18.32%	21.50%	19.18%	22.14%	18.73%	388
PP45 (SMMMS)	14	16.32	11.94%	6.95%	12.48%	6.45%	13.39%	386
PP45-CP	21	23.43	9.32%	4.90%	9.76%	4.43%	9.85%	387
PP45-AgNPs/CP	27	30.22	8.74%	3.82%	8.93%	3.41%	8.74%	387

*CV% of 5 scans for each sample

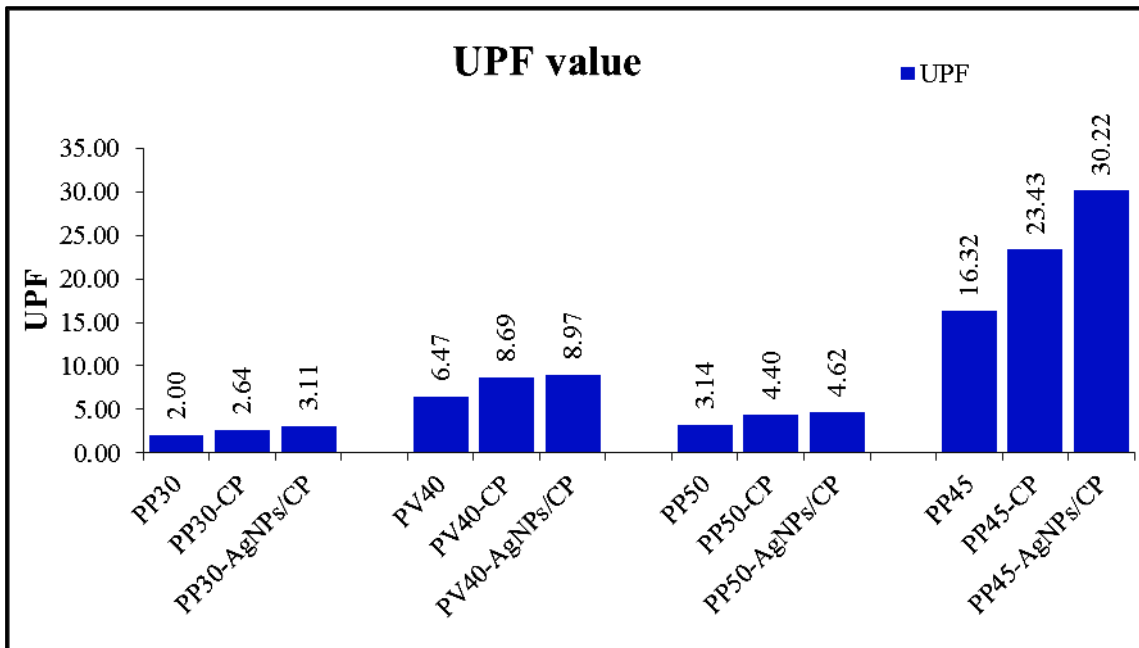


Figure 4.93: UPF values of nano-composites

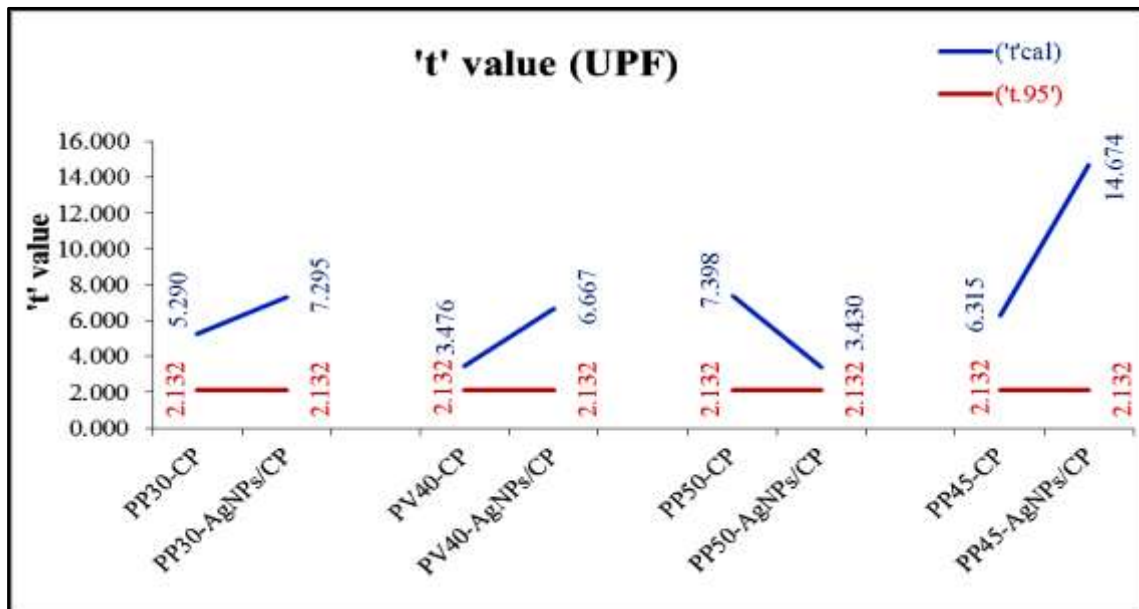


Figure 4.94: 't'-Test value (UPF)

Table 4.35: 't'-Test (UV transmittance profile)

Parameters	Mean	('t_{cal}')
PP30 (SMS)	2.00	--
PP30-CP	2.64	5.290
PP30-AgNPs/CP	3.11	7.295
PV40 (SMS)	6.47	--
PV40-CP	8.69	3.476
PV40-AgNPs/CP	8.97	6.667
PP50 (SMS)	3.14	--
PP50-CP	4.40	7.398
PP50-AgNPs/CP	4.62	3.430
PP45 (SMMMS)	16.32	--
PP45-CP	23.43	6.315
PP45-AgNPs/CP	30.22	14.674

('t_{cal}') = Calculated 't' value,

('t_{.95}') = 2.132

('t_{.99}') = 3.747

The UV transmittance profile of all the samples were analysed statistically to find out the effect of CP extract and AgNPs/CP through the sample mean paired 't-test'. The statistical analysis has shown higher calculated 't_{cal}' values at 95% confidence level and degrees of freedom of '4' ($\therefore \eta = 5-1$) (Table 4.35 and Figure 4.94). Hence, it is statistically proved that after application of the CP leave extract and AgNPs/CP, have a significant effect on the UV transmittance profile of the respective nonwoven textile materials.

Figure 4.95-uvs to Figure 4.98-uvs executes graphically the UV transmittance profiles for all the samples under study.

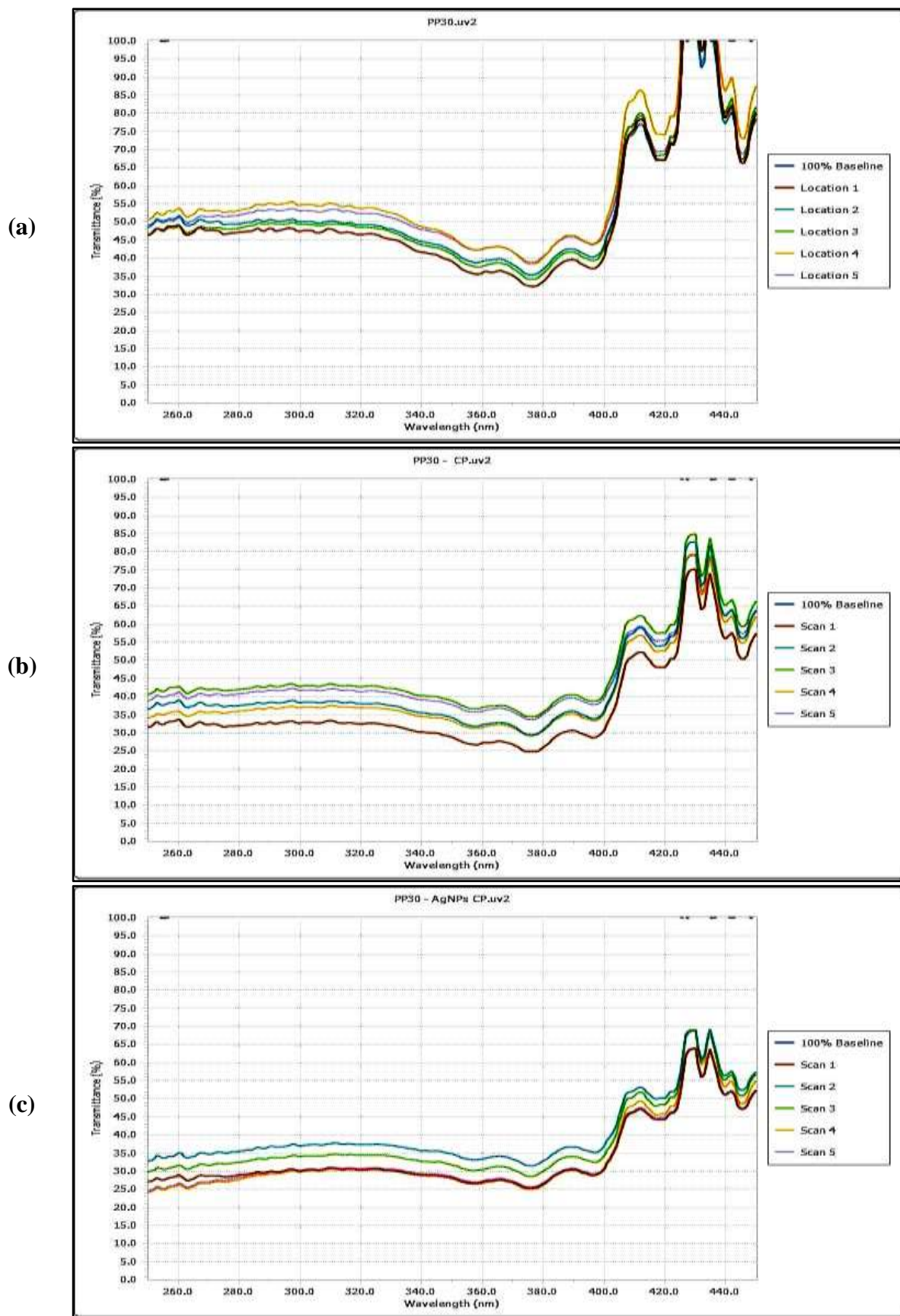
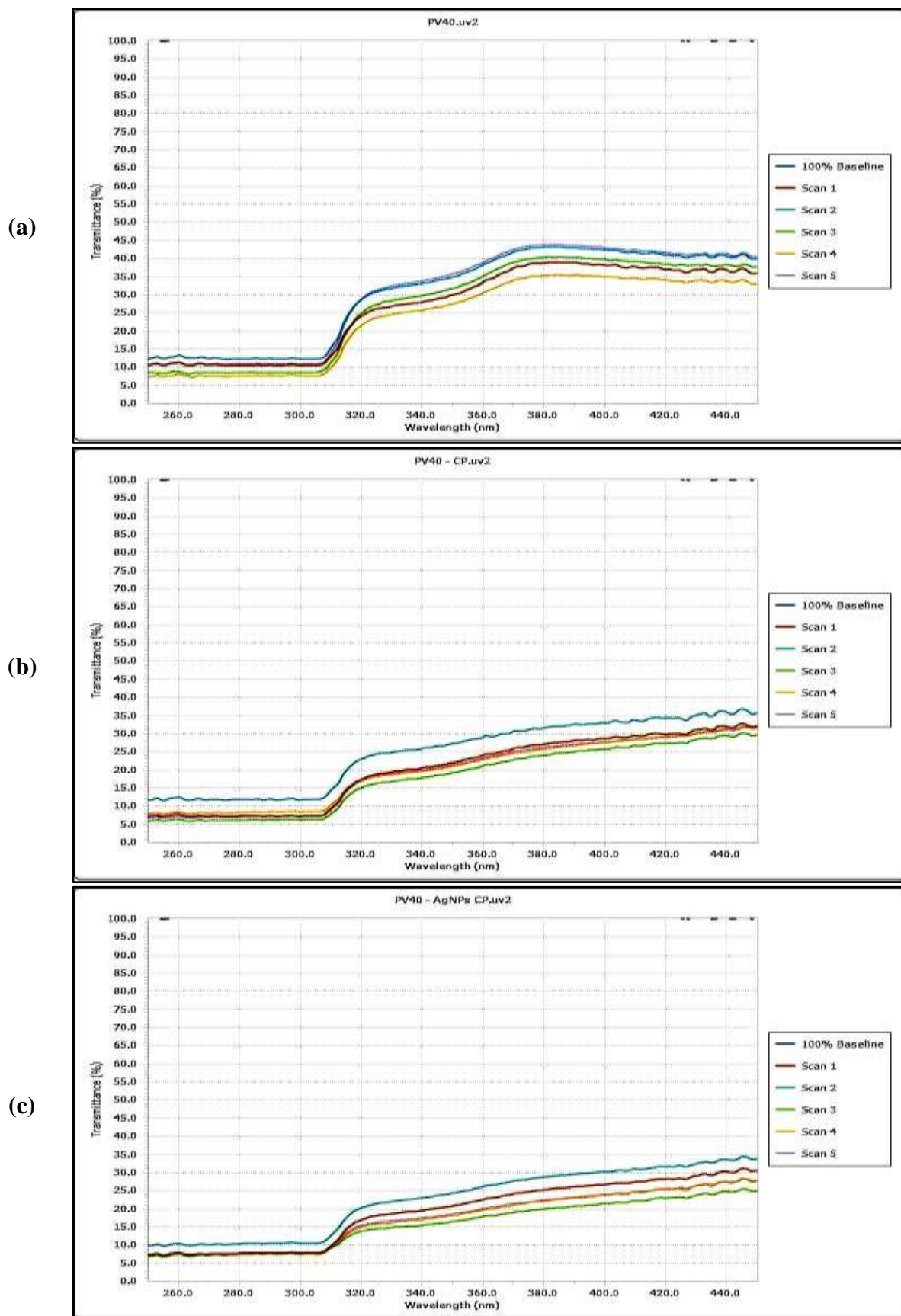


Figure 4.95: UV Transmittance profile of a) PP30, b) PP30-CP, and c) PP30-AgNPs/CP



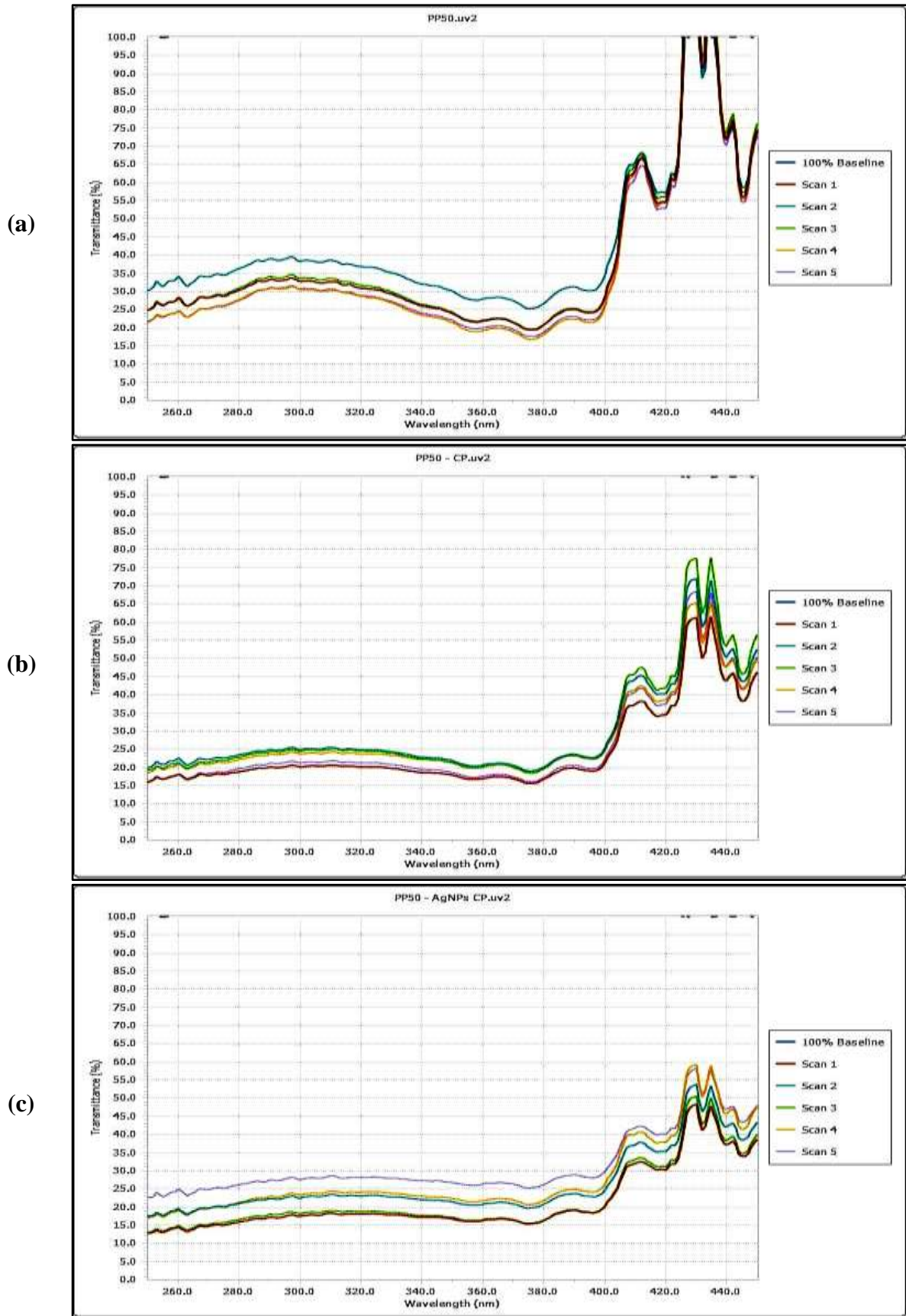


Figure 4.97: UV Transmittance profile of a) PP50, b) PP50-CP, and c) PP50-AgNPs/CP

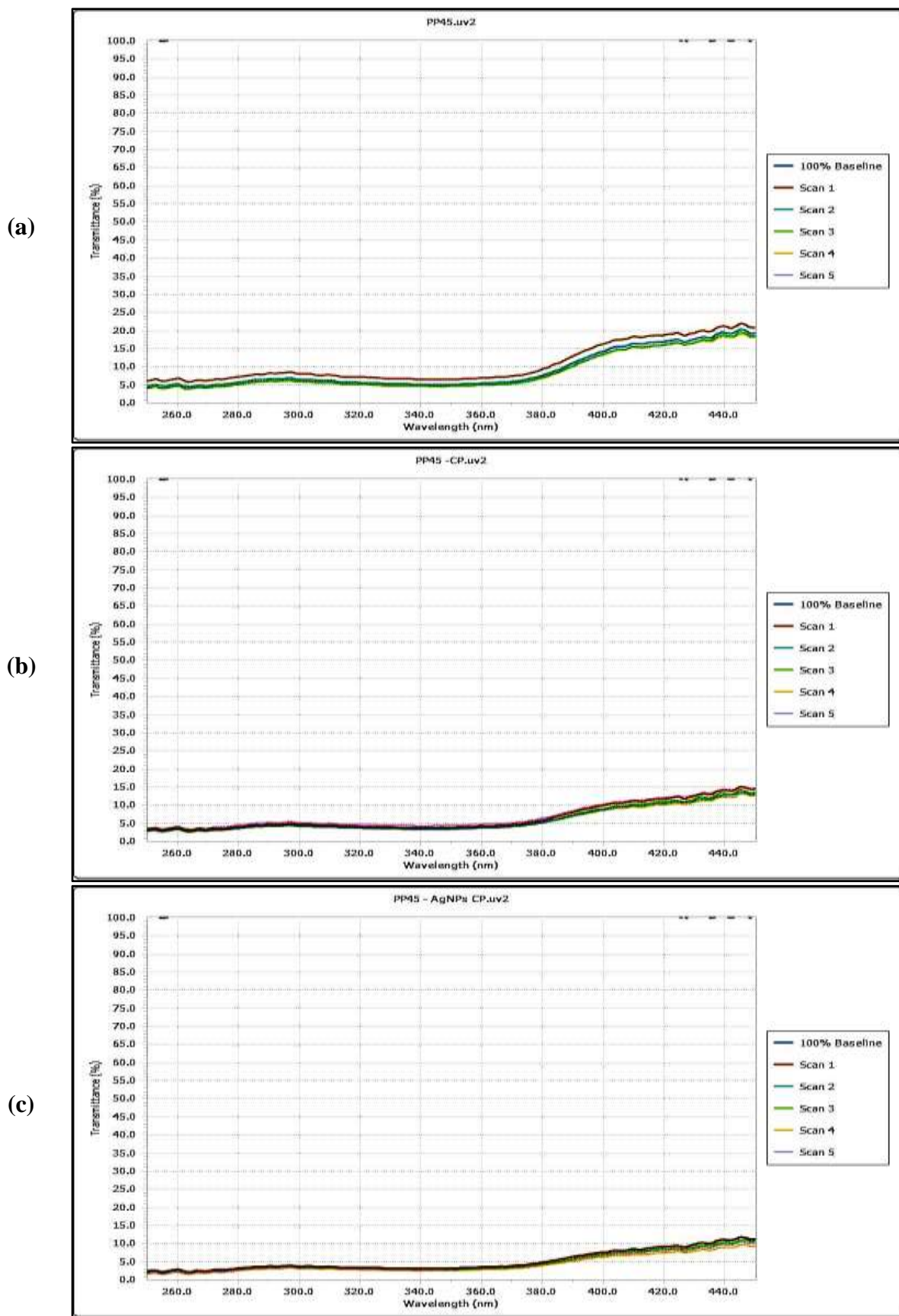


Figure 4.98: UV Transmittance profile of a) PP45, b) PP45-CP, and c) PP45-AgNPs/CP

4.4.2 PHASE-IV: CONCLUSIONS

I) Antibacterial assessment: According to the results of the antibacterial test, none of the parent PP and PV-nonwoven samples shown any bacterial inhibition against any of the bacterial cultures. It was expected of this behaviour. However, for CP treated and AgNPs/CP treated samples, the effectiveness and stability of the antibacterial activities mapped against SA and EC bacteria have showed extremely good findings. Additionally, statistical analysis demonstrated that the ZOI value significantly changed following the application of the CP leave extract and AgNPs/CP.

II) Structural assessments:

Morphological assessment (ESEM): ESEM micrographs have effectively exposed the surface morphology, structure, and orientation of the component fibres in the base materials. Similar to this, ESEM pictures have verified that CP particles had strong penetration, well-deposition, and adhesion to the fibre surface. However, the chosen deposition method has been supported by ESEM pictures that show a consistent distribution of nanoparticles @AgNPs/CP on the surface of the fibres. Hence, the technique used in the current study was deemed adequate for a virtue-based deposition of AgNPs on the PP and PV non-woven fabric.

FTIR analysis: The FTIR spectrum characterisation peaks demonstrate a common chemical composition (in respective parent nonwoven, CP treated, and AgNPs/CP treated samples), as well as additional chemical compositions for PV-AgNP/CP nano-composite i.e. phenolic (O-H) bending vibration and aromatic amine (C-N) stretching vibration. The integration of AgNPs into the AgNPs/CP nano-composites has been revealed by these spectra peaks linked to phenolic and aromatic amine groups.

III) Physical assessments:

Physical properties: The physical property findings suggest that all of the AgNPs/CP loaded samples have uniformly displayed a more rise in GSM value when compared to CP extract treated samples. The thickness measurement showed the same behaviour with small extent. This behaviour is mostly explained by the added component density. In comparison to when it was loaded with AgNPs, the lighter CP extract has resulted in a less significant shift in the composite values. The percent (%) variations in the values, however, were far smaller in each case.

Low-stress properties: Similar to the physical characteristics, fabric bending modulus (BM) and crease recovery angle ($^{\circ}$), particularly for PP the treatment with AgNPs/CP has demonstrated a notable increase. The impact in PV-nonwoven fabric has only been seen in the machine-direction. However, the statistical analysis revealed that the CP extract and AgNPs/CP treatments had no statistically significant effects in either direction the MD or the CD.

Comfort-associated properties: The findings for air permeability showed a little reduction in air permeability ($\text{m}^3/\text{m}^2/\text{hr}$) with the application of CP extract, and the value further decreased with the addition of AgNPs/CP. The statistical study also revealed that treating nonwoven textile materials with CP extract and AgNPs/CP can have a substantial impact in the form of a decrease in the air permeability value. The majority of samples, including the control, had a 'very poor' OMMC grade. The base material is rated as 'very poor' grade, has poor moisture management, and falls under the category of 'water proof fabrics'. Only the PV40-AgNPs/CP nano-composite, which is classed as a 'moisture management fabric', significantly improved its ability to handle water.

IV) UV Transmission properties: The "Poor protection" class for the tested UV radiations is applied to all non-woven textiles with measured UPF rating levels. The development of PP and PV nano-composite -AgNPs/CP, however can result in increased UVA and UVB type radiation protection due to a favourable decrease in UVA and UVB type radiation transmission %. The statistical analysis further demonstrated that the UV transmittance profile of the corresponding nonwoven textile materials is significantly impacted by the application of CP leave extract and AgNPs/CP.